Volume 68A
Number 1
Jan.–Feb. 1964

Physics and Chemistry

U.S. DEPARTMENT OF COMMERCE

SECTION A

JOURNAL OF RESEARCH

NATIONAL BUREAU OF STANDARDS

Journal of Research

of the

National Bureau of Standards

A. Physics and Chemistry

Jan.–Feb. • 1964

VOLUME • 68A

NUMBER • 1

Editor: C. W. Beckett

Associate Editors: D. D. Wagman
J. M. Richardson

Publication dates:
Feb. 1, Apr. 1, June 1, Aug. 1, Oct. 1, Dec. 1, 1964

JOURNAL OF RESEARCH

The National Bureau of Standards Journal of Research reports research and development in the fields of activity shown at right. Also included from time to time are survey articles on topics closely related to the Bureau's scientific and technical program.

The Journal is published in four separate sections as follows:

A. Physics and Chemistry

Contains papers of interest primarily to scientists working in these fields. Issued six times a year. Annual subscription: domestic, $4.00; foreign, $4.75.

B. Mathematics and Mathematical Physics

Presents studies and compilations designed mainly for the mathematician and the theoretical physicist. Issued quarterly. Annual subscription: domestic, $2.25; foreign, $2.75.

C. Engineering and Instrumentation

Reports research and development results of interest chiefly to the engineer and the applied scientist. Issued quarterly. Annual subscription: domestic, $2.25; foreign, $2.75.

D. Radio Science (formerly Radio Propagation)

Published in cooperation with U.S. National Committee of URSI. Presents papers in radio propagation, communications, and radio science generally. Issued monthly. Annual subscription: domestic, $9.00; foreign, $11.50.

Functions and Activities

The functions of the National Bureau of Standards are set forth in the Act of Congress, March 3, 1901, as amended. These include the development and maintenance of the national standards of measurement and the provision of means and methods for making measurements consistent with these standards; the determination of physical constants and properties of materials; the development of methods and instruments for testing materials, devices, and structures; advisory services to government agencies on scientific and technical problems; invention and development of devices to serve special needs of the Government; and the development of standard practices, codes, and specifications. The work includes basic and applied research, development, engineering instrumentation, testing, evaluation, calibration services, and various consultation and information services. The Bureau also serves as the Federal technical research center in a number of specialized fields. The scope of activities of the National Bureau of Standards is suggested in the following listing of the divisions and sections engaged in technical work.

Washington, D.C.

Electricity. Resistance and Reactance. Electrochemistry. Electrical Instruments. Magnetic Measurements. Dielectrics. High Voltage. Absolute Electrical Measurements.

Metrology. Photometry and Colorimetry. Refractometry. Photographic Research. Length. Engineering Metrology. Mass and Volume.

Heat. Temperature Physics. Heat Measurements. Cryogenic Physics. Equation of State. Statistical Physics.

Radiation Physics. X-ray. Radioactivity. Radiation Theory. High Energy Radiation. Radiological Equipment. Nucleonic Instrumentation. Neutron Physics.

Analytical and Inorganic Chemistry. Pure Substances. Spectrochemistry. Solution Chemistry. Standard Reference Materials. Applied Analytical Research. Crystal Chemistry.

Mechanics. Sound. Pressure and Vacuum. Fluid Mechanics. Engineering Mechanics. Rheology. Combustion Controls.

Polymers. Macromolecules: Synthesis and Structure. Polymer Chemistry. Polymer Physics. Polymer Characterization. Polymer Evaluation and Testing. Applied Polymer Standards and Research. Dental Research.

Metallurgy. Engineering Metallurgy. Metal Reactions. Metal Physics. Electrolysis and Metal Deposition.

Inorganic Solids. Engineering Ceramics. Glass. Solid State Chemistry. Crystal Growth. Physical Properties. Crystallography.

Building Research. Structural Engineering. Fire Research. Mechanical Systems. Organic Building Materials. Codes and Safety Standards. Heat Transfer. Inorganic Building Materials. Metallic Building Materials.

Applied Mathematics. Numerical Analysis. Computation. Statistical Engineering. Mathematical Physics. Operations Research.

Data Processing Systems. Components and Techniques. Computer Technology. Measurements Automation. Engineering Applications. Systems Analysis.

Atomic Physics. Spectroscopy. Infrared Spectroscopy. Far Ultraviolet Physics. Solid State Physics. Electron Physics. Atomic Physics. Plasma Spectroscopy.

Instrumentation. Engineering Electronics. Electron Devices. Electronic Instrumentation. Mechanical Instruments. Basic Instrumentation.

Physical Chemistry. Thermochemistry. Surface Chemistry. Organic Chemistry. Molecular Spectroscopy. Elementary Processes. Mass Spectrometry. Photochemistry and Radiation Chemistry.

Office of Weights and Measures.

Boulder, Colo.

Cryogenic Engineering Laboratory

Cryogenic Processes. Cryogenic Properties of Solids. Cryogenic Technical Services. Properties of Cryogenic Fluids.

Central Radio Propagation Laboratory

Ionosphere Research and Propagation. Low Frequency and Very Low Frequency Research. Ionosphere Research. Prediction Services. Sun-Earth Relationships. Field Engineering. Radio Warning Services. Vertical Soundings Research.

(Continued on inside back cover)

JOURNAL OF RESEARCH of the National Bureau of Standards—A. Physics and Chemistry
Vol. 68A, No. 1, January–February 1964

Fast Neutron Dose Measurements for a D–D Neutron Source in Water*

W. B. Beverly and V. Spiegel, Jr.

(June 27, 1963)

The penetration of D–D neutrons in water has been studied through measurements of first collision dose. A relative measurement of first collision dose as a function of distance from the neutron source was made at 0°. At large penetrations the results appear to approach asymptotically the slope predicted by the theoretical calculations of Goldstein et al. [6] for a monoenergetic, isotropic 4.0-Mev neutron source in water. However as expected, the measurements close to the source where the average neutron spectrum is relatively soft indicate a steeper slope than the theoretical calculation. Further calculations will be required to obtain an explicit check of this experiment.

1. Introduction

This experiment is a continuation of a series of experiments performed at this laboratory pertaining to the slowing down of neutrons in hydrogenous media [1–3].[1] The 14-Mev experiment in water of Caswell et al. [1] was the only previous one in which an attempt was made to measure fast neutron dose. Fast neutron dose was also measured by Otis [4] using the fission neutrons from a U^{235} disk source. Experiments such as these are needed to check the calculation methods and input data used for neutron shielding and reactor physics.

The first collision neutron dose (or "kerma," see ref. [5]) at 0° with respect to the incident deuteron beam was measured as a function of distance in water from the D–D neutron source which emitted neutrons of 4.0-Mev maximum energy. This source is well-defined in energy versus angle. It should be possible to make a critical check between this experiment and appropriate penetration calculations. Unfortunately, at present there are no calculations which can be compared directly to our experiment but Goldstein [6] has calculated the dose expected for a 2- and a 4-Mev monoenergetic, isotropic source. It would be expected that a similar calculation made using our D–D spectrum would show the dose to be between the 2- and the 4-Mev curve with its slope approaching that of the 4-Mev curve at large distance.

The absolute neutron dose was not measured in this experiment because it was not possible to measure accurately the beam current or the pressure of the gas target. The associated particle method of obtaining an absolute measurement was undesirable due to the duct effect of the associated equipment. Consequently, only the slope of the experimental curve can be compared to the calculations of Goldstein.

2. Experimental Arrangement

Neutrons were produced by the $D(d,n)He^3$ reaction using an analyzed deuteron beam from a 2-Mev Van de Graaff accelerator. The deuteron beam impinged upon a modified gas target of the type described by Richardson [7] which was located in a tank of water 115 cm wide x 142 cm long x 60 cm deep. The gas cell of the target was coupled to the 2-in. beam tube by a 2 cm diam by 30 cm long thin

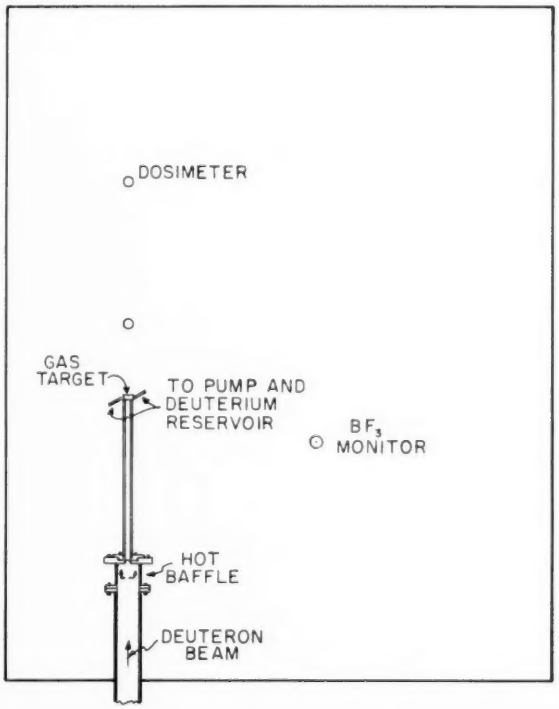

FIGURE 1. *Experimental arrangement.*

*Work sponsored by the U.S. Atomic Energy Commission.

[1] Figures in brackets indicate the literature references at the end of this paper.

wall brass tube in order to reduce duct effects. The gas cell was positioned 26 cm from the nearest wall and 30 cm from the bottom and 28 cm from the top of the tank. This arrangement is shown in figure 1.

The gas target had a cell 1.24 cm long and used a 0.1 mil nickel entrance foil. The entrance aperture was ⅜-in. diam and the impinging deuteron beam was first collimated by a heated baffle so that the remaining beam would completely pass through the entrance foil into the gas cell. The heated baffle is used to collimate a deuteron beam without production of undesired neutrons by the $D(d,n)He^3$ reaction. The foil was cooled by continuously circulating the deuterium gas. This permitted the use of 2-μa current for as long as 30 hr without burning out the foil. The pressure was maintained at 760 mm Hg in the cell. This target differed from the one described by Richardson in that a thick gold backing was used instead of an exit foil. The gold backing was rotated frequently in order to reduce the buildup of a "drive-in" target.

The deuteron beam incident energy was 1.36-Mev. Using the data of Whaling [8], the average energy loss of the beam in passing through the 0.1 mil entrance foil was computed to be 380-kev and that in the gas cell to be 150-kev. The resultant average deuteron energy in the gas cell was 0.905-Mev which produced neutrons of 4.0-Mev average energy at 0° with a neutron energy spread of 180-kev. A small number of lower energy neutrons were also produced by the formation of a "drive-in" target in the gold backing of the gas cell. Their relative intensity was measured by first forming a "drive-in" target by bombarding the gas cell with a deuteron beam for approximately 5 hr. The yield at 0° in air of the deuterium-gas filling was then measured and compared to the yield obtained by replacing the deuterium with hydrogen. This measurement showed that 3.1 percent of the neutron flux at 0° was due to "drive-in" neutrons. The idealized neutron spectrum from both the gas target and the gold backing is shown in figure 2. The angular distribution of the neutron yield [9] and energy [10] are shown in figure 3.

A polyethylene-ethylene proportional counter dosimeter modeled after the secondary counter described by Hurst [11] was used to measure the neutron first collision dose [12]. This counter and its energy response is described in detail by Caswell et al. [13]. The energy response is shown in figure 4.

The signal was brought out of the dosimeter by a 3-ft RG–59/U coaxial cable passed through a ⅜ in. thin-wall, watertight brass tube attached to

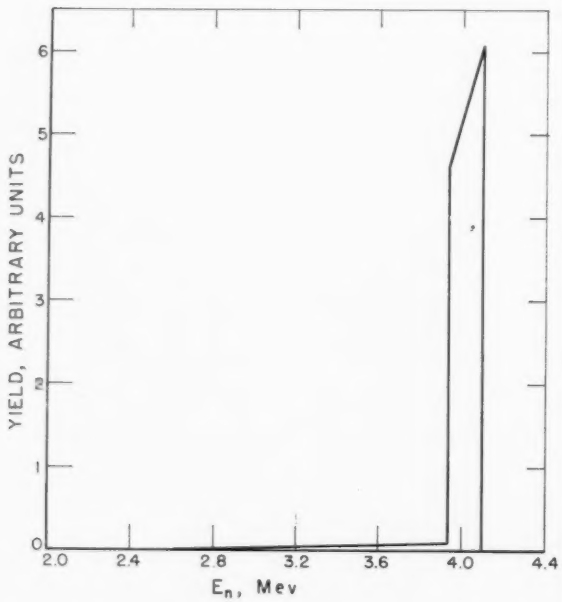

FIGURE 2. *Neutron spectrum at 0° (gas target plus gold backing).*

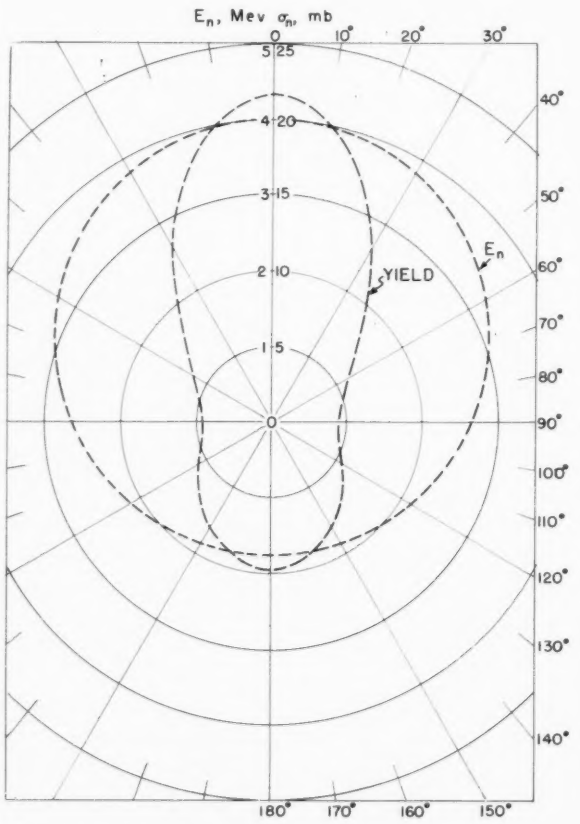

FIGURE 3. *Angular and energy distribution of the D–D source.*
The differential cross section (in mb/ster) is shown by the dotted curve marked yield. The average energy at any given angle is given by the intersection of the off center dotted circle marked E_n with a radius vector drawn from the origin in that direction. The concentric circles give the scale for both yield (mb/ster) and energy (Mev).

one end of the dosimeter. The other end of the brass tube was attached to and passed through a small (4 in. x 2 in. x ⅜ in.) brass plate which had two parallel grooves shaped to slide along a track. This track was mounted horizontally at the top of the water tank just above the water level and parallel to the beam direction. This permitted the dosimeter to be dropped into the water and positioned at various distances along 0° with its long axis vertical and perpendicular to the beam direction. The dosimeter was operated at 2150 v. High voltage was supplied by a regulated power supply.

The signal was bought from the dosimeter to a gain-of-sixteen, transistorized preamplifier powered by batteries. The signal was then carried by a 40-ft cable through a variable attenuator to an RCL linear amplifier and 256-channel analyzer. A constant pulse from a mercury-relay pulser could be fed into the input of the preamplifier thus permitting a quick check on the overall gain of the electronics and the gain could be quickly adjusted to the desired level by means of the variable attenuator.

It was necessary in the computing of neutron doses to reject small pulses which were caused by electrons ejected by gamma rays. Previous experience with this dosimeter [1] had indicated that the gamma ray contribution would be negligible if a 0.1-Mev bias were selected and all pulses falling below this bias were discarded. This was corroborated experimentally by first determining the 0.1-Mev bias by extrapolating the steep part of a 0.1-Mev $T(P,n)He^3$ neutron spectrum to zero and then adjusting electronic gains so that this intercept would fall in channel 17. The dosimeter was then exposed to the 87-kev gamma ray of Cd^{109} and to the higher energy gamma rays of radium. All the pulses from the 87-kev gamma ray fell below the 0.1-Mev bias but a few pulses from the radium source fell as high as six channels above the bias. The dose falling above the 0.1-Mev bias was measured for the 4.0-Mev monoenergetic neutron source and for the radium source and these were compared when the total energy deposition in the dosimeter was the same for each. This neutron-gamma ray discrimination ratio was found to be about 120. The 0.1-Mev cutoff as determined experimentally was reproducible to within one channel although the absolute accuracy was estimated to be no better than two or three channels.

The dosimeter was checked for possible drift by periodically measuring the dose in air from a plutonium-beryllium source. A slight drift was noticed when the energy calibrations were finished and the dosimeter was first placed in the water. The data were corrected for this drift and the resultant error due to dosimeter drift is estimated to be not greater than 5 percent.

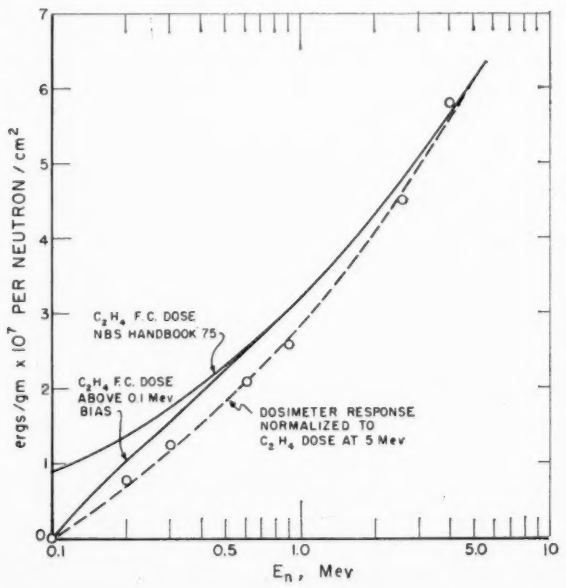

FIGURE 4. *Dosimeter response.*

3. First-Collision Dose Measurement

The D–D neutron first collison dose was measured as described by promenading the dosimeter at 2.5 cm intervals from 15 to 45 cm at 0° and then calculating the dose using a 0.1-Mev bias. The neutron flux was monitored during these runs by a cylindrical BF_3 counter placed at 100° to the incident deuteron beam and approximately 40 cm from the target. The measured dose is given in table 1 and is plotted in figure 5. A computation of the dose was made using the neutron spectra of Goldstein [6] for a 2.0- and a 4.0-Mev neutron source and our dosimeter response and these are also shown in figure 5 with the experimental curve arbitrarily normalized to the 4.0-Mev curve at 10 cm. R, as given in figure 5 and table 1, is the distance from the center of the gas target to the center of the dosimeter, while r is the distance from the target-water boundary to the center of the dosimeter.

TABLE 1. *D–D neutron first collision dose in water*

First run at 0°		
r	R	R^2 dose, arbitrary units
cm	cm	
14.25	14.87	1202.5±7.4
16.95	17.57	865.3±5.9
19.27	19.89	667.0±8.0
21.84	22.46	442.4±5.5
24.41	25.03	318.0±3.5
26.79	27.41	221.7±3.1
29.42	30.04	149.5±2.4
32.03	32.65	105.2±1.6
34.36	34.98	76.1±3.2
37.04	37.66	50.4±0.9
39.39	40.01	36.6±1.4
44.51	45.13	13.8±0.4

There was some uncertainty in determining the best value of R and r due to (1) the finite size of the neutron source and the variation in yield along its length, (2) the finite size of the dosimeter, and (3) the

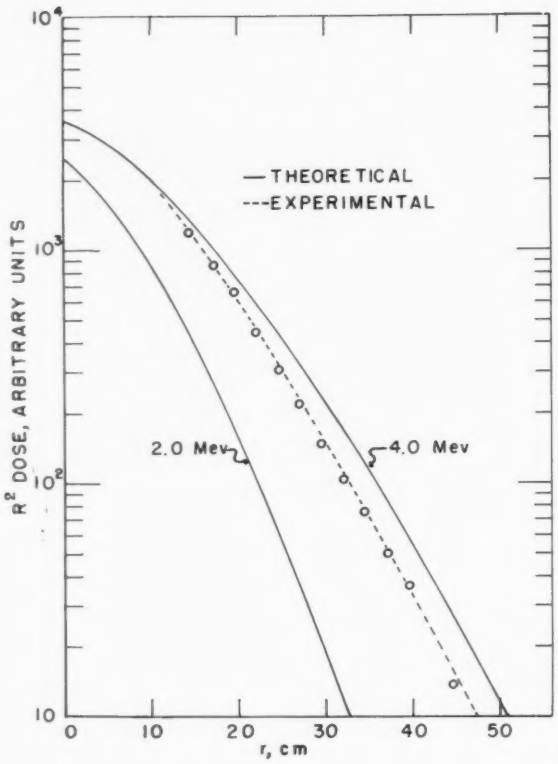

FIGURE 5. *D–D neutron dose in water.*

anisotropy of the neutron flux incident upon the dosimeter. In the ideal situation of a point source of neutrons located at the center of a void sphere of radius r_1 and at a distance r_2 from a point dosimeter, R would be given exactly by r_2 while r would be given by r_2-r_1. In our experiment, the upper limit of the difference between the nominal values of R and r chosen above and the values of $\sqrt{\overline{R^2}}$ and $\sqrt{\overline{r^2}}$ computed for the worst case by taking into account the above effects was found to be small enough to warrant being ignored. The first effect would cause $\sqrt{\overline{R^2}}$ to be less than 0.02 cm longer than R while the second and third effects opposed each other and would cause $\sqrt{\overline{r^2}}$ to be less than 0.10 cm shorter than r.

The statistical errors for the first collision dose were computed by approximating the dosimeter spectrum with one of the form $Y=MX+B$ where Y is the counts per channel and X is the channel. M and B are adjusted so that $Y=0$ for $X=256$ and $\int_{X_I}^{X_F} Y dX=$ True Counts. The standard deviation as computed in this manner will be given by

$$\delta^2_{\text{Dose}}=\frac{X_F^4}{6(X_F-X_I)^2}\sum_{i=I}^{F} Y_i$$

where X_I=channel 18, X_I=channel 256, and $\sum_{i=I}^{F} Y_i$= total counts above the 0.1-Mev bias. The standard deviation as computed in this manner will be larger than the true standard deviation. When two or more commensurate runs were made at the same distance, they were averaged together by weighting each measurement according to its separate standard deviation.

4. Conclusion

A calculation to compare directly to this experiment is not yet available. However the 4- and 2-Mev monoenergetic, isotropic calculation of Goldstein [6] should bracket the experimental results. The slope of the penetration curve of this experiment is steeper at small distances but appears to approach at larger distances the slope of the 4.0-Mev calculation. This steeper slope close to the source is probably due to the contributions of neutrons of energies around 3.5-Mev which are emitted into forward angles, and which have a short mean free path and therefore scatter quickly and contribute to the dose seen by the dosimeter at 0°.

It is desirable that a calculation be made of the dose distribution at 0° with exactly the D–D neutron spectrum and angular distribution and the experimentally observed dosimeter response [13] of figure 4 to provide a more exact comparison with this experiment. Another possibility in the future is to extend the 0° curve to larger distances. This would require much higher currents on the gas target and greatly increased detector sensitivity.

The authors express their appreciation to R. S. Caswell for his many helpful discussions and suggestions during the course of this experiment. A special note of appreciation is due to J. Cooper for his suggestions on the analysis of the results. We are also indebted to W. Bailey for his aid in setting up the experiment and to R. T. Weppner for his assembling of the dosimeter.

5. References

[1] R. S. Caswell, R. F. Gabbard, D. W. Padgett, and W. P. Doering, Nuclear Sci. and Eng. **2,** 143–159 (1957).
[2] V. Spiegel, Jr., D. W. Oliver, and R. S. Caswell, Nuclear Sci. Eng. **4,** 546–562 (1958).
[3] V. Spiegel, Jr., and A. C. B. Richardson, Nuclear Sci. Eng. **10,** 11–15 (1961).
[4] D. R. Otis, ORNL CF–57–3–48 (12 Mar. 1957).
[5] National Bureau of Standards Handbook **84,** (1962).
[6] R. Aronson, J. Certaine, and H. Goldstein, NYO 6269 (1954).
[7] A. C. B. Richardson, Rev. Sci. Instr. **31,** 1202–1203 (1960).
[8] W. Whaling, Handbuch der Physik **XXXIV,** 193–215 (1958).
[9] N. Jarmie, and J. D. Seagrave, LA–2014 (1957).
[10] L. Blumberg, and S. I. Schlesinger, AECU–3118 (1956).
[11] G. S. Hurst, Brit. J. Rad. **XXVII,** 353–357 (1954).
[12] National Bureau of Standards Handbook **75** (1961).
[13] R. S. Caswell, W. B. Beverly and V. Spiegel, Jr., Symposium on Neutron Detection, Dosimetry and Standardization, Harwell, U.K. (1962).

(Paper 68A1–250)

JOURNAL OF RESEARCH of the National Bureau of Standards—A. Physics and Chemistry
Vol. 68A, No. 1, January–February 1964

X-Ray Spectrometric Analysis of Noble Metal Dental Alloys

B. W. Mulligan,[1] H. J. Caul, S. D. Rasberry, and B. F. Scribner

(October 9, 1963)

The analysis of noble metal dental alloys for the various constituent elements is a difficult and tedious task by chemical or fire assay procedures. X-ray spectroscopy offered the possibility of increased speed, especially if solid metal samples were employed. This technique was investigated particularly with respect to the analysis of dental alloys having the nominal composition in percent, of gold 72, silver 12, copper 10, platinum 2, palladium 2, and zinc 2. Alloys were prepared by melting the component elements in a high frequency furnace and casting the metal into disk form. Compositions of the castings were determined by chemical analysis. Optimum procedures for casting the sample and for X-ray analysis were established, and analytical curves were developed relating concentrations to measured intensities of the X-ray lines Au L_β, Ag K_α, Cu K_α, Pt L_α, Pd K_α, and Zn K_α. The observed typical coefficients of variation for the method were Au 0.34 percent, Ag 0.44 percent, Cu 2.2 percent, Pt 1.6 percent, Pd 1.2 percent, and Zn 0.72 percent. The results indicate that the method is sufficiently accurate and has marked advantages of speed and simplicity compared to chemical analysis.

1. Introduction

The analysis of noble metal alloys by traditional methods of solution chemistry [3] [2] is one of the more complex and time-consuming tasks confronting the analytical chemist. Three to four man-weeks are usually required for the analysis of three samples in duplicate. The methods involve painstaking separations with numerous precipitations and filtrations.

Fire assay techniques also are used but chiefly for the determination of gold. If platinum and palladium are present in the sample being assayed, the alloy has a much higher melting point and there are more losses due to volatilization [2]. In addition, further chemical separations are necessary to remove the platinum and palladium before gravimetrically determining the gold. In the assay technique the base metals are either absorbed into the cupel or volatilized and hence are not determined.

In conjunction with the problem of analysis of gold alloys for the Research Group of the American Dental Association, the development and evaluation of an instrumental method of analysis was considered. X-ray spectrometry with its high precision offered the best possibility for a rapid method, especially if wet chemical processes could be eliminated in preparing the samples. A typical composition for the alloys to be analyzed was, in percent, gold 72, silver 12, copper 10, platinum 2, palladium 2, and zinc 2.

There are only a few references in the literature concerning the X-ray spectrometric determination of the noble metals. MacNevin and Hakkila [6] made determinations of palladium, platinum, rhodium, and iridium in a liquid sample that was applied to heavy chromatographic paper, dried, and compared with a previously calibrated color chart. Bacon and Popoff [1] described quantitative X-ray fluorescence analyses of glass for 15 or more elements including platinum and silver. Other references of interest include the determination of platinum in a petroleum reforming catalyst [4], and the determination of silver in photographic films [5].

2. Experimental Procedure

In order to investigate the direct X-ray spectrometric analysis of solid alloys, samples were synthesized initially by melting together in a high frequency furnace solid metal pieces of the desired component elements. Four samples were prepared in this manner.

The molten alloys of these elements were cast in the shape of disks approximately ⅛-in. thick with a diameter of 1¼ in. to fit the sample holders of the X-ray spectrometer to be employed. Each disk so cast weighed about 35 g. The surfaces of the disks were then precision machined for the X-ray measurements. The compositions of the castings were determined by wet chemical analysis according to the method of Gilchrist [3], and the results of the analysis are shown in table 1.

TABLE 1. *Results of chemical analysis*

Element	Alloy No.			
	1	2	3	4
	Percent	*Percent*	*Percent*	*Percent*
Au	68.27	72.01	78.08	79.08
Ag	11.63	10.86	8.13	13.88
Cu	11.88	9.95	7.86	6.01
Pt	6.34	3.76	2.17	.00
Pd	.00	1.97	2.84	1.04
Zn	1.87	1.44	.94	.00
Totals	[3] 99.99	99.99	100.02	100.02

[1] Present address Army Materiel Command, Harry Diamond Laboratories, Washington, D.C., 20438.
[2] Figures in brackets indicate the literature references at the end of this paper.

The optimum conditions for X-ray fluorescence intensity measurements were determined experimentally and are given in table 2. Using these parameters, measurements of intensities at the X-ray wavelengths listed were made on the disks for all six constituent elements. The resultant analytical curves were found generally to be linear and the precision of repeated determinations appeared favorable for an analytical method. Before carrying the development of the method further, it was considered advisable to establish a preparation technique requiring a smaller quantity of precious metal per sample. The technique generally applied to prepare castings in dentistry, known as investment casting or the "lost wax" process [8, 9], appeared promising. This technique was applied, using a small centrifugal casting machine, to obtain disks of the gold alloys varying in thickness from ⅛ to 1/64 in. The various steps of this process are illustrated in figures 1 and 2. Disks are cut from wax sheets of the desired thickness and mounted vertically on edge on the tip of a brass cone as shown in figure 1. A metal cylinder is then

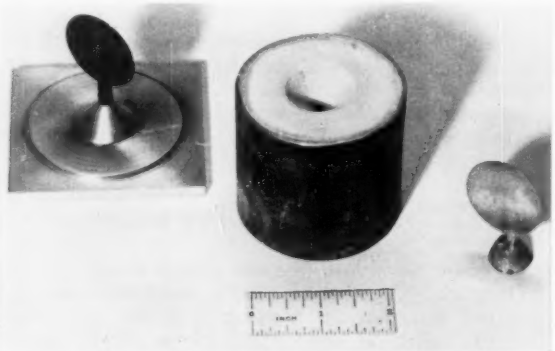

FIGURE 1. *Preparation of sample—(left) Wax disk mounted on metal cone; (center) metal cylinder (inverted) containing mold cavity of wax disk; (right) noble metal alloy disk before removal of sprue.*

FIGURE 2. *Preparation of sample—furnace and centrifugal casting machine with mounted mold cylinder.*

TABLE 2. *Operating parameters [1] for noble metal alloy analysis*

Element	X-ray line	Degrees, 2θ LiF crystal	Wavelength X-ray tube			Counts per determination
			Å	kv	ma	
Au	L_β	31.19	1.083	50	30	256,000
Ag	K_α	15.95	0.559	50	45	256,000
Cu	K_α	44.96	1.540	50	45	256,000
Pt	L_α	38.05	1.313	50	45	128,000
Pd	K_α	16.70	.585	50	45	128,000
Zn	K_α	41.74	1.435	50	45	128,000

[1] Norelco Inverted-Sample Three-Position Spectrograph with molybdenum target X-ray tube, lithium fluoride crystal, and scintillation counter detector (Philips Electronic Instruments, Mt. Vernon, N.Y.).

placed around the disk and cone and the cylinder is filled with an investment material (consisting of 50% crystobolite and 50% gypsum). The investment hardens in a few minutes and the filled cylinder is placed in a furnace and heated to approximately 700° C. During the heating the wax volatilizes completely leaving a mold cavity having the dimensions of the wax disk.

The heated cylinder is removed from the furnace, cooled to about 500 °C, and mounted on the centrifugal casting machine shown in figure 2. In the machine the mold is shown adjacent to the small refractory melting cup at the center. The gold alloy is melted in the cup by means of a torch and is cast immediately by releasing the spring loaded arm of the machine. The molten metal is forced into the mold cavity where it solidifies in disk form. The furnace in the background served for preparing the mold.

After cooling, the mold is broken apart and the metal disk and sprue are extracted. The sprue is cut from the disk by means of a jeweler's saw, and the metal disk sample is mounted in methyl methacrylate resin for handling during surface preparation and analysis. The exposed surface of the resin-mounted sample is prepared for analysis by wet grinding to a flat surface, finishing with a 600-grit abrasive.

X-ray intensity measurements for the selected wavelengths were made for all of the disks, and no differences could be detected within the precision of the determinations among the disks of the same alloy having different thicknesses. Subsequently, disks of 1/32-in. thickness were selected as the best compromise between rigidity of sample and minimum amount of alloy per sample. The disk and sprue together weighed about 20 g with the sprue accounting for slightly over half of this weight.

Samples of the four previously analyzed gold alloys were prepared in duplicate by this technique and X-ray fluorescence measurements were made in the spectrometer in a sequence designed to minimize effects of instrumental drift [7]. The overall time required for this procedure was approximately 5 hr, which included about 3 hr for sample preparation and about 2 hr for X-ray measurements. The effect of melting and casting on the apparent composition of the alloys will be discussed later in the text.

3. Results and Discussion

The analytical curves obtained from these runs for gold, silver, copper, platinum, palladium, and zinc are shown in figures 3 through 8. Each point on a curve is the mean of four individual determinations. The precision of the method, calculated as the coefficient of variation for an individual determination in a group of four, is given in table 3.

In the case of platinum, sample number two resulted in a higher count compared to the linear relationship of the other three samples for reasons as yet unknown. A least squares treatment of the data indicated that the point was in error by 0.14 percent.

The theoretical precision that should be obtained solely on the basis of the counting statistics is equal to the reciprocal of the square root of the total number of counts per measurement. In the case of gold, silver, and copper, where 256,000 counts were measured per determination, this would be about 0.20 percent. For platinum, palladium, and zinc, where 128,000 counts were measured, it would be about 0.28 percent. This precision was approached in the case of gold and silver, but not in the other cases, possibly because of the greater influence of background variation (which could not be measured simultaneously) when the line-to-background ratio is low.

TABLE 3. *Reproducibility of single determinations*

Au concentration	CV [1]	Ag concentration	CV	Cu concentration	CV
%		%		%	
68.27	0.43	11.63	0.17	11.88	2.07
72.01	.23	10.86	.66	9.95	2.32
78.08	.41	8.13	.30	7.86	2.60
79.08	.30	13.88	.63	6.01	1.74
Pt concentration	**CV**	**Pd concentration**	**CV**	**Zn concentration**	**CV**
%		%		%	
6.34	1.15	0.00	2.24	1.87	0.73
3.76	1.63	1.97	1.32	1.44	.81
2.17	2.64	2.84	1.18	0.94	.62
[2] 0.00	1.36	1.04	1.19	.00	2.15

[1] CV = Observed coefficient of variation for an individual determination in a group of four

$$CV = \frac{100}{\bar{c}} \sqrt{\frac{(\Sigma c - \bar{c})^2}{n-1}}$$

[2] Coefficient of variation for zero concentration is the value for the background radiation.

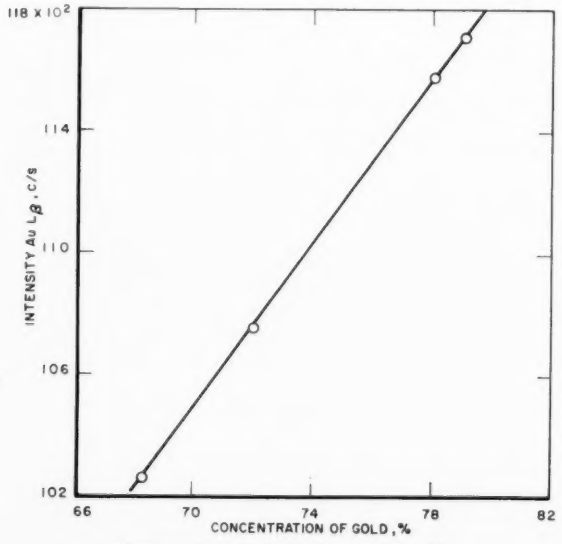

FIGURE 3. *Analytical curve for gold.*

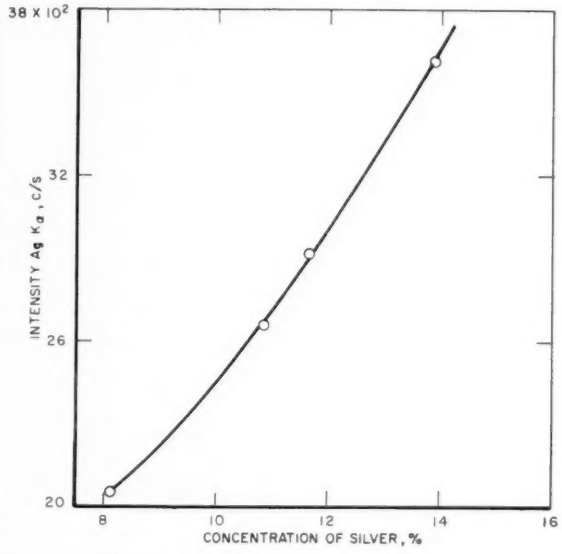

FIGURE 4. *Analytical curve for silver.*

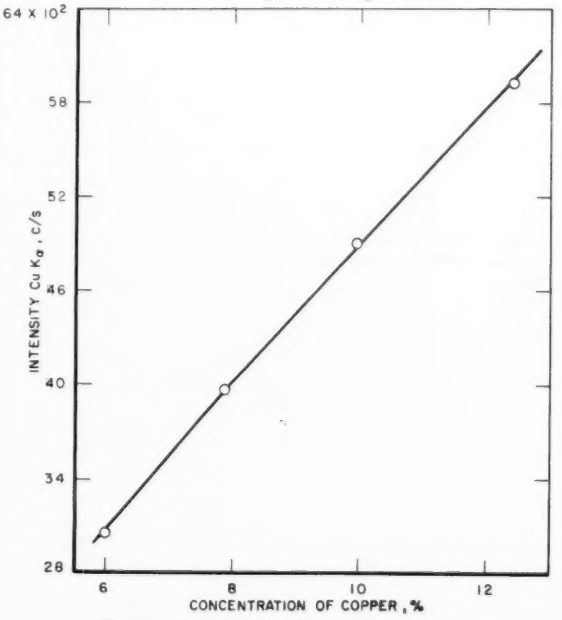

FIGURE 5. *Analytical curve for copper.*

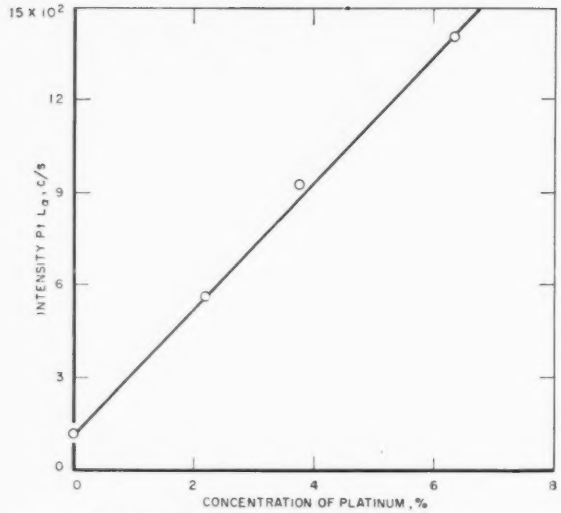

FIGURE 6. *Analytical curve for platinum.*

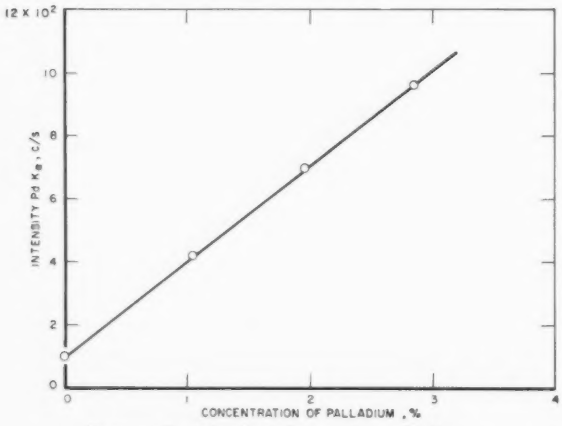

FIGURE 7. *Analytical curve for palladium.*

A possible drawback to this procedure is the loss of more volatile constituents in the melting and casting operation. To investigate this possibility, samples were repeatedly melted and cast in an automatic machine which cast the metal when a selected temperature was reached. The samples were melted, then heated to 1080 °C and cooled to 870 °C six times before casting. The castings were then analyzed by the X-ray procedure described and compared with samples of the same material melted once at 1080 °C and cast immediately. Within the precision of the method no differences could be detected between the samples prepared by the two casting procedures, indicating negligible loss on melting.

The spectrometer used (table 2) is a research-type instrument in which individual determinations must be made sequentially (since it has only one crystal and detector) and wavelength settings must be changed manually. More automatic multi-channel instruments are available which would decrease the measurement time by a substantial factor.

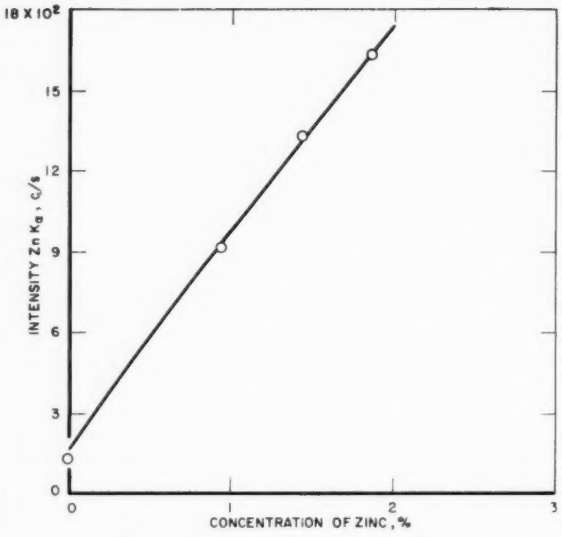

FIGURE 8. *Analytical curve for zinc.*

The results indicate that the method is sufficiently precise and has distinct advantages of simplicity of sample preparation and speed of measurement compared to chemical analysis. The melting and casting procedure employed in this work would appear to offer advantages as a general method for preparing samples and standards especially for X-ray spectrometry. The casting procedure probably could be speeded up by use of a permanent split mold instead of the investment mold. The extension of the technique to the analysis of silver alloys is currently in progress.

The authors are indebted to Charles L. Gordon of the National Bureau of Standards for the chemical analysis of the noble metal alloys and to Dennis Worthen and Laszlo de Simon of the Walter Reed Army Medical Center for their assistance in specimen preparation.

4. References

[1] Bacon, J. F., Popoff, V., Pittsburgh Conference on Analytical Chemistry and Applied Spectroscopy, Pittsburgh, Pa., March, 1955 (an abstract).
[2] Bugbee, E. E., Textbook of Fire Assaying, 3d ed., 1940, p. 103 (John Wiley & Sons, New York, N. Y.).
[3] Gilchrist, R., J. Res. NBS **20,** 745 (1938).
[4] Gunn, E. L., Anal. Chem. **28,** 1433 (1956).
[5] Lofstrom, J. G., Smith, T. D., Norelco Reptr. **3,** 9 (1956).
[6] MacNevin, W. M., Hakkila, E. A., Anal. Chem. **29,** 1019 (1957).
[7] National Bureau of Standards Circ. 600 (1959), pp. 11 and 12. Superintendent of Documents, U.S. Government Printing Office, Washington, D.C., 20402.
[8] Peyton, F. A., et al., Restorative Dental Materials, p. 306 (C. V. Mosby Co., St. Louis, Mo., 1960).
[9] Skinner, E. W., Phillips, R. W. The Science of Dental Materials, 5th ed., p. 412 (W. B. Saunders Co., Phila., Pa., 1960).

(Paper 68A1–251)

JOURNAL OF RESEARCH of the National Bureau of Standards—A. Physics and Chemistry
Vol. 68A, No. 1, January–February 1964

The First Spectrum of Manganese, Mn I

Miguel A. Catalán,[1] William F. Meggers,[2] and Olga Garcia-Riquelme[3]

June 29, 1963

In 1894, two short series of threefold spectral terms were discovered in the arc spectrum of manganese, and in 1922 other regularities involving fivefold and sixfold terms were discovered by Catalán who coined the word "multiplet" for the group of related lines resulting from combinations of such complex terms. Multiplet analyses of complex spectra promptly led to the present formal quantum interpretation of all such phenomena, but comparable progress in the analysis of the Mn I spectrum was handicapped by the paucity of experimental data.

New observations of about 2500 wavelengths and intensities plus 440 Zeeman patterns made available in 1948–49 have now been completely exploited to derive additional atomic energy levels and thereby explain more of the observed Mn I lines. The result is that a total of 42 even terms with 125 levels and 60 g-values have now been designated and allocated to electron configurations, and 94 odd terms with 266 levels, 164 g-values, plus 13 miscellaneous levels. These terms are distributed among four multiplicities (doublets, quartets, sextets, octets), and transitions between even and odd terms account for more than 2030 lines ranging in wavelength from 1785 Å to 17608 Å.

I. Introduction

The spectra of manganese have interested and engaged scientists for nearly 120 years. In 1910 Kayser [1][4] listed 67 publications on this subject since 1845, and in 1934 Kayser and Konen [2] compiled a bibliography of 154 additional items through 1931. In the present paper only a few of the above will be referred to for historical background, but most of the papers published since 1931 that describe or interpret the Mn I spectrum will be mentioned to extend the bibliography.

In 1894 Kayser and Runge [3] reported finding the first regularities among lines in the arc spectrum of manganese; they found five triplets with wave number differences of 173 and 129 K (K=kayser=1 cm^{-1}) and arranged them in two spectral series, one "sharp" and one "diffuse," like those in the simpler spectra of alkaline-earth elements. (This precious information was presented in a footnote on page 104 of a paper primarily dedicated to the spectra of tin, lead, arsenic, antimony, and bismuth.)

Nearly three decades after Kayser and Runge [3] discovered the first rudimentary series in the arc spectrum of manganese, Catalán [4] extended those series and calculated the first ionization potential of manganese as 7.41 electron volts. Catalán said (p. 146) "Whilst the manganese series of ordinary type were under investigation, it was noted that there was a strong tendency for lines of similar character to appear in groups (of 9, 12, or 15 lines) and that such groups included some of the most intense lines in the spectrum". For such a group of related spectral lines, "multiplet" was suggested (p. 147). "The accuracy of the separations, some of them being identical with those of the ordinary series, together with the fact that the lines of each group are of the same character, strongly suggests that the multiplets have a real physical significance. Further evidence for their reality is afforded by the occurrence of similar multiplets in the spectra of other elements" (p. 163). In fact, Catalán's first paper on regularities in the spectrum of manganese reporting triplets and multiplets that reveal terms with five or six levels [4] also reported three multiplets in the spectrum of ionized manganese and three multiplets of the neutral atom of chromium. Even before that paper was printed, a manuscript copy of it inspired Sommerfeld [5] to write on the explanation of complex spectra (manganese, chromium, etc.) according to the method of inner quantum numbers. Almost simultaneously, Back [6] accurately measured the Zeeman effect of 49 lines in the arc- and 12 lines in the spark spectrum of manganese with the object of investigating magnetic term splitting of the complex terms found by Catalán, and Landé [7] provided an explanation of all Zeeman patterns with the aid of magnetic quantum numbers and experimental magnetic splitting factors for different types of spectral terms and multiplicities.

It was then clear that the regularities among 169 lines of Mn I presented by Catalán [4] arose from spectral terms belonging to sextet and octet systems. As a check of Landé's scheme, and an example of the usefulness of Zeeman effect in analyzing complex spectra, Back [6] found from Zeeman data the first multiplet of the quartet system. Since multiplets usually occur in triplicate ($\Delta l=0,\pm 1$), Catalán [8] promptly found two additional quartet multiplets associated with the one described by Back.

In 1926 McLennan and McLay [9] extended the work of Catalán and Back on Mn I by making absorption experiments, finding 14 additional multi-

[1] Institute of Optics, Madrid. Died 11 November 1957. This report has been prepared by the surviving authors to honor their deceased colleague.
[2] National Bureau of Standards, Washington.
[3] Institute of Optics, Madrid.
[4] Figures in brackets indicate the literature references at the end of this paper.

711-046—64——2

plets, providing energy diagrams for quartets, sextets, and octets, and tables of 90 energy levels and 257 classified lines ranging in wavelength from 1874.7 Å to 17607.5 Å. Although terms of doublet multiplicity were sought, none was found at that time. This list of levels and terms, with some additions from Russell [10] and from Catalán [11], and with modernized notation, appeared in a volume of Atomic Energy States published in 1932 by Bacher and Goudsmit [12]; it presented 99 energy levels distributed in 17 quartet, 16 sextet, and 15 octet, terms then recognized for the Mn I spectrum. The following year, T. Dunham, Jr., [13] found ten new quartet and two sextet terms (but never published them), and Meggers [14] detected one quartet and two sextet terms in new observations of near infrared spectra. Aside from the above, fifteen years passed without progress in the analysis of Mn I. A strong incentive to extend this analysis came in 1946 when C. E. Moore began her critical and comprehensive compilation of Atomic Energy Levels as Derived from the Analyses of Optical Spectra.

In 1949 a major advance in the analysis of Mn I was made by Miss Olga Garcia-Riquelme [15] who was assigned the task as a thesis problem by Professor Catalán at the University of Madrid. By assembling all known energy levels of Mn I and by compiling wavelengths and intensities of manganese lines from many spectroscopic papers (by 15 different authors), Garcia-Riquelme succeeded in finding 58 new energy levels and 15 new terms for Mn I, thus producing a total of 30 even terms (85 levels), 30 odd terms (124 levels), plus 21 miscellaneous odd levels beyond the ionization limit. The permitted transitions between these levels accounted for 711 observed lines ranging in wavelength from 1876.48 A to 17607.5 Å. All the established spectral terms of Mn I were assigned to quartet, sextet, and octet systems; doublet terms were still unrecognized.

In order to complete the bibliography on description and interpretation of Mn I spectra during the period 1931 to 1949, we mention a paper by Slevogt [16] and one by Paul [17]. The former quotes earlier data on 233 lines (between 6024.67 and 8933.03 A) and remeasured the wavelengths of 113 of these; the latter reported observations on 57 Mn I lines with wavelengths between 1923.05 Å and 1085.01 Å absorbed by manganese vapor. Paul explained 10 of these as transitions from the ground state to highly excited levels, but only three of these have been confirmed in this analysis of Mn I.

In 1948 Catalán decided that an improved description of the Mn I spectrum (including reliable wavelengths, realistic relative intensities for several thousand lines, and Zeeman data for hundreds of lines) was prerequisite to a more complete and satisfactory term analysis of this spectrum.

2. Experiments

To improve the data of Mn I Catalán spent most of 1948 in the United States, where he recorded the vacuum ultraviolet arc spectrum of manganese at Princeton University, and photographed the arc spectrum throughout the visible and adjacent ultraviolet at the National Bureau of Standards.

The vacuum ultraviolet arc and spark spectra of manganese were photographed with a two-m radius grating at Princeton University through the courtesy of Allen G. Shenstone who previously described [18] the apparatus and procedure. The manganese spectra were recorded in this vacuum spectrograph from 1460 Å to 2180 Å with a scale of 4.8 Å per mm, and all these spectrograms were measured and converted to wavelengths by Catalán.

In 1933, Meggers photographed and measured an ultraviolet range (2100 Å to 2800 Å) of manganese spectra with the largest quartz Littrow spectrograph constructed by Adam Hilger, Ltd., of London. Provided with a quartz lens of three-m focal length and Cornu prisms of 60-cm total base, this spectrograph produced reciprocal dispersions of 0.4 to 1.0 Å/mm at the above-mentioned wavelengths. These results were presented to Catalán in 1948 in addition to several dozen new lines between 10500 Å and 12000 Å recorded by Meggers on Eastman 1–Z photographic plates to extend his earlier observations [14] made with Eastman 1–Q plates.

In 1948 Meggers and Catalán reobserved the arc and spark spectra of manganese between 2200 Å and 7800 Å with the aid of a concave grating supplied by R. W. Wood [19]. In a Wadsworth-type mounting, this grating of 30,000 lines per inch on aluminized pyrex glass with 22 feet radius of curvature provided ghost-free spectra with reciprocal dispersions of 1.7 to 2.4 Å per mm in the first order. The second order spectra with double dispersion were photographed between 2500 Å and 4500 Å. All these spectrograms were measured relative to international standards of wavelength provided by the iron arc, and improved wavelengths and estimated intensities of more than 2000 lines characteristic of Mn I were thus obtained in 1949. Excepting several hundred wavelengths since reported in papers on the Zeeman effect, none of these new data has been published heretofore. To complete this description of the Mn I spectra, we (like others) have quoted 16 infrared wavelengths (12900 Å to 17608 Å) emitted by arcs of 60 to 80 amperes and detected with a thermopile in 1919 by Randall and Barker [20].

This improved description of the Mn I spectrum promptly led to the detection of doublet terms and extension of other multiplicities, so that by 1952 as compared with 1949, the total number of even levels had increased to 118 from 87, the number of odd levels to 217 from 124, and the number of classified lines to 1500 from 711. This improvement in the term analysis of Mn I, including g (magnetic splitting) factors for 108 levels, was summarized in 1952 by Charlotte E. Moore [21].

Although Back [6] in 1923 clearly demonstrated the great value of Zeeman effect in spectral term analyses, a quarter of a century elapsed before fur-

ther determinations of inner quantum numbers and magnetic splitting factors were undertaken for Mn I.

Through the courtesy of George R. Harrison, Catalán was invited, in 1949, to photograph the Zeeman effect in manganese spectra with the Bitter magnet and large concave gratings previously described by Harrison and Bitter [22]. The electrodes were prepared with pure manganese powder mixed with pure silver powder, then pressed and sintered to form solid rods about 3 mm square. These electrodes were ignited in a d-c arc operated in a magnet producing a field of 85,000 oersteds, and the spectra were photographed between 2300 Å and 6500 Å. These spectrograms were measured and computed partly at the National Bureau of Standards in Washington and partly at the Institute of Optics in Madrid.

In those experiments, the magnetic field intensity was determined from the splitting of the resonance lines (3280.7 and 3382.9 Å) of the silver matrix, and/or from the resonance lines (3933.7 Å and 3968.5 Å) of ionized calcium, present as an impurity, assuming that the Zeeman patterns of those lines agree exactly with the Landé predictions [7]. Then all displacements of Zeeman components and magnetic splitting factors were expressed in Lorentz units (the unit displacement characterizing all singlet levels). As a result of these experiments, Zeeman data have been obtained for 440 lines of Mn I, ranging from 2461.0 Å to 6021.8 A, thus providing material for several reports extending over a decade.

The observations of normal Zeeman splitting in Mn I by Back [6] in 1923 were made in magnetic fields of 37,000 oersteds, whereas the Zeeman-effect spectrograms obtained by Catalán in 1949 recorded magnetic splitting in fields of 85,000 oersteds. Catalán and Velasco [23] observed changes in g-values of Mn I with magnetic fields above 80,000 oersteds which distort some Zeeman patterns. These distortions in the case of $z\,^6F^\circ_{0\frac{1}{2}}$ and $z\,^6F^\circ_{1\frac{1}{2}}$ levels were ascribed to repulsions between magnetic levels with equal M-values, belonging to adjacent levels of a spectral term, and it was shown that the theory of partial Paschen-Back effects provides a simple rule for obtaining correct g-values in spite of asymmetries in Zeeman patterns. This was elaborated by Catalán [24] who discussed in detail a dozen distorted patterns and concluded that the experimental g-values agreed with those predicted for LS coupling by Landé [7]. Finally, Espinosa [25, 26], in connection with his doctoral thesis, made a complete theoretical interpretation of the very complex Paschen-Back patterns of the $z\,^6P^\circ - e\,^6D$ and $a\,^6S - z\,^6P^\circ$ multiplets of Mn I.

The major contributions to g-factors for Mn I levels have been published in two papers separated by nine years. The first, by Catalán and Garcia-Riquelme [27], reported measurements of Zeeman patterns for 128 lines ranging in wavelength from 2794.817 Å to 4823.528 Å, and derived g-factors for 93 levels, the latter ranging in value from 0 to 67752.84 K. The second, by Riquelme et al. [28], presented measurements and interpretations of the Zeeman patterns of 314 lines (2573 Å to 6022 Å), including derived g-values for 105 energy levels. The data for 251 lines were totally interpreted, whereas 63 lines showing some Paschen-Back effect were partially interpreted as confirming the spectral classification. In addition to the above, Garcia-Riquelme [29] has compiled and exploited inferior Zeeman data for about 100 lines of Mn I, most of which appeared as pseudo doublets, triplets, or quartets because they were incompletely observed or resolved. In most cases, the Landé type of Zeeman pattern could be recognized and for classified lines the observed Zeeman effect confirms the classification quantitatively. Because most of the Zeeman data for Mn I have been published elsewhere [23, 24, 25, 26, 27, 28] they will not be repeated here; only the type numbers [32, 34] will be listed in our list of classified lines, and the average derived g-values in our table of spectral terms.

Following the new observations of wavelengths and intensities of more than 2000 spectral lines belonging to Mn I, and the measurement of Zeeman patterns for nearly 500 lines, Catalán and Garcia-Riquelme undertook a complete revision of the analysis and quantum interpretation of this spectrum. A preview of this overall revision was summarized by Moore [21] in 1952 when 368 energy levels were reported to account for more than 1500 lines. This work continued practically until Catalán's death in 1957, and further progress was made by Garcia-Riquelme until 1962 when the total number of accepted levels rose to 404 and classified lines exceeded 2000. At this point, several hundred unclassified lines, mostly weak, hazy, and without Zeeman data, were sent to the National Bureau of Standards where Meggers applied an electronic computer to a final search for new energy levels by adding the wave numbers of lines to the wave numbers of levels and seeking constant sums within tolerated limits. Among hundreds of "new energy levels", only two were accepted as physically real; they constitute the term $a\,^2I$ with level values of 37148.66 and 37164.25 K. We conclude that the available material on Mn I does not permit further progress in the analysis of this spectrum. This conclusion and the fact that our material is more homogeneous and extensive than any existing description of Mn I justify publication of this paper.

3. Results

Our final results for Mn I classified lines are presented in table 1, in which col. 1 contains the observed wavelength (λ) in angstroms (Å); col. 2, the intensity and character; col. 3, the wave number (σ) in kaysers (K); col. 4, the observed minus calculated wave number in kaysers (K); col. 5, the symbols for associated energy levels; and col. 6, the Zeeman type. Since the "Air" wavelengths were measured before 1950, they were converted to vacuum wave numbers with the aid of Kayser's Table [30] which was recently superseded by a new table published by Coleman, Bozman, and Meggers [31]. Because

TABLE 1. Mn I—*Classified lines*

1	2	3	4	5	6
λ	Int.	σ	o−c	Term designation	Zeeman type
Å		K	K		
Vac					
1785. 355	7*h*	56011. 26	−1. 16	$a\ ^6S_{2½}$—$s\ ^6P^o_{3½}$	
1785. 465	5*h*	56007. 81	−0. 10	$a\ ^6S_{2½}$—$s\ ^6P^o_{2½}$	
1785. 829	6*h*	55996. 40	−0. 22	$a\ ^6S_{2½}$—$s\ ^6P^o_{1½}$	
1788. 152	2*h*	55923. 65	−0. 16	$a\ ^6S_{2½}$—$55923^o_{2½}$	
1875. 727	10*r*	53312. 66	1. 29	$a\ ^6S_{2½}$—$t\ ^6P^o_{1½}$	
1876. 445	15*r*	53292. 26	0. 68	$a\ ^6S_{2½}$—$t\ ^6P^o_{2½}$	
1877. 518	20*r*	53261. 80	0. 38	$a\ ^6S_{2½}$—$t\ ^6P^o_{3½}$	
1882. 366	3	53124. 63	0. 54	$a\ ^6S_{2½}$—$y\ ^4D^o_{3½}$	
1882. 900	1	53109. 56	0. 35	$a\ ^6S_{2½}$—$y\ ^4D^o_{2½}$	
1883. 085	0	53104. 34	1. 15	$a\ ^6S_{2½}$—$y\ ^4D^o_{1½}$	
1890. 962	1	52883. 13	−0. 74	$a\ ^6S_{2½}$—$x\ ^6D^o_{2½,\ 1½}$	
1891. 414	3	52870. 49	0. 39	$a\ ^6S_{2½}$—$x\ ^6D^o_{3½}$	
1913. 752	(15)	52253. 57	0. 33	$a\ ^6S_{2½}$—$u\ ^6P^o_{3½}$	
1918. 328	(15)	52128. 73	0. 08	$a\ ^6S_{2½}$—$u\ ^6P^o_{2½}$	
1922. 516	(12)	52015. 17	0. 17	$a\ ^6S_{2½}$—$u\ ^6P^o_{1½}$	
1949. 100	3	51305. 73	0. 32	$a\ ^6S_{2½}$—$x\ ^4P^o_{2½}$	
1996. 056	50R	50098. 79	−0. 37	$a\ ^6S_{2½}$—$v\ ^6P^o_{1½}$	
1999. 511	100R	50012. 23	−0. 30	$a\ ^6S_{2½}$—$v\ ^6P^o_{2½}$	
Air					
2003. 849	200R	49887. 73	−0. 35	$a\ ^6S_{2½}$—$y\ ^6P^o_{3½}$	
2017. 630	3	49547. 04	−0. 84	$a\ ^6D_{4½}$—$66600^o_{3½}$?	
2018. 332	4	49529. 78	0. 00	$a\ ^6D_{2½}$—$66981^o_{3½}$	
2070. 988	5	48270. 66	−0. 25	$a\ ^6S_{2½}$—$y\ ^6F^o_{2½}$	
2072. 917	12	48225 74	−0. 25	$a\ ^6S_{2½}$—$y\ ^6F^o_{3½}$	
2092. 159	500R	47782. 26	−0. 17	$a\ ^6S_{2½}$—$u\ ^6P^o_{1½}$	
2092. 516	50R	47774. 09	−0. 43	$a\ ^6S_{2½}$—$y\ ^6D^o_{3½}$	
2093. 407	200R	47753. 77	−0. 22	$a\ ^6S_{2½}$—$y\ ^6D^o_{2½}$	
2097. 554	30	47659. 38	−0. 14	$a\ ^6S_{2½}$—$w\ ^6P^o_{2½}$	
2106. 052	100R	47467. 10	0. 44	$a\ ^6S_{2½}$—$y\ ^6D^o_{1½}$	
2109. 585	300R	47387. 60	−0. 02	$a\ ^6S_{2½}$—$w\ ^6P^o_{3½}$	
2173. 195	3*h*	46001. 72	0. 95	$a\ ^6S_{2½}$—$y\ ^8P^o_{3½}$?	
2174. 12	0*h*	45981. 2	−0. 2	$a\ ^6S_{2½}$—$y\ ^8P^o_{2½}$	
2176. 014	2	45941. 14	0. 21	$a\ ^6S_{2½}$—$z\ ^4D^o_{2½}$	
2182. 773	15	45798. 90	−0. 28	$a\ ^6D_{4½}$—$w\ ^6D^o_{3½}$	
2184. 912	10	45754. 07	−0. 20	$a\ ^6S_{2½}$—$z\ ^4D^o_{3½}$	
2190. 884	2	45629. 37	−0. 39	$a\ ^6D_{2½}$—$y\ ^2D^o_{2½}$	
2191. 413	100	45618. 36	−0. 16	$a\ ^6D_{4½}$—$w\ ^6D^o_{4½}$	
2193. 762	20	45569. 51	0. 04	$a\ ^6D_{3½}$—$w\ ^6D^o_{3½}$	
2196. 503	3	45512. 65	−0. 15	$a\ ^6D_{1½}$—$y\ ^2D^o_{2½}$	
2198. 131	10	45478. 94	−0. 39	$a\ ^6D_{3½}$—$w\ ^6D^o_{2½}$	
2199. 41	1*h*	45452. 5	−0. 5	$a\ ^6D_{4½}$—$v\ ^4F^o_{3½}$	
2201. 960	7	45399. 88	−0. 07	$a\ ^6D_{2½}$—$w\ ^6D^o_{3½}$	
2202. 489	2	45388. 97	0. 16	$a\ ^6D_{3½}$—$w\ ^6D^o_{4½}$	
2205. 057	10	45336. 11	0. 00	$a\ ^6D_{2½}$—$w\ ^6D^o_{1½}$	
2206. 343	2	45309. 70	−0. 11	$a\ ^6D_{2½}$—$w\ ^6D^o_{2½}$	
2208. 806	200R	45259. 17	0. 00	$a\ ^6S_{2½}$—$x\ ^6P^o_{1½}$	
2210. 582	8*h*	45222. 81	−0. 48	$a\ ^6D_{3½}$—$v\ ^4F^o_{3½}$	
2211. 720	8	45199. 55	−0. 13	$a\ ^6D_{1½}$—$w\ ^6D^o_{0½}$	
2212. 055	15	45192. 70	−0. 15	$a\ ^6D_{1½}$—$w\ ^6D^o_{2½}$	
2213. 855	300R	45155. 96	−0. 15	$a\ ^6S_{2½}$—$x\ ^6P^o_{2½}$	
2214. 10	10	45150. 4	−0. 1	$a\ ^6D_{0½}$—$w\ ^6D^o_{1½}$	
2215. 086	3	45130. 89	−0. 12	$a\ ^6D_{0½}$—$w\ ^6D^o_{0½}$	
2218. 903	3*h*	45053. 24	−0. 53	$a\ ^6D_{2½}$—$v\ ^4F^o_{3½}$	
2221. 837	500R	44993. 76	−0. 16	$a\ ^6S_{2½}$—$x\ ^6P^o_{3½}$	
2249. 911	5*s*	44432. 39	−0. 13	$a\ ^6D_{3½}$—$y\ ^2G^o_{4½}$	
2258. 714	2	44259. 24	−0. 22	$a\ ^6D_{2½}$—$z\ ^2F^o_{3½}$	

TABLE 1. Mn I—*Classified lines*—Continued

1	2	3	4	5	6
λ	Int.	σ	o−c	Term designation	Zeeman type
Å Air		*K*	*K*		
2262. 294	8*s*	44189. 21	−0. 02	$a\ ^6D_{3½}$—$w\ ^4G^o_{2½}$	
2277. 065	0*h*	43902. 60	−0. 15	$a\ ^6D_{1½}$—$w\ ^4G^o_{2½}$	
2288. 449	20	43684. 22	−0. 41	$a\ ^4D_{3½}$—$66981^o_{3½}$	
2292. 189	30	43612. 95	−0. 40	$a\ ^4D_{3½}$—$66910^o_{2½}$	
2293. 122	2	43595. 21	−0. 29	$a\ ^6S_{2½}$—$z\ ^6F^o_{3½}$	
2296. 880	5	43523. 88	−0. 20	$a\ ^6S_{2½}$—$z\ ^6F^o_{3½}$	
2298. 876	20	43486. 10	−0. 28	$a\ ^4D_{3½}$—$u\ ^4F^o_{3½}$	
2300. 300	8	43459. 18	−0. 16	$a\ ^4D_{2½}$—$67008^o_{2½}$	
2300. 728	3H	43451. 10	−0. 18	$a\ ^6D_{2½}$—$w\ ^4F^o_{3½}$	
2301. 260	1*d*	43441. 07	−0. 08	$a\ ^4D_{3½}$—$v\ ^2G^o_{3½}$	
2301. 748	4	43431. 84	−0. 26	$a\ ^4D_{2½}$—$66981^o_{3½}$	
2305. 518	5	43360. 83	0. 01	$a\ ^4D_{2½}$—$66910^o_{2½}$	
2305. 703	15H	43357. 35	−0. 63	$a\ ^4D_{3½}$—$66654^o_{2½}$	
2309. 057	2*h*	43294. 38	−0. 21	$a\ ^4D_{2½}$—$u\ ^4F^o_{1½}$	
2309. 374	10	43288. 45	0. 01	$a\ ^4D_{2½}$—$u\ ^4F^o_{2½}$	
2312. 304	20	43233. 59	−0. 26	$a\ ^4D_{2½}$—$u\ ^4F^o_{3½}$	
2318. 17	1*h*	43124. 2	−0. 1	$a\ ^4D_{1½}$—$u\ ^4F^o_{1½}$	
2318. 501	2*h*	43118. 04	−0. 08	$a\ ^4D_{1½}$—$u\ ^4F^o_{2½}$	
2321. 995	10*h*	43053. 16	0. 00	$a\ ^4G_{4½}$—$u\ ^2G^o_{3½}$	
2322. 106	3*h*	43051. 11	0. 26 0. 14	$a\ ^4G_{3½}$—$u\ ^2G^o_{3½}$ $a\ ^4D_{2½}$—$66600^o_{3½}$	
2323. 748	30*h*	43020. 70	0. 00	$a\ ^4G_{5½}$—$u\ ^2G^o_{4½}$	
2324. 803	5*h*	43001. 17	0. 16	$a\ ^4G_{4½}$—$u\ ^2G^o_{4½}$	
2327. 308	2H	42954. 89	−0. 12	$a\ ^4D_{2½}$—$66504^o_{1½}$	
2342. 088	3H	42683. 85	0. 02	$a\ ^4G_{2½}$—$t\ ^4G^o_{2½}$	
2342. 771	1H	42676. 87	−0. 26	$a\ ^4G_{3½}$—$t\ ^4G^o_{2½}$	
2346. 126	1H	42610. 38	0. 06	$a\ ^4G_{2½}$—$t\ ^4G^o_{3½}$	
2346. 383	2*h*	42605. 72	−0. 21	$a\ ^4G_{4½}$—$t\ ^4G^o_{3½}$	
2346. 497	5*h*	42603. 65	0. 03	$a\ ^4G_{3½}$—$t\ ^4G^o_{3½}$	
2349. 263	3*h*	42553. 50	0. 07	$a\ ^4G_{3½}$—$t\ ^4G^o_{4½}$	
2350. 352	10*h*	42533. 78	0. 04	$a\ ^4G_{4½}$—$t\ ^4G^o_{4½}$	
2352. 937	20*h*	42487. 05	−0. 05	$a\ ^4G_{5½}$—$t\ ^4G^o_{5½}$	
2354. 020	4*h*	42467. 51	0. 10	$a\ ^4G_{4½}$—$t\ ^4G^o_{5½}$	
2357. 899	2*h*	42397. 65	−0. 02	$a\ ^4D_{2½}$—$w\ ^2D^o_{2½}$	
2362. 719	1	42311. 17	0. 07	$a\ ^4G_{3½}$—$w\ ^2H^o_{4½}$	
2363. 823	4	42291. 41	0. 00	$a\ ^4G_{4½}$—$w\ ^2H^o_{4½}$	
2363. 956	1	42289. 03	−0. 07	$a\ ^4G_{3½}$—$w\ ^2H^o_{4½}$	
2366. 575	1	42242. 24	−0. 14	$a\ ^4D_{1½}$—$w\ ^2D^o_{1½}$	
2366. 744	5	42239. 22	0. 06	$a\ ^4G_{5½}$—$w\ ^2H^o_{5½}$	
2367. 851	1	42219. 47	0. 00	$a\ ^4G_{5½}$—$w\ ^2H^o_{5½}$	
2372. 116	10*d*	42143. 56	−0. 01	$a\ ^6S_{2½}$—$z\ ^6D^o_{1½}$	
2377. 183	30R	42053. 75	0. 02	$a\ ^6S_{2½}$—$z\ ^6D^o_{2½}$	
2382. 175	2	41965. 63	0. 02	$a\ ^4D_{3½}$—$w\ ^2G^o_{4½}$	
2384. 049	40R	41932. 65	0. 01	$a\ ^6S_{2½}$—$z\ ^6D^o_{3½}$	
2397. 732	2	41693. 37	−0. 19	$a\ ^4G_{3½}$—$66981^o_{3½}$	
2401. 830	2	41622. 24	−0. 04	$a\ ^4G_{3½}$—$66910^o_{2½}$	
2403. 748	2	41589. 03	−0. 23	$a\ ^4G_{3½}$—$u\ ^4F^o_{4½}$	
2404. 882	5	41569. 42	−0. 15	$a\ ^4G_{4½}$—$u\ ^4F^o_{4½}$	
2405. 274	3	41562. 65	−0. 10	$a\ ^4G_{2½}$—$u\ ^4F^o_{1½}$	
2405. 628	2*h*	41556. 53	−0. 07	$a\ ^4G_{2½}$—$u\ ^4F^o_{2½}$	
2406. 017	2	41549. 82	−0. 08	$a\ ^4G_{3½}$—$u\ ^4F^o_{2½}$	
2409. 198	2	41494. 96	−0. 35	$a\ ^4G_{3½}$—$u\ ^4F^o_{3½}$	
2411. 415	2	41456. 81	0. 03	$a\ ^4G_{2½}$—$v\ ^2G^o_{3½}$	
2417. 502	2	41352. 44	−0. 09	$a\ ^4D_{3½}$—$x\ ^2G^o_{3½}$	
2417. 909	2	41345. 48	−0. 01	$a\ ^4G_{4½}$—$v\ ^2G^o_{4½}$	
2418. 042	4	41343. 20	0. 02	$a\ ^4G_{3½}$—$v\ ^2G^o_{4½}$	

TABLE 1. Mn I—*Classified lines*—Continued

1	2	3	4	5	6
λ	Int.	σ	o−c	Term designation	Zeeman type
Å Air		K	K		
2420.110	30	41307.88	0.02	$a\ ^4G_{3\frac{1}{2}}$—$u\ ^4G^\circ_{5\frac{1}{2}}$	
2420.403	30	41302.88	0.04	$a\ ^4G_{3\frac{1}{2}}$—$u\ ^4H^\circ_{6\frac{1}{2}}$	
2421.254	20*d*	41288.38	0.21	$a\ ^4G_{4\frac{1}{2}}$—$u\ ^4G^\circ_{5\frac{1}{2}}$	
			−0.39	$a\ ^4D_{3\frac{1}{2}}$—$x\ ^2G^\circ_{4\frac{1}{2}}$	
2423.099	6	41256.93	0.05	$a\ ^4G_{3\frac{1}{2}}$—$u\ ^4G^\circ_{4\frac{1}{2}}$	
2424.260	30	41237.17	−0.02	$a\ ^4G_{4\frac{1}{2}}$—$u\ ^4G^\circ_{4\frac{1}{2}}$	
2424.385	1	41235.04	0.16	$a\ ^4G_{2\frac{1}{2}}$—$u\ ^4G^\circ_{4\frac{1}{2}}$	
2428.286	8	41168.81	−0.03	$a\ ^4G_{4\frac{1}{2}}$—$u\ ^4G^\circ_{3\frac{1}{2}}$	
2428.423	25	41166.49	−0.04	$a\ ^4G_{3\frac{1}{2}}$—$u\ ^4G^\circ_{3\frac{1}{2}}$	
2428.586	2*h*	41163.72	−0.02	$a\ ^4D_{2\frac{1}{2}}$—$u\ ^4D^\circ_{2\frac{1}{2}}$	
2429.233	30	41152.76	−0.05	$a\ ^4G_{3\frac{1}{2}}$—$u\ ^4H^\circ_{5\frac{1}{2}}$	
2430.395	35	41133.08	−0.04	$a\ ^4G_{4\frac{1}{2}}$—$u\ ^4H^\circ_{5\frac{1}{2}}$	
2431.520	40	41114.06	−0.09	$a\ ^4G_{2\frac{1}{2}}$—$u\ ^4G^\circ_{2\frac{1}{2}}$	
2431.587	4*h*	41112.92	−0.10	$a\ ^4D_{3\frac{1}{2}}$—$u\ ^4D^\circ_{3\frac{1}{2}}$	
2431.915	10	41107.38	−0.07	$a\ ^4G_{3\frac{1}{2}}$—$u\ ^4G^\circ_{3\frac{1}{2}}$	
2432.360	8	41099.86	−0.14	$a\ ^4D_{2\frac{1}{2}}$—$x\ ^2G^\circ_{3\frac{1}{2}}$	
2432.898	7	41090.77	0.11	$a\ ^4G_{3\frac{1}{2}}$—$u\ ^4H^\circ_{4\frac{1}{2}}$	
2434.071	30	41070.97	0.00	$a\ ^4G_{4\frac{1}{2}}$—$u\ ^4H^\circ_{5\frac{1}{2}}$	
2434.208	35	41068.65	−0.01	$a\ ^4G_{3\frac{1}{2}}$—$u\ ^4H^\circ_{4\frac{1}{2}}$	
2435.137	40	41053.00	−0.43	$a\ ^4G_{2\frac{1}{2}}$—$u\ ^4H^\circ_{3\frac{1}{2}}$	
2435.376	5	41048.96	−0.08	$a\ ^4G_{4\frac{1}{2}}$—$u\ ^4H^\circ_{3\frac{1}{2}}$	
2435.511	20	41046.69	−0.04	$a\ ^4G_{3\frac{1}{2}}$—$u\ ^4H^\circ_{3\frac{1}{2}}$	
2440.415	2	40964.19	−0.24	$a\ ^4D_{1\frac{1}{2}}$—$u\ ^4D^\circ_{2\frac{1}{2}}$	
2446.159	1	40868.03	−0.03	$a\ ^4G_{2\frac{1}{2}}$—$u\ ^2F^\circ_{3\frac{1}{2}}$	
2446.561	2	40861.31	−0.05	$a\ ^4G_{3\frac{1}{2}}$—$u\ ^2F^\circ_{3\frac{1}{2}}$	
2446.610	2	40860.49	0.00	$a\ ^4D_{2\frac{1}{2}}$—$u\ ^4D^\circ_{3\frac{1}{2}}$	
2449.047	2	40819.83	0.02	$a\ ^4D_{0\frac{1}{2}}$—$u\ ^4D^\circ_{0\frac{1}{2}}$	
2453.870	6	40739.62	0.03	$a\ ^4G_{2\frac{1}{2}}$—$u\ ^2F^\circ_{2\frac{1}{2}}$	
2454.262	3	40733.11	0.22	$a\ ^4G_{3\frac{1}{2}}$—$u\ ^2F^\circ_{2\frac{1}{2}}$	
2456.878	3*h*	40689.74	−0.08	$a\ ^4P_{2\frac{1}{2}}$—$t\ ^4G^\circ_{3\frac{1}{2}}$	
2458.312	2	40666.01	0.18	$a\ ^4G_{2\frac{1}{2}}$—$w\ ^2D^\circ_{2\frac{1}{2}}$	
2459.694	50	40643.16	−0.02	$a\ ^4G_{3\frac{1}{2}}$—$v\ ^4G^\circ_{4\frac{1}{2}}$	
2460.887	40	40623.46	−0.03	$a\ ^4G_{4\frac{1}{2}}$—$v\ ^4G^\circ_{4\frac{1}{2}}$	
2461.011	50	40621.41	−0.16	$a\ ^4G_{3\frac{1}{2}}$—$v\ ^4G^\circ_{5\frac{1}{2}}$	6, 7*b*
2462.190	7	40601.96	0.08	$a\ ^4G_{4\frac{1}{2}}$—$v\ ^4G^\circ_{5\frac{1}{2}}$	
2462.596	3	40595.27	−0.03	$a\ ^4G_{2\frac{1}{2}}$—$v\ ^4G^\circ_{3\frac{1}{2}}$	
2462.776	20	40592.31	−0.05	$a\ ^4G_{2\frac{1}{2}}$—$v\ ^4G^\circ_{2\frac{1}{2}}$	
2462.863	5	40590.88	−0.03	$a\ ^4G_{4\frac{1}{2}}$—$v\ ^4G^\circ_{3\frac{1}{2}}$	
2463.005	40	40588.53	−0.07	$a\ ^4G_{3\frac{1}{2}}$—$v\ ^4G^\circ_{3\frac{1}{2}}$	
2463.182	6	40585.61	−0.05	$a\ ^4G_{2\frac{1}{2}}$—$v\ ^4G^\circ_{2\frac{1}{2}}$	
2468.207	2	40502.99	−0.08	$a\ ^4G_{5\frac{1}{2}}$—65768$^\circ_{4\frac{1}{2}}$	
2469.407	40	40483.31	−0.07	$a\ ^4G_{4\frac{1}{2}}$—65768$^\circ_{4\frac{1}{2}}$	
2470.330	4	40468.19	−0.04	$a\ ^4D_{3\frac{1}{2}}$—$x\ ^2D^\circ_{2\frac{1}{2}}$	
2478.803	2*h*	40329.87	0.24	$a\ ^4G_{3\frac{1}{2}}$—$v\ ^2F^\circ_{3\frac{1}{2}}$	
2481.431	1	40287.16	−0.01	$a\ ^4D_{3\frac{1}{2}}$—63583$^\circ_{2\frac{1}{2}}$	
2483.743	8	40249.66	0.03	$a\ ^4D_{3\frac{1}{2}}$—63546$^\circ_{3\frac{1}{2}}$	
2485.114	10*hw*	40227.46	0.31	$a\ ^4D_{3\frac{1}{2}}$—63523$^\circ_{2\frac{1}{2}}$	
2485.842	5*h*	40215.68	−0.02	$a\ ^4D_{2\frac{1}{2}}$—$x\ ^2D^\circ_{2\frac{1}{2}}$	
2491.414	2	40125.75	−0.05	$a\ ^4D_{1\frac{1}{2}}$—$x\ ^2D^\circ_{1\frac{1}{2}}$	
2494.391	20	40077.86	0.00	$a\ ^4D_{3\frac{1}{2}}$—63374$^\circ_{4\frac{1}{2}}$	
2494.585	5	40074.74	−0.15	$a\ ^4D_{3\frac{1}{2}}$—63371$^\circ_{2\frac{1}{2}}$	
2496.048	7	40051.25	0.01	$a\ ^4D_{3\frac{1}{2}}$—$y\ ^2H^\circ_{4\frac{1}{2}}$	
2496.415	3	40045.37	−0.01	$a\ ^4D_{1\frac{1}{2}}$—$x\ ^2D^\circ_{2\frac{1}{2}}$	
2497.084	4	40034.64	0.00	$a\ ^4D_{2\frac{1}{2}}$—63583$^\circ_{2\frac{1}{2},1\frac{1}{2}}$	
2497.597	4	40026.42	−0.03	$a\ ^4D_{0\frac{1}{2}}$—$x\ ^2D^\circ_{1\frac{1}{2}}$	
2497.725	15	40024.37	0.28	$a\ ^4G_{2\frac{1}{2}}$—$w\ ^2G^\circ_{3\frac{1}{2}}$	

TABLE 1. Mn I—*Classified lines*—Continued

	2	3	4	5	6
λ	Int.	σ	o−c	Term designation	Zeeman type
Å Air		*K*	*K*		
2499.429	8	39997.08	−0.02	$a\ ^4D_{2\frac{1}{2}}$—$63546^{\circ}_{3\frac{1}{2}}$	
2500.692	4	39976.88	0.03	$a\ ^4G_{4\frac{1}{2}}$—$w\ ^2G^{\circ}_{4\frac{1}{2}}$	
2500.840	2	39974.52	−0.02 −0.10	$a\ ^4G_{3\frac{1}{2}}$—$w\ ^2G^{\circ}_{4\frac{1}{2}}$ $a\ ^4D_{2\frac{1}{2}}$—$63523^{\circ}_{2\frac{1}{2}}$	
2507.756	2*h*	39864.28	−0.04	$a\ ^4D_{1\frac{1}{2}}$—$63583^{\circ}_{2\frac{1}{2},1\frac{1}{2}}$	
2511.351	2	39807.21	0.21	$a\ ^4P_{2\frac{1}{2}}$—$67008^{\circ}_{2\frac{1}{2}}$	
2511.538	4*h*	39804.26	−0.04	$a\ ^4D_{1\frac{1}{2}}$—$63523^{\circ}_{2\frac{1}{2}}$	
2513.086	1	39779.74	−0.02	$a\ ^4P_{2\frac{1}{2}}$—$66981^{\circ}_{3\frac{1}{2}}$	
2514.314	40	39760.31	−0.23	$a\ ^4P_{1\frac{1}{2}}$—$67008^{\circ}_{2\frac{1}{2}}$	
2517.580	2	39708.74	0.26	$a\ ^4P_{2\frac{1}{2}}$—$66910^{\circ}_{2\frac{1}{2}}$	
2517.677	1	39707.21	0.03	$a\ ^4G_{2\frac{1}{2}}$—$w\ ^2F^{\circ}_{3\frac{1}{2}}$	
2517.960	1	39702.75	−0.04	$a\ ^4G_{4\frac{1}{2}}$—$w\ ^2F^{\circ}_{3\frac{1}{2}}$	
2521.986	7	39639.37	0.08	$a\ ^4G_{2\frac{1}{2}}$—$v\ ^4H^{\circ}_{3\frac{1}{2}}$	
2522.185	2	39636.25	0.15	$a\ ^4P_{2\frac{1}{2}}$—$u\ ^4F^{\circ}_{2\frac{1}{2}}$	
2522.274	4	39634.84	−0.06	$a\ ^4G_{4\frac{1}{2}}$—$v\ ^4H^{\circ}_{3\frac{1}{2}}$	
2524.472	10	39600.34	0.08	$a\ ^4G_{3\frac{1}{2}}$—$v\ ^4H^{\circ}_{4\frac{1}{2}}$	
2525.669	8	39581.57	0.06	$a\ ^4P_{2\frac{1}{2}}$—$u\ ^4F^{\circ}_{3\frac{1}{2}}$	
2528.184	2	39542.20	0.03	$a\ ^4G_{2\frac{1}{2}}$—$w\ ^2F^{\circ}_{3\frac{1}{2}}$	
2528.700	8	39534.13	0.03	$a\ ^4G_{4\frac{1}{2}}$—$v\ ^4H^{\circ}_{5\frac{1}{2}}$	
2533.050	20	39466.24	0.10	$a\ ^4G_{3\frac{1}{2}}$—$v\ ^4H^{\circ}_{4\frac{1}{2}}$	
2533.896	2*h*	39453.07	−0.04	$a\ ^4P_{2\frac{1}{2}}$—$66654^{\circ}_{2\frac{1}{2}}$	
2536.878	5H	39406.69	0.04	$a\ ^4P_{1\frac{1}{2}}$—$66654^{\circ}_{2\frac{1}{2}}$	
2539.642	9	39363.81	0.04	$a\ ^4G_{4\frac{1}{2}}$—$x\ ^2G^{\circ}_{5\frac{1}{2}}$	
2539.792	5	39361.48	0.02	$a\ ^4G_{3\frac{1}{2}}$—$x\ ^2G^{\circ}_{4\frac{1}{2}}$	
2542.491	10	39319.70	0.00	$a\ ^4G_{3\frac{1}{2}}$—$x\ ^2G^{\circ}_{4\frac{1}{2}}$	
2543.593	2*h*	39302.67	0.00	$a\ ^4P_{2\frac{1}{2}}$—$66504^{\circ}_{1\frac{1}{2}}$	
2543.763	4	39300.04	0.03	$a\ ^4G_{4\frac{1}{2}}$—$x\ ^2G^{\circ}_{4\frac{1}{2}}$	
2546.582	4*h*	39256.54	0.33	$a\ ^4P_{1\frac{1}{2}}$—$66504^{\circ}_{1\frac{1}{2}}$	
2548.80	3H	39222.4	0.0	$a\ ^4P_{0\frac{1}{2}}$—$66504^{\circ}_{1\frac{1}{2}}$	
2557.040	3	39096.00	−0.15	$a\ ^4D_{3\frac{1}{2}}$—$v\ ^4F^{\circ}_{4\frac{1}{2}}$	
2565.952	4*h*	38960.22	0.09	$a\ ^6D_{4\frac{1}{2}}$—$s\ ^6P^{\circ}_{3\frac{1}{2}}$	
2566.230	1*h*	38956.00	−0.09	$a\ ^4D_{2\frac{1}{2}}$—$v\ ^4F^{\circ}_{3\frac{1}{2}}$	
2566.783	2	38947.61	0.05	$a\ ^4P_{2\frac{1}{2}}$—$u\ ^2F^{\circ}_{3\frac{1}{2}}$	
2567.40	1H	38938.3	0.1	$a\ ^4D_{2\frac{1}{2}}$—$v\ ^4F^{\circ}_{3\frac{1}{2}}$	
2572.755	50R	38857.20	−0.06	$z\ ^8P^{\circ}_{3\frac{1}{2}}$—$e\ ^8P_{4\frac{1}{2}}$	
2575.509	20R	38815.66	−0.03	$z\ ^8P^{\circ}_{2\frac{1}{2}}$—$e\ ^8P_{3\frac{1}{2}}$	
2577.470	6	38786.13	−0.04	$a\ ^4G_{5\frac{1}{2}}$—$x\ ^2H^{\circ}_{5\frac{1}{2}}$	
2578.358	2	38772.77	0.14	$a\ ^4P_{1\frac{1}{2}}$—$u\ ^2F^{\circ}_{2\frac{1}{2}}$	
2578.548	2	38769.92	−0.02	$a\ ^4G_{4\frac{1}{2}}$—$x\ ^2H^{\circ}_{4\frac{1}{2}}$	
2578.695	2*h*	38767.71	−0.13	$a\ ^4D_{1\frac{1}{2}}$—$v\ ^4F^{\circ}_{2\frac{1}{2}}$	
2579.18	1	38760.4	0.0	$a\ ^4P_{2\frac{1}{2}}$—$w\ ^2D^{\circ}_{1\frac{1}{2}}$	
2580.180	3	38745.40	0.07	$a\ ^4P_{2\frac{1}{2}}$—$w\ ^2D^{\circ}_{2\frac{1}{2}}$	
2581.183	2*h*	38730.34	−0.08	$a\ ^6D_{3\frac{1}{2}}$—$s\ ^6P^{\circ}_{3\frac{1}{2}}$	
2581.478	3*h*	38725.91	0.00	$a\ ^6D_{3\frac{1}{2}}$—$s\ ^6P^{\circ}_{2\frac{1}{2}}$	
2582.270	5	38714.04	0.14	$a\ ^4P_{1\frac{1}{2}}$—$w\ ^2D^{\circ}_{1\frac{1}{2}}$	
2583.275	7	38698.98	0.11	$a\ ^4P_{1\frac{1}{2}}$—$w\ ^2D^{\circ}_{2\frac{1}{2}}$	
2584.100	10	38686.62	0.11	$z\ ^8P^{\circ}_{3\frac{1}{2}}$—$e\ ^8P_{3\frac{1}{2}}$	
2584.302	100R	38683.60	−0.27 0.07	$z\ ^8P^{\circ}_{2\frac{1}{2}}$—$e\ ^8P_{2\frac{1}{2}}$ $z\ ^8P^{\circ}_{4\frac{1}{2}}$—$e\ ^8P_{4\frac{1}{2}}$	7*b*
2584.540	2	38680.04	−0.01	$a\ ^4P_{0\frac{1}{2}}$—$w\ ^2D^{\circ}_{1\frac{1}{2}}$	
2587.100	1*h*	38641.77	−0.04	$a\ ^6D_{3\frac{1}{2}}$—$55923^{\circ}_{2\frac{1}{2}}$	
2592.298	6	38564.29	0.01	$a\ ^4G_{2\frac{1}{2}}$—$x\ ^2D^{\circ}_{1\frac{1}{2}}$	
2592.944	60R	38554.68	−0.01	$z\ ^8P^{\circ}_{3\frac{1}{2}}$—$e\ ^8P_{2\frac{1}{2}}$	4
2595.763	80R	38512.81	0.03	$z\ ^8P^{\circ}_{4\frac{1}{2}}$—$e\ ^8P_{3\frac{1}{2}}$	
2597.722	2	38483.77	−0.09	$a\ ^4G_{2\frac{1}{2}}$—$x\ ^2D^{\circ}_{2\frac{1}{2}}$	
2598.172	6	38477.11	−0.05	$a\ ^4G_{3\frac{1}{2}}$—$x\ ^2D^{\circ}_{2\frac{1}{2}}$	
2600.220	8H*w*	38446.80	0.00	$a\ ^6D_{4\frac{1}{2}}$—$y\ ^8F^{\circ}_{3\frac{1}{2}}$	

TABLE 1. Mn I—*Classified lines*—Continued

1	2	3	4	5	6
λ	Int.	σ	o−c	Term designation	Zeeman type
Å Air		K	K		
2600.650	6Hw	38440.45	0.00	$a\ ^6D_{4\frac{1}{2}}$—$v\ ^6F^\circ_{5\frac{1}{2}}$	
2601.486	2	38428.09	−0.05	$a\ ^6D_{1\frac{1}{2}}$—$s\ ^6P^\circ_{1\frac{1}{2}}$	
2603.487	1Hw	38398.57	−0.3	$z\ ^8P^\circ_{2\frac{1}{2}}$—$h\ ^8D$	
2606.137	1H	38359.52	0.05	$a\ ^6D_{0\frac{1}{2}}$—$s\ ^6P^\circ_{1\frac{1}{2}}$	
2612.233	5Hw	38270.01	0.2	$z\ ^8P^\circ_{3\frac{1}{2}}$—$h\ ^8D$	
2612.860	20	38260.83	0.08	$a\ ^4G_{3\frac{1}{2}}$—$z\ ^2H^\circ_{4\frac{1}{2}}$	
2613.006	1	38258.69	0.13	$a\ ^4G_{3\frac{1}{2}}$—63546$^\circ_{3\frac{1}{2}}$	
2614.550	3	38236.10	0.02	$a\ ^4G_{3\frac{1}{2}}$—63523$^\circ_{2\frac{1}{2}}$	
2615.850	5Hw	38217.10	0.01	$a\ ^6D_{3\frac{1}{2}}$—$y\ ^8F^\circ_{4\frac{1}{2}}$	
2616.300	4Hw	38210.52	0.00	$a\ ^6D_{3\frac{1}{2}}$—$v\ ^6F^\circ_{4\frac{1}{2}}$	
2617.564	1	38192.07	−0.04	$a\ ^4G_{3\frac{1}{2}}$—$w\ ^4H^\circ_{3\frac{1}{2}}$	
2618.470	4	38178.86	−0.01	$a\ ^4G_{5\frac{1}{2}}$—$w\ ^4H^\circ_{4\frac{1}{2}}$	
2618.911	20	38172.43	0.01	$a\ ^4G_{4\frac{1}{2}}$—$w\ ^4H^\circ_{3\frac{1}{2}}$	
2619.510	25	38163.70	0.00	$a\ ^4G_{4\frac{1}{2}}$—$y\ ^2H^\circ_{3\frac{1}{2}}$	
2619.819	5	38159.20	0.02	$a\ ^4G_{4\frac{1}{2}}$—$w\ ^4H^\circ_{4\frac{1}{2}}$	
2619.980	10	38156.86	−0.01	$a\ ^4G_{3\frac{1}{2}}$—$w\ ^4H^\circ_{4\frac{1}{2}}$	
2622.895	25	38114.45	0.04	$a\ ^4G_{2\frac{1}{2}}$—$w\ ^4H^\circ_{3\frac{1}{2}}$	
2623.284	8	38108.80	0.01	$a\ ^4G_{5\frac{1}{2}}$—63374$^\circ_{4\frac{1}{2}}$	
2623.362	5	38107.67	−0.04	$a\ ^4G_{3\frac{1}{2}}$—$w\ ^4H^\circ_{3\frac{1}{2}}$	
2624.043	50	38097.78	−0.02	$a\ ^4G_{5\frac{1}{2}}$—$w\ ^4H^\circ_{6\frac{1}{2}}$	4
2624.466	1Hw	38096.2	0.2	$z\ ^8P^\circ_{4\frac{1}{2}}$—$h\ ^8D$	
2624.642	2	38089.08	−0.02	$a\ ^4G_{4\frac{1}{2}}$—63374$^\circ_{4\frac{1}{2}}$	
2624.800	10	38086.79	0.00	$a\ ^4G_{3\frac{1}{2}}$—63374$^\circ_{4\frac{1}{2}}$	
2625.120	3	38082.15	−0.02	$a\ ^4G_{5\frac{1}{2}}$—$y\ ^2H^\circ_{4\frac{1}{2}}$	
2626.635	20	38060.19	0.02	$a\ ^4G_{3\frac{1}{2}}$—$y\ ^2H^\circ_{3\frac{1}{2}}$	
2627.48	1Hw	38048.0	0.0	$a\ ^6D_{2\frac{1}{2}}$—$y\ ^8F^\circ_{3\frac{1}{2}}$	
2627.990	2Hw	38040.56	0.00	$a\ ^6D_{2\frac{1}{2}}$—$v\ ^6F^\circ_{3\frac{1}{2}}$	
2628.100		38038.97	0.16	$a\ ^4G_{2\frac{1}{2}}$—63319$^\circ_{3\frac{1}{2}}$	
2630.260	8	38007.74	0.00	$a\ ^4G_{2\frac{1}{2}}$—$x\ ^2F^\circ_{3\frac{1}{2}}$	
2630.565	25	38003.33	−0.02	$a\ ^4G_{4\frac{1}{2}}$—$z\ ^2H^\circ_{5\frac{1}{2}}$	
2630.721	2	38001.08	0.04	$a\ ^4G_{3\frac{1}{2}}$—$x\ ^2F^\circ_{3\frac{1}{2}}$	
2635.551	4Hw	37931.42	0.00	$a\ ^6D_{1\frac{1}{2}}$—$y\ ^8F^\circ_{2\frac{1}{2}}$	
2636.131	2Hw	37923.09	0.00	$a\ ^6D_{1\frac{1}{2}}$—$v\ ^6F^\circ_{2\frac{1}{2}}$	
2640.340	1Hw	37862.6	0.0	$a\ ^6D_{0\frac{1}{2}}$—$y\ ^8F^\circ_{1\frac{1}{2}}$	
2640.619	4	37858.64	−0.02	$a\ ^4G_{2\frac{1}{2}}$—$x\ ^2F^\circ_{2\frac{1}{2}}$	
2640.887	1Hw	37854.80	0.00	$a\ ^6D_{0\frac{1}{2}}$—$v\ ^6F^\circ_{1\frac{1}{2}}$	
2642.403	3	37833.08	0.01	$a\ ^4G_{2\frac{1}{2}}$—$y\ ^2D^\circ_{1\frac{1}{2}}$	
2645.168	1	37793.54	0.00	$a\ ^4G_{3\frac{1}{2}}$—$y\ ^2D^\circ_{2\frac{1}{2}}$	
2648.800	3Hw	37741.72	0.02	$z\ ^8P^\circ_{2\frac{1}{2}}$—$g\ ^8S_{3\frac{1}{2}}$	
2654.824	1	37656.09	0.09	$a\ ^6D_{2\frac{1}{2}}$—$x\ ^4D^\circ_{3\frac{1}{2}}$	
2655.787	10h	37642.43	0.13	$a\ ^4D_{3\frac{1}{2}}$—$w\ ^4F^\circ_{4\frac{1}{2}}$	
2657.528	1	37617.77	0.08	$a\ ^6D_{1\frac{1}{2}}$—$x\ ^4D^\circ_{2\frac{1}{2}}$	
2657.898	8Hl	37612.54	−0.05	$z\ ^8P^\circ_{3\frac{1}{2}}$—$g\ ^8S_{3\frac{1}{2}}$	
3658.349	2	37606.16	0.03	$a\ ^4D_{3\frac{1}{2}}$—$w\ ^4F^\circ_{3\frac{1}{2}}$	
2661.20	2h	37566.3	0.3	$a\ ^4G_{4\frac{1}{2}}$—$w\ ^6D^\circ_{3\frac{1}{2}}$	
2665.064	4h	37511.41	0.01	$a\ ^4P_{2\frac{1}{2}}$—$u\ ^4D^\circ_{2\frac{1}{2}}$	
2667.263	1	37480.49	0.20	$a\ ^4G_{2\frac{1}{2}}$—$w\ ^6D^\circ_{2\frac{1}{2}}$	
2667.751	1	37473.63	0.04	$a\ ^4G_{3\frac{1}{2}}$—$w\ ^6D^\circ_{2\frac{1}{2}}$	
2667.882	1	37471.79	0.04	$b\ ^4D_{2\frac{1}{2}}$—$t\ ^4G^\circ_{3\frac{1}{2}}$	
2668.370	3h	37464.94	0.00 −0.02	$a\ ^4P_{1\frac{1}{2}}$—$u\ ^4D^\circ_{2\frac{1}{2}}$ $b\ ^4D_{3\frac{1}{2}}$—$t\ ^4G^\circ_{4\frac{1}{2}}$	
2670.237	4Hw	37438.74	−0.05	$z\ ^8P^\circ_{4\frac{1}{2}}$—$g\ ^8S_{3\frac{1}{2}}$	
2670.435	4Hw	37435.97	0.02	$a\ ^4P_{1\frac{1}{2}}$—$u\ ^4D^\circ_{1\frac{1}{2}}$	
2672.85	1	37402.2	0.1	$a\ ^4P_{1\frac{1}{2}}$—$u\ ^4D^\circ_{1\frac{1}{2}}$	
2673.651	1	37390.95	0.27	$a\ ^4P_{1\frac{1}{2}}$—$u\ ^4D^\circ_{0\frac{1}{2}}$	
2676.090	3	37356.87	0.04	$a\ ^4P_{0\frac{1}{2}}$—$u\ ^4D^\circ_{0\frac{1}{2}}$	

TABLE 1. Mn I—*Classified lines*—Continued

1	2	3	4	5	6
λ	Int.	σ	o−c	Term designation	Zeeman type
Å Air		*K*	*K*		
2676. 326	10	37353. 57	−0. 03	$a\ ^4D_{2\frac{1}{2}}$—$w\ ^4F^o_{3\frac{1}{2}}$	
2682. 244	2	37271. 16	0. 01	$a\ ^4D_{2\frac{1}{2}}$—$w\ ^4F^o_{2\frac{1}{2}}$	
2685. 941	8H	37219. 86	0. 00	$a\ ^4G_{4\frac{1}{2}}$—$v\ ^4F^o_{3\frac{1}{2}}$	
2686. 777	6	37208. 28	0. 13	$a\ ^4P_{2\frac{1}{2}}$—$u\ ^4D^o_{3\frac{1}{2}}$	
2687. 400	8*h*	37199. 66	0. 04	$a\ ^4G_{3\frac{1}{2}}$—$v\ ^4F^o_{2\frac{1}{2}}$	
2688. 078	2	37190. 28	0. 06	$a\ ^4D_{2\frac{1}{2}}$—$z\ ^2G^o_{3\frac{1}{2}}$	
2690. 977	2	37150. 21	−0. 05	$z\ ^8P^o_{3\frac{1}{2}}$—$h\ ^6D_{4\frac{1}{2}}$	
2692. 655	20	37127. 06	−0. 02	$a\ ^4G_{5\frac{1}{2}}$—$v\ ^4F^o_{4\frac{1}{2}}$	
2693. 757	2	37109. 12	−0. 04	$a\ ^4G_{2\frac{1}{2}}$—$v\ ^4F^o_{1\frac{1}{2}}$	
2694. 560	8	37100. 82	−0. 01	$a\ ^4D_{1\frac{1}{2}}$—$w\ ^4F^o_{2\frac{1}{2}}$	
2698. 890	2	37041. 30	−0. 05	$a\ ^4D_{1\frac{1}{2}}$—$w\ ^4F^o_{1\frac{1}{2}}$	
2703. 129	20H*w*	36983. 21	0. 48	$z\ ^8P^o_{4\frac{1}{2}}$—$h\ ^6D_{3\frac{1}{2}}$	
2703. 658	50H*w*	36975. 96	−0. 57	$z\ ^8P^o_{4\frac{1}{2}}$—$h\ ^6D_{4\frac{1}{2}}$	
2703. 92	40H*w*	36972. 4	0. 1	$z\ ^8P^o_{2\frac{1}{2}}$—$g\ ^8D_{3\frac{1}{2}}$	
2706. 142	5	36942. 04	0. 04	$a\ ^4D_{0\frac{1}{2}}$—$w\ ^4F^o_{1\frac{1}{2}}$	
2713. 320	100H*w*	36844. 31	0. 25	$z\ ^8P^o_{3\frac{1}{2}}$—$g\ ^8D_{4\frac{1}{2}}$	
2717. 028	4	36794. 04	0. 06	$a\ ^4G_{2\frac{1}{2}}$—$y\ ^2F^o_{3\frac{1}{2}}$	
2720. 387	2*h*	36748. 61	0. 00	$a\ ^4G_{4\frac{1}{2}}$—$y\ ^2F^o_{3\frac{1}{2}}$	
2720. 550	5*h*	36746. 41	0. 11	$a\ ^4G_{3\frac{1}{2}}$—$y\ ^2F^o_{3\frac{1}{2}}$	
2726. 13	100H*w*	36671. 2	−0. 1	$z\ ^8P^o_{4\frac{1}{2}}$—$g\ ^8D_{5\frac{1}{2}}$	
2727. 381	1	36654. 37	0. 04	$b\ ^4D_{3\frac{1}{2}}$—$67008^o_{2\frac{1}{2}}$	
2729. 420	10	36627. 00	−0. 09	$b\ ^4D_{3\frac{1}{2}}$—$66981^o_{3\frac{1}{2}}$	
2732. 260	2	36588. 93	0. 00	$b\ ^4D_{2\frac{1}{2}}$—$67008^o_{2\frac{1}{2}}$	
2733. 167	1	36576. 78	0. 01	$a\ ^4D_{0\frac{1}{2}}$—$z\ ^2D^o_{1\frac{1}{2}}$	
2734. 164	1	36563. 45	0. 09 −0. 02	$a\ ^4P_{2\frac{1}{2}}$—$x\ ^2D^o_{2\frac{1}{2}}$ $a\ ^4P_{0\frac{1}{2}}$—$x\ ^2D^o_{1\frac{1}{2}}$	
2734. 297	1	36561. 67	−0. 02	$b\ ^4D_{\frac{1}{2}}$—$66981^o_{3\frac{1}{2}}$	
2734. 736	15	36555. 80	−0. 01	$b\ ^4D_{3\frac{1}{2}}$—$66910^o_{2\frac{1}{2}}$	
2734. 997	4	36552. 31	−0. 14	$a\ ^4D_{2\frac{1}{2}}$—$z\ ^2D^o_{2\frac{1}{2}}$	
2735. 310	1*hw*	36548. 13	−0. 07	$z\ ^8P^o_{2\frac{1}{2}}$—$g\ ^6D_{2\frac{1}{2}}$	
2737. 640	2	36517. 03	0. 13	$a\ ^4P_{1\frac{1}{2}}$—$x\ ^2D^o_{2\frac{1}{2}}$	
2738. 552	5	36504. 87	−0. 03	$a\ ^4G_{2\frac{1}{2}}$—$y\ ^2G^o_{3\frac{1}{2}}$	
2738. 861	25	36500. 75	−0. 04	$b\ ^4D_{3\frac{1}{2}}$—$u\ ^4F^o_{4\frac{1}{2}}$	
2739. 627	4	36490. 54	0. 13	$b\ ^4D_{\frac{1}{2}}$—$66910^o_{2\frac{1}{2}}$	
2740. 161	1*h*	36483. 43	0. 00	$b\ ^4D_{3\frac{1}{2}}$—$u\ ^4F^o_{3\frac{1}{2}}$	
2740. 546	3H*w*	36478. 31	0. 01	$a\ ^4G_{5\frac{1}{2}}$—$61744^o_{5\frac{1}{2}}$	
2742. 735	15	36449. 19	0. 41	$a\ ^4G_{3\frac{1}{2}}$—$y\ ^2G^o_{4\frac{1}{2}}$?	
2742. 930	1	36446. 60	0. 18	$a\ ^4G_{2\frac{1}{2}}$—$z\ ^2F^o_{2\frac{1}{2}}$	
2743. 446	10	36439. 75	0. 03	$a\ ^4G_{3\frac{1}{2}}$—$z\ ^2F^o_{2\frac{1}{2}}$	
2743. 790	5	36435. 18	−0. 09	$a\ ^4D_{3\frac{1}{2}}$—$x\ ^4G^o_{4\frac{1}{2}}$	
2744. 023	9	36432. 08	0. 03	$b\ ^4D_{0\frac{1}{2}}$—$u\ ^4F^o_{1\frac{1}{2}}$	
2744. 268	6*h*	36428. 84	−0. 25 0. 00	$a\ ^4G_{4\frac{1}{2}}$—$y\ ^2G^o_{4\frac{1}{2}}$ $b\ ^4D_{3\frac{1}{2}}$—$u\ ^4F^o_{3\frac{1}{2}}$	
2744. 519	6	36425. 51	−0. 04	$a\ ^4G_{4\frac{1}{2}}$—$z\ ^2F^o_{3\frac{1}{2}}$	
2744. 748	1	36422. 46	0. 00	$a\ ^4D_{1\frac{1}{2}}$—$w\ ^4D^o_{0\frac{1}{2}}$	
2745. 082	3	36418. 03	0. 00 −0. 05	$b\ ^4D_{2\frac{1}{2}}$—$u\ ^4F^o_{2\frac{1}{2}}$ $b\ ^4D_{1\frac{1}{2}}$—$u\ ^4F^o_{1\frac{1}{2}}$	
2745. 549	10	36411. 84	−0. 09	$b\ ^4D_{1\frac{1}{2}}$—$u\ ^4F^o_{2\frac{1}{2}}$	
2745. 913	2*h*	36407. 01	0. 09	$z\ ^8P^o_{3\frac{1}{2}}$—$g\ ^6D_{4\frac{1}{2}}$	
2747. 785	4*d*	36382. 21	0. 08 −0. 09	$a\ ^4D_{1\frac{1}{2}}$—$z\ ^2D^o_{2\frac{1}{2}}$ $a\ ^4P_{2\frac{1}{2}}$—$63583^o_{2\frac{1}{2}, 1\frac{1}{2}}$	
2749. 205	20*h*	36363. 42	−0. 02	$b\ ^4D_{2\frac{1}{2}}$—$u\ ^4F^o_{3\frac{1}{2}}$	
2750. 602	3	36344. 95	0. 19	$a\ ^4P_{2\frac{1}{2}}$—$63546^o_{3\frac{1}{2}}$	
2752. 259	3	36323. 07	−0. 04	$a\ ^4D_{0\frac{1}{2}}$—$w\ ^4D^o_{0\frac{1}{2}}$	

TABLE 1. Mn I—*Classified lines*—Continued

1	2	3	4	5	6
λ	Int.	σ	o−c	Term designation	Zeeman type
Å Air		K	K		
2752. 322	7	36322. 24	−0. 04	$a\ ^4P_{2\frac{1}{2}}$—$63523^{\circ}_{2\frac{1}{2}}$	
2752. 635	3	36318. 10	−0. 11	$b\ ^4D_{2\frac{1}{2}}$—$v\ ^2G^{\circ}_{3\frac{1}{2}}$	
2753. 851	3	36302. 07	0. 08	$a\ ^4P_{0\frac{1}{2}}$—$63583^{\circ}_{2\frac{1}{2}, 1\frac{1}{2}}$	
2753. 995	3Hw	36300. 18	−0. 26	$b\ ^4D_{3\frac{1}{2}}$—$66654^{\circ}_{2\frac{1}{2}}$	
2755. 777	2	36276. 70	−0. 01	$b\ ^4D_{3\frac{1}{2}}$—$v\ ^2G^{\circ}_{4\frac{1}{2}}$	
2755. 839	2	36275. 88	0. 06	$a\ ^4P_{1\frac{1}{2}}$—$63523^{\circ}_{2\frac{1}{2}}$	
2756. 267	4	36270. 25	0. 00	$a\ ^4D_{1\frac{1}{2}}$—$w\ ^4D^{\circ}_{1\frac{1}{2}}$	
2758. 950	4	36234. 98	−0. 06 −0. 13	$b\ ^4D_{2\frac{1}{2}}$—$66654^{\circ}_{2\frac{1}{2}}$ $a\ ^4D_{2\frac{1}{2}}$—$x\ ^4G^{\circ}_{3\frac{1}{2}}$	
2760. 920	100hl	36209. 13	0. 00	$a\ ^6D_{4\frac{1}{2}}$—$t\ ^6P^{\circ}_{3\frac{1}{2}}$	
2761. 350	4	36203. 50	0. 03	$a\ ^4G_{3\frac{1}{2}}$—$w\ ^4G^{\circ}_{3\frac{1}{2}}$	
2761. 797	3	36197. 64	0. 04	$a\ ^4G_{3\frac{1}{2}}$—$u\ ^4G^{\circ}_{4\frac{1}{2}}$	
2761. 985	2h	36195. 17	0. 00	$a\ ^4G_{4\frac{1}{2}}$—$w\ ^4G^{\circ}_{3\frac{1}{2}}$	
2762. 853	3h	36183. 80	0. 02	$a\ ^4G_{4\frac{1}{2}}$—$w\ ^4G^{\circ}_{5\frac{1}{2}}$	
2763. 665	3	36173. 17	−0. 30	$a\ ^4D_{3\frac{1}{2}}$—$v\ ^4D^{\circ}_{3\frac{1}{2}}$	
2763. 87	3	36170. 4	−0. 5	$a\ ^4D_{0\frac{1}{2}}$—$w\ ^4D^{\circ}_{1\frac{1}{2}}$	
2763. 907	8h	36170. 00	−0. 02	$a\ ^4P_{2\frac{1}{2}}$—$63371^{\circ}_{2\frac{1}{2}}$	
2764. 027	1	36168. 44	0. 03	$b\ ^4D_{3\frac{1}{2}}$—$u\ ^4G^{\circ}_{4\frac{1}{2}}$	
2767. 450	10	36123. 70	0. 14	$a\ ^4P_{1\frac{1}{2}}$—$63371^{\circ}_{2\frac{1}{2}}$	
2769. 410	2	36098. 13	−0. 05	$a\ ^4D_{1\frac{1}{2}}$—$x\ ^4G^{\circ}_{2\frac{1}{2}}$	
2770. 242	3	36087. 30	0. 06	$a\ ^4P_{2\frac{1}{2}}$—$x\ ^2F^{\circ}_{3\frac{1}{2}}$	
2771. 430	30	36071. 83	0. 03	$a\ ^6D_{4\frac{1}{2}}$—$y\ ^4D^{\circ}_{3\frac{1}{2}}$	
2772. 032	2	36063. 99	−0. 06	$a\ ^4D_{3\frac{1}{2}}$—$x\ ^4F^{\circ}_{2\frac{1}{2}}$	
2773. 021	5	36051. 13	−0. 02	$a\ ^4D_{2\frac{1}{2}}$—$w\ ^4D^{\circ}_{2\frac{1}{2}}$	
2773. 659	10	36042. 84	−0. 04	$a\ ^4D_{3\frac{1}{2}}$—$w\ ^4D^{\circ}_{3\frac{1}{2}}$	
2774. 289	1	36034. 66	0. 00	$b\ ^4D_{2\frac{1}{2}}$—$u\ ^4G^{\circ}_{3\frac{1}{2}}$	
2776. 218	80hl	36009. 62	0. 04	$a\ ^6D_{3\frac{1}{2}}$—$t\ ^6P^{\circ}_{2\frac{1}{2}}$	
2777. 464	6	35993. 47	−0. 09	$a\ ^4D_{3\frac{1}{2}}$—$x\ ^4F^{\circ}_{3\frac{1}{2}}$	
2778. 544	60h	35979. 47	0. 05	$a\ ^6D_{3\frac{1}{2}}$—$t\ ^6P^{\circ}_{3\frac{1}{2}}$	
2779. 993	40	35960. 72	−0. 05	$a\ ^4D_{3\frac{1}{2}}$—$x\ ^4F^{\circ}_{4\frac{1}{2}}$	
2781. 733	1	35938. 23	0. 07	$a\ ^4P_{2\frac{1}{2}}$—$x\ ^2F^{\circ}_{2\frac{1}{2}}$	
2782. 259	1	35931. 44	−0. 16	$a\ ^4D_{2\frac{1}{2}}$—$v\ ^4D^{\circ}_{2\frac{1}{2}}$	
2782. 711	50H	35925. 60	0. 00	$a\ ^6D_{4\frac{1}{2}}$—$w\ ^6F^{\circ}_{3\frac{1}{2}}$	
2783. 080	10	35920. 84	−0. 10	$a\ ^4D_{2\frac{1}{2}}$—$v\ ^4D^{\circ}_{3\frac{1}{2}}$	
2785. 334	1	35891. 77	0. 07	$a\ ^4P_{1\frac{1}{2}}$—$x\ ^2F^{\circ}_{2\frac{1}{2}}$	
2786. 185	3	35880. 81	−0. 02	$a\ ^4D_{1\frac{1}{2}}$—$w\ ^4D^{\circ}_{2\frac{1}{2}}$	
2786. 266	3	35879. 77	0. 03	$a\ ^4P_{2\frac{1}{2}}$—$y\ ^2D^{\circ}_{2\frac{1}{2}}$	
2787. 264	2	35866. 93	−0. 02	$a\ ^4D_{2\frac{1}{2}}$—$x\ ^4F^{\circ}_{1\frac{1}{2}}$	
2787. 813	15h	35859. 86	0. 01	$a\ ^6D_{2\frac{1}{2}}$—$t\ ^6P^{\circ}_{1\frac{1}{2}}$	
2788. 682	3	35848. 68	−0. 09	$a\ ^4D_{1\frac{1}{2}}$—$u\ ^4P^{\circ}_{0\frac{1}{2}}$	
2789. 192	25	35842. 13	0. 04	$a\ ^6D_{3\frac{1}{2}}$—$y\ ^4D^{\circ}_{3\frac{1}{2}}$	6
2789. 355	15hw	35840. 03	−0. 03	$a\ ^6D_{2\frac{1}{2}}$—$t\ ^6P^{\circ}_{2\frac{1}{2}}$	
2789. 731	3	35835. 20	−0. 05	$a\ ^4D_{2\frac{1}{2}}$—$u\ ^4P^{\circ}_{1\frac{1}{2}}$	
2790. 353	30	35827. 21	0. 00	$a\ ^6D_{3\frac{1}{2}}$—$y\ ^4D^{\circ}_{2\frac{1}{2}}$	
2790. 925	4	35819. 87	−0. 06	$a\ ^4D_{3\frac{1}{2}}$—$u\ ^4P^{\circ}_{2\frac{1}{2}}$	
2791. 085	20	35817. 82	0. 01	$a\ ^6D_{4\frac{1}{2}}$—$x\ ^6D^{\circ}_{3\frac{1}{2}}$	
2791. 584	4	35811. 42	−0. 10	$a\ ^4D_{2\frac{1}{2}}$—$x\ ^4F^{\circ}_{2\frac{1}{2}}$	
2791. 707	2h	35809. 84	−0. 06	$a\ ^6D_{2\frac{1}{2}}$—$t\ ^6P^{\circ}_{3\frac{1}{2}}$	
2793. 24	6h	35790. 2	−0. 2	$a\ ^4D_{2\frac{1}{2}}$—$w\ ^4D^{\circ}_{3\frac{1}{2}}$	
2794. 817	10000R	35769. 99	0. 02	$a\ ^6S_{2\frac{1}{2}}$—$y\ ^6P^{\circ}_{3\frac{1}{2}}$	4
2796. 938	5	35742. 88	−0. 01	$a\ ^6D_{1\frac{1}{2}}$—$t\ ^6P^{\circ}_{1\frac{1}{2}}$	
2797. 194	3	35740. 88	−0. 15	$a\ ^4D_{2\frac{1}{2}}$—$x\ ^4F^{\circ}_{3\frac{1}{2}}$	
2798. 270	8000R	35725. 86	0. 01	$a\ ^6S_{2\frac{1}{2}}$—$y\ ^6P^{\circ}_{2\frac{1}{2}}$	6
2799. 841	50	35705. 81	−0. 01	$a\ ^6D_{4\frac{1}{2}}$—$x\ ^6D^{\circ}_{4\frac{1}{2}}$	6, 7b
2800. 63	6H	35695. 75	0. 00	$a\ ^6D_{3\frac{1}{2}}$—$w\ ^6F^{\circ}_{4\frac{1}{2}}$	
2801. 084	6000R	35689. 97	−0. 01	$a\ ^6S_{2\frac{1}{2}}$—$y\ ^6P^{\circ}_{1\frac{1}{2}}$	4

TABLE 1. Mn I—*Classified lines*—Continued

1	2	3	4	5	6
λ	Int.	σ	o−c	Term designation	Zeeman type
Å Air		K	K		
2802.168	10	35676.16	−0.01	$a\ ^4G_{2\frac{1}{2}}$—$x\ ^4H^0_{3\frac{1}{2}}$	
2802.399	5	35673.22	−0.01	$a\ ^4G_{3\frac{1}{2}}$—$w\ ^4F^0_{4\frac{1}{2}}$	
2802.454	10	35672.51	−0.06	$a\ ^6D_{2\frac{1}{2}}$—$y\ ^4D^0_{3\frac{1}{2}}$	
2802.619	3	35670.42	−0.03	$a\ ^4G_{4\frac{1}{2}}$—$x\ ^4H^0_{5\frac{1}{2}}$	
2802.697	2	35669.43	−0.04	$a\ ^4G_{3\frac{1}{2}}$—$x\ ^4H^0_{3\frac{1}{2}}$	
2802.805	15	35668.06	−0.08	$a\ ^4G_{3\frac{1}{2}}$—$x\ ^4H^0_{4\frac{1}{2}}$	
2803.623	10	35657.65	−0.04	$a\ ^6D_{2\frac{1}{2}}$—$y\ ^4D^0_{2\frac{1}{2}}$	
2803.946	2	35653.54	0.00	$a\ ^4G_{4\frac{1}{2}}$—$w\ ^4F^0_{4\frac{1}{2}}$	
2804.095	20	35651.64	−0.03	$a\ ^6D_{2\frac{1}{2}}$—$y\ ^4D^0_{1\frac{1}{2}}$	
2804.216	2	35649.98	0.05	$a\ ^4P_{2\frac{1}{2}}$—$w\ ^6D^0_{3\frac{1}{2}}$	
2804.363	15	35648.24	−0.06	$a\ ^4G_{4\frac{1}{2}}$—$x\ ^4H^0_{5\frac{1}{2}}$	
2804.929	6	35641.05	−0.15	$a\ ^4D_{1\frac{1}{2}}$—$x\ ^4F^0_{2\frac{1}{2}}$	
2806.136	30	35625.72	−0.02	$a\ ^4G_{5\frac{1}{2}}$—$x\ ^4H^0_{6\frac{1}{2}}$	
2806.794	10	35617.37	0.00	$a\ ^4G_{4\frac{1}{2}}$—$w\ ^4F^0_{3\frac{1}{2}}$	
2806.977	4	35615.04	−0.02	$a\ ^4G_{3\frac{1}{2}}$—$w\ ^4F^0_{3\frac{1}{2}}$	
2808.015	20	35601.88	0.01	$a\ ^6D_{3\frac{1}{2}}$—$x\ ^6D^0_{2\frac{1}{2}}$	
2808.385	8	35597.19	−0.09	$a\ ^4D_{0\frac{1}{2}}$—$x\ ^4F^0_{1\frac{1}{2}}$	
2809.103	25	35588.09	−0.01	$a\ ^6D_{3\frac{1}{2}}$—$x\ ^6D^0_{3\frac{1}{2}}$	
2811.337	4	35559.81	0.02	$a\ ^4P_{2\frac{1}{2}}$—$w\ ^6D^0_{2\frac{1}{2}}$	
2812.090	1	35550.29	0.13	$b\ ^4D_{0\frac{1}{2}}$—$w\ ^2D^0_{1\frac{1}{2}}$	
2812.840	20	35540.82	0.09	$a\ ^6D_{1\frac{1}{2}}$—$y\ ^4D^0_{2\frac{1}{2}}$	
2812.933	2	35539.64	0.01	$a\ ^4P_{1\frac{1}{2}}$—$w\ ^6D^0_{1\frac{1}{2}}$	
2813.489	20	35532.61	−0.23 0.00	$a\ ^6D_{1\frac{1}{2}}$—$y\ ^4D^0_{0\frac{1}{2}}$ $a\ ^4G_{3\frac{1}{2}}$—$w\ ^4F^0_{2\frac{1}{2}}$	
2813.989	12H	35526.30	0.00	$a\ ^6D_{2\frac{1}{2}}$—$w\ ^6F^0_{3\frac{1}{2}}$	
2814.462	2	35520.33	0.17	$a\ ^4P_{1\frac{1}{2}}$—$w\ ^6D^0_{0\frac{1}{2}}$	
2815.018	8	35513.32	−0.01	$a\ ^4P_{1\frac{1}{2}}$—$w\ ^6D^0_{2\frac{1}{2}}$	
2815.609	8*h*	35505.86	0.08	$a\ ^4P_{0\frac{1}{2}}$—$w\ ^6D^0_{1\frac{1}{2}}$	
2817.164	5*h*	35486.27	−0.04	$a\ ^4P_{0\frac{1}{2}}$—$w\ ^6D^0_{0\frac{1}{2}}$	
2817.667	10	35479.93	0.10	$a\ ^4G_{2\frac{1}{2}}$—$w\ ^4F^0_{1\frac{1}{2}}$	
2817.969	30*l*	35476.13	0.02	$a\ ^6D_{3\frac{1}{2}}$—$x\ ^6D^0_{4\frac{1}{2}}$	
2818.770	20	35466.05	0.01	$a\ ^6D_{0\frac{1}{2}}$—$y\ ^4D^0_{1\frac{1}{2}}$	
2818.919	10	35464.17	0.00	$a\ ^6D_{0\frac{1}{2}}$—$y\ ^4D^0_{0\frac{1}{2}}$	
2819.326	4	35458.42	0.04	$a\ ^4G_{2\frac{1}{2}}$—$z\ ^2G^0_{3\frac{1}{2}}$	
2819.727	4	35454.01	0.02	$a\ ^4G_{4\frac{1}{2}}$—$z\ ^2G^0_{3\frac{1}{2}}$	
2821.452	20	35432.34	−0.01	$a\ ^6D_{2\frac{1}{2}}$—$x\ ^6D^0_{2\frac{1}{2},1\frac{1}{2}}$	
2822.275	2*h*	35422.00	0.00	$a\ ^4H_{6\frac{1}{2}}$—$x\ ^2I^0_{6\frac{1}{2}}$	
2822.549	30	35418.57	−0.01	$a\ ^6D_{2\frac{1}{2}}$—$x\ ^6D^0_{3\frac{1}{2}}$	
2823.268	5H	35409.55	0.00	$a\ ^6D_{1\frac{1}{2}}$—$w\ ^6F^0_{2\frac{1}{2}}$	
2823.813	1	35402.71	−0.04	$a\ ^4G_{3\frac{1}{2}}$—$z\ ^2G^0_{4\frac{1}{2}}$	
2825.552	2	35380.86	0.11	$a\ ^4G_{3\frac{1}{2}}$—$z\ ^2G^0_{4\frac{1}{2}}$	
2828.762	6H	35340.78	0.00	$a\ ^6D_{0\frac{1}{2}}$—$w\ ^6F^0_{1\frac{1}{2}}$	
2830.793	20	35315.42	0.03	$a\ ^6D_{1\frac{1}{2}}$—$x\ ^6D^0_{2\frac{1}{2},1\frac{1}{2}}$	
2833.171	3*h*	35285.78	−0.04	$a\ ^4P_{2\frac{1}{2}}$—$v\ ^4F^0_{2\frac{1}{2}}$	
2836.310	20	35246.74	0.02	$a\ ^6D_{0\frac{1}{2}}$—$x\ ^6D^0_{1\frac{1}{2}}$	
2836.898	4*h*	35239.43	0.07	$a\ ^4P_{1\frac{1}{2}}$—$v\ ^4F^0_{2\frac{1}{2}}$	
2839.997	15	35200.98	0.03	$a\ ^6D_{4\frac{1}{2}}$—$u\ ^6P^0_{3\frac{1}{2}}$	
2840.983	1	35188.76	0.10	$a\ ^4P_{2\frac{1}{2}}$—$v\ ^4F^0_{1\frac{1}{2}}$	
2844.764	2	35141.97	−0.23	$a\ ^4P_{1\frac{1}{2}}$—$v\ ^4F^0_{1\frac{1}{2}}$	
2858.655	30	34971.24	0.00	$a\ ^6D_{3\frac{1}{2}}$—$u\ ^6P^0_{3\frac{1}{2}}$	6
2863.827	2*h*	34908.09	0.02	$b\ ^4D_{3\frac{1}{2}}$—$w\ ^2G^0_{4\frac{1}{2}}$	
2866.646	2H	34873.76	0.28	$a\ ^4P_{2\frac{1}{2}}$—$y\ ^2F^0_{2\frac{1}{2}}$?	
2868.880	7	34846.60	−0.05	$a\ ^6D_{3\frac{1}{2}}$—$u\ ^6P^0_{2\frac{1}{2}}$	
2870.464	1*h*	34827.37	0.35	$a\ ^4P_{1\frac{1}{2}}$—$y\ ^2F^0_{2\frac{1}{2}}$?	
2871.583	1*h*	34813.78	0.21	$a\ ^4D_{3\frac{1}{2}}$—$y\ ^4G^0_{4\frac{1}{2}}$	
2872.583	30	34801.69	−0.03	$a\ ^6D_{2\frac{1}{2}}$—$u\ ^6P^0_{3\frac{1}{2}}$	5

TABLE 1. Mn I—*Classified lines*—Continued

1	2	3	4	5	6
λ	Int.	σ	o−c	Term designation	Zeeman type
Å Air		*K*	*K*		
2880.270	1*h*	34708.81	0.08	$a\ ^4G_{2\frac{1}{2}}$—$w\ ^4D^\circ_{1\frac{1}{2}}$	
2882.899	20	34677.16	0.03	$a\ ^6D_{2\frac{1}{2}}$—$u\ ^6P^\circ_{2\frac{1}{2}}$	
2890.388	1*h*	34587.31	−0.18	$a\ ^4D_{2\frac{1}{2}}$—$y\ ^4G^\circ_{3\frac{1}{2}}$	
2891.945	2*h*	34568.69	0.08	$b\ ^4D_{2\frac{1}{2}}$—$w\ ^2F^\circ_{3\frac{1}{2}}$	
2892.388	2	34563.39	−0.09	$a\ ^6D_{2\frac{1}{2}}$—$u\ ^6P^\circ_{1\frac{1}{2}}$	
2892.493	5	34562.13	−0.01	$a\ ^4G_{3\frac{1}{2}}$—$z\ ^2I^\circ_{3\frac{1}{2}}$	
2892.657	20	34560.19	0.02	$a\ ^6D_{1\frac{1}{2}}$—$u\ ^6P^\circ_{2\frac{1}{2}}$	5
2894.625	10	34536.69	0.03	$a\ ^4G_{2\frac{1}{2}}$—$x\ ^4G^\circ_{2\frac{1}{2}}$	
2895.188	8	34529.97	0.01	$a\ ^4G_{3\frac{1}{2}}$—$x\ ^4G^\circ_{2\frac{1}{2}}$	
2897.428	5	34503.28	0.01	$a\ ^4G_{2\frac{1}{2}}$—$x\ ^4G^\circ_{3\frac{1}{2}}$	
2897.651	1	34500.63	−0.09	$b\ ^4D_{3\frac{1}{2}}$—$v\ ^4H^\circ_{3\frac{1}{2}}$	
2897.797	15	34498.89	0.01	$a\ ^4G_{4\frac{1}{2}}$—$x\ ^4G^\circ_{3\frac{1}{2}}$	
2897.990	10	34496.59	0.02	$a\ ^4G_{3\frac{1}{2}}$—$x\ ^4G^\circ_{3\frac{1}{2}}$	
2900.545	20	34466.20	0.00	$a\ ^4G_{3\frac{1}{2}}$—$x\ ^4G^\circ_{4\frac{1}{2}}$	5
2902.203	25	34446.51	−0.01 0.00	$a\ ^6D_{1\frac{1}{2}}$—$u\ ^6P^\circ_{1\frac{1}{2}}$ $a\ ^4G_{4\frac{1}{2}}$—$x\ ^4G^\circ_{4\frac{1}{2}}$	
2902.399	5	34444.19	−0.01	$a\ ^4G_{3\frac{1}{2}}$—$x\ ^4G^\circ_{4\frac{1}{2}}$	
2905.825	1*h*	34403.58	−0.02	$b\ ^4D_{2\frac{1}{2}}$—$w\ ^2F^\circ_{2\frac{1}{2}}$	
2906.340	4*h*	34397.49	−0.01	$b\ ^4D_{1\frac{1}{2}}$—$w\ ^3F^\circ_{2\frac{1}{2}}$	
2907.214	40	34387.15	−0.01	$a\ ^4G_{3\frac{1}{2}}$—$x\ ^4G^\circ_{3\frac{1}{2}}$	6
2907.993	15	34377.93	0.08	$a\ ^6D_{0\frac{1}{2}}$—$u\ ^6P^\circ_{1\frac{1}{2}}$	
2908.878	10	34367.47	0.00	$a\ ^4G_{4\frac{1}{2}}$—$x\ ^4G^\circ_{3\frac{1}{2}}$	
2909.630	1	34358.59	−0.14	$b\ ^4D_{3\frac{1}{2}}$—$u\ ^4D^\circ_{2\frac{1}{2}}$	
2910.242	3	34351.37	−0.01	$a\ ^4G_{4\frac{1}{2}}$—$z\ ^2I^\circ_{3\frac{1}{2}}$	
2911.839	1*h*	34332.53	−0.02	$z\ ^8P^\circ_{2\frac{1}{2}}$—$f\ ^6D_{1\frac{1}{2}}$	
2912.000	2*h*	34330.63	−0.13	$z\ ^8P^\circ_{2\frac{1}{2}}$—$f\ ^6D_{2\frac{1}{2}}$	
2912.226	3*h*	34327.97	0.02	$z\ ^8P^\circ_{2\frac{1}{2}}$—$f\ ^6D_{3\frac{1}{2}}$	
2913.518	1	34312.74	0.13	$a\ ^4G_{3\frac{1}{2}}$—$w\ ^4D^\circ_{2\frac{1}{2}}$	
2914.599	600*hw*	34300.02	0.00	$z\ ^8P^\circ_{2\frac{1}{2}}$—$f\ ^8D$	
2916.375	1*h*	34279.13	0.07	$a\ ^4P_{2\frac{1}{2}}$—$w\ ^4G^\circ_{3\frac{1}{2}}$	
2917.637	1	34264.31	−0.03	$b\ ^4D_{2\frac{1}{2}}$—$u\ ^4D^\circ_{1\frac{1}{2}}$	
2919.122	8	34246.88	0.03	$a\ ^4G_{2\frac{1}{2}}$—$v\ ^4D^\circ_{1\frac{1}{2}}$	
2920.458	8	34231.21	−0.02	$b\ ^4D_{3\frac{1}{2}}$—$x\ ^2G^\circ_{4\frac{1}{2}}$	4
2920.599	5	34229.56	−0.03	$b\ ^4D_{2\frac{1}{2}}$—$x\ ^2G^\circ_{3\frac{1}{2}}$	
2921.112	1	34223.55	0.32	$a\ ^4P_{1\frac{1}{2}}$—$w\ ^4G^\circ_{2\frac{1}{2}}$	
2923.145	2	34199.75	−0.01	$a\ ^4G_{-\frac{1}{2}}$—$v\ ^4D^\circ_{\frac{1}{2}}$	
2923.229	2*h*	34198.76	−0.01	$z\ ^8P^\circ_{3\frac{1}{2}}$—$f\ ^6D_{3\frac{1}{2}}$	
2923.577	3*h*	34194.69	−0.06	$z\ ^8P^\circ_{3\frac{1}{2}}$—$f\ ^6D_{4\frac{1}{2}}$	
2923.715	10	34193.08	0.02	$a\ ^4G_{3\frac{1}{2}}$—$v\ ^4D^\circ_{2\frac{1}{2}}$	
2924.430	10	34184.72	0.01	$a\ ^4G_{4\frac{1}{2}}$—$v\ ^4D^\circ_{3\frac{1}{2}}$	
2924.629	2	34182.39	−0.01	$a\ ^4G_{3\frac{1}{2}}$—$v\ ^4D^\circ_{3\frac{1}{2}}$	
2925.58	500*hw*	34171.3	−0.2	$z\ ^8P^\circ_{3\frac{1}{2}}$—$f\ ^8D_{4\frac{1}{2}}$	P−B
2928.678	40	34135.14	0.03	$a\ ^4G_{2\frac{1}{2}}$—$x\ ^4F^\circ_{1\frac{1}{2}}$	
2930.245	20	34116.89	0.00	$a\ ^6D_{4\frac{1}{2}}$—$x\ ^6F^\circ_{5\frac{1}{2}}$	4
2933.442	3	34079.71	0.03	$a\ ^4G_{2\frac{1}{2}}$—$x\ ^4F^\circ_{2\frac{1}{2}}$	
2934.020	30	34072.99	0.01	$a\ ^4G_{3\frac{1}{2}}$—$x\ ^4F^\circ_{2\frac{1}{2}}$	
2935.643	15	34054.15	0.03	$a\ ^4G_{4\frac{1}{2}}$—$w\ ^4D^\circ_{3\frac{1}{2}}$	4
2935.844	3	34051.82	0.01	$a\ ^4G_{3\frac{1}{2}}$—$w\ ^4D^\circ_{3\frac{1}{2}}$	
2936.156	10	34048.20	0.00	$a\ ^6D_{4\frac{1}{2}}$—$x\ ^6F^\circ_{4\frac{1}{2}}$	6
2938.496	2*h*	34021.09	0.07	$z\ ^8P^\circ_{4\frac{1}{2}}$—$f\ ^6D_{4\frac{1}{2}}$	
2939.904	20	34004.80	0.00	$a\ ^4G_{4\frac{1}{2}}$—$x\ ^4F^\circ_{3\frac{1}{2}}$	
2940.331	400*hw*	33999.86	0.00	$z\ ^8P^\circ_{4\frac{1}{2}}$—$f\ ^8D_{5\frac{1}{2}}$	
2940.483	2	33997.91	0.2	$z\ ^8P^\circ_{4\frac{1}{2}}$—$f\ ^8D_{4\frac{1}{2}}$	
2941.038	40	33991.69	−0.01	$a\ ^4G_{5\frac{1}{2}}$—$x\ ^4F^\circ_{4\frac{1}{2}}$	4
2941.681	5	33984.26	−0.04	$a\ ^6D_{1\frac{1}{2}}$—$x\ ^4P^\circ_{0\frac{1}{2}}$	
2942.740	8	33972.03	0.02	$a\ ^4G_{4\frac{1}{2}}$—$x\ ^4F^\circ_{4\frac{1}{2}}$	

TABLE 1. Mn I—*Classified lines*—Continued

1	2	3	4	5	6
λ	Int.	σ	o−c	Term designation	Zeeman type
Å Air		*K*	*K*		
2943. 550	1	33962. 68	0. 02	$a\ ^6D_{4\frac{1}{2}}$—$x\ ^6F^\circ_{3\frac{1}{2}}$	
2947. 634	3	33915. 63	0. 00	$a\ ^6D_{0\frac{1}{2}}$—$x\ ^4P^\circ_{0\frac{1}{2}}$	
2950. 979	3	33877. 19	0. 02	$a\ ^6D_{1\frac{1}{2}}$—$x\ ^4P^\circ_{1\frac{1}{2}}$	
2953. 008	10	33853. 91	0. 02	$a\ ^6D_{2\frac{1}{2}}$—$x\ ^4P^\circ_{2\frac{1}{2}}$	
2956. 101	20	33818. 49	0. 00	$a\ ^6D_{3\frac{1}{2}}$—$x\ ^6F^\circ_{4\frac{1}{2}}$	4
2956. 971	10	33808. 54	0. 04	$a\ ^6D_{0\frac{1}{2}}$—$x\ ^4P^\circ_{1\frac{1}{2}}$	
2963. 250	10	33736. 90	−0. 03	$a\ ^6D_{1\frac{1}{2}}$—$x\ ^4P^\circ_{2\frac{1}{2}}$	
2963. 606	20	33732. 85	−0. 10	$a\ ^6D_{3\frac{1}{2}}$—$x\ ^6F^\circ_{3\frac{1}{2}}$	6
2966. 374	1	33701. 38	0. 12	$a\ ^4P_{2\frac{1}{2}}$—$w\ ^4F^\circ_{3\frac{1}{2}}$	
2970. 956	4	33649. 40	−0. 02	$a\ ^6D_{3\frac{1}{2}}$—$x\ ^6F^\circ_{2\frac{1}{2}}$	
2974. 089	20	33613. 96	0. 00	$a\ ^4H_{6\frac{1}{2}}$—$t\ ^4G^\circ_{5\frac{1}{2}}$	4
2976. 588	1	33585. 74	−0. 01	$a\ ^4G_{5\frac{1}{2}}$—$z\ ^4I^\circ_{5\frac{1}{2}}$	
2976. 987	1	33581. 23	0. 00	$a\ ^4G_{4\frac{1}{2}}$—$z\ ^4I^\circ_{4\frac{1}{2}}$	
2977. 190	1	33578. 95	0. 03	$a\ ^4G_{3\frac{1}{2}}$—$z\ ^4I^\circ_{4\frac{1}{2}}$	
2977. 303	3	33577. 67	0. 02	$a\ ^4G_{5\frac{1}{2}}$—$z\ ^4I^\circ_{6\frac{1}{2}}$	
2977. 755	1	33572. 57	0. 22	$a\ ^4P_{1\frac{1}{2}}$—$w\ ^4F^\circ_{2\frac{1}{2}}$	
2977. 922	1	33570. 69	0. 3	$a\ ^4D_{3\frac{1}{2}}$—$u\ ^6F^\circ$	
2978. 114	8*h*	33568. 53	−0. 12	$a\ ^4H_{5\frac{1}{2}}$—$t\ ^4G^\circ_{4\frac{1}{2}}$	
2978. 333	2	33566. 06	0. 00	$a\ ^4G_{4\frac{1}{2}}$—$z\ ^4I^\circ_{5\frac{1}{2}}$	
2978. 566	15	33563. 44	0. 01	$a\ ^6D_{2\frac{1}{2}}$—$x\ ^6F^\circ_{3\frac{1}{2}}$	
2979. 994	8*h*	33547. 35	−0. 11	$a\ ^4H_{4\frac{1}{2}}$—$t\ ^4G^\circ_{3\frac{1}{2}}$	
2980. 493	2*h*	33541. 74	0. 14	$a\ ^4H_{3\frac{1}{2}}$—$t\ ^4G^\circ_{2\frac{1}{2}}$	
2984. 002	2	33502. 29	−0. 03	$a\ ^4H_{5\frac{1}{2}}$—$t\ ^4G^\circ_{5\frac{1}{2}}$	
2985. 992	20	33479. 97	0. 07	$a\ ^6D_{2\frac{1}{2}}$—$x\ ^6F^\circ_{2\frac{1}{2}}$	6
2986. 407	2*h*	33475. 32	0. 05	$a\ ^4H_{4\frac{1}{2}}$—$t\ ^4G^\circ_{4\frac{1}{2}}$	
2987. 052	1*h*	33468. 10	0. 01	$a\ ^4H_{3\frac{1}{2}}$—$t\ ^4G^\circ_{3\frac{1}{2}}$	
2990. 135	1	33433. 58	0. 00	$b\ ^4D_{0\frac{1}{2}}$—$x\ ^2D^\circ_{1\frac{1}{2}}$	
2991. 387	1	33419. 59	−0. 02	$b\ ^4D_{1\frac{1}{2}}$—$x\ ^2D^\circ_{1\frac{1}{2}}$	
2992. 109	5	33411. 53	0. 00	$a\ ^6D_{2\frac{1}{2}}$—$x\ ^6F^\circ_{1\frac{1}{2}}$	
2996. 183	2	33366. 10	0. 08	$a\ ^4H_{6\frac{1}{2}}$—$w\ ^2H^\circ_{5\frac{1}{2}}$	
2996. 470	10	33362. 90	−0. 04	$a\ ^6D_{1\frac{1}{2}}$—$x\ ^6F^\circ_{2\frac{1}{2}}$	4
2997. 826	6H	33347. 81	0. 07	$a\ ^4F_{4\frac{1}{2}}$—$u\ ^2G^\circ_{4\frac{1}{2}}$	6, 7*b*
2998. 056	1	33345. 25	−0. 04	$b\ ^4D_{2\frac{1}{2}}$—$x\ ^2D^\circ_{2\frac{1}{2}}$	
2998. 600	1*h*	33339. 20	0. 01	$b\ ^4D_{1\frac{1}{2}}$—$x\ ^2D_{2\frac{1}{2}}$	
3002. 378	2*hw*	33297. 25	0. 03	$a\ ^4F_{3\frac{1}{2}}$—$u\ ^2G^\circ_{3\frac{1}{2}}$	
3002. 616	20	33294. 61	0. 04	$a\ ^6D_{1\frac{1}{2}}$—$x\ ^6F^\circ_{1\frac{1}{2}}$	6
3003. 125	2	33288. 97	−0. 04	$a\ ^6D_{4\frac{1}{2}}$—$y\ ^4F^\circ_{4\frac{1}{2}}$	
3006. 629	4	33250. 18	0. 02	$a\ ^6D_{1\frac{1}{2}}$—$x\ ^6F^\circ_{0\frac{1}{2}}$	
3007. 102	7H	33244. 95	−0. 12	$a\ ^4F_{3\frac{1}{2}}$—$u\ ^2G^\circ_{4\frac{1}{2}}$	
3007. 650	80	33238. 89	0. 03	$a\ ^4G_{2\frac{1}{2}}$—$y\ ^4H^\circ_{3\frac{1}{2}}$	5
3008. 050	3	33234. 47	0. 00	$a\ ^4G_{4\frac{1}{2}}$—$y\ ^4H^\circ_{3\frac{1}{2}}$	
3008. 258	40	33232. 17	0. 01	$a\ ^4G_{3\frac{1}{2}}$—$y\ ^4H^\circ_{3\frac{1}{2}}$	
3008. 822	4	33225. 95	0. 05	$a\ ^6D_{0\frac{1}{2}}$—$x\ ^6F^\circ_{1\frac{1}{2}}$	
3009. 378	5	33219. 80	0. 02	$a\ ^4G_{5\frac{1}{2}}$—$y\ ^4H^\circ_{4\frac{1}{2}}$	5
3011. 165	50	33200. 09	0. 00	$a\ ^4G_{4\frac{1}{2}}$—$y\ ^4H^\circ_{4\frac{1}{2}}$	
3011. 376	70	33197. 76	−0. 02	$a\ ^4G_{3\frac{1}{2}}$—$y\ ^4H^\circ_{4\frac{1}{2}}$	
3012. 854	8	33181. 48	−0. 01	$a\ ^6D_{0\frac{1}{2}}$—$x\ ^6F^\circ_{0\frac{1}{2}}$	6
3013. 933	1*h*	33169. 60	−0. 01	$b\ ^4D_{3\frac{1}{2}}$—63523$^\circ_{2\frac{1}{2}}$	
3014. 666	70	33161. 54	−0. 02	$a\ ^4G_{5\frac{1}{2}}$—$y\ ^4H^\circ_{5\frac{1}{2}}$	6
3015. 183	1	33155. 85	0. 04	$b\ ^4P_{2\frac{1}{2}}$—66981$^\circ_{3\frac{1}{2}}$	
3015. 915	2	33147. 80	0. 16 0. 2	$a\ ^4P_{1\frac{1}{2}}$—$z\ ^2D^\circ_{1\frac{1}{2}}$ $a\ ^4D_{1\frac{1}{2}}$—$u\ ^6F^\circ$	
3016. 454	100	33141. 88	0. 01	$a\ ^4G_{4\frac{1}{2}}$—$y\ ^4H^\circ_{5\frac{1}{2}}$	5
3019. 018	2	33113. 74	−0. 05	$a\ ^4P_{0\frac{1}{2}}$—$z\ ^2D^\circ_{1\frac{1}{2}}$	
3021. 673	2*h*	33084. 64	0. 11	$b\ ^4P_{2\frac{1}{2}}$—66910$^\circ_{2\frac{1}{2}}$	
3022. 743	120	33072. 93	0. 00	$a\ ^4G_{3\frac{1}{2}}$—$y\ ^4H^\circ_{3\frac{1}{2}}$	4

TABLE 1. Mn I—*Classified lines*—Continued

1	2	3	4	5	6
λ	Int.	σ	o−c	Term designation	Zeeman type
Å Air		*K*	*K*		
3023.993	1*h*	33059.26	−0.04	*a* $^6D_{3½}$—*y* $^4F^o_{4½}$	
3027.836	1*h*	33017.30	−0.05	*b* $^4D_{3½}$—63371$^o_{2½}$	
3033.324	1*h*	32957.57	0.01	*b* $^4P_{2½}$—*u* $^4F^o_{3½}$	
3034.408	1*h*	32945.80	−0.05	*b* $^4D_{1½}$—63371$^o_{2½}$	
3038.616	3	32900.17	−0.07 0.06	*b* $^4D_{2½}$—63319$^o_{3½}$ *a* $^4P_{2½}$—*z* $^2D^o_{2½}$	
3039.169	1	32849.19	0.21	*a* $^4P_{1½}$—*w* $^4D^o_{½½}$	
3040.600	100	32878.71	0.02	*a* $^4G_{2½}$—*y* $^4G^o_{2½}$	
3041.220	30	32872.00	0.01	*a* $^4G_{3½}$—*y* $^4G^o_{2½}$	P−B
3041.483	1	32869.16	−0.01	*b* $^4D_{2½}$—*x* $^2F^o_{3½}$	
3042.319	3	32860.13	0.00	*a* $^4P_{0½}$—*w* $^4D^o_{½½}$	
3042.734	30	32855.65	0.00	*a* $^4G_{2½}$—*y* $^4G^o_{3½}$	
3042.905	2	32853.80	0.15	*a* $^4P_{1½}$—*z* $^2D^o_{2½}$	
3043.139	15	32851.28	0.02	*a* $^4G_{4½}$—*y* $^4G^o_{3½}$	P−B
3043.355	60	32848.95	0.00	*a* $^4G_{3½}$—*y* $^4G^o_{3½}$	P−B
3043.768	20	32844.49	−0.01	*a* $^4G_{5½}$—*y* $^4G^o_{4½}$	
3044.566	500*r*	32835.88	0.09	*a* $^6D_{4½}$—*v* $^6P^o_{3½}$	4
3045.590	80	32824.84	0.03	*a* $^4G_{4½}$—*y* $^4G^o_{4½}$	P−B
3045.804	30	32822.53	0.03	*a* $^4G_{3½}$—*y* $^4G^o_{4½}$	P−B
3046.588	4	32814.09	−0.05	*a* $^4F_{4½}$—*t* $^4G^o_{5½}$	
3047.032	150	32809.31	−0.01	*a* $^4G_{5½}$—*y* $^4G^o_{5½}$	6, 7*b*
3048.860	40	32789.64	0.01	*a* $^4G_{4½}$—*y* $^4G^o_{5½}$	P−B
3049.967	2*h*	32777.73	−0.07	*a* $^4F_{3½}$—*t* $^4G^o_{4½}$	
3050.100	3*h*	32776.31	−0.07	*a* $^4F_{2½}$—*t* $^4G_{3½}$	
3053.296	2	32742.00	0.23	*a* $^4P_{1½}$—*w* $^4D^o_{1½}$	
3054.362	400*r*	32730.57	0.04	*a* $^6D_{3½}$—*v* $^6P^o_{2½}$	4
3055.915	2	32713.94	−0.05	*b* $^4D_{1½}$—*x* $^2F^o_{2½}$	
3056.471	4	32707.99	0.07	*a* $^4P_{0½}$—*w* $^4D^o_{1½}$	
3056.992	4	32702.41	0.04	*b* $^4D_{0½}$—*y* $^2D^o_{1½}$	
3057.733	1	32694.49	−0.01	*b* $^4D_{2½}$—*y* $^2D^o_{1½}$	
3058.305	2	32688.38	−0.62	*b* $^4D_{1½}$—*y* $^2D^o_{1½}$	
3059.217	5H*w*	32678.63	−0.09	*b* $^4P_{2½}$—66504$^o_{1½}$	
3062.120	200	32647.65	0.01	*a* $^6D_{2½}$—*v* $^6P^o_{1½}$	4
3064.045	2*h*	32627.14	0.00	*a* $^4D_{3½}$—55923$^o_{2½}$	
3066.022	250	32606.11	0.03	*a* $^6D_{3½}$—*v* $^6P^o_{3½}$	6
3067.858	1	32586.59	−0.06	*z* $^6P^o_{3½}$—*e* $^8P_{4½}$	
3070.270	300	32560.99	−0.02	*a* $^6D_{2½}$—*v* $^6P^o_{2½}$	6
3073.180	300	32530.69	0.01	*a* $^6D_{1½}$—*v* $^6P^o_{1½}$	6
3079.635	200	32461.98	−0.03	*a* $^6D_{0½}$—*v* $^6P^o_{1½}$	4
3081.340	100	32444.02	−0.03	*a* $^6D_{1½}$—*v* $^6P^o_{2½}$	5
3082.060	40	32436.44	−0.12	*a* $^6D_{2½}$—*v* $^6P^o_{3½}$	5
3082.246	2	32434.48	−0.24	*a* $^4H_{6½}$—*u* $^4G^o_{5½}$	
3082.507	2H*w*	32431.74	−0.12	*b* $^4D_{2½}$—*w* $^6D^o_{3½}$	
3082.713	15	32429.57	−0.13	*a* $^4H_{6½}$—*u* $^4H^o_{6½}$	6, 7*b*
3084.025	1*h*	32415.77	−0.13	*z* $^6P^o_{3½}$—*e* $^8P_{3½}$	
3084.879	2*h*	32406.80	−0.32	*b* $^4D_{3½}$—*w* $^6D^o_{2½}$?	
3087.378	1	32380.57	0.17	*a* $^4H_{5½}$—*v* $^2G^o_{4½}$	
3087.791	3*h*	32376.24	0.35	*b* $^4D_{0½}$—*w* $^6D^o_{1½}$?	
3087.944	2*h*	32374.64	0.03	*a* $^4D_{2½}$—55923$^o_{2½}$	
3089.686	1H*w*	32356.38	−0.04	*b* $^4D_{0½}$—*w* $^6D^o_{0½}$	
3091.098	3*h*	32341.60	−0.12	*b* $^4D_{2½}$—*w* $^6D^o_{2½}$	
3091.673	4*h*	32335.59	−0.03	*b* $^4D_{1½}$—*w* $^6D^o_{2½}$	
3092.549	7	32326.43	0.08	*a* $^4P_{2½}$—*v* $^4D^o_{1½}$	
3092.872	10	32323.05	−0.03	*a* $^4H_{5½}$—*u* $^4G^o_{5½}$	
3093.121	2	32320.45	0.16	*a* $^4P_{1½}$—*u* $^4P^o_{1½}$	
3093.352	4	32318.04	−0.02	*a* $^4H_{5½}$—*u* $^4H^o_{6½}$	

TABLE 1. Mn I—*Classified lines*—Continued

1	2	3	4	5	6
λ	Int.	σ	o − c	Term designation	Zeeman type
Å Air		K	K		
3093. 467	1	32316. 84	0. 24	$b\ {}^4D_{3\frac{1}{2}}$—$w\ {}^6D^\circ_{4\frac{1}{2}}$	
3093. 689	2	32314. 52	−0. 03	$a\ {}^4H_{3\frac{1}{2}}$—$v\ {}^2G^\circ_{3\frac{1}{2}}$	
3094. 818	1	32302. 73	0. 01	$b\ {}^4G_{5\frac{1}{2}}$—$v\ {}^2H^\circ_{5\frac{1}{2}}$	
3095. 244	1	32298. 29	0. 01	$z\ {}^6P^\circ_{2\frac{1}{2}}$—$e\ {}^8P_{2\frac{1}{2}}$	
3096. 384	6	32286. 39	−0. 05	$a\ {}^4P_{0\frac{1}{2}}$—$u\ {}^4P^\circ_{0\frac{1}{2}}$	
3097. 010	20	32279. 87	−0. 02 0. 20	$a\ {}^4P_{1\frac{1}{2}}$—$v\ {}^4D^\circ_{1\frac{1}{2}}$ $a\ {}^4H_{6\frac{1}{2}}$—$u\ {}^4H^\circ_{5\frac{1}{2}}$	
3097. 063	30	32279. 31	0. 05	$a\ {}^4P_{2\frac{1}{2}}$—$v\ {}^4D^\circ_{2\frac{1}{2}}$	
3097. 758	5	32272. 07	−0. 03	$a\ {}^4H_{5\frac{1}{2}}$—$u\ {}^4G^\circ_{4\frac{1}{2}}$	
3098. 092	10	32268. 57	−0. 03	$a\ {}^4P_{2\frac{1}{2}}$—$v\ {}^4D^\circ_{3\frac{1}{2}}$	
3099. 301	1	32256. 01	−0. 26	$a\ {}^4H_{4\frac{1}{2}}$—66600$^\circ_{3\frac{1}{2}}$	
3100. 267	8	32245. 96	−0. 08	$a\ {}^4P_{0\frac{1}{2}}$—$v\ {}^4D^\circ_{1\frac{1}{2}}$	
3100. 310	10	32245. 51	0. 00	$a\ {}^4P_{0\frac{1}{2}}$—$v\ {}^4D^\circ_{0\frac{1}{2}}$	
3101. 529	30	32232. 84	0. 04	$a\ {}^4P_{1\frac{1}{2}}$—$v\ {}^4D^\circ_{2\frac{1}{2}}$	4
3101. 836	2	32229. 65	−0. 05	$a\ {}^4H_{4\frac{1}{2}}$—$u\ {}^4G^\circ_{3\frac{1}{2}}$	
3103. 280	1	32214. 65	0. 04	$a\ {}^4P_{2\frac{1}{2}}$—$x\ {}^4F^\circ_{1\frac{1}{2}}$	
3106. 336	2	32182. 96	0. 05	$a\ {}^4P_{2\frac{1}{2}}$—$u\ {}^4P^\circ_{1\frac{1}{2}}$	
3106. 748	10	32178. 69	−0. 03	$a\ {}^4H_{4\frac{1}{2}}$—$u\ {}^4G^\circ_{4\frac{1}{2}}$	6
3107. 776	20	32168. 05	−0. 10 0. 02	$a\ {}^4P_{1\frac{1}{2}}$—$x\ {}^4F^\circ_{1\frac{1}{2}}$ $a\ {}^4H_{5\frac{1}{2}}$—$u\ {}^4H^\circ_{5\frac{1}{2}}$	6
3108. 634	10	32159. 17	−0. 01	$a\ {}^4P_{2\frac{1}{2}}$—$x\ {}^4F^\circ_{2\frac{1}{2}}$	6
3109. 435	4Hw	32150. 89	−0. 19	$b\ {}^4D_{3\frac{1}{2}}$—$v\ {}^4F^\circ_{3\frac{1}{2}}$	
3110. 681	50	32138. 01	0. 00	$a\ {}^4P_{2\frac{1}{2}}$—$w\ {}^4D^\circ_{3\frac{1}{2}}$	4
3111. 147	2	32133. 20	0. 05	$b\ {}^4D_{3\frac{1}{2}}$—$v\ {}^4F^\circ_{2\frac{1}{2}}$	
3113. 118	10	32112. 85	0. 13	$a\ {}^4P_{1\frac{1}{2}}$—$x\ {}^4F^\circ_{2\frac{1}{2}}$	4
3113. 362	4	32110. 33	−0. 04	$a\ {}^4H_{4\frac{1}{2}}$—$u\ {}^4G^\circ_{3\frac{1}{2}}$	5
3113. 800	15	32105. 81	−0. 07	$a\ {}^4H_{5\frac{1}{2}}$—$u\ {}^4H^\circ_{4\frac{1}{2}}$	5
3114. 115	3	32102. 57	−0. 03	$a\ {}^4P_{0\frac{1}{2}}$—$u\ {}^4P^\circ_{1\frac{1}{2}}$	
3114. 440	1	32099. 22	−0. 13	$a\ {}^4H_{3\frac{1}{2}}$—$u\ {}^4G^\circ_{4\frac{1}{2}}$	
3115. 462	40	32088. 69	0. 00	$a\ {}^4P_{2\frac{1}{2}}$—$x\ {}^4F^\circ_{1\frac{1}{2}}$	4
3115. 754	3Hw	32085. 68	0. 00	$b\ {}^4D_{2\frac{1}{2}}$—$v\ {}^4F^\circ_{2\frac{1}{2}}$	
3116. 822	2	32074. 68	0. 03	$a\ {}^4H_{4\frac{1}{2}}$—$u\ {}^4H^\circ_{3\frac{1}{2}}$	
3117. 505	3Hw	32067. 66	−0. 09	$b\ {}^4D_{2\frac{1}{2}}$—$v\ {}^4F^\circ_{2\frac{1}{2}}$	
3118. 099	8Hw	32061. 55	−0. 10	$b\ {}^4D_{1\frac{1}{2}}$—$v\ {}^4F^\circ_{2\frac{1}{2}}$	
3120. 337	30h	32038. 56	−0. 05	$b\ {}^4D_{3\frac{1}{2}}$—$v\ {}^4F^\circ_{4\frac{1}{2}}$	4
3121. 072	6	32031. 02	0. 02	$a\ {}^4H_{3\frac{1}{2}}$—$u\ {}^4G^\circ_{3\frac{1}{2}}$	6
3121. 914	1hw	32022. 38	0. 3	$z\ {}^6P^\circ_{1\frac{1}{2}}$—$h\ {}^8D$	
3122. 880	10	32012. 47	−0. 03	$a\ {}^4H_{4\frac{1}{2}}$—$u\ {}^4H^\circ_{4\frac{1}{2}}$	6
3125. 013	8	31990. 62	0. 05	$a\ {}^4H_{4\frac{1}{2}}$—$u\ {}^4H^\circ_{3\frac{1}{2}}$	5
3126. 192	2	31978. 56	0. 10	$b\ {}^4D_{0\frac{1}{2}}$—$v\ {}^4F^\circ_{1\frac{1}{2}}$	
3126. 846	10	31971. 87	−0. 05	$a\ {}^4H_{3\frac{1}{2}}$—$u\ {}^4G^\circ_{2\frac{1}{2}}$	5
3129. 971	3	31939. 95	0. 02	$a\ {}^4F_{3\frac{1}{2}}$—66981$^\circ_{3\frac{1}{2}}$	
3130. 624	2	31933. 29	0. 16	$a\ {}^4H_{3\frac{1}{2}}$—$u\ {}^4H^\circ_{4\frac{1}{2}}$	
3132. 284	15h	31916. 36	0. 06	$a\ {}^4F_{4\frac{1}{2}}$—$u\ {}^4F^\circ_{4\frac{1}{2}}$	6, 7b
3132. 789	10	31911. 22	0. 02	$a\ {}^4H_{3\frac{1}{2}}$—$u\ {}^4H^\circ_{3\frac{1}{2}}$	6
3134. 922	4h	31889. 51	0. 01	$a\ {}^4D_{3\frac{1}{2}}$—$x\ {}^4D^\circ_{2\frac{1}{2}}$	
3135. 188	2	31886. 80	0. 06	$z\ {}^6P^\circ_{1\frac{1}{2}}$—$i\ {}^6D_{0\frac{1}{2}}$	7b?
3136. 958	10	31868. 82	0. 22	$a\ {}^4P_{1\frac{1}{2}}$—$u\ {}^4P^\circ_{2\frac{1}{2}}$	4
3138. 222	5	31855. 98	0. 04	$a\ {}^4D_{2\frac{1}{2}}$—$w\ {}^4P^\circ_{2\frac{1}{2}}$	
3141. 555	1	31822. 18	−0. 13	$z\ {}^6P^\circ_{1\frac{1}{2}}$—$e\ {}^4D_{1\frac{1}{2}}$	
3141. 821	5	31819. 49	0. 03	$a\ {}^4D_{2\frac{1}{2}}$—$w\ {}^4P^\circ_{1\frac{1}{2}}$	
3142. 401	1	31813. 61	−0. 02 0. 03	$a\ {}^4F_{3\frac{1}{2}}$—$u\ {}^4F^\circ_{4\frac{1}{2}}$ $z\ {}^6P^\circ_{2\frac{1}{2}}$—$e\ {}^4D_{1\frac{1}{2}}$	

TABLE 1. Mn I—*Classified lines*—Continued

1	2	3	4	5	6
λ	Int.	σ	o−c	Term designation	Zeeman type
Å Air		*K*	*K*		
3142.669	20*w*	31810.90	0.05	*a* $^4D_{3\frac{1}{2}}$—*x* $^4D^{\circ}_{3\frac{1}{2}}$	6, 7*b*
3144.119	1	31776.23	−0.04	*a* $^4F_{3\frac{1}{2}}$—*u* $^4F^{\circ}_{2\frac{1}{2}}$	
3144.222	1	31795.19	0.15	*a* $^4F_{2\frac{1}{2}}$—66910$^{\circ}_{2\frac{1}{2}}$	
3144.872	3*h*	31788.62	0.01	*z* $^6P^{\circ}_{1\frac{1}{2}}$—*i* $^6D_{1\frac{1}{2}}$	
3145.458	2*h*	31782.69	0.06	*z* $^6P^{\circ}_{1\frac{1}{2}}$—*e* $^4D_{2\frac{1}{2}}$	
3145.727	1*h*	31779.98	0.10	*z* $^6P^{\circ}_{2\frac{1}{2}}$—*i* $^6D_{1\frac{1}{2}}$	
3146.324	6*h*	31773.95	0.05	*z* $^6P^{\circ}_{2\frac{1}{2}}$—*e* $^4D_{2\frac{1}{2}}$	
3148.182	200*h*	31755.20	0.03	*z* $^6P^{\circ}_{2\frac{1}{2}}$—*f* $^8S_{3\frac{1}{2}}$	4
3148.857	8	31748.39	−0.04	*a* $^4H_{6\frac{1}{2}}$—*v* $^4G^{\circ}_{5\frac{1}{2}}$	4
3149.529	6*h*	31741.62	−0.06	*a* $^4F_{3\frac{1}{2}}$—*u* $^4F^{\circ}_{3\frac{1}{2}}$	
3149.928	5	31737.60	−0.08	*a* $^4D_{1\frac{1}{2}}$—*w* $^4P^{\circ}_{0\frac{1}{2}}$	4
3150.616	2	31730.67	−0.04	*a* $^4D_{2\frac{1}{2}}$—*x* $^4D^{\circ}_{1\frac{1}{2}}$	
3150.800	1	31728.81	0.00	*a* $^4F_{2\frac{1}{2}}$—*u* $^4F^{\circ}_{1\frac{1}{2}}$	
3151.415	10*h*	31722.62	−0.04	*a* $^4F_{2\frac{1}{2}}$—*u* $^4F^{\circ}_{2\frac{1}{2}}$	
3152.248	5	31714.24	−0.02	*a* $^2H_{5\frac{1}{2}}$—*v* $^2H^{\circ}_{5\frac{1}{2}}$	6, 7*b*
3152.517	4H*w*	31711.53	0.06	*z* $^6P^{\circ}_{1\frac{1}{2}}$—*i* $^6D_{2\frac{1}{2}}$	
3153.393	7H*w*	31702.72	−0.02	*z* $^6P^{\circ}_{2\frac{1}{2}}$—*i* $^6D_{2\frac{1}{2}}$	
3155.094	1	31685.63	0.01	*a* $^4D_{1\frac{1}{2}}$—*w* $^4P^{\circ}_{2\frac{1}{2}}$	
3155.781	10	31678.73	−0.01	*a* $^4F_{1\frac{1}{2}}$—*u* $^4F^{\circ}_{1\frac{1}{2}}$	6, 7*b*
3156.245	2*h*	31674.07	0.04	*z* $^6P^{\circ}_{2\frac{1}{2}}$—*e* $^4D_{3\frac{1}{2}}$	
3156.392	1*h*	31672.60	0.01	*a* $^4F_{1\frac{1}{2}}$—*u* $^4F^{\circ}_{2\frac{1}{2}}$	
3157.658	3*h*	31659.90	0.07	*z* $^6P^{\circ}_{3\frac{1}{2}}$—*e* $^4D_{3\frac{1}{2}}$	
3157.811	3	31658.37	−0.03	*a* $^4H_{5\frac{1}{2}}$—*v* $^4G^{\circ}_{4\frac{1}{2}}$	
3158.723	10	31649.12	−0.02	*a* $^4D_{1\frac{1}{2}}$—*w* $^4P^{\circ}_{1\frac{1}{2}}$	6
3159.825	4	31638.19	−0.14	*a* $^4D_{0\frac{1}{2}}$—*w* $^4P^{\circ}_{0\frac{1}{2}}$	
3159.952	20	31636.92	−0.05	*a* $^4D_{2\frac{1}{2}}$—*x* $^4D^{\circ}_{2\frac{1}{2}}$	6, 7*b*
3160.155	6	31634.89	−0.01	*a* $^4F_{4\frac{1}{2}}$—*u* $^4G^{\circ}_{5\frac{1}{2}}$	4
3161.050	200*h*	31625.93	−0.06	*z* $^8P^{\circ}_{3\frac{1}{2}}$—*f* $^8S_{3\frac{1}{2}}$	6
3162.210	1*h*	31614.33	−0.10	*b* $^4D_{-\frac{1}{2}}$—*y* $^2F^{\circ}_{3\frac{1}{2}}$	
3163.365	1	31602.79	0.01	*a* $^2H_{4\frac{1}{2}}$—*v* $^2H^{\circ}_{5\frac{1}{2}}$	
3163.534	1	31601.10	−0.3	*a* $^4G_{5\frac{1}{2}}$—*u* $^6F^{\circ}$	
3165.253	1	31583.94	0.02	*a* $^4F_{4\frac{1}{2}}$—*u* $^4G^{\circ}_{4\frac{1}{2}}$	
3166.827	10*h*	31568.24	0.08	*z* $^6P^{\circ}_{2\frac{1}{2}}$—*i* $^6D_{3\frac{1}{2}}$	
3167.153	2	31564.99	−0.03	*a* $^4H_{4\frac{1}{2}}$—*v* $^4G^{\circ}_{4\frac{1}{2}}$	
3167.619	3	31560.35	−0.04	*a* $^4D_{3\frac{1}{2}}$—*x* $^4D^{\circ}_{1\frac{1}{2}}$	
3167.827	8*h*	31558.28	−0.04	*a* $^4D_{-\frac{1}{2}}$—*x* $^4D^{\circ}_{3\frac{1}{2}}$	5
3167.935	1	31557.20	−0.06	*b* $^4P_{1\frac{1}{2}}$—*u* $^2F^{\circ}_{2\frac{1}{2}}$	
3168.254	4*h*	31554.02	0.06	*z* $^6P^{\circ}_{3\frac{1}{2}}$—*i* $^6D_{3\frac{1}{2}}$	
3168.680	2	31549.78	−0.01	*a* $^4D_{0\frac{1}{2}}$—*w* $^4P^{\circ}_{1\frac{1}{2}}$	
3169.356	4	31543.06	0.04	*a* $^2H_{4\frac{1}{2}}$—*v* $^2H^{\circ}_{4\frac{1}{2}}$	6, 7
3170.427	4	31532.40	−0.04	*a* $^4H_{4\frac{1}{2}}$—*v* $^4G^{\circ}_{3\frac{1}{2}}$	
3173.845	3	31498.44	−0.09	*b* $^4P_{1\frac{1}{2}}$—*w* $^2D^{\circ}_{1\frac{1}{2}}$	
3174.746	20H*w*	31489.50	−0.10	*a* $^4F_{1\frac{1}{2}}$—66654$^{\circ}_{2\frac{1}{2}}$	
3175.355	3*h*	31483.47	−0.03	*b* $^4P_{1\frac{1}{2}}$—*w* $^2D^{\circ}_{2\frac{1}{2}}$	
3175.576	12	31481.28	0.03	*a* $^4F_{3\frac{1}{2}}$—*u* $^4G^{\circ}_{4\frac{1}{2}}$	4
3175.713	10	31479.91	0.06	*a* $^4F_{4\frac{1}{2}}$—*u* $^4H^{\circ}_{5\frac{1}{2}}$	
3177.044	10	31466.72	0.07	*a* $^4D_{1\frac{1}{2}}$—*x* $^4D^{\circ}_{2\frac{1}{2}}$	5
3177.616	5	31461.06	0.02	*a* $^4D_{0\frac{1}{2}}$—*x* $^4D^{\circ}_{1\frac{1}{2}}$	5
3178.501	200	31452.30	0.04	*z* $^8P^{\circ}_{4\frac{1}{2}}$—*f* $^8S_{3\frac{1}{2}}$	4
3178.730	2	31450.03	−0.10	*a* $^4H_{3\frac{1}{2}}$—*v* $^4G^{\circ}_{2\frac{1}{2}}$	

TABLE 1. Mn I—*Classified lines*—Continued

1	2	3	4	5	6
λ	Int.	σ	o − c	Term designation	Zeeman type
Å Air		*K*	*K*		
3181. 269	1	31424. 94	0. 03	$a\ ^4H_{4½}$—65768$^{\circ}_{4½}$	
3181. 990	1	31417. 82	0. 12	$a\ ^4F_{4½}$—$u\ ^4H^{\circ}_{4½}$	
3182. 498	2	31412. 90	0. 00	$a\ ^4F_{3½}$—$u\ ^4G^{\circ}_{3½}$	
3185. 096	10*h*	31387. 18	−0. 02	$z\ ^6P^{\circ}_{3½}$—$i\ ^6D_{4½}$	
3186. 507	1*h*	31373. 28	0. 03	$b\ ^4D_{3½}$—$z\ ^2F^{\circ}_{2½}$	
3187. 213	2	31366. 33	0. 00	$b\ ^4D_{2½}$—$y\ ^2G^{\circ}_{3½}$	
3189. 959	15	31339. 33	0. 04	$a\ ^4F_{2½}$—$u\ ^4G^{\circ}_{3½}$	4
3192. 242	10	31315. 11	0. 08	$a\ ^4F_{3½}$—$u\ ^4H^{\circ}_{4½}$	
3193. 788	1	31301. 76	0. 01	$b\ ^4D_{1½}$—$z\ ^2F^{\circ}_{2½}$	
3194. 663	1*h*	31293. 19	0. 09	$a\ ^4F_{3½}$—$u\ ^4H^{\circ}_{3½}$	
3194. 855	1*h*	31291. 31	−0. 06	$b\ ^4D_{2½}$—$z\ ^2F^{\circ}_{3½}$	
3195. 988	2	31280. 22	0. 01	$a\ ^4F_{2½}$—$u\ ^4G^{\circ}_{2½}$	
3201. 113	10	31230. 14	0. 00	$a\ ^4F_{1½}$—$u\ ^4G^{\circ}_{2½}$	5
3202. 205	4	31219. 49	0. 00	$a\ ^4F_{2½}$—$u\ ^4H^{\circ}_{3½}$	
3203. 131	4	31210. 47	0. 07	$a\ ^4F_{4½}$—$u\ ^2F^{\circ}_{3½}$	
3206. 910	80	31173. 69	−0. 01	$a\ ^6D_{4½}$—$y\ ^6F^{\circ}_{3½}$	5
3211. 270	4*h*	31131. 36	0. 23	$b\ ^4D_{3½}$—$w\ ^4G^{\circ}_{4½}$	
3212. 887	200	31115. 70	−0. 02	$a\ ^6D_{4½}$—$y\ ^6F^{\circ}_{4½}$	6
3216. 947	100*r*	31076. 42	0. 00	$a\ ^6S_{2½}$—$z\ ^4P^{\circ}_{1½}$	5
3224. 758	150R	31001. 15	0. 00	$a\ ^6S_{2½}$—$z\ ^4P^{\circ}_{2½}$	6
3226. 048	100	30988. 76	−0. 15	$a\ ^6D_{3½}$—$y\ ^6F^{\circ}_{2½}$	5
3227. 039	2	30979. 24	−0. 02	$a\ ^4F_{3½}$—$u\ ^2F^{\circ}_{2½}$	
3228. 092	1000R	30969. 14	0. 00	$a\ ^6D_{4½}$—$y\ ^6F^{\circ}_{5½}$	4
3230. 231	10	30948. 64	0. 03	$a\ ^4F_{4½}$—$v\ ^4G^{\circ}_{5½}$	
3230. 716	500R	30943. 98	−0. 01	$a\ ^6D_{3½}$—$y\ ^6F^{\circ}_{3½}$	5
3233. 939	200H	30913. 12	0. 04	$z\ ^6P^{\circ}_{1½}$—$h\ ^6D_{0½}$	
3233. 997		30912. 67	0. 09	$z\ ^6P^{\circ}_{1½}$—$h\ ^6D_{1½}$	
3234. 112		30911. 46	−0. 02	$z\ ^6P^{\circ}_{1½}$—$h\ ^6D_{2½}$	
3234. 737	4	30905. 53	0. 03	$a\ ^4F_{3½}$—$w\ ^2D^{\circ}_{2½}$	4
3234. 912	10*h*	30903. 82	−0. 03	$z\ ^6P^{\circ}_{2½}$—$h\ ^6D_{1½}$	
3235. 025	200*h*	30902. 74	−0. 01	$z\ ^6P^{\circ}_{2½}$—$h\ ^6D_{2½}$	P − B
3235. 307	300*h*	30900. 05	0. 00	$z\ ^6P^{\circ}_{2½}$—$h\ ^6D_{3½}$	P − B
3236. 515	5*h*	30888. 55	0. 00	$z\ ^6P^{\circ}_{3½}$—$h\ ^6D_{2½}$	
3236. 778	1000	30886. 04	0. 03 0. 19	$a\ ^6D_{3½}$—$y\ ^6F^{\circ}_{4½}$ ($z\ ^6P^{\circ}_{3½}$—$h\ ^6D_{3½}$)	4
3237. 019	1	30883. 74	0. 03	$z\ ^8P^{\circ}_{3½}$—$f\ ^6S_{2½}$	
3237. 443	500H*w*	30879. 67	0. 02	$z\ ^6P^{\circ}_{3½}$—$h\ ^6D_{4½}$	P − B
3238. 720	5	30867. 51	−0. 04	$a\ ^4F_{3½}$—$v\ ^4G^{\circ}_{4½}$	4
3240. 408	150	30851. 52	0. 01	$a\ ^6D_{4½}$—$y\ ^6D^{\circ}_{4½}$	6, 7*b*
3240. 613	100	30849. 49	0. 03	$a\ ^6D_{2½}$—$y\ ^6F^{\circ}_{1½}$	P − B
3240. 882	6	30846. 93	0. 01	$a\ ^4F_{2½}$—$w\ ^2D^{\circ}_{1½}$	
3242. 139	1	30834. 97	0. 00	$a\ ^4F_{3½}$—$v\ ^4G^{\circ}_{3½}$	
3242. 463	2*h*	30831. 89	0. 00	$a\ ^4F_{2½}$—$w\ ^2D^{\circ}_{2½}$	
3243. 777	500	30819. 40	0. 01	$a\ ^6D_{2½}$—$y\ ^6F^{\circ}_{2½}$	6
3246. 153	3	30796. 84	−0. 01	$a\ ^4F_{1½}$—$w\ ^2D^{\circ}_{1½}$	
3248. 512	700*r*	30774. 48	0. 01	$a\ ^6D_{2½}$—$y\ ^6F^{\circ}_{3½}$	4
3249. 894	6	30761. 40	0. 04	$a\ ^4F_{2½}$—$v\ ^4G^{\circ}_{3½}$	P − B
3251. 134	150	30749. 66	0. 02	$a\ ^6D_{1½}$—$y\ ^6F^{\circ}_{0½}$	5
3252. 949	500*r*	30732. 50	0. 00	$a\ ^6D_{1½}$—$y\ ^6F^{\circ}_{1½}$	6
3254. 037	100	30722. 23	0. 00	$a\ ^6D_{4½}$—$y\ ^6D^{\circ}_{3½}$	4
3255. 508	5	30708. 35	0. 00	$a\ ^4F_{1½}$—$v\ ^4G^{\circ}_{2½}$	P − B
3256. 137	500*r*	30702. 42	−0. 01	$a\ ^6D_{1½}$—$y\ ^6F^{\circ}_{2½}$	4
3258. 414	400*r*	30680. 96	−0. 01	$a\ ^6D_{0½}$—$y\ ^6F^{\circ}_{0½}$	6
3260. 238	300*r*	30663. 80	−0. 03	$a\ ^6D_{0½}$—$y\ ^6F^{\circ}_{1½}$	4
3262. 333	3	30644. 10	−0. 22	$a\ ^4H_{4½}$—$w\ ^2F^{\circ}_{3½}$	
3263. 037	2	30637. 49	0. 01	$a\ ^4H_{3½}$—$v\ ^4H^{\circ}_{3½}$	

TABLE 1. Mn I—*Classified lines*—Continued

1	2	3	4	5	6
λ	Int.	σ	o−c	Term designation	Zeeman type
Å Air		K	K		
3264.710	300	30621.79	−0.01	$a\ ^6D_{3\frac{1}{2}}$—$y\ ^6D^\circ_{4\frac{1}{2}}$	4
3267.789	80	30592.94	−0.06	$a\ ^4H_{6\frac{1}{2}}$—$v\ ^4H^\circ_{6\frac{1}{2}}$	6, 7*b*
3268.720	70	30584.23	0.03	$b\ ^4P_{2\frac{1}{2}}$—$u\ ^4D^\circ_{3\frac{1}{2}}$	4
3270.353	60	30568.96	−0.05	$a\ ^4H_{5\frac{1}{2}}$—$v\ ^4H^\circ_{5\frac{1}{2}}$	6, 7*b*
3270.781	5*h*	30564.96	0.01	$a\ ^4H_{3\frac{1}{2}}$—$w\ ^2F^\circ_{3\frac{1}{2}}$	
3273.016	50	30544.09	−0.01	$a\ ^4H_{4\frac{1}{2}}$—$v\ ^4H^\circ_{4\frac{1}{2}}$	6, 7*b*
3278.062	15*h*	30497.07	0.01	$a\ ^4H_{3\frac{1}{2}}$—$v\ ^4H^\circ_{3\frac{1}{2}}$	
3278.551	100	30492.52	0.00	$a\ ^6D_{3\frac{1}{2}}$—$y\ ^6D^\circ_{3\frac{1}{2}}$	6, 7*b*
3279.751	5	30481.37	0.01	$a\ ^4H_{5\frac{1}{2}}$—$v\ ^4H^\circ_{5\frac{1}{2}}$	
3280.370	5	30475.62	−0.01	$a\ ^4H_{4\frac{1}{2}}$—$v\ ^4H^\circ_{5\frac{1}{2}}$	
3280.763	100	30471.96	−0.03	$a\ ^6D_{3\frac{1}{2}}$—$y\ ^6D^\circ_{2\frac{1}{2}}$	
3281.415	1	30465.91	−0.23	$b\ ^4D_{3\frac{1}{2}}$—$w\ ^4F^\circ_{3\frac{1}{2}}$	
3281.532	2	30464.82	0.09	$a\ ^4H_{3\frac{1}{2}}$—$v\ ^4H^\circ_{4\frac{1}{2}}$	
3285.482	1*h*	30428.20	0.02	$a\ ^2I_{5\frac{1}{2}}$—$w\ ^2H^\circ_{5\frac{1}{2}}$	
3288.548	1H	30399.83	−0.11	$a\ ^4H_{3\frac{1}{2}}$—$w\ ^2F^\circ_{2\frac{1}{2}}$	
3288.644	2H	30398.94	0.01	$b\ ^4G_{5\frac{1}{2}}$—$t\ ^4G^\circ_{4\frac{1}{2}}$	
3289.106	1	30394.67	0.03	$b\ ^4D_{1\frac{1}{2}}$—$w\ ^4F^\circ_{2\frac{1}{2}}$	
3290.969	25	30377.46	−0.06	$a\ ^6D_{3\frac{1}{2}}$—$w\ ^6P^\circ_{2\frac{1}{2}}$	4
3294.030	1*h*?	30349.24	0.11	$b\ ^4D_{0\frac{1}{2}}$—$w\ ^4F^\circ_{1\frac{1}{2}}$	
3294.934	1*h*	30340.91	−0.35	$b\ ^4D_{2\frac{1}{2}}$—$w\ ^4F^\circ_{1\frac{1}{2}}$	
3295.840	20	30332.57	−0.03	$b\ ^4G_{5\frac{1}{2}}$—$t\ ^4G^\circ_{5\frac{1}{2}}$	6, 7*b*
3296.025	40	30330.88	−0.03	$a\ ^6D_{2\frac{1}{2}}$—$w\ ^6P^\circ_{1\frac{1}{2}}$	4
3296.879	150	30323.01	0.01	$a\ ^6D_{2\frac{1}{2}}$—$y\ ^6D^\circ_{3\frac{1}{2}}$	4
3298.228	120	30310.61	−0.01	$a\ ^4P_{2\frac{1}{2}}$—$y\ ^4S^\circ_{1\frac{1}{2}}$	4
3300.943	10	30285.68	0.14	$a\ ^4P_{2\frac{1}{2}}$—$v\ ^4P^\circ_{2\frac{1}{2}}$	6, 7*b*
3303.280	100	30264.25	0.09	$a\ ^4P_{1\frac{1}{2}}$—$y\ ^4S^\circ_{1\frac{1}{2}}$	6
3303.681	1*h*	30260.58	−0.16	$b\ ^4G_{4\frac{1}{2}}$—$t\ ^4G^\circ_{3\frac{1}{2}}$	
3304.898	15*h*	30249.44	−0.13	$b\ ^4P_{1\frac{1}{2}}$—$u\ ^4D^\circ_{2\frac{1}{2}}$	
3306.004	2	30239.32	0.24	$a\ ^4P_{1\frac{1}{2}}$—$v\ ^4P^\circ_{2\frac{1}{2}}$	
3306.998	40	30230.23	−0.08	$a\ ^4P_{0\frac{1}{2}}$—$y\ ^4S^\circ_{1\frac{1}{2}}$	4
3308.065	8*h*	30220.48	−0.10	$b\ ^4P_{1\frac{1}{2}}$—$u\ ^4D^\circ_{1\frac{1}{2}}$	6
3308.778	40	30213.97	0.02	$a\ ^6D_{1\frac{1}{2}}$—$w\ ^6P^\circ_{1\frac{1}{2}}$	6
3309.428	2	30208.04	0.04	$a\ ^6D_{2\frac{1}{2}}$—$w\ ^6P^\circ_{2\frac{1}{2}}$	
3311.586	6*hw*	30188.35	−0.20	$b\ ^4G_{4\frac{1}{2}}$—$t\ ^4G^\circ_{4\frac{1}{2}}$	
3311.895	100*l*	30185.54	0.03	$a\ ^6D_{1\frac{1}{2}}$—$y\ ^6D^\circ_{2\frac{1}{2}}$	
3313.050	1H?	30175.01	0.07	$b\ ^4G_{2\frac{1}{2}}$—$t\ ^4G^\circ_{2\frac{1}{2}}$	
3313.200	50*hl*	30173.65	−0.05	$z\ ^6P^\circ_{1\frac{1}{2}}$—$g\ ^6D_{1\frac{1}{2}}$	P−B
3313.458	10*h*	30171.30	−0.04	$z\ ^6P^\circ_{1\frac{1}{2}}$—$g\ ^6D_{2\frac{1}{2}}$	
3313.560	40*h*	30170.36	−0.22	$z\ ^6P^\circ_{1\frac{1}{2}}$—$g\ ^6D_{0\frac{1}{2}}$	P−B
3314.146	10*hl*	30165.03	0.06	$z\ ^6P^\circ_{2\frac{1}{2}}$—$g\ ^6D_{1\frac{1}{2}}$	P−B
3314.415	50*hl*	30162.59	−0.02	$z\ ^6P^\circ_{2\frac{1}{2}}$—$g\ ^6D_{2\frac{1}{2}}$	P−B
3314.889	100*hl*	30158.27	0.23	$z\ ^6P^\circ_{2\frac{1}{2}}$—$g\ ^6D_{3\frac{1}{2}}$	P−B
3315.343	4*h*	30154.14	0.00	$b\ ^4G_{3\frac{1}{2}}$—$t\ ^4G^\circ_{3\frac{1}{2}}$	
3315.975	7*hl*	30148.40	−0.01	$z\ ^6P^\circ_{3\frac{1}{2}}$—$g\ ^6D_{2\frac{1}{2}}$	
3316.319	20	30145.27	−0.01	$a\ ^6D_{0\frac{1}{2}}$—$w\ ^6P^\circ_{1\frac{1}{2}}$	4
3316.459	60*hl*	30144.00	0.16	$z\ ^6P^\circ_{3\frac{1}{2}}$—$g\ ^6D_{3\frac{1}{2}}$	P−B
3317.289	200*hl*	30136.46	0.15	$z\ ^6P^\circ_{3\frac{1}{2}}$—$g\ ^6D_{4\frac{1}{2}}$	P−B
3318.874	1*h*	30122.08	−0.14	$b\ ^4G_{4\frac{1}{2}}$—$t\ ^4G^\circ_{5\frac{1}{2}}$	
3319.873	3	30113.00	0.22	$a\ ^4P_{1\frac{1}{2}}$—$v\ ^4P^\circ_{1\frac{1}{2}}$	
3320.692	100	30105.57	−0.05	$a\ ^6D_{3\frac{1}{2}}$—$w\ ^6P^\circ_{3\frac{1}{2}}$	6
3322.295	6	30091.05	0.01	$a\ ^6D_{1\frac{1}{2}}$—$w\ ^6P^\circ_{2\frac{1}{2}}$	
3323.633	6	30078.93	0.00	$a\ ^4P_{0\frac{1}{2}}$—$v\ ^4P^\circ_{1\frac{1}{2}}$	4
3330.663	100*c*	30015.45	0.31	$a\ ^6D_{2\frac{1}{2}}$—$y\ ^6D^\circ_{1\frac{1}{2}}$	
3334.557	8	29980.40	0.10	$a\ ^4P_{1\frac{1}{2}}$—$v\ ^4P^\circ_{0\frac{1}{2}}$	4
3335.039	3	29976.06	0.03	$b\ ^4D_{2\frac{1}{2}}$—$z\ ^2D^\circ_{1\frac{1}{2}}$	

TABLE 1. Mn I—*Classified lines*—Continued

1	2	3	4	5	6
λ	Int.	σ	o−c	Term designation	Zeeman type
Å (Air)		K	K		
3338.002	1	29949.46	0.16	$a\ ^4F_{4\frac{1}{2}}$—$v\ ^4H^\circ_{4\frac{1}{2}}$	
3338.288	1*h*	29946.90	0.05	$a\ ^4F_{3\frac{1}{2}}$—$w\ ^2F^\circ_{3\frac{1}{2}}$	
3338.346	2*h*	29946.37	−0.08	$a\ ^4P_{0\frac{1}{2}}$—$v\ ^4P^\circ_{0\frac{1}{2}}$	
3339.126	2*h*	29939.38	−0.03	$b\ ^4P_{2\frac{1}{2}}$—$x\ ^2D^\circ_{2\frac{1}{2}}$	
3339.486	1*h*	29936.15	0.05	$a\ ^6D_{2\frac{1}{2}}$—$w\ ^6P^\circ_{3\frac{1}{2}}$	
3342.065	4	29913.05	0.02	$a\ ^4H_{6\frac{1}{2}}$—$x\ ^2H^\circ_{5\frac{1}{2}}$	
3343.722	60	29898.23	0.05	$a\ ^6D_{1\frac{1}{2}}$—$y\ ^6D^\circ_{1\frac{1}{2}}$	
3345.349	50	29883.68	0.00	$a\ ^6D_{1\frac{1}{2}}$—$y\ ^6D^\circ_{0\frac{1}{2}}$	4
3345.656	2	29880.94	0.11	$a\ ^4F_{4\frac{1}{2}}$—$v\ ^4H^\circ_{5\frac{1}{2}}$	
3349.494	2	29846.71	0.08	$a\ ^4F_{3\frac{1}{2}}$—$v\ ^4H^\circ_{4\frac{1}{2}}$	
3350.409	10*h*	29838.56	−0.13	$b\ ^4P_{0\frac{1}{2}}$—$u\ ^4D^\circ_{1\frac{1}{2}}$	4
3351.423	10	29829.53	0.02	$a\ ^6D_{0\frac{1}{2}}$—$y\ ^6D^\circ_{1\frac{1}{2}}$	
3351.656	20*c*	29827.46	0.04	$a\ ^4D_{3\frac{1}{2}}$—$y\ ^4D^\circ_{3\frac{1}{2}}$	6, 7*b*
3353.054	1	29815.02	0.01	$a\ ^6D_{0\frac{1}{2}}$—$y\ ^6D^\circ_{0\frac{1}{2}}$	
3353.328	4*h*	29812.58	0.04	$a\ ^4D_{3\frac{1}{2}}$—$y\ ^4D^\circ_{2\frac{1}{2}}$	
3354.135	1*h*	29805.41	0.06	$a\ ^4F_{2\frac{1}{2}}$—$v\ ^4H^\circ_{3\frac{1}{2}}$	
3354.183	1*h*	29804.98	0.13	$a\ ^4H_{5\frac{1}{2}}$—$x\ ^2H^\circ_{4\frac{1}{2}}$	
3355.479	10	29793.47	0.05	$b\ ^4P_{0\frac{1}{2}}$—$u\ ^4D^\circ_{0\frac{1}{2}}$	6
3356.788	1*h*	29781.86	0.02	$a\ ^4F_{3\frac{1}{2}}$—$w\ ^2F^\circ_{3\frac{1}{2}}$	
3359.419	20H	29758.53	0.18	$b\ ^4P_{2\frac{1}{2}}$—$63583^\circ_{2\frac{1}{2},\ 1\frac{1}{2}}$	
3360.681	10	29747.36	−0.08	$b\ ^4D_{3\frac{1}{2}}$—$z\ ^2D^\circ_{2\frac{1}{2}}$	5
3361.054	2	29744.06	−0.08	$a\ ^2H_{5\frac{1}{2}}$—$t\ ^4G^\circ_{5\frac{1}{2}}$	
3362.535	1	29730.96	0.15	$a\ ^6D_{1\frac{1}{2}}$—$y\ ^4P^\circ_{0\frac{1}{2}}$	
3364.188	6	29716.35	0.08	$b\ ^4D_{1\frac{1}{2}}$—$w\ ^4D^\circ_{0\frac{1}{2}}$	
3365.137	8*cw*	29707.97	−0.04	$a\ ^4H_{4\frac{1}{2}}$—$x\ ^2H^\circ_{5\frac{1}{2}}$?	
3365.693	3	29703.06	0.07	$a\ ^6D_{2\frac{1}{2}}$—$y\ ^4P^\circ_{1\frac{1}{2}}$	
3366.235	10	29698.28	−0.05	$b\ ^4P_{2\frac{1}{2}}$—$63523^\circ_{2\frac{1}{2}}$	6
3368.086	1	29681.96	−0.08	$b\ ^4D_{2\frac{1}{2}}$—$z\ ^2D^\circ_{2\frac{1}{2}}$	
3368.194	7*h*	29681.00	0.02	$z\ ^6P^\circ_{1\frac{1}{2}}$—$h\ ^6S_{2\frac{1}{2}}$	
3369.188	10*h*	29672.25	0.00	$z\ ^6P^\circ_{2\frac{1}{2}}$—$h\ ^6S_{2\frac{1}{2}}$	
3370.813	15*h*	29657.95	−0.10	$z\ ^6P^\circ_{3\frac{1}{2}}$—$h\ ^6S_{2\frac{1}{2}}$	
3372.087	15	29646.74	0.00	$a\ ^4F_{4\frac{1}{2}}$—$x\ ^2G^\circ_{4\frac{1}{2}}$	6
3375.223	3	29619.20	0.07	$a\ ^6D_{3\frac{1}{2}}$—$y\ ^4P^\circ_{2\frac{1}{2}}$	
3376.527	6	29607.76	−0.07	$a\ ^4F_{3\frac{1}{2}}$—$x\ ^2G^\circ_{3\frac{1}{2}}$	
3378.871	3	29587.22	0.02	$a\ ^4D_{3\frac{1}{2}}$—$x\ ^6D^\circ_{2\frac{1}{2}}$	
3380.283	5*c*	29574.86	−0.03	$a\ ^4D_{2\frac{1}{2}}$—$y\ ^4D^\circ_{3\frac{1}{2}}$	
3380.444	10*c*	29573.46	0.03	$a\ ^4D_{3\frac{1}{2}}$—$x\ ^6D^\circ_{3\frac{1}{2}}$	
3380.817	10	29570.19	0.03	$b\ ^4D_{2\frac{1}{2}}$—$w\ ^4D^\circ_{1\frac{1}{2}}$	
3381.981	4*c*	29560.01	0.00	$a\ ^4D_{2\frac{1}{2}}$—$y\ ^4D^\circ_{2\frac{1}{2}}$	
3382.673	3	29553.96	−0.03	$a\ ^4D_{2\frac{1}{2}}$—$y\ ^4D^\circ_{1\frac{1}{2}}$	
3383.585	9*h*	29546.00	−0.07	$b\ ^4P_{2\frac{1}{2}}$—$63371^\circ_{2\frac{1}{2}}$	
3386.863	1	29517.40	0.04	$a\ ^6D_{0\frac{1}{2}}$—$y\ ^4P^\circ_{1\frac{1}{2}}$	
3389.287	2	29496.29	0.09	$a\ ^2H_{5\frac{1}{2}}$—$w\ ^2H^\circ_{5\frac{1}{2}}$	6, 7*b*
3393.843	1	29456.70	0.04	$a\ ^2H_{4\frac{1}{2}}$—$w\ ^2H^\circ_{4\frac{1}{2}}$	6, 7*b*
3396.367	2*h*	29434.81	0.05	$b\ ^4G_{5\frac{1}{2}}$—$u\ ^4F^\circ_{4\frac{1}{2}}$	
3399.878	1	29404.41	0.08	$a\ ^2I_{6\frac{1}{2}}$—$u\ ^4H^\circ_{6\frac{1}{2}}$	
3401.578	3	29389.72	0.03	$a\ ^4D_{1\frac{1}{2}}$—$y\ ^4D^\circ_{2\frac{1}{2}}$	
3402.490	2	29381.84	0.04 −0.11	$a\ ^4D_{1\frac{1}{2}}$—$y\ ^4D^\circ_{1\frac{1}{2}}$ $b\ ^4P_{1\frac{1}{2}}$—$x\ ^2D^\circ_{1\frac{1}{2}}$	
3406.122	1	29350.51	−0.17	$b\ ^4G_{4\frac{1}{2}}$—$66981^\circ_{3\frac{1}{2}}$	
3407.962	20	29334.66	−0.01	$a\ ^4D_{2\frac{1}{2}}$—$x\ ^6D^\circ_{3\frac{1}{2},\ 1\frac{1}{2}}$	4
3408.188	1	29332.72	0.07	$a\ ^6D_{1\frac{1}{2}}$—$y\ ^4P^\circ_{2\frac{1}{2}}$	
3409.561	3*c*	29320.91	0.01	$a\ ^4D_{2\frac{1}{2}}$—$x\ ^6D^\circ_{3\frac{1}{2}}$	
3410.345	1	29314.17	−0.04	$b\ ^4P_{2\frac{1}{2}}$—$x\ ^2F^\circ_{3\frac{1}{2}}$	
3410.800	5	29310.26	0.01	$a\ ^4H_{6\frac{1}{2}}$—$y\ ^2H^\circ_{5\frac{1}{2}}$	
3411.816	1	29301.53	0.00	$b\ ^4P_{1\frac{1}{2}}$—$x\ ^2D^\circ_{2\frac{1}{2}}$	

TABLE 1. Mn I—*Classified lines*—Continued

1	2	3	4	5	6
λ	Int.	σ	o−c	Term designation	Zeeman type
Å Air		K	K		
3412. 543	3*hl*	29295. 29	0. 02	$a\ ^2F_{3\frac{1}{2}}$—$l\ ^4G^o_{2\frac{1}{2}}$	
3413. 815	1	29284. 37	0. 05	$a\ ^4D_{0\frac{1}{2}}$—$y\ ^4D^o_{1\frac{1}{2}}$	
3417. 158	6	29255. 73	−0. 06	$b\ ^4P_{2\frac{1}{2}}$—$y\ ^2D^o_{2\frac{1}{2}}$	
3418. 276	15	29246. 15	0. 01	$b\ ^4D_{3\frac{1}{2}}$—$w\ ^4D^o_{3\frac{1}{2}}$	5
3420. 794	50	29224. 63	−0. 03	$a\ ^4H_{6\frac{1}{2}}$—$w\ ^4H^o_{6\frac{1}{2}}$	6, 7*b*
3421. 491	1	29218. 67	0. 06	$b\ ^4G_{2\frac{1}{2}}$—67008$^o_{2\frac{1}{2}}$	
3422. 418	1	29210. 76	0. 08	$b\ ^4G_{5\frac{1}{2}}$—$v\ ^2G^o_{4\frac{1}{2}}$	
3422. 826	10	29207. 28	−0. 05	$a\ ^4H_{5\frac{1}{2}}$—$w\ ^4H^o_{5\frac{1}{2}}$	6, 7*b*
3423. 137	2	29204. 63	0. 04	$a\ ^4H^4_{4\frac{1}{2}}$—$z\ ^2H^o_{4\frac{1}{2}}$	6
3423. 841	10	29198. 62	0. 01	$a\ ^4H_{5\frac{1}{2}}$—$y\ ^2H^o_{5\frac{1}{2}}$	
3424. 375	5	29194. 07	−0. 02	$a\ ^4H_{5\frac{1}{2}}$—$w\ ^4H^o_{4\frac{1}{2}}$	
3425. 929	1	29180. 82	0. 08	$b\ ^4D_{2\frac{1}{2}}$—$w\ ^4D^o_{2\frac{1}{2}}$	
3427. 865	10	29164. 34	−0. 01	$a\ ^4D_{1\frac{1}{2}}$—$x\ ^6D^o_{2\frac{1}{2},\ 1\frac{1}{2}}$	
3427. 957	3	29163. 56	−0. 02	$a\ ^4D_{1\frac{1}{2}}$—$x\ ^6D^o_{0\frac{1}{2}}$	
3428. 782	15	29156. 55	0. 00	$b\ ^4D_{0\frac{1}{2}}$—$u\ ^4P^o_{0\frac{1}{2}}$	6
3429. 155	4	29153. 37	0. 01	$b\ ^4G_{5\frac{1}{2}}$—$u\ ^4G^o_{5\frac{1}{2}}$	
3429. 741	2	29148. 39	0. 05	$b\ ^4G_{5\frac{1}{2}}$—$u\ ^4H^o_{6\frac{1}{2}}$	
3430. 428	1	29142. 56	−0. 02	$b\ ^4D_{1\frac{1}{2}}$—$u\ ^4P^o_{0\frac{1}{2}}$	
3433. 025	5*h*	29120. 51	0. 04	$b\ ^4P_{1\frac{1}{2}}$—63583$^o_{2\frac{1}{2},\ 1\frac{1}{2}}$	
3433. 572	50	29115. 87	−0. 06	$b\ ^4D_{3\frac{1}{2}}$—$v\ ^4D^o_{3\frac{1}{2}}$	6
3433. 911	1	29113. 00	−0. 02	$a\ ^4H_{5\frac{1}{2}}$—$w\ ^4H^o_{6\frac{1}{2}}$	
3434. 473	2	29108. 23	−0. 05	$b\ ^4D_{2\frac{1}{2}}$—$v\ ^4D^o_{1\frac{1}{2}}$	
3434. 823	1	29105. 27	0. 04	$a\ ^4H_{4\frac{1}{2}}$—$y\ ^2H^o_{5\frac{1}{2}}$	
3435. 193	5	29102. 13	−0. 05	$b\ ^4D_{1\frac{1}{2}}$—$v\ ^4D^o_{1\frac{1}{2}}$	P−B
3435. 254	4	29101. 62	−0. 03	$b\ ^4D_{1\frac{1}{2}}$—$v\ ^4D^o_{0\frac{1}{2}}$	P−B
3435. 375	5	29100. 59	−0. 12 0. 04	$a\ ^4H_{4\frac{1}{2}}$—$w\ ^4H^o_{4\frac{1}{2}}$ $a\ ^4H_{3\frac{1}{2}}$—63523$^o_{2\frac{1}{2}}$	6, 7*b*
3439. 579	3	29065. 02	0. 02	$a\ ^4D_{0\frac{1}{2}}$—$x\ ^6D^o_{1\frac{1}{2}}$	
3439. 673	3	29064. 23	0. 00	$a\ ^4D_{0\frac{1}{2}}$—$x\ ^6D^o_{0\frac{1}{2}}$	
3440. 044	10	29061. 10	−0. 09	$b\ ^4D_{2\frac{1}{2}}$—$v\ ^4D^o_{2\frac{1}{2}}$	6
3440. 769	1	29054. 97	−0. 12	$b\ ^4D_{1\frac{1}{2}}$—$v\ ^4D^o_{2\frac{1}{2}}$	
3440. 907	1	29053. 79	−0. 07	$b\ ^4G_{2\frac{1}{2}}$—$u\ ^4F^o_{1\frac{1}{2}}$	
3441. 177	2	29051. 53	−0. 02	$a\ ^4H_{4\frac{1}{2}}$—$w\ ^4H^o_{3\frac{1}{2}}$	
3442. 756	5	29038. 20	−0. 06	$a\ ^4H_{3\frac{1}{2}}$—$z\ ^2H^o_{3\frac{1}{2}}$	6, 7*b*
3443. 657	5*h*	29030. 60	−0. 03	$a\ ^4H_{4\frac{1}{2}}$—63374$^o_{4\frac{1}{2}}$	
3444. 237	2*hc*	29025. 72	−0. 26	$b\ ^4P_{2\frac{1}{2}}$—$w\ ^6D^o_{3\frac{1}{2}}$	
3446. 519	1	29006. 50	−0. 01	$b\ ^4D_{3\frac{1}{2}}$—$x\ ^4F^o_{2\frac{1}{2}}$	
3446. 766	2	29004. 42	0. 01	$b\ ^4D_{0\frac{1}{2}}$—$x\ ^4F^o_{1\frac{1}{2}}$	
3446. 822	5	29003. 95	−0. 06	$a\ ^4H_{4\frac{1}{2}}$—$y\ ^2H^o_{4\frac{1}{2}}$	6
3448. 429	1*h*	28990. 44	0. 00	$b\ ^4D_{1\frac{1}{2}}$—$x\ ^4F^o_{1\frac{1}{2}}$	
3449. 036	1	28985. 34	0. 00	$b\ ^4D_{3\frac{1}{2}}$—$w\ ^4D^o_{3\frac{1}{2}}$	
3450. 607	20	28972. 14	−0. 04	$a\ ^4H_{3\frac{1}{2}}$—$w\ ^4H^o_{3\frac{1}{2}}$	6
3450. 932	1*h*	28969. 41	−0. 14	$b\ ^4G_{4\frac{1}{2}}$—66600$^o_{3\frac{1}{2}}$	4
3451. 475	7	28964. 85	0. 01	$b\ ^4D_{2\frac{1}{2}}$—$u\ ^4P^o_{1\frac{1}{2}}$	
3452. 201	5	28958. 76	0. 02	$b\ ^4D_{1\frac{1}{2}}$—$u\ ^4P^o_{1\frac{1}{2}}$	
3452. 440	5*w*	28956. 75	0. 18	$a\ ^4D_{3\frac{1}{2}}$—$u\ ^6P^o_{3\frac{1}{2}}$	
3453. 426	2*h*	28948. 49	0. 01	$a\ ^6D_{4\frac{1}{2}}$—$y\ ^4P^o_{3\frac{1}{2}}$	
3453. 505	2*hw*	28947. 83	−0. 06	$b\ ^4G_{2\frac{1}{2}}$—$v\ ^2G^o_{3\frac{1}{2}}$	
3453. 861	1	28944. 84	−0. 04 −0. 04	$a\ ^4H_{4\frac{1}{2}}$—$z\ ^2H^o_{5\frac{1}{2}}$ $a\ ^4H_{4\frac{1}{2}}$—$x\ ^2F^o_{3\frac{1}{2}}$	
3454. 110	2	28942. 76	−0. 22	$b\ ^4G_{4\frac{1}{2}}$—$u\ ^4G^o_{5\frac{1}{2}}$	
3454. 309	1	28941. 09	−0. 02	$b\ ^4D_{2\frac{1}{2}}$—$x\ ^4F^o_{2\frac{1}{2}}$	

TABLE 1. Mn I—*Classified lines*—Continued

1	2	3	4	5	6
λ	Int.	σ	o−c	Term designation	Zeeman type
Å Air		*K*	*K*		
3454.926	8	28935.92	0.08	$b\ ^4P_{2\frac{1}{2}}$—$w\ ^6D^\circ_{2\frac{1}{2}}$	
			−0.10	$b\ ^4D_{3\frac{1}{2}}$—$x\ ^4F^\circ_{3\frac{1}{2}}$	
3455.045	8	28934.92	−0.09	$b\ ^4D_{1\frac{1}{2}}$—$x\ ^4F^\circ_{2\frac{1}{2}}$	
3456.268	1	28924.69	0.05	$a\ ^4H_{3\frac{1}{2}}$—$y\ ^2H^\circ_{4\frac{1}{2}}$	
3456.850	1	28919.81	−0.13	$b\ ^4D_{2\frac{1}{2}}$—$w\ ^4D^\circ_{3\frac{1}{2}}$	
3458.246	2*h*	28908.14	−0.05	$b\ ^4P_{1\frac{1}{2}}$—63371$^\circ_{2\frac{1}{2}}$	
3458.842	5	28903.16	−0.07	$b\ ^4D_{3\frac{1}{2}}$—$x\ ^4F^\circ_{4\frac{1}{2}}$	
3462.755	10	28870.50	−0.12	$b\ ^4D_{2\frac{1}{2}}$—$x\ ^4F^\circ_{3\frac{1}{2}}$	P−B
3463.356	3	28865.49	−0.02	$a\ ^4H_{3\frac{1}{2}}$—$x\ ^2F^\circ_{3\frac{1}{2}}$	
3463.657	15	28862.98	0.03	$b\ ^4G_{3\frac{1}{2}}$—66600$^\circ_{3\frac{1}{2}}$	6
3470.013	15	28810.12	−0.12	$b\ ^4G_{2\frac{1}{2}}$—66600$^\circ_{3\frac{1}{2}}$	7*b*?
3472.986	1	28785.45	0.05	$b\ ^4G_{3\frac{1}{2}}$—$u\ ^4G^\circ_{4\frac{1}{2}}$	
3475.776	20	28762.35	−0.04	$b\ ^4D_{3\frac{1}{2}}$—$u\ ^4P^\circ_{2\frac{1}{2}}$	4
3478.645	2*hl*	28738.63	0.05	$b\ ^4P_{0\frac{1}{2}}$—63583$^\circ_{1\frac{1}{2}}$	
			−0.02	$a\ ^2I_{5\frac{1}{2}}$—$v\ ^4G^\circ_{5\frac{1}{2}}$	
3480.609	5*h*	28722.41	0.14	$a\ ^4P_{2\frac{1}{2}}$—55923$^\circ_{2\frac{1}{2}}$	
3481.053	1	28718.75	−0.02	$a\ ^6D_{3\frac{1}{2}}$—$y\ ^8P^\circ_{3\frac{1}{2}}$	
3481.342	2	28716.36	−0.07	$a\ ^4H_{3\frac{1}{2}}$—$x\ ^2F^\circ_{2\frac{1}{2}}$	
3483.084	20	28702.00	0.02	$a\ ^6D_{4\frac{1}{2}}$—$z\ ^4D^\circ_{3\frac{1}{2}}$	
3483.689	6	28697.02	0.03	$b\ ^4D_{2\frac{1}{2}}$—$u\ ^4P^\circ_{2\frac{1}{2}}$	
3484.355	2	28691.54	0.06	$a\ ^2G_{4\frac{1}{2}}$—$v\ ^2H^\circ_{5\frac{1}{2}}$	
3485.724	2*h*	28680.27	−0.15	$z\ ^8P^\circ_{3\frac{1}{2}}$—$e\ ^6D_{3\frac{1}{2}}$	
3486.239	2*h*	28676.03	0.22	$a\ ^4P_{1\frac{1}{2}}$—55923$^\circ_{2\frac{1}{2}}$	
3487.658	1	28664.36	0.02	$b\ ^4G_{2\frac{1}{2}}$—$u\ ^4G^\circ_{3\frac{1}{2}}$	
3488.309	5	28659.01	0.08	$a\ ^6D_{3\frac{1}{2}}$—$z\ ^4D^\circ_{2\frac{1}{2}}$	
3491.548	1	28632.43	0.06	$a\ ^6D_{2\frac{1}{2}}$ $z\ ^4D^\circ_{1\frac{1}{2}}$	
3492.786	1	28622.28	0.06	$a\ ^2H_{5\frac{1}{2}}$—$v\ ^2G^\circ_{4\frac{1}{2}}$	
3493.352	1	28617.64	0.00	$a\ ^2H_{4\frac{1}{2}}$—$v\ ^2G^\circ_{3\frac{1}{2}}$	
3494.861	2*h*	28605.29	0.03	$b\ ^4G_{2\frac{1}{2}}$—$u\ ^4G^\circ_{2\frac{1}{2}}$	
3503.727	2	28532.91	0.13	$a\ ^6D_{0\frac{1}{2}}$—$z\ ^4D^\circ_{0\frac{1}{2}}$	
3504.085	2*h*	28529.99	0.07	$a\ ^6D_{2\frac{1}{2}}$—$y\ ^8P^\circ_{2\frac{1}{2}}$	
3505.408	1	28519.22	0.07	$a\ ^4F_{4\frac{1}{2}}$—$w\ ^4H^\circ_{5\frac{1}{2}}$	
3505.863	2	28515.52	0.11	$a\ ^6D_{1\frac{1}{2}}$—$z\ ^4D^\circ_{1\frac{1}{2}}$	
3507.158	2*h*	28504.99	0.06	$a\ ^4F_{3\frac{1}{2}}$—63546$^\circ_{3\frac{1}{2}}$	
3507.538	3*h*	28501.90	−0.01	$z\ ^8P^\circ_{4\frac{1}{2}}$—$e\ ^6D_{4\frac{1}{2}}$	
3509.067	3	28489.48	0.07	$a\ ^6D_{2\frac{1}{2}}$—$z\ ^4D^\circ_{2\frac{1}{2}}$	
3509.168	1	28488.66	−0.02	$b\ ^4G_{5\frac{1}{2}}$—$v\ ^4G^\circ_{4\frac{1}{2}}$	
3511.188	4	28472.28	0.01	$a\ ^6D_{3\frac{1}{2}}$—$z\ ^4D^\circ_{3\frac{1}{2}}$	
3511.831	20	28467.06	−0.01	$b\ ^4G_{3\frac{1}{2}}$—$v\ ^4G^\circ_{3\frac{1}{2}}$	6, 7
3514.330	1	28446.82	0.08	$a\ ^6D_{0\frac{1}{2}}$—$z\ ^4D^\circ_{1\frac{1}{2}}$	
3515.690	3*h*	28435.82	−0.01	$a\ ^4F_{4\frac{1}{2}}$—63374$^\circ_{4\frac{1}{2}}$	
3516.053	2	28432.88	−0.02	$a\ ^2G_{3\frac{1}{2}}$—$v\ ^2H^\circ_{4\frac{1}{2}}$	
3518.989	2*h*	28409.16	−0.05	$a\ ^4F_{4\frac{1}{2}}$—$y\ ^2H^\circ_{4\frac{1}{2}}$	
			0.03	$a\ ^4D_{1\frac{1}{2}}$—$u\ ^6P^\circ_{2\frac{1}{2}}$	
3523.530	3	28372.54	0.09	$a\ ^6D_{1\frac{1}{2}}$—$z\ ^4D^\circ_{2\frac{1}{2}}$	
3525.212	1*h*	28359.01	−0.16	$b\ ^4G_{2\frac{1}{2}}$—$u\ ^2F^\circ_{3\frac{1}{2}}$	
3526.322	1	28350.09	0.01	$a\ ^4F_{4\frac{1}{2}}$—$z\ ^2H^\circ_{5\frac{1}{2}}$	
			0.01	$a\ ^4F_{4\frac{1}{2}}$—$x\ ^2F^\circ_{3\frac{1}{2}}$	
3526.492	1	28348.72	0.15	$b\ ^4G_{5\frac{1}{2}}$—65768$^\circ_{4\frac{1}{2}}$	
3529.534	1	28324.29	0.03	$b\ ^4P_{1\frac{1}{2}}$—$w\ ^6D^\circ_{1\frac{1}{2}}$	
3531.836	1600	28305.82	−0.05	$z\ ^8P^\circ_{2\frac{1}{2}}$—$e\ ^8D_{3\frac{1}{2}}$	P−B
3531.998	1800	28304.53	−0.04	$z\ ^8P^\circ_{2\frac{1}{2}}$—$e\ ^8D_{2\frac{1}{2}}$	P−B
3532.110	2000	28303.63	0.00	$z\ ^8P^\circ_{2\frac{1}{2}}$—$e\ ^8D_{1\frac{1}{2}}$	P−B
3535.297	10	28278.11	−0.19	$b\ ^4G_{4\frac{1}{2}}$—$v\ ^4G^\circ_{4\frac{1}{2}}$	6, 7*b*
3538.002	5	28256.50	−0.19	$b\ ^4G_{4\frac{1}{2}}$—$v\ ^4G^\circ_{3\frac{1}{2}}$	
3539.371	2	28245.57	−0.15	$b\ ^4G_{4\frac{1}{2}}$—$v\ ^4G^\circ_{3\frac{1}{2}}$	
3541.234	1	28230.70	0.00	$b\ ^4G_{2\frac{1}{2}}$—$u\ ^2F^\circ_{2\frac{1}{2}}$	
3547.794	4000	28178.51	0.00	$z\ ^8P^\circ_{3\frac{1}{2}}$—$e\ ^8D_{4\frac{1}{2}}$	P−B
3548.022	3000	28176.69	0.00	$z\ ^8P^\circ_{3\frac{1}{2}}$—$e\ ^8D_{3\frac{1}{2}}$	P−B

TABLE 1. Mn I—*Classified lines*—Continued

1	2	3	4	5	6
λ	Int.	σ	o−c	Term designation	Zeeman type
Å Air		K	K		
3548.182	1000	28175.43	0.04	$z\ ^8P^o_{3½}$—$e\ ^8D_{2½}$	P−B
3552.757	10	28139.14	0.02	$b\ ^4G_{3½}$—$v\ ^4G^o_{3½}$	
3552.901	4	28138.00	−0.19	$b\ ^4G_{4½}$—65768$^o_{4½}$	
3553.121	1	28136.26	0.08	$b\ ^4G_{3½}$—$v\ ^4G^o_{2½}$	
3555.066	2	28120.87	0.21	$a\ ^4P_{1½}$—$w\ ^4P^o_{1½}$	
3559.373	2	28086.84	0.03	$a\ ^4P_{0½}$—$w\ ^4P^o_{1½}$	
3559.434	2	28086.36	−0.05	$b\ ^4G_{2½}$—$v\ ^4G^o_{3½}$	
3559.808	10	28083.41	−0.06	$b\ ^4G_{2½}$—$v\ ^4G^o_{2½}$	
3561.736	1	28068.21	−0.01	$a\ ^2F_{3½}$—$v\ ^2G^o_{3½}$	
3566.330	1	28032.05	0.14	$a\ ^4P_{1½}$—$x\ ^4D^o_{1½}$	
3566.731	3	28028.91	−0.01	$a\ ^2H_{4½}$—$u\ ^2F^o_{3½}$	
3569.494	6000	28007.21	0.00	$z\ ^8P^o_{3½}$—$e\ ^8D_{3½}$	P−B
3569.804	3000	28004.78	0.00	$z\ ^8P^o_{4½}$—$e\ ^8D_{4½}$	P−B
3570.028	1000	28003.02	0.06	$z\ ^8P^o_{4½}$—$e\ ^8D_{3½}$	P−B
3572.354	1	27984.79	0.16	$a\ ^4P_{2½}$—$x\ ^4D^o_{2½}$	
3575.356	1	27961.29	−0.03	$a\ ^2F_{3½}$—$v\ ^2G^o_{4½}$	
3575.967	4H	27956.51	0.00	$z\ ^6P^o_{1½}$—$f\ ^6D_{0½}$	
3576.073	8H	27955.68	−0.01	$z\ ^6P^o_{1½}$—$f\ ^6D_{1½}$	
3576.303	4H	27953.89	−0.01	$z\ ^6P^o_{1½}$—$f\ ^6D_{2½}$	
3577.187	2H	27946.98	0.02	$z\ ^6P^o_{2½}$—$f\ ^6D_{1½}$	
3577.416	5H	27945.19	0.02	$z\ ^6P^o_{2½}$—$f\ ^6D_{2½}$	
3577.870	2000	27941.64	0.01	$a\ ^6D_{4½}$—$x\ ^6P^o_{3½}$	4
3578.285	3	27938.40	0.23	$a\ ^4P_{1½}$—$x\ ^4D^o_{2½}$	
3579.637	8	27927.85	−0.31	$z\ ^6P^o_{3½}$—$f\ ^6D_{3½}$	
3580.112	40H*l*	27924.14	0.00	$z\ ^6P^o_{3½}$—$f\ ^6D_{4½}$	
3581.545	5H*w*	27912.97	0.20	$a\ ^4F_{4½}$—$w\ ^6D^o_{3½}$	
3582.425	20*c*	27906.11	0.13	$a\ ^4P_{2½}$—$x\ ^4D^o_{3½}$	4
3583.187	2	27900.18	−0.04	$a\ ^2H_{5½}$—$v\ ^4G^o_{4½}$	
3583.675	40	27896.38	−0.07	$a\ ^4D_{2½}$—$x\ ^4P^o_{1½}$	4
3585.966	1	27878.56	−0.05	$a\ ^2H_{5½}$—$v\ ^4G^o_{5½}$	
3586.540	1000*h*	27874.10	−0.01	$a\ ^6D_{3½}$—$x\ ^6P^o_{2½}$	4
3590.664	2	27842.09	0.05	$b\ ^4G_{3½}$—$w\ ^2G^o_{4½}$	
3591.806	15	27833.23	−0.03	$a\ ^4D_{1½}$—$x\ ^4P^o_{0½}$	4
3592.556	1	27827.42	−0.02	$b\ ^4G_{2½}$—$v\ ^2F^o_{3½}$	
3595.110	500*h*	27807.65	0.00	$a\ ^6D_{2½}$—$x\ ^6P^o_{1½}$	4
3597.560	1	27788.72	−0.02	$a\ ^2H_{4½}$—$v\ ^4G^o_{4½}$	
3599.504	4H*w*	27773.71	0.02	$a\ ^4H_{6½}$—$y\ ^2I^o_{6½}$	
3601.268	20	27760.11	0.00	$a\ ^2H_{5½}$—65768$^o_{4½}$	4
3601.772	20*c*	27756.22	0.01	$a\ ^4D_{2½}$—$x\ ^4P^o_{2½}$	6
3604.670	15*c*	27733.91	0.00	$a\ ^4D_{0½}$—$x\ ^4P^o_{0½}$	6
3605.683	20	27726.12	−0.01	$a\ ^4D_{1½}$—$x\ ^4P^o_{1½}$	6
3606.489	2H	27719.92	−0.04	$a\ ^4F_{3½}$—$w\ ^6D^o_{2½}$	
3606.702	1H	27718.28	0.00	$a\ ^4D_{3½}$—$x\ ^6F^o_{3½}$	
3607.530	1000	27711.92	0.00	$a\ ^6D_{3½}$—$x\ ^6P^o_{3½}$	6
3608.485	1000	27704.59	0.00	$a\ ^6D_{2½}$—$x\ ^6P^o_{2½}$	6
3610.298	1000	27690.68	−0.01	$a\ ^6D_{1½}$—$x\ ^6P^o_{1½}$	6
3612.612	2H	27672.94	0.29	$a\ ^4F_{2½}$—$w\ ^6D^o_{1½}$	
3615.375	10H	27651.78	0.03	$a\ ^4H_{3½}$—$y\ ^2F^o_{2½}$	5
3618.646	2	27626.80	0.02	$a\ ^4D_{0½}$—$x\ ^4P^o_{1½}$	
3619.272	600	27622.02	0.00	$a\ ^6D_{0½}$—$x\ ^6P^o_{1½}$	4
3620.751	1*h*	27610.73	−0.04	$a\ ^4H_{3½}$—$y\ ^2F^o_{3½}$	
3621.483	6H*w*	27605.15	−0.01	$a\ ^4H_{6½}$—61744$^o_{5½}$	
3623.783	500*h*	27587.63	0.00	$a\ ^6D_{1½}$—$x\ ^6P^o_{2½}$	5
3626.299	3H*w*	27568.49	−0.06	$a\ ^4H_{3½}$—$y\ ^2I^o_{3½}$	
3629.738	400*h*	27542.38	−0.02	$a\ ^6D_{2½}$—$x\ ^6P^o_{3½}$	5

TABLE 1. Mn I—*Classified lines*—Continued

1	2	3	4	5	6
λ	Int.	σ	o−c	Term designation	Zeeman type
Å Air		*K*	*K*		
3635.699	10	27497.22	0.03	$a\ ^2H_{4½}$—$v\ ^2F^o_{3½}$	4
3636.190	2H*w*	27493.51	−0.01	$a\ ^4H_{3½}$—61744$^o_{5½}$	
3638.032	1*h*	27479.59	0.09	$a\ ^2F_{3½}$—$u\ ^2F^o_{3½}$	
3639.145	5	27471.18	0.02	$a\ ^6D_{4½}$—$z\ ^4F^o_{3½}$	
3639.580	1	27467.90	0.14	$b\ ^4G_{5½}$—$v\ ^4H^o_{4½}$	
3640.086	15*h*	27464.08	0.16 0.08	$a\ ^4F_{3½}$—$v\ ^4F^o_{3½}$ $a\ ^4H_{5½}$—$y\ ^2G^o_{4½}$	
3641.405	30*h*	27454.13	0.01	$a\ ^4F_{4½}$—$v\ ^4F^o_{4½}$	6, 7*b*
3643.018	3	27441.98	−0.06	$a\ ^4H_{4½}$—$y\ ^2G^o_{3½}$	5
3646.707	3	27414.22	−0.07	$a\ ^6D_{3½}$—$z\ ^4F^o_{2½}$	
3648.698	6	27399.26	−0.03	$b\ ^4G_{5½}$—$v\ ^4H^o_{5½}$	6
3652.292	3H	27372.30	−0.08	$a\ ^4F_{2½}$—$v\ ^4F^o_{2½}$	
3652.510	1*h*	27370.66	0.04	$a\ ^4H_{4½}$—$y\ ^2G^o_{4½}$	
3653.514	2	27363.14	−0.07	$a\ ^6D_{2½}$—$z\ ^4F^o_{1½}$	
3653.581	2	27362.64	−0.03	$a\ ^4H_{3½}$—$y\ ^2G^o_{3½}$	
3654.291	2*h*	27357.32	−0.28	$b\ ^4G_{4½}$—$w\ ^2F^o_{3½}$	
3655.097	3*h*	27351.29	−0.16 0.26	$a\ ^4F_{3½}$—$v\ ^4F^o_{4½}$ $a\ ^2F_{3½}$—$u\ ^2F^o_{2½}$	
3657.906	20*c*	27330.29	−0.04	$a\ ^4H_{6½}$—$w\ ^4G^o_{5½}$	5
3660.404	100	27311.64	0.00	$b\ ^4G_{5½}$—$v\ ^4H^o_{6½}$	4
3663.135	1*h*	27291.27	0.02	$a\ ^4H_{3½}$—$y\ ^2G^o_{4½}$	
3663.373	2*h*	27289.50	−0.21	$b\ ^4G_{4½}$—$v\ ^4H^o_{3½}$	
2667.714	10	27257.21	−0.17	$b\ ^4G_{4½}$—$v\ ^4H^o_{4½}$	6
3668.201	1	27253.59	0.01	$a\ ^2H_{5½}$—$w\ ^2G^o_{4½}$	
3668.547	1*h*	27251.02	0.02	$b\ ^4G_{3½}$—$w\ ^2F^o_{3½}$	
3669.198	4	27246.18	−0.07	$a\ ^6D_{1½}$—$z\ ^4F^o_{1½}$	
3669.398	15	27244.70	−0.07	$a\ ^6D_{2½}$—$z\ ^4F^o_{2½}$	
3669.837	50	27241.44	−0.01	$a\ ^6D_{3½}$—$z\ ^4F^o_{3½}$	
3670.505	100	27236.48	0.01	$a\ ^6D_{4½}$—$z\ ^4F^o_{4½}$	6
3672.037	1	27225.12	−0.03	$a\ ^4F_{1½}$—$v\ ^4F^o_{1½}$	
3672.915	1	27218.61	−0.08	$a\ ^4H_{5½}$—$w\ ^4G^o_{5½}$	
3673.515	2	27214.16	0.00	$a\ ^2F_{2½}$—$u\ ^2F^o_{3½}$	
3674.514	1	27206.76	0.02	$a\ ^2F_{2½}$—$v\ ^4G^o_{3½}$	
3675.670	10H*l*	27198.21	−0.08	$b\ ^4G_{2½}$—$w\ ^2F^o_{3½}$	
3676.960	80	27188.67	−0.24	$b\ ^4G_{4½}$—$v\ ^4H^o_{5½}$	4
3677.469	1	27184.90	−0.05	$a\ ^2H_{4½}$—$w\ ^2G^o_{3½}$	
3677.716	4*h*	27183.08	−0.03	$b\ ^4G_{3½}$—$v\ ^4H^o_{3½}$	
3678.470	3	27177.50	−0.08	$a\ ^6D_{0½}$—$z\ ^4F^o_{1½}$	
3680.146	20	27165.12	−0.08	$b\ ^4G_{5½}$—$x\ ^2G^o_{4½}$	4
3682.090	60	27150.79	0.01	$b\ ^4G_{3½}$—$v\ ^4H^o_{4½}$	4
2683.363	4	27141.40	−0.04	$a\ ^4H_{4½}$—$w\ ^4G^o_{4½}$	
3684.522	20	27132.87	0.00	$b\ ^4D_{3½}$—$v\ ^4P^o_{2½}$	4
3684.866	20*h*	27130.33	−0.07	$b\ ^4G_{2½}$—$v\ ^4H^o_{3½}$	
3685.215	15	27127.76	−0.05	$a\ ^6D_{1½}$—$z\ ^4F^o_{2½}$	
3685.561	7	27125.22	−0.09	$a\ ^4H_{4½}$—$w\ ^4G^o_{3½}$	
3689.097	2	27099.22	0.01 0.10	$a\ ^2F_{3½}$—65768$^o_{4½}$ $a\ ^4D_{1½}$—$x\ ^6F^o_{0½}$	4
3689.989	1*h*	27092.67	0.12	$b\ ^4D_{2½}$—$y\ ^4S^o_{1½}$	
3690.808	10	27086.66	−0.01	$a\ ^4H_{6½}$—$y\ ^4I^o_{5½}$	
3690.933	5*h*	27085.74	0.05 −0.25	$a\ ^2F_{2½}$—$u\ ^2F^o_{2½}$ $b\ ^4G_{3½}$—$w\ ^2F^o_{2½}$	
3692.187	2*h*	27076.54	−0.02	$a\ ^4D_{3½}$—$y\ ^4F^o_{2½}$	
3692.817	40	27071.92	−0.01	$a\ ^6D_{2½}$—$z\ ^4F^o_{3½}$	4
3693.426	4	27067.46	−0.01	$b\ ^4D_{2½}$—$v\ ^4P^o_{2½}$	

TABLE 1. Mn I—*Classified lines*—Continued

1	2	3	4	5	6
λ	Int.	σ	o−c	Term designation	Zeeman type
Å Air		K	K		
3693. 671	100	27065. 66	0. 00	$a\ ^4H_{6\frac{1}{2}}$—$y\ ^4I^\circ_{7\frac{1}{2}}$	4
3694. 056	20c	27062. 84	0. 23	$a\ ^4D_{3\frac{1}{2}}$—$y\ ^4F^\circ_{3\frac{1}{2}}$	6
3694. 116		27062. 40	−0. 21		P−B
3696. 093	2h	27047. 93	−0. 03	$a\ ^4H_{3\frac{1}{2}}$—$w\ ^4G^\circ_{2\frac{1}{2}}$	
3696. 547	100cw	27044. 61	−0. 02	$a\ ^4D_{3\frac{1}{2}}$—$y\ ^4F^\circ_{4\frac{1}{2}}$	4
3700. 147	8	27018. 29	−0. 29	$b\ ^4G_{4\frac{1}{2}}$—$x\ ^2G^\circ_{3\frac{1}{2}}$	
3700. 300	15	27017. 18	0. 01	$a\ ^4P_{2\frac{1}{2}}$—$z\ ^4S^\circ_{1\frac{1}{2}}$	4
3701. 728	80	27006. 75	−0. 01	$a\ ^6D_{3\frac{1}{2}}$—$z\ ^4F^\circ_{4\frac{1}{2}}$	4
3706. 082	150	26975. 03	0. 00	$a\ ^4H_{5\frac{1}{2}}$—$y\ ^4I^\circ_{6\frac{1}{2}}$	
3706. 663	10	26970. 80	0. 09	$a\ ^4P_{1\frac{1}{2}}$—$z\ ^4S^\circ_{1\frac{1}{2}}$	6, 7b
3708. 148	1h	26960. 00	−0. 04	$a\ ^4F_{2\frac{1}{2}}$—$y\ ^2F^\circ_{2\frac{1}{2}}$	
3708. 870	3	26954. 75	−0. 07	$b\ ^4G_{4\frac{1}{2}}$—$x\ ^2G^\circ_{4\frac{1}{2}}$	
3709. 656	1	26949. 04	0. 00	$b\ ^4D_{0\frac{1}{2}}$—$v\ ^4P^\circ_{1\frac{1}{2}}$	
3709. 831	3	26947. 77	0. 00	$a\ ^2F_{3\frac{1}{2}}$—$v\ ^2F^\circ_{3\frac{1}{2}}$	6
3710. 749	8	26941. 10	−0. 07	$b\ ^4D_{2\frac{1}{2}}$—$v\ ^4P^\circ_{1\frac{1}{2}}$	4
3711. 349	4	26936. 75	−0. 11	$a\ ^4P_{0\frac{1}{2}}$—$z\ ^4S^\circ_{1\frac{1}{2}}$	4
3711. 590	6	26935. 00	−0. 07	$b\ ^4D_{1\frac{1}{2}}$—$v\ ^4P^\circ_{1\frac{1}{2}}$	
3713. 789	6h	26919. 05	−0. 01	$a\ ^4F_{2\frac{1}{2}}$—$y\ ^2F^\circ_{3\frac{1}{2}}$	4
3714. 771	1	26911. 93	−0. 05	$b\ ^4G_{3\frac{1}{2}}$—$x\ ^2G^\circ_{3\frac{1}{2}}$	
3715. 046	5h	26909. 94	−0. 03	$a\ ^4F_{1\frac{1}{2}}$—$y\ ^2F^\circ_{2\frac{1}{2}}$	5
3715. 525	4	26906. 47	−0. 24	$a\ ^2I_{5\frac{1}{2}}$—$x\ ^2H^\circ_{5\frac{1}{2}}$	
3718. 129	4	26887. 63	−0. 03	$a\ ^2I_{6\frac{1}{2}}$—$x\ ^2H^\circ_{5\frac{1}{2}}$	
3718. 924	100	26881. 88	0. 01	$a\ ^4H_{4\frac{1}{2}}$—$y\ ^4I^\circ_{5\frac{1}{2}}$	
3720. 908	5	26867. 55	0. 02	$a\ ^4H_{4\frac{1}{2}}$—$y\ ^4I^\circ_{4\frac{1}{2}}$	6
3722. 062	1	26859. 22	−0. 05	$b\ ^4G_{2\frac{1}{2}}$—$x\ ^2G^\circ_{3\frac{1}{2}}$	
3725. 548	2	26834. 08	0. 01	$a\ ^4D_{2\frac{1}{2}}$—$y\ ^4F^\circ_{1\frac{1}{2}}$	
3726. 949	20	26824. 00	−0. 03	$a\ ^4D_{2\frac{1}{2}}$—$y\ ^4F^\circ_{2\frac{1}{2}}$	6
3727. 986	4	26816. 54	−0. 02	$b\ ^4D_{0\frac{1}{2}}$—$v\ ^4P^\circ_{0\frac{1}{2}}$	6
3728. 894	100c	26810. 01	−0. 07	$a\ ^4D_{2\frac{1}{2}}$—$y\ ^4F^\circ_{3\frac{1}{2}}$	4
3729. 523	2Hl	26805. 48	0. 14	$a\ ^4F_{4\frac{1}{2}}$—61744$^\circ_{5\frac{1}{2}}$	
3729. 942	3	26802. 47	−0. 12	$b\ ^4D_{1\frac{1}{2}}$—$v\ ^4P^\circ_{0\frac{1}{2}}$	
3731. 012	10	26794. 79	−0. 06	$a\ ^4H_{6\frac{1}{2}}$—$x\ ^4H^\circ_{5\frac{1}{2}}$	
3731. 938	100	26788. 14	−0. 02	$a\ ^4H_{3\frac{1}{2}}$—$y\ ^4I^\circ_{4\frac{1}{2}}$	5
3733. 643	1h	26775. 91	0. 09	$a\ ^4F_{4\frac{1}{2}}$—$y\ ^2G^\circ_{4\frac{1}{2}}$	
			−0. 01	$a\ ^4D_{3\frac{1}{2}}$—$z\ ^4H^\circ_{4\frac{1}{2}}$	
3736. 909	50	26752. 53	−0. 07	$a\ ^4H_{6\frac{1}{2}}$—$x\ ^4H^\circ_{6\frac{1}{2}}$	6, 7b
3738. 014	1h	26744. 60	0. 03	$a\ ^4F_{3\frac{1}{2}}$—$y\ ^2G^\circ_{3\frac{1}{2}}$	
3741. 019	10	26723. 11	−0. 07	$a\ ^2H_{5\frac{1}{2}}$—$v\ ^4H^\circ_{6\frac{1}{2}}$	
3742. 269	1H	26714. 19	0. 00	$a\ ^2F_{2\frac{1}{2}}$—$v\ ^2F^\circ_{3\frac{1}{2}}$	
3743. 525	10	26705. 23	−0. 13	$a\ ^4H_{3\frac{1}{2}}$—$x\ ^4H^\circ_{4\frac{1}{2}}$	
3744. 362	2	26699. 26	−0. 09	$a\ ^2H_{4\frac{1}{2}}$—$v\ ^4H^\circ_{5\frac{1}{2}}$	
3746. 623	40	26683. 15	−0. 06	$a\ ^4H_{5\frac{1}{2}}$—$x\ ^4H^\circ_{5\frac{1}{2}}$	6, 7b
3748. 021	8h	26673. 19	0. 04	$a\ ^4F_{3\frac{1}{2}}$—$y\ ^2G^\circ_{4\frac{1}{2}}$	
3748. 332	1	26670. 98	0. 02	$a\ ^4F_{2\frac{1}{2}}$—$y\ ^2G^\circ_{3\frac{1}{2}}$	
3748. 515	7hl	26669. 68	0. 07	$a\ ^4F_{3\frac{1}{2}}$—$z\ ^2F^\circ_{3\frac{1}{2}}$	
			0. 02	$b\ ^2I_{6\frac{1}{2}}$—$v\ ^2H^\circ_{5\frac{1}{2}}$	
3749. 353	10	26663. 71	−0. 04	$a\ ^4D_{1\frac{1}{2}}$—$y\ ^4F^\circ_{1\frac{1}{2}}$	6
3750. 766	60	26653. 67	−0. 04	$a\ ^4D_{1\frac{1}{2}}$—$y\ ^4F^\circ_{2\frac{1}{2}}$	4
3752. 554	5	26640. 97	0. 01	$a\ ^4H_{3\frac{1}{2}}$—$x\ ^4H^\circ_{4\frac{1}{2}}$	
3753. 303	2h	26635. 66	0. 13	$a\ ^2F_{3\frac{1}{2}}$—$w\ ^2G^\circ_{3\frac{1}{2}}$	
3753. 866	8	26631. 66	−0. 01	$b\ ^4G_{5\frac{1}{2}}$—$x\ ^2H^\circ_{5\frac{1}{2}}$	
3754. 224	5Hw	26629. 12	−0. 29	$z\ ^4P^\circ_{1\frac{1}{2}}$—$f\ ^4D_{0\frac{1}{2}}$	

TABLE 1. Mn I—*Classified lines*—Continued

1	2	3	4	5	6
λ	Int.	σ	o−c	Term designation	Zeeman type
Å Air		*K*	*K*		
3755.385	1H*w*	26620.89	0.14	$z\ ^4P^\circ_{3\frac{1}{2}}$—$f\ ^4D_{1\frac{1}{2}}$	
3756.449	5	26613.35	0.04	$a\ ^4H_{4\frac{1}{2}}$—$x\ ^4H^\circ_{3\frac{1}{2}}$	
3756.643	30	26611.98	0.00	$a\ ^4H_{4\frac{1}{2}}$—$x\ ^4H^\circ_{4\frac{1}{2}}$	
3758.912	4*h*	26595.91	−0.09	$a\ ^4F_{2\frac{1}{2}}$—$z\ ^2F^\circ_{3\frac{1}{2}}$	
3759.354	2*h*	26592.79	0.11	$a\ ^2F_{3\frac{1}{2}}$—$w\ ^2G^\circ_{4\frac{1}{2}}$	
3759.775	6	26589.81	−0.02	$a\ ^4H_{4\frac{1}{2}}$—$x\ ^4H^\circ_{3\frac{1}{2}}$	
3761.010	5H*w*	26581.08	0.20	$z\ ^4P^\circ_{0\frac{1}{2}}$—$f\ ^4D_{0\frac{1}{2}}$	
3761.629	1	26576.70	−0.04	$a\ ^2H_{5\frac{1}{2}}$—$x\ ^2G^\circ_{4\frac{1}{2}}$	
3763.372	40	26564.40	0.00	$a\ ^4D_{0\frac{1}{2}}$—$y\ ^4F^\circ_{1\frac{1}{2}}$	5
3763.650	2*h*	26562.43	0.02	$a\ ^4F_{1\frac{1}{2}}$—$z\ ^2F^\circ_{2\frac{1}{2}}$	
3766.052	10H	26545.49	0.01	$z\ ^4P^\circ_{1\frac{1}{2}}$—$f\ ^4D_{1\frac{1}{2}}$	
3767.695	20	26533.92	−0.02	$a\ ^4H_{3\frac{1}{2}}$—$x\ ^4H^\circ_{3\frac{1}{2}}$	
3767.876	2	26532.64	0.03	$a\ ^4H_{3\frac{1}{2}}$—$x\ ^4H^\circ_{4\frac{1}{2}}$	
3768.176	10	26530.53	0.02	$a\ ^4F_{4\frac{1}{2}}$—$w\ ^4G^\circ_{3\frac{1}{2}}$	
3770.226	1H?	26516.11	−0.15	$a\ ^4D_{2\frac{1}{2}}$—$z\ ^4H^\circ_{3\frac{1}{2}}$	
3771.439	15	26507.58	0.00	$b\ ^2I_{6\frac{1}{2}}$—$x\ ^2I^\circ_{6\frac{1}{2}}$	6, 7*b*
3772.955	10H	26496.93	−0.02	$z\ ^4P^\circ_{0\frac{1}{2}}$—$f\ ^4D_{1\frac{1}{2}}$	
3773.858	10	26490.58	0.00	$b\ ^2I_{5\frac{1}{2}}$—$x\ ^2I^\circ_{5\frac{1}{2}}$	6, 7*b*
3774.669	20*h*	26484.89	0.07	$z\ ^4P^\circ_{2\frac{1}{2}}$—$f\ ^4D_{2\frac{1}{2}}$	
3776.289	2*h*	26473.53	0.11	$a\ ^2G_{4\frac{1}{2}}$—$w\ ^2H^\circ_{5\frac{1}{2}}$	
3776.537	40	26471.79	0.00	$a\ ^6D_{4\frac{1}{2}}$—$z\ ^6F^\circ_{3\frac{1}{2}}$	
3781.192	1*h*	26439.20	−0.03	$a\ ^4F_{3\frac{1}{2}}$—$w\ ^4G^\circ_{3\frac{1}{2}}$	
3783.297	2	26424.49	−0.26	$b\ ^4G_{4\frac{1}{2}}$—$x\ ^2H^\circ_{4\frac{1}{2}}$	
3784.233	1	26417.96	−0.01	$a\ ^4H_{5\frac{1}{2}}$—$z\ ^2G^\circ_{4\frac{1}{2}}$	
3785.422	30*h*	26409.66	0.11	$z\ ^4P^\circ_{1\frac{1}{2}}$—$f\ ^4D_{2\frac{1}{2}}$	4
3786.836	3	26399.80	−0.03	$a\ ^2I_{5\frac{1}{2}}$—$z\ ^2H^\circ_{4\frac{1}{2}}$	7*b*
3787.446	1	26395.55	0.03	$a\ ^4H_{4\frac{1}{2}}$—$z\ ^2G^\circ_{3\frac{1}{2}}$	
3789.757	1*h*	26379.45	−0.19	$a\ ^4D_{1\frac{1}{2}}$—$v\ ^6P^\circ_{1\frac{1}{2}}$	
3790.214	200*h*	26376.27	−0.02	$a\ ^6D_{4\frac{1}{2}}$—$z\ ^6F^\circ_{4\frac{1}{2}}$	6
3791.081	2*h*	26370.22	0.03	$a\ ^2F_{2\frac{1}{2}}$—$w\ ^2G^\circ_{3\frac{1}{2}}$	
3794.497	2	26346.50	−0.04	$a\ ^2G_{3\frac{1}{2}}$—$w\ ^2H^\circ_{4\frac{1}{2}}$	
3799.256	60	26313.50	0.00	$a\ ^6D_{3\frac{1}{2}}$—$z\ ^6F^\circ_{2\frac{1}{2}}$	5
3800.551	60*h*	26304.53	0.06	$z\ ^4P^\circ_{2\frac{1}{2}}$—$f\ ^4D_{3\frac{1}{2}}$	4
3801.901	80	26295.19	0.00	$a\ ^4G_{5\frac{1}{2}}$—$z\ ^4G^\circ_{5\frac{1}{2}}$	6, 7*b*
3802.137	1	26293.56	−0.04	$a\ ^2I_{6\frac{1}{2}}$—$w\ ^4H^\circ_{5\frac{1}{2}}$	
3803.073	2	26287.09	0.02	$a\ ^4F_{4\frac{1}{2}}$—$y\ ^4I^\circ_{5\frac{1}{2}}$	
3804.021	6	26280.54	0.01	$a\ ^4G_{5\frac{1}{2}}$—$z\ ^4G^\circ_{4\frac{1}{2}}$	
3804.752	20*c*	26275.49	−0.01	$a\ ^4G_{4\frac{1}{2}}$—$z\ ^4G^\circ_{5\frac{1}{2}}$	
3806.715	2000*h*	26261.94	0.00	$a\ ^6D_{4\frac{1}{2}}$—$z\ ^6F^\circ_{5\frac{1}{2}}$	4
3806.881	10	26260.80	−0.04	$a\ ^4G_{4\frac{1}{2}}$—$z\ ^4G^\circ_{4\frac{1}{2}}$	
3807.203	10	26258.58	0.05	$a\ ^4G_{3\frac{1}{2}}$—$z\ ^4G^\circ_{4\frac{1}{2}}$	
3808.506	10	26249.59	0.02	$a\ ^4G_{2\frac{1}{2}}$—$z\ ^4G^\circ_{3\frac{1}{2}}$	
3809.146	5	26245.18	0.00	$a\ ^4G_{4\frac{1}{2}}$—$z\ ^4G^\circ_{3\frac{1}{2}}$	
3809.485	10	26242.85	−0.02	$a\ ^4G_{3\frac{1}{2}}$—$z\ ^4G^\circ_{3\frac{1}{2}}$	
3809.593	500*h*	26242.10	0.02	$a\ ^6D_{3\frac{1}{2}}$—$z\ ^6F^\circ_{3\frac{1}{2}}$	6
3810.679	40	26234.62	0.03	$a\ ^4G_{2\frac{1}{2}}$—$z\ ^4G^\circ_{2\frac{1}{2}}$	
3811.659	6	26227.88	−0.01	$a\ ^4G_{3\frac{1}{2}}$—$z\ ^4G^\circ_{2\frac{1}{2}}$	
3813.024	1	26218.49	0.09	$a\ ^2F_{3\frac{1}{2}}$—$v\ ^4H^\circ_{4\frac{1}{2}}$	
3816.746	100	26192.92	−0.01	$a\ ^6D_{2\frac{1}{2}}$—$z\ ^6F^\circ_{1\frac{1}{2}}$	5, C
3820.081	1*h*	26170.06	0.00	$a\ ^4F_{3\frac{1}{2}}$—$y\ ^4I^\circ_{4\frac{1}{2}}$	
3820.903	1*h*	26164.42	0.14	$b\ ^4P_{2\frac{1}{2}}$—$w\ ^4D^\circ_{1\frac{1}{2}}$	
3823.508	1500*h*	26146.60	0.02	$a\ ^6D_{3\frac{1}{2}}$—$z\ ^6F^\circ_{4\frac{1}{2}}$	4
3823.891	100*h*	26143.98	0.00	$a\ ^6D_{2\frac{1}{2}}$—$z\ ^6F^\circ_{2\frac{1}{2}}$	6, C
3826.617	5*h*	26125.36	0.00	$z\ ^6P^\circ_{1\frac{1}{2}}$—$g\ ^6S_{2\frac{1}{2}}$	
3826.734	1*h*	26124.55	0.02	$a\ ^2I_{6\frac{1}{2}}$—$z\ ^2H^\circ_{5\frac{1}{2}}$	

711-046—64——3

TABLE 1. Mn I—*Classified lines*—Continued

1	2	3	4	5	6
λ	Int.	σ	o−c	Term designation	Zeeman type
Å Air		K	K		
3827.890	10H	26116.67	0.04	$z\ {}^6P^{\circ}_{3\frac{1}{2}}$—$g\ {}^6S_{2\frac{1}{2}}$	
3829.679	100	26104.47	0.29	$a\ {}^6D_{1\frac{1}{2}}$—$z\ {}^6F^{\circ}_{0\frac{1}{2}}$	5, C
3829.986	8*h*	26102.38	−0.05	$z\ {}^6P^{\circ}_{3\frac{1}{2}}$—$g\ {}^6S_{2\frac{1}{2}}$	
3833.865	500	26075.97	0.00	$a\ {}^6D_{1\frac{1}{2}}$—$z\ {}^6F^{\circ}_{1\frac{1}{2}}$	6, C
3834.368	1000	26072.55	−0.01	$a\ {}^6D_{2\frac{1}{2}}$—$z\ {}^6F^{\circ}_{3\frac{1}{2}}$	4
3836.908	1*h*	26055.29	−0.10	$b\ {}^4G_{2\frac{1}{2}}$—$x\ {}^2D^{\circ}_{1\frac{1}{2}}$	
3838.191	2*hl*	26046.58	−0.09	$a\ {}^2H_{5\frac{1}{2}}$—$x\ {}^2H^{\circ}_{4\frac{1}{2}}$	
3839.779	500*h*	26035.81	0.30	$a\ {}^6D_{0\frac{1}{2}}$—$z\ {}^6F^{\circ}_{0\frac{1}{2}}$	6, C
3841.074	600*h*	26027.03	0.01	$a\ {}^6D_{1\frac{1}{2}}$—$z\ {}^6F^{\circ}_{2\frac{1}{2}}$	4, C
3843.988	500*h*	26007.30	0.00	$a\ {}^6D_{0\frac{1}{2}}$—$z\ {}^6F^{\circ}_{1\frac{1}{2}}$	4, C
3845.009	7*h*	26000.40	0.13	$a\ {}^4F_{4\frac{1}{2}}$—$w\ {}^4F^{\circ}_{4\frac{1}{2}}$	
3845.795	1	25995.08	0.05	$a\ {}^4F_{4\frac{1}{2}}$—$x\ {}^4H^{\circ}_{5\frac{1}{2}}$	
3847.234	1*h*	25985.36	−0.03	$a\ {}^2F_{2\frac{1}{2}}$—$v\ {}^4H^{\circ}_{3\frac{1}{2}}$	
3846.046	1	25979.88	0.28	$a\ {}^2F_{3\frac{1}{2}}$—$x\ {}^2G^{\circ}_{3\frac{1}{2}}$	
3850.380	1*h*	25964.12	0.02	$a\ {}^4F_{4\frac{1}{2}}$—$w\ {}^4F^{\circ}_{3\frac{1}{2}}$	
3852.512	6*h*	25949.76	−0.06	$a\ {}^2G_{4\frac{1}{2}}$—66981$^{\circ}_{3\frac{1}{2}}$	
3853.476	30	25943.27	−0.03	$b\ {}^4G_{5\frac{1}{2}}$—$w\ {}^4H^{\circ}_{6\frac{1}{2}}$	4
3854.674	1	25935.17	−0.02	$a\ {}^2H_{4\frac{1}{2}}$—$x\ {}^2H^{\circ}_{4\frac{1}{2}}$	
3855.114	4*h*	25932.24	−0.03	$b\ {}^4P_{1\frac{1}{2}}$—$z\ {}^2D^{\circ}_{1\frac{1}{2}}$	
3856.539	50	25922.66	0.11	$a\ {}^4P_{2\frac{1}{2}}$—$y\ {}^4D^{\circ}_{3\frac{1}{2}}$	4
3857.280	1	25917.68	−0.19	$b\ {}^4G_{4\frac{1}{2}}$—$z\ {}^2H^{\circ}_{4\frac{1}{2}}$	
3857.563	1*h*	25915.78	−0.06	$a\ {}^4F_{3\frac{1}{2}}$—$x\ {}^4H^{\circ}_{3\frac{1}{2}}$	
			−0.06	$a\ {}^2F_{3\frac{1}{2}}$—$x\ {}^2G^{\circ}_{4\frac{1}{2}}$	
3857.753	1	25914.51	0.00	$a\ {}^4F_{3\frac{1}{2}}$—$x\ {}^4H^{\circ}_{4\frac{1}{2}}$	
3858.749	5	25907.82	0.15	$a\ {}^4P_{2\frac{1}{2}}$—$y\ {}^4D^{\circ}_{2\frac{1}{2}}$	
3859.397	1	25903.47	0.03	$a\ {}^4G_{5\frac{1}{2}}$—$x\ {}^6F^{\circ}_{5\frac{1}{2}}$	
3860.258	3*h*	25897.69	0.09	$a\ {}^4F_{3\frac{1}{2}}$—$w\ {}^4F^{\circ}_{4\frac{1}{2}}$	
3862.320	1*h*	25883.86	0.11	$a\ {}^4G_{4\frac{1}{2}}$—$x\ {}^6F^{\circ}_{5\frac{1}{2}}$	
3865.672	20	25861.42	0.21	$a\ {}^4P_{1\frac{1}{2}}$—$y\ {}^4D^{\circ}_{2\frac{1}{2}}$	
3866.574	2	25855.39	0.20	$a\ {}^4P_{1\frac{1}{2}}$—$y\ {}^4D^{\circ}_{1\frac{1}{2}}$	
3868.535	1	25842.28	0.05	$a\ {}^4F_{2\frac{1}{2}}$—$x\ {}^4H^{\circ}_{3\frac{1}{2}}$	
3870.822	4	25827.01	−0.22	$b\ {}^4G_{4\frac{1}{2}}$—$w\ {}^4H^{\circ}_{5\frac{1}{2}}$	
3871.345	1H	25823.52	0.00	$a\ {}^2G_{4\frac{1}{2}}$—$u\ {}^4F^{\circ}_{4\frac{1}{2}}$	
3871.671	6*h*	25821.34	0.00	$a\ {}^4P_{0\frac{1}{2}}$—$y\ {}^4D^{\circ}_{1\frac{1}{2}}$	
2871.953	2	25819.47	0.00	$a\ {}^4P_{0\frac{1}{2}}$—$y\ {}^4D^{\circ}_{0\frac{1}{2}}$	
3872.127	10	25818.31	−0.20	$b\ {}^4G_{4\frac{1}{2}}$—$y\ {}^2H^{\circ}_{5\frac{1}{2}}$	
3873.200	10	25811.16	−0.11	$b\ {}^4G_{3\frac{1}{2}}$—$z\ {}^2H^{\circ}_{4\frac{1}{2}}$	
3874.743	1*h*	25800.87	0.15	$a\ {}^4F_{4\frac{1}{2}}$—$z\ {}^2G^{\circ}_{3\frac{1}{2}}$?	
3876.712	3	25787.77	−0.05	$a\ {}^4F_{2\frac{1}{2}}$—$w\ {}^4F^{\circ}_{3\frac{1}{2}}$	
3878.155	5*h*	25778.18	−0.06	$a\ {}^2G_{3\frac{1}{2}}$—67008$^{\circ}_{2\frac{1}{2}}$	
3883.249	20	25744.36	0.10	$b\ {}^2I_{6\frac{1}{2}}$—$z\ {}^2K^{\circ}_{7\frac{1}{2}}$	4
3887.380	2	25717.00	−0.29	$b\ {}^4G_{4\frac{1}{2}}$—$y\ {}^2H^{\circ}_{4\frac{1}{2}}$	
3888.841	7	25707.35	−0.04	$b\ {}^4G_{3\frac{1}{2}}$—$w\ {}^4H^{\circ}_{4\frac{1}{2}}$	
3889.461	20	25703.25	0.00	$b\ {}^2I_{5\frac{1}{2}}$—$z\ {}^2K^{\circ}_{6\frac{1}{2}}$	5
3891.624	5	25688.96	−0.04	$a\ {}^4H_{6\frac{1}{2}}$—$z\ {}^2I^{\circ}_{5\frac{1}{2}}$	
3892.621	15	25682.38	0.05	$a\ {}^4P_{2\frac{1}{2}}$—$x\ {}^6D^{\circ}_{2\frac{1}{2},1\frac{1}{2}}$	
3893.199	1	25678.57	−0.04	$b\ {}^4P_{1\frac{1}{2}}$—$w\ {}^4D^{\circ}_{0\frac{1}{2}}$	
3894.714	60	25668.58	0.02	$a\ {}^4P_{2\frac{1}{2}}$—$x\ {}^6D^{\circ}_{3\frac{1}{2}}$	4
3896.339	20	25657.87	−0.29	$b\ {}^4G_{4\frac{1}{2}}$—$z\ {}^2H^{\circ}_{5\frac{1}{2}}$	4
			−0.29	$b\ {}^4G_{4\frac{1}{2}}$—$x\ {}^2F^{\circ}_{3\frac{1}{2}}$	
3896.743	2*h*	25655.21	−0.10	$b\ {}^4P_{2\frac{1}{2}}$—$v\ {}^4D^{\circ}_{2\frac{1}{2}}$	
			−0.09	$a\ {}^4F_{1\frac{1}{2}}$—$w\ {}^4F^{\circ}_{2\frac{1}{2}}$	
3898.368	50*c*	25644.52	−0.13	$b\ {}^4P_{2\frac{1}{2}}$—$v\ {}^4D^{\circ}_{3\frac{1}{2}}$	4

TABLE 1. Mn I—*Classified lines*—Continued

1	2	3	4	5	6
λ	Int.	σ	o−c	Term designation	Zeeman type
Å Air		K	K		
3899. 336	10	25638. 15	−0. 13	$b\ {}^4P_{1½}$—$z\ {}^2D^{\circ}_{2½}$	4
3899. 620	30	25636. 29	0. 42	$a\ {}^4P_{1½}$—$x\ {}^6D^{\circ}_{2½, 1½}$	
3903. 525	10	25610. 64	−0. 05	$b\ {}^4G_{3½}$—$y\ {}^2H^{\circ}_{4½}$	
3904. 328	20	25605. 37	−0. 15	$b\ {}^4G_{2½}$—$w\ {}^4H^{\circ}_{3½}$	5
3904. 852	15	25601. 94	−0. 08	$a\ {}^4P_{0½}$—$x\ {}^6D^{\circ}_{1½}$	P−B
3904. 967	15	25601. 18	−0. 07	$a\ {}^4P_{0½}$—$x\ {}^6D^{\circ}_{0½}$	P−B
3905. 237	5*h*	25599. 42	−0. 02	$a\ {}^2G_{4½}$—$v\ {}^2G^{\circ}_{4½}$	6, 7*b*
3907. 815	1	25582. 53	−0. 10	$b\ {}^4G_{3½}$—63319$^{\circ}_{3½}$	
3909. 795	3H	25569. 57	−0. 03	$b\ {}^4D_{3½}$—55923$^{\circ}_{2½}$	
3910. 222	5H	25566. 78	0. 00	$z\ {}^4P^{\circ}_{2½}$—$i\ {}^6D_{1½}$	
3911. 144	20*hw*	25560. 75	−0. 05	$z\ {}^4P^{\circ}_{2½}$—$e\ {}^4D_{2½}$	
3911. 425	20*c*	25558. 92	−0. 04	$b\ {}^4P^{\circ}_{2½}$—$u\ {}^4P^{\circ}_{1½}$	6, 7*b*
3912. 553	1	25551. 55	−0. 01	$b\ {}^4G_{3½}$—$x\ {}^2F^{\circ}_{3½}$	
3912. 754	5	25550. 24	−0. 14	$b\ {}^4P_{0½}$—$z\ {}^2D^{\circ}_{1½}$	4
3914. 210	5H*lwd*	25540. 73	−0. 38	$z\ {}^4P^{\circ}_{0½}$—$i\ {}^6D_{0½}$	
3916. 407	6*h*	25526. 40	0. 00	$b\ {}^4P_{1½}$—$w\ {}^4D^{\circ}_{1½}$	6
3916. 601	10H*w*	25525. 14	−0. 07	$z\ {}^4P^{\circ}_{1½}$—$e\ {}^4D_{1½}$	
3918. 319	60*c*	25513. 95	−0. 11 −0. 07	$b\ {}^4P_{2½}$—$w\ {}^4D^{\circ}_{3½}$ $a\ {}^4H_{6½}$—$x\ {}^4G^{\circ}_{5½}$	4 4
3919. 332	3	25507. 36	−0. 16	$a\ {}^2G_{3½}$—$v\ {}^2G^{\circ}_{3½}$?	6, 7*b*
3920. 657	1	25498. 74	−0. 11	$b\ {}^4G_{2½}$—$x\ {}^2F^{\circ}_{3½}$	
3921. 766	30H*w*	25491. 52	0. 01	$z\ {}^4P^{\circ}_{1½}$—$i\ {}^6D_{1½}$	P−B
3922. 066	10H	25489. 57	−0. 07	$z\ {}^4P^{\circ}_{2½}$—$i\ {}^6D_{2½}$	P−B
3922. 681	40H*w*	25485. 58	0. 05	$z\ {}^4P^{\circ}_{1½}$—$e\ {}^4D_{2½}$	
3923. 325	30	25481. 39	−0. 03	$a\ {}^4H_{5½}$—$x\ {}^4G^{\circ}_{4½}$	4
3924. 075	40H	25476. 52	−0. 16	$z\ {}^4P^{\circ}_{0½}$—$e\ {}^4D_{1½}$	
3925. 912	4	25464. 60	−0. 14	$b\ {}^4P_{2½}$—$x\ {}^4F^{\circ}_{3½}$	4
3926. 476	100H*w*	25460. 95	0. 02	$z\ {}^4P^{\circ}_{2½}$—$e\ {}^4D_{3½}$	
3928. 314	6	25449. 03	−0. 12	$a\ {}^2H_{5½}$—$w\ {}^4H^{\circ}_{5½}$	6
3929. 248	30H*w*	25443. 02	0. 04	$z\ {}^4P^{\circ}_{0½}$—$i\ {}^6D_{1½}$	
3929. 662	20	25440. 30	−0. 11	$a\ {}^4H_{4½}$—$x\ {}^4G^{\circ}_{3½}$	4
3931. 517	10	25428. 30	−0. 01	$a\ {}^2H_{4½}$—$z\ {}^2H^{\circ}_{4½}$	6, 7*b*
3933. 666	50H*w*	25414. 42	0. 05	$z\ {}^4P^{\circ}_{1½}$—$i\ {}^6D_{2½}$	
3935. 544	10	25402. 28	−0. 10	$a\ {}^4H_{5½}$—$x\ {}^4G^{\circ}_{5½}$	6
3936. 766	30	25394. 40	−0. 03	$a\ {}^4H_{3½}$—$x\ {}^4G^{\circ}_{2½}$	5
3937. 763	10	25387. 97	−0. 07	$a\ {}^4H_{4½}$—$x\ {}^4G^{\circ}_{4½}$	6
3941. 951	7	25360. 99	−0. 05	$a\ {}^4H_{3½}$—$x\ {}^4G^{\circ}_{3½}$	
3942. 881	50H*wl*	25355. 01	−0. 05	$z\ {}^4P^{\circ}_{2½}$—$i\ {}^6D_{3½}$	4
3943. 719	1	25349. 63	−0. 14	$b\ {}^4G_{2½}$—$x\ {}^2F^{\circ}_{3½}$	
3951. 977	20	25296. 66	−0. 06	$b\ {}^4P_{0½}$—$w\ {}^4D^{\circ}_{0½}$	6
3952. 842	100	25291. 12	0. 01	$b\ {}^4P_{2½}$—$u\ {}^4P^{\circ}_{2½}$	6
3954. 579	10	25280. 01	−0. 07	$a\ {}^2H_{5½}$—$z\ {}^2H^{\circ}_{5½}$	6
3955. 314	1	25275. 31	0. 04	$a\ {}^2H_{4½}$—$w\ {}^4H^{\circ}_{3½}$	
3958. 603	1*h*	25254. 32	−0. 03	$a\ {}^2H_{4½}$—63374$^{\circ}_{4½}$	
3959. 138	1	25250. 90	0. 18	$e\ {}^6S_{2½}$—66654$^{\circ}_{2½}$	
3962. 776	1	25227. 73	0. 00	$a\ {}^2H_{4½}$—$y\ {}^2H^{\circ}_{4½}$	
3972. 077	1	25168. 65	0. 05 0. 05	$a\ {}^2H_{4½}$—$z\ {}^2H^{\circ}_{5½}$ $a\ {}^2H_{4½}$—$x\ {}^2F^{\circ}_{3½}$	
3975. 880	40	25144. 58	0. 07	$b\ {}^4P_{0½}$—$w\ {}^4D^{\circ}_{1½}$	4
3977. 076	50	25137. 02	0. 04	$b\ {}^4P_{1½}$—$w\ {}^4D^{\circ}_{2½}$	4
3978. 781	2*h*	25126. 24	0. 00	$a\ {}^4H_{4½}$—$v\ {}^4D^{\circ}_{3½}$	
3980. 142	10	25117. 65	0. 03	$a\ {}^2G_{4½}$—$u\ {}^2F^{\circ}_{3½}$	4

TABLE 1. Mn I—*Classified lines*—Continued

1	2	3	4	5	6
λ	Int.	σ	o−c	Term designation	Zeeman type
Å Air		*K*	*K*		
3982.164	30	25104.90	−0.02	$b\ {}^4P_{1\frac{1}{2}}$—$u\ {}^4P^\circ_{0\frac{1}{2}}$	P−B
3982.576	100	25102.30	0.07	$a\ {}^4G_{2\frac{1}{2}}$—$y\ {}^4F^\circ_{1\frac{1}{2}}$	
3982.900	40	25100.26	−0.02	$e\ {}^6S_{2\frac{1}{2}}$—66504$i^\circ_{1\frac{1}{2}}$	
3984.172	20	25092.25	0.06	$a\ {}^4G_{2\frac{1}{2}}$—$y\ {}^4F^\circ_{2\frac{1}{2}}$	P−B
3985.236	100	25085.55	0.06	$a\ {}^4G_{3\frac{1}{2}}$—$y\ {}^4F^\circ_{2\frac{1}{2}}$	
3986.377	2	25078.34	0.10	$a\ {}^4G_{2\frac{1}{2}}$—$y\ {}^4F^\circ_{3\frac{1}{2}}$	4
3986.822	200	25075.57	0.01	$a\ {}^4G_{5\frac{1}{2}}$—$y\ {}^4F^\circ_{4\frac{1}{2}}$	4
3987.092	100	25073.87	0.02	$a\ {}^4G_{4\frac{1}{2}}$—$y\ {}^4F^\circ_{3\frac{1}{2}}$	P−B
3987.455	20	25071.59	0.05	$a\ {}^4G_{3\frac{1}{2}}$—$y\ {}^4F^\circ_{3\frac{1}{2}}$	P−B
3988.666	8	25063.98	−0.01	$b\ {}^4P_{1\frac{1}{2}}$—$v\ {}^4D^\circ_{0\frac{1}{2}}$	
3989.699	1	25057.49	−0.04	$a\ {}^4H_{3\frac{1}{2}}$—$v\ {}^4D^\circ_{2\frac{1}{2}}$	6
3989.952	30	25055.90	0.03	$a\ {}^4G_{4\frac{1}{2}}$—$y\ {}^4F^\circ_{4\frac{1}{2}}$	
3990.737	1	25050.97	0.04	$b\ {}^4D_{3\frac{1}{2}}$—$w\ {}^4P^\circ_{2\frac{1}{2}}$	
3991.596	20	25045.58	0.12	$b\ {}^4D_{0\frac{1}{2}}$—$w\ {}^4P^\circ_{0\frac{1}{2}}$	P−B
3993.858	6	25031.40	−0.09	$b\ {}^4D_{1\frac{1}{2}}$—$w\ {}^4P^\circ_{0\frac{1}{2}}$	
3995.012	1*h*	25024.17	0.06	$b\ {}^4G_{3\frac{1}{2}}$—$w\ {}^6D^\circ_{3\frac{1}{2}}$?	
3996.101	5H*s*	25017.34	−0.09	$b\ {}^4P_{1\frac{1}{2}}$—$v\ {}^4D^\circ_{2\frac{1}{2}}$	4
3997.771	3*h*	25006.89	−0.03	$a\ {}^4H_{5\frac{1}{2}}$—$x\ {}^4F^\circ_{4\frac{1}{2}}$	
3999.573	1*h*	24995.63	−0.02	$a\ {}^4H_{4\frac{1}{2}}$—$w\ {}^4D^\circ_{3\frac{1}{2}}$	
4001.190	15	24985.52	−0.01	$b\ {}^4D_{2\frac{1}{2}}$—$w\ {}^4P^\circ_{2\frac{1}{2}}$	P−B
4002.169	15	24979.42	−0.01	$b\ {}^4D_{1\frac{1}{2}}$—$w\ {}^4P^\circ_{1\frac{1}{2}}$	P−B
4002.559	1	24976.98	0.05	$a\ {}^4F_{1\frac{1}{2}}$—$w\ {}^4D^\circ_{0\frac{1}{2}}$	
4003.258	20H*l*	24972.63	0.05	$b\ {}^4G_{5\frac{1}{2}}$—$v\ {}^4F^\circ_{4\frac{1}{2}}$	
4005.775	1	24956.93	0.01	$b\ {}^4D_{0\frac{1}{2}}$—$w\ {}^4P^\circ_{1\frac{1}{2}}$	
4007.041	10	24949.04	−0.01	$b\ {}^4D_{2\frac{1}{2}}$—$w\ {}^4P^\circ_{1\frac{1}{2}}$	P−B
4008.022	20	24942.94	−0.01	$b\ {}^4D_{1\frac{1}{2}}$—$w\ {}^4P^\circ_{1\frac{1}{2}}$	P−B
4011.535	30	24921.09	0.01	$b\ {}^4P_{1\frac{1}{2}}$—$u\ {}^4P^\circ_{1\frac{1}{2}}$	6
4011.913	10*h*	24918.75	−0.05	$a\ {}^2G_{3\frac{1}{2}}$—$u\ {}^2F^\circ_{3\frac{1}{2}}$	6
4012.761	2	24913.48	−0.06	$a\ {}^4H_{4\frac{1}{2}}$—$x\ {}^4F^\circ_{4\frac{1}{2}}$	
4016.671	5	24889.23	0.05	$a\ {}^4F_{4\frac{1}{2}}$—$z\ {}^2I^\circ_{5\frac{1}{2}}$	4
4018.106	1000*h*	24880.34	−0.01	$a\ {}^6D_{4\frac{1}{2}}$—$z\ {}^6D^\circ_{3\frac{1}{2}}$	4
4018.583	2*h*	24877.39	−0.05	$a\ {}^2G_{4\frac{1}{2}}$—$v\ {}^4G^\circ_{5\frac{1}{2}}$	5
4020.072	10	24868.17	0.00	$b\ {}^4D_{0\frac{1}{2}}$—$x\ {}^4D^\circ_{1\frac{1}{2}}$	
4021.354	2	24860.25	−0.05	$b\ {}^4D_{2\frac{1}{2}}$—$x\ {}^4D^\circ_{1\frac{1}{2}}$	
4022.335	2*h*	24854.18	−0.02 −0.04	$b\ {}^4D_{1\frac{1}{2}}$—$x\ {}^4D^\circ_{1\frac{1}{2}}$ $a\ {}^2F_{3\frac{1}{2}}$—63523$^\circ_{2\frac{1}{2}}$	
4023.719	1	24845.63	0.02	$a\ {}^4F_{4\frac{1}{2}}$—$x\ {}^4G^\circ_{3\frac{1}{2}}$	5
4025.938	4	24831.94	−0.02	$b\ {}^4D_{3\frac{1}{2}}$—$x\ {}^4D^\circ_{2\frac{1}{2}}$	4
4026.437	80	24828.86	0.00	$a\ {}^4G_{5\frac{1}{2}}$—$z\ {}^4H^\circ_{6\frac{1}{2}}$	6
4028.595	5H	24815.56	−0.01	$a\ {}^4G_{5\frac{1}{2}}$—$z\ {}^4H^\circ_{5\frac{1}{2}}$	4
4030.755	20000R*w*	24802.26	0.01	$a\ {}^6S_{2\frac{1}{2}}$—$z\ {}^6P^\circ_{3\frac{1}{2}}$	
4031.791	100	24795.89	0.01	$a\ {}^4G_{4\frac{1}{2}}$—$z\ {}^4H^\circ_{5\frac{1}{2}}$	6
4033.068	15000R*w*	24788.04	−0.01	$a\ {}^6S_{2\frac{1}{2}}$—$z\ {}^6P^\circ_{2\frac{1}{2}}$	
4033.587	4	24784.85	0.00	$a\ {}^4G_{3\frac{1}{2}}$—$z\ {}^4H^\circ_{4\frac{1}{2}}$	
4033.652	3	24784.45	0.03	$a\ {}^4G_{2\frac{1}{2}}$—$z\ {}^4H^\circ_{3\frac{1}{2}}$	
4034.485	10000R*w*	24779.33	0.01	$a\ {}^6S_{2\frac{1}{2}}$—$z\ {}^6P^\circ_{1\frac{1}{2}}$	4
4035.729	1000	24771.70	−0.03	$a\ {}^6D_{3\frac{1}{2}}$—$z\ {}^6D^\circ_{2\frac{1}{2}}$	4
4036.244	4	24768.51	−0.22	$a\ {}^2P_{1\frac{1}{2}}$—$z\ {}^2P^\circ_{1\frac{1}{2}}$	
4036.562	5	24766.58	0.02	$b\ {}^4D_{2\frac{1}{2}}$—$x\ {}^4D^\circ_{2\frac{1}{2}}$	
4037.561	5	24760.45	−0.01	$b\ {}^4D_{1\frac{1}{2}}$—$x\ {}^4D^\circ_{2\frac{1}{2}}$	
4038.728	20	24753.30	−0.01	$b\ {}^4D_{3\frac{1}{2}}$—$x\ {}^4D^\circ_{3\frac{1}{2}}$	6, 7*b*
4039.250	1H*l*	24750.10	−0.04	$b\ {}^4G_{3\frac{1}{2}}$—$v\ {}^4F^\circ_{2\frac{1}{2}}$	
4040.424	2	24742.95	0.01	$a\ {}^4F_{3\frac{1}{2}}$—$x\ {}^4G^\circ_{3\frac{1}{2}}$	
4041.357	2000*h*	24737.20	0.01	$a\ {}^6D_{4\frac{1}{2}}$—$z\ {}^6D^\circ_{4\frac{1}{2}}$	6, 7*b*
4043.682	1*h*	24722.98	−0.05	$b\ {}^4P_{0\frac{1}{2}}$—$u\ {}^4P^\circ_{0\frac{1}{2}}$	
4045.115	50	24714.22	0.02	$a\ {}^4F_{4\frac{1}{2}}$—$x\ {}^4G^\circ_{5\frac{1}{2}}$	4

TABLE 1. Mn I—*Classified lines*—Continued

1	2	3	4	5	6
λ	Int.	σ	o−c	Term designation	Zeeman type
Å Air		*K*	*K*		
4045. 203	50	24713. 68	−0. 04	$a\ ^4H_{6½}$—$z\ ^4I^o_{7½}$	4
4046. 711	1*h*	24704. 47	−0. 04	$a\ ^4H_{6½}$—$z\ ^4I^o_{6½}$	
4046. 996	3	24702. 73	0. 01	$a\ ^4F_{2½}$—$x\ ^4G^o_{2½}$	6
4048. 747	1000*h*	24692. 05	0. 00	$a\ ^6D_{2½}$—$z\ ^6D^o_{1½}$	4, C
4048. 998	40	24690. 52	−0. 05	$a\ ^4F_{3½}$—$x\ ^4G^o_{4½}$	4
4049. 423	1*h*	24687. 93	0. 02	$b\ ^4D_{2½}$—$x\ ^4D^o_{3½}$	
4050. 306	1	24682. 54	−0. 09	$b\ ^4P_{0½}$—$v\ ^4D^o_{1½}$	
4051. 255	2*h*	24676. 76	−0. 03	$a\ ^4D_{2½}$—$y\ ^6F^o_{3½}$	
4052. 476	50	24669. 33	0. 00	$a\ ^4F_{2½}$—$x\ ^4G^o_{3½}$	4
4055. 215	20	24652. 67	0. 02	$a\ ^4F_{1½}$—$x\ ^4G^o_{2½}$	5
4055. 548	1000*h*	24650. 64	0. 00	$a\ ^6D_{3½}$—$z\ ^6D^o_{3½}$	6, 7*b*
4057. 954	100*hl*	24636. 03	0. 00	$z\ ^6P^o_{1½}$—$f\ ^6S_{2½}$	4
4058. 936	500	24630. 06	−0. 02	$a\ ^6D_{1½}$—$z\ ^6D^o_{0½}$	4, C
4059. 388	150*hl*	24627. 32	0. 02	$z\ ^6P^o_{2½}$—$f\ ^6S_{2½}$	6
4061. 737	200*hl*	24613. 09	−0. 01	$z\ ^6P^o_{3½}$—$f\ ^6S_{2½}$	4
4063. 530	400	24602. 22	0. 01	$a\ ^6D_{2½}$—$z\ ^6D^o_{3½}$	6, 7*b*
4065. 083	100	24592. 82	−0. 05	$a\ ^4H_{5½}$—$z\ ^4I^o_{6½}$	
4066. 235	10	24585. 86	−0. 03	$a\ ^2G_{4½}$—$v\ ^2F^o_{3½}$	5
4067. 238	5	24579. 79	0. 00	$a\ ^2I_{6½}$—61744$^o_{5½}$	
4068. 011	100	24575. 10	0. 01	$a\ ^6D_{1½}$—$z\ ^6D^o_{1½}$	6, 7*b*
4070. 280	200	24561. 42	0. 01	$a\ ^6D_{0½}$—$z\ ^6D^o_{0½}$	6, 7C
4070. 682	2*h*	24559. 00	0. 02	$a\ ^4F_{3½}$—$w\ ^4D^o_{2½}$	
4071. 949	1	24551. 36	−0. 03	$a\ ^4D_{1½}$—$y\ ^6F^o_{2½}$	
4073. 976	10	24539. 14	−0. 05	$b\ ^4P_{0½}$—$u\ ^4P^o_{1½}$	4
4075. 251	40*h*	24531. 46	0. 02	$a\ ^4F_{4½}$—$v\ ^4D^o_{3½}$	4
4076. 708	2	24522. 70	−0. 06	$a\ ^4H_{4½}$—$z\ ^4I^o_{4½}$	
4079. 241	500	24507. 47	−0. 01 −0. 12	$a\ ^6D_{3½}$—$z\ ^6D^o_{4½}$ $a\ ^4H_{4½}$—$z\ ^4I^o_{5½}$	5
4079. 415	500	24506. 34	−0. 08	$a\ ^6D_{0½}$—$z\ ^6D^o_{1½}$	4, C
4082. 945	600	24485. 24	−0. 01	$a\ ^6D_{1½}$—$z\ ^6D^o_{2½}$	4, C
4083. 634	500	24481. 11	−0. 01	$a\ ^6D_{2½}$—$z\ ^6D^o_{3½}$	4
4085. 480	1	24470. 04	−0. 06	$a\ ^2F_{3½}$—$x\ ^2F^o_{3½}$	
4087. 073	1	24460. 51	0. 00	$a\ ^2F_{2½}$—$w\ ^4H^o_{3½}$	
4087. 617	1H	24457. 25	−0. 07	$a\ ^4D_{3½}$—$y\ ^6D^o_{2½}$	
4088. 565	6	24451. 58	−0. 02	$b\ ^2I_{6½}$—$w\ ^2H^o_{5½}$	
4089. 941	60	24443. 36	−0. 03	$a\ ^4H_{3½}$—$z\ ^4I^o_{4½}$	5
4090. 618	10	24439. 31	−0. 1?	$a\ ^4F_{3½}$—$v\ ^4D^o_{2½}$	4
4090. 910	3	24437. 57	0. 00	$b\ ^2I_{5½}$—$w\ ^2H^o_{4½}$	
4092. 388	40*h*	24428. 74	−0. 03	$a\ ^4F_{3½}$—$v\ ^4D^o_{3½}$	6
4094. 070	6	24418. 70	−0. 13	$a\ ^2G_{3½}$—$v\ ^2F^o_{2½}$	
4095. 052	10	24412. 85	−0. 06	$a\ ^4F_{2½}$—$v\ ^4D^o_{1½}$	4
4095. 252	30	24411. 66	−0. 02	$a\ ^2F_{3½}$—$y\ ^2D^o_{2½}$	4
4096. 676	5	24403. 17	−0. 25	$b\ ^4G_{4½}$—$y\ ^2F^o_{3½}$	
4099. 399	8	24386. 96	−0. 11	$a\ ^2G_{3½}$—$v\ ^2F^o_{3½}$	6
4099. 899	5*h*	24383. 99	−0. 13	$a\ ^2H_{5½}$—$v\ ^4F^o_{4½}$	
4102. 970	30	24365. 74	−0. 08	$a\ ^4F_{2½}$—$v\ ^4D^o_{2½}$	6
4103. 463	10	24362. 81	−0. 03	$a\ ^4F_{1½}$—$v\ ^4D^o_{1½}$	P−B
4103. 560	5	24362. 22	−0. 09	$a\ ^4F_{1½}$—$v\ ^4D^o_{0½}$	P−B
4105. 365	60*c*	24351. 52	−0. 01	$a\ ^4F_{4½}$—$x\ ^4F^o_{3½}$	5
4107. 873	10	24336. 66	−0. 02	$a\ ^2I_{5½}$—$w\ ^4G^o_{4½}$	4
4110. 802	30	24319. 32	−0. 03	$a\ ^4F_{3½}$—$x\ ^4F^o_{2½}$	

TABLE 1. Mn I—*Classified lines*—Continued

1	2	3	4	5	6
λ	Int.	σ	o−c	Term designation	Zeeman type
Å Air		K	K		
4110.894	60*c*	24318.77	0.03	$a\ ^4F_{4\frac{1}{2}}$—$x\ ^4F^\circ_{4\frac{1}{2}}$	6, 7
4111.416	2	24315.68	−0.07	$a\ ^4F_{1\frac{1}{2}}$—$v\ ^4D^\circ_{2\frac{1}{2}}$	
4113.243	30	24304.88	0.10 −0.08	$a\ ^4P_{1\frac{1}{2}}$—$x\ ^4P^\circ_{0\frac{1}{2}}$ ($a\ ^2I_{6\frac{1}{2}}$—$w\ ^4G^\circ_{5\frac{1}{2}}$)	4
4113.880	20	24301.12	−0.05	$a\ ^4F_{2\frac{1}{2}}$—$x\ ^4F^\circ_{1\frac{1}{2}}$	5
4114.381	25	24298.16	−0.02	$a\ ^4F_{3\frac{1}{2}}$—$w\ ^4D^\circ_{3\frac{1}{2}}$	6
4114.594	10H*l*	24296.90	0.08	$b\ ^4G_{3\frac{1}{2}}$—$y\ ^2F^\circ_{3\frac{1}{2}}$	
4115.033	1*h*	24294.31	0.03	$b\ ^4G_{5\frac{1}{2}}$—$y\ ^2G^\circ_{4\frac{1}{2}}$	
4116.598	8H*l*	24285.08	−0.01	$b\ ^4G_{2\frac{1}{2}}$—$y\ ^2F^\circ_{2\frac{1}{2}}$	6, 7*b*
4119.010	5	24270.85	−0.08	$a\ ^4P_{0\frac{1}{2}}$—$x\ ^4P^\circ_{0\frac{1}{2}}$	
4122.367	20	24251.09	−0.01	$a\ ^4F_{1\frac{1}{2}}$—$x\ ^4F^\circ_{1\frac{1}{2}}$	
4122.757	12	24248.80	−0.06	$a\ ^4F_{3\frac{1}{2}}$—$x\ ^4F^\circ_{3\frac{1}{2}}$	
4123.280	15	24245.72	−0.02	$a\ ^4F_{2\frac{1}{2}}$—$x\ ^4F^\circ_{2\frac{1}{2}}$	
4123.542	20	24244.18	0.07	$a\ ^4P_{2\frac{1}{2}}$—$x\ ^4P^\circ_{1\frac{1}{2}}$	
4125.415	1*h*	24233.17	−0.06	$a\ ^4D_{2\frac{1}{2}}$—$w\ ^6P^\circ_{1\frac{1}{2}}$	
4125.813	8*c*	24230.83	0.03	$a\ ^2G_{4\frac{1}{2}}$—$w\ ^2G^\circ_{4\frac{1}{2}}$	6
4126.710	1*h*	24225.57	0.25	$a\ ^4D_{2\frac{1}{2}}$—$y\ ^6D^\circ_{3\frac{1}{2}}$	
4126.876	1	24224.60	0.03	$a\ ^4F_{2\frac{1}{2}}$—$w\ ^4D^\circ_{3\frac{1}{2}}$	
4127.751	1	24219.46	0.06	$a\ ^4F_{1\frac{1}{2}}$—$u\ ^4P^\circ_{1\frac{1}{2}}$	
4130.256	2*h*	24204.77	−0.02 0.01	$a\ ^4D_{2\frac{1}{2}}$—$y\ ^6D^\circ_{2\frac{1}{2}}$ $a\ ^2F_{2\frac{1}{2}}$—$x\ ^2F^\circ_{2\frac{1}{2}}$	
4131.111	150	24199.76	−0.03	$a\ ^4H_{6\frac{1}{2}}$—$y\ ^4H^\circ_{6\frac{1}{2}}$	6, 7*b*
4131.449	10	24197.78	0.13	$a\ ^4P_{1\frac{1}{2}}$—$x\ ^4P^\circ_{1\frac{1}{2}}$	6, 7*b*
4132.282	6	24192.90	0.13	$z\ ^4F^\circ_{3\frac{1}{2}}$—$f\ ^4G_{4\frac{1}{2}}$	4
4134.619	20	24179.23	0.06	$a\ ^2F_{2\frac{1}{2}}$—$y\ ^2D^\circ_{1\frac{1}{2}}$	5
4135.034	100	24176.80	0.02	$a\ ^4H_{5\frac{1}{2}}$—$y\ ^4H^\circ_{5\frac{1}{2}}$	6, 7*b*
4137.266	40	24163.76	−0.04	$a\ ^4P_{0\frac{1}{2}}$—$x\ ^4P^\circ_{1\frac{1}{2}}$	4
4141.063	100	24141.60	−0.02	$a\ ^4H_{4\frac{1}{2}}$—$y\ ^4H^\circ_{4\frac{1}{2}}$	6, 7*b*
4147.529	60	24103.97	0.10	$a\ ^4P_{2\frac{1}{2}}$—$x\ ^4P^\circ_{2\frac{1}{2}}$	6, 7*b*
4148.796	80	24096.61	−0.02	$a\ ^4H_{3\frac{1}{2}}$—$y\ ^4H^\circ_{3\frac{1}{2}}$	6, 7*b*
4149.648	1H	24091.66	−0.07	$a\ ^2F_{3\frac{1}{2}}$—$w\ ^6D^\circ_{2\frac{1}{2}}$	
4150.262	1	24088.10	−0.05	$a\ ^4H_{5\frac{1}{2}}$—$y\ ^4H^\circ_{5\frac{1}{2}}$	
4151.023	10*hl*	24083.68	0.28 −0.22	$a\ ^4H_{4\frac{1}{2}}$—$y\ ^4H^\circ_{5\frac{1}{2}}$ $b\ ^4G_{4\frac{1}{2}}$—$y\ ^2G^\circ_{4\frac{1}{2}}$	
4151.663	3*h*	24079.97	−0.39	$b\ ^4G_{4\frac{1}{2}}$—$z\ ^2F^\circ_{3\frac{1}{2}}$	
4152.556	1	24074.79	−0.04	$a\ ^2G_{3\frac{1}{2}}$—$w\ ^2G^\circ_{3\frac{1}{2}}$	
4154.218	1	24065.16	0.06	$b\ ^4G_{5\frac{1}{2}}$—$w\ ^4G^\circ_{4\frac{1}{2}}$	
4154.631	2	24062.76	−0.15	$a\ ^4D_{1\frac{1}{2}}$—$w\ ^6P^\circ_{1\frac{1}{2}}$	
4154.726	1	24062.22	−0.03	$a\ ^4H_{3\frac{1}{2}}$—$y\ ^4H^\circ_{4\frac{1}{2}}$	
4155.525	40	24057.59	0.18	$a\ ^4P_{1\frac{1}{2}}$—$x\ ^4P^\circ_{2\frac{1}{2}}$	4
4157.019	60	24048.94	−0.03 0.22	$b\ ^4G_{5\frac{1}{2}}$—$w\ ^4G^\circ_{5\frac{1}{2}}$ $b\ ^4G_{3\frac{1}{2}}$—$y\ ^2G^\circ_{3\frac{1}{2}}$?	6
4158.692	8	24039.24	−0.03	$a\ ^2P_{0\frac{1}{2}}$—$z\ ^2P^\circ_{0\frac{1}{2}}$	6
4159.957	1	24031.96	−0.02	$a\ ^2G_{3\frac{1}{2}}$—$w\ ^2G^\circ_{4\frac{1}{2}}$	
4164.979	10*h*	24002.96	−0.02	$a\ ^2P_{0\frac{1}{2}}$—$z\ ^2P^\circ_{1\frac{1}{2}}$	5
4166.208	6	23995.90	−0.11	$b\ ^4G_{2\frac{1}{2}}$—$y\ ^2G^\circ_{3\frac{1}{2}}$	
4167.197	2*h*	23990.21	−0.03	$b\ ^4G_{3\frac{1}{2}}$—$z\ ^2F^\circ_{2\frac{1}{2}}$	
4169.440	1*h*	23977.30	0.00	$b\ ^4G_{3\frac{1}{2}}$—$y\ ^2G^\circ_{4\frac{1}{2}}$	
4175.891	2*h*	23940.26	0.26	$a\ ^4D_{1\frac{1}{2}}$—$w\ ^6P^\circ_{2\frac{1}{2}}$	
4176.608	100*c*	23936.15	−0.03	$a\ ^4H_{6\frac{1}{2}}$—$y\ ^4G^\circ_{5\frac{1}{2}}$	4
4179.875	4*h*	23917.44	−0.02	$a\ ^4D_{2\frac{1}{2}}$—$y\ ^6D^\circ_{1\frac{1}{2}}$	
4182.254	20H*w*	23903.84	−0.03	$a\ ^2H_{5\frac{1}{2}}$—$y\ ^2I^\circ_{6\frac{1}{2}}$	
4184.956	2*h*	23888.40	−0.14	$e\ ^8S_{3\frac{1}{2}}$—63319$^\circ_{3\frac{1}{2}}$	
4189.990	100	23859.70	−0.02	$a\ ^4H_{5\frac{1}{2}}$—$y\ ^4G^\circ_{4\frac{1}{2}}$	4

TABLE 1. Mn I—*Classified lines*—Continued

1	2	3	4	5	6
λ	Int.	σ	o−c	Term designation	Zeeman type
Å Air		*K*	*K*		
4190.901	1*h*	23854.51	−0.21	*b* $^4G_{4\frac{1}{2}}$—*w* $^4G^\circ_{4\frac{1}{2}}$	
4193.745	1	23838.34	−0.08	*a* $^4D_{3\frac{1}{2}}$—*w* $^6P^\circ_{3\frac{1}{2}}$	
			−0.25	*b* $^4G_{4\frac{1}{2}}$—*w* $^4G^\circ_{3\frac{1}{2}}$	
4199.250	1*h*	23807.09	−0.13	*a* $^2I_{5\frac{1}{2}}$—*x* $^4H^\circ_{4\frac{1}{2}}$	
4201.778	60	23792.77	−0.02	*a* $^4H_{4\frac{1}{2}}$—*y* $^4G^\circ_{3\frac{1}{2}}$	4
4202.612	1	23788.05	0.00	*a* $^2G_{4\frac{1}{2}}$—*v* $^4H^\circ_{5\frac{1}{2}}$	
4203.113	3	23785.21	0.14	*a* $^2I_{5\frac{1}{2}}$—*x* $^4H^\circ_{5\frac{1}{2}}$	
4207.956	1*hl*	23757.84	−0.08	*a* $^2G_{3\frac{1}{2}}$—*w* $^2F^\circ_{3\frac{1}{2}}$	
4209.677	2	23748.12	0.00	*b* $^4G_{3\frac{1}{2}}$—*w* $^4G^\circ_{4\frac{1}{2}}$	
4209.864	1*h*	23747.07	−0.07	*a* $^4D_{1\frac{1}{2}}$—*y* $^6D^\circ_{1\frac{1}{2}}$	
4210.519	2*h*	23743.37	−0.01	*b* $^4G_{3\frac{1}{2}}$—*w* $^4G^\circ_{3\frac{1}{2}}$	
4211.753	50	23736.42	−0.04	*a* $^4H_{3\frac{1}{2}}$—*y* $^4G^\circ_{2\frac{1}{2}}$	5
4211.942	10H*l*	23735.35	0.01	*a* $^2H_{5\frac{1}{2}}$—61744$^\circ_{5\frac{1}{2}}$	
4212.443	8	23732.53	−0.11	*a* $^4D_{1\frac{1}{2}}$—*y* $^6D^\circ_{0\frac{1}{2}}$	
4215.842	1	23713.40	−0.02	*a* $^4H_{3\frac{1}{2}}$—*y* $^4G^\circ_{3\frac{1}{2}}$	
4217.186	1*h*	23705.84	0.02	*a* $^2H_{5\frac{1}{2}}$—*y* $^2G^\circ_{4\frac{1}{2}}$	
4218.405	5H*w*	23698.99	0.10	*a* $^2H_{4\frac{1}{2}}$—*y* $^2I^\circ_{5\frac{1}{2}}$	
4220.610	50*cw*	23686.61	−0.06	*b* $^4P_{2\frac{1}{2}}$—*y* $^4S^\circ_{1\frac{1}{2}}$	4
4221.562	9*h*	23681.27	−0.03	*b* $^4G_{2\frac{1}{2}}$—*w* $^4G^\circ_{2\frac{1}{2}}$	
4224.336	5	23665.72	−0.04	*a* $^2H_{4\frac{1}{2}}$—*y* $^2G^\circ_{3\frac{1}{2}}$	
4225.080	2	23661.55	−0.04	*b* $^4P_{2\frac{1}{2}}$—*v* $^4P^\circ_{2\frac{1}{2}}$	
4225.785	1	23657.60	−0.10	*a* $^2G_{3\frac{1}{2}}$—*v* $^4H^\circ_{4\frac{1}{2}}$	
4230.144	10	23633.22	−0.07	*a* $^4D_{0\frac{1}{2}}$—*y* $^6D^\circ_{0\frac{1}{2}}$	
4235.154	400	23605.27	−0.04	*a* $^4D_{2\frac{1}{2}}$—*y* $^4P^\circ_{1\frac{1}{2}}$	4
4235.300	800	23604.45	−0.01	*a* $^4D_{3\frac{1}{2}}$—*y* $^4P^\circ_{2\frac{1}{2}}$	4
4237.104	2H	23594.41	0.07	*a* $^2H_{4\frac{1}{2}}$—*y* $^2G^\circ_{4\frac{1}{2}}$	
4239.737	200	23579.75	−0.02	*a* $^4D_{1\frac{1}{2}}$—*y* $^4P^\circ_{0\frac{1}{2}}$	4
4247.689	1	23535.61	−0.03	*b* $^4G_{5\frac{1}{2}}$—*x* $^4H^\circ_{4\frac{1}{2}}$	
4250.722	1*h*	23518.82	0.09	*b* $^4G_{5\frac{1}{2}}$—*w* $^4F^\circ_{4\frac{1}{2}}$	
4251.345	2*hw*	23515.37	0.09	*b* $^2I_{6\frac{1}{2}}$—*u* $^4H^\circ_{6\frac{1}{2}}$	
4257.669	200	23480.44	0.02	*a* $^4D_{0\frac{1}{2}}$—*y* $^4P^\circ_{0\frac{1}{2}}$	6
4258.369	7	23476.58	−0.06	*a* $^2H_{5\frac{1}{2}}$—*w* $^4G^\circ_{4\frac{1}{2}}$	
4259.349	10	23471.18	−0.06	*b* $^4G_{5\frac{1}{2}}$—*x* $^4H^\circ_{6\frac{1}{2}}$	4
4261.301	30	23460.43	−0.08	*a* $^2H_{5\frac{1}{2}}$—*w* $^4G^\circ_{5\frac{1}{2}}$	6
4265.928	400	23434.99	0.00	*a* $^4D_{1\frac{1}{2}}$—*y* $^4P^\circ_{1\frac{1}{2}}$	
4271.282	2	23405.61	0.19	*a* $^2F_{3\frac{1}{2}}$—*y* $^2F^\circ_{2\frac{1}{2}}$	
4278.676	20	23365.16	0.00	*a* $^2H^\circ_{4\frac{1}{2}}$—*w* $^4G^\circ_{4\frac{1}{2}}$	6
4279.545	8H	23360.42	0.00	*a* $^2H^\circ_{4\frac{1}{2}}$—*w* $^4G^\circ_{3\frac{1}{2}}$	
4281.100	500	23351.93	0.00	*a* $^4D_{2\frac{1}{2}}$—*y* $^4P^\circ_{2\frac{1}{2}}$	6
4284.083	100	23335.67	0.03	*a* $^4D_{0\frac{1}{2}}$—*y* $^4P^\circ_{1\frac{1}{2}}$	5
4290.111	10	23302.89	−0.22	*b* $^4G_{4\frac{1}{2}}$—*x* $^4H^\circ_{5\frac{1}{2}}$	4
4300.194	20	23248.25	0.00	*b* $^4G_{5\frac{1}{2}}$—*z* $^2G^\circ_{4\frac{1}{2}}$	5
4305.670	10	23218.68	0.02	*b* $^4G_{3\frac{1}{2}}$—*x* $^4H^\circ_{4\frac{1}{2}}$	
4305.985	4	23216.98	−0.09	*a* $^2H_{5\frac{1}{2}}$—*y* $^4I^\circ_{5\frac{1}{2}}$	
			0.13	*a* $^2H_{5\frac{1}{2}}$—*y* $^4I^\circ_{6\frac{1}{2}}$	
4308.633	1	23202.71	−0.02	*a* $^2H_{5\frac{1}{2}}$—*y* $^4I^\circ_{4\frac{1}{2}}$	
4312.554	100	23181.62	0.01	*a* $^4D_{1\frac{1}{2}}$—*y* $^4P^\circ_{2\frac{1}{2}}$	5
4314.424	2*h*	23171.57	0.03	*a* $^4F_{4\frac{1}{2}}$—*y* $^4G^\circ_{4\frac{1}{2}}$	
4315.235	8	23167.22	−0.06	*b* $^4G_{2\frac{1}{2}}$—*x* $^4H^\circ_{3\frac{1}{2}}$	
4315.532	1*h*	23165.62	0.04	*b* $^4G_{3\frac{1}{2}}$—*w* $^4F^\circ_{3\frac{1}{2}}$	
4320.284	4H	23140.14	0.06	*a* $^2F_{2\frac{1}{2}}$—*y* $^2F^\circ_{2\frac{1}{2}}$	
4326.181	5	23108.60	−0.20	*b* $^4G_{4\frac{1}{2}}$—*z* $^2G^\circ_{3\frac{1}{2}}$	

TABLE 1. Mn I—*Classified lines*—Continued

1	2	3	4	5	6
λ	Int.	σ	o−c	Term designation	Zeeman type
Å Air		K	K		
4326.747	1	23105.57	−0.02	$a\ ^2H_{4\frac{1}{2}}$—$y\ ^4I^\circ_{3\frac{1}{2}}$	
4327.951	10Hw	23099.15	0.05	$a\ ^2F_{2\frac{1}{2}}$—$y\ ^2F^\circ_{3\frac{1}{2}}$	
4328.676	2	23095.28	−0.04	$a\ ^4F_{3\frac{1}{2}}$—$y\ ^4G^\circ_{3\frac{1}{2}}$	
4329.430	3	23091.26	0.01	$a\ ^2H_{4\frac{1}{2}}$—$y\ ^4I^\circ_{3\frac{1}{2}}$	
4330.938	1	23083.22	0.09	$b\ ^4G_{3\frac{1}{2}}$—$w\ ^4F^\circ_{2\frac{1}{2}}$	
4337.414	30c	23048.76	−0.03	$b\ ^4P_{1\frac{1}{2}}$—$y\ ^4S^\circ_{1\frac{1}{2}}$	
4338.135	2h	23044.92	0.00	$a\ ^2F_{3\frac{1}{2}}$—$y\ ^2G^\circ_{4\frac{1}{2}}$	
4338.819	3h	23041.29	−0.09	$a\ ^2F_{3\frac{1}{2}}$—$z\ ^2F^\circ_{3\frac{1}{2}}$	
4342.105	1	23023.85	0.14 −0.04	$b\ ^4P_{1\frac{1}{2}}$—$v\ ^4P^\circ_{2\frac{1}{2}}$ $a\ ^2G_{4\frac{1}{2}}$—$x\ ^2H^\circ_{4\frac{1}{2}}$	
4346.331	5h	23001.47	0.00	$z\ ^8P^\circ_{2\frac{1}{2}}$—$e\ ^6S_{2\frac{1}{2}}$	
4352.100	1?	22970.98	0.04	$b\ ^4G_{2\frac{1}{2}}$—$w\ ^4F^\circ_{1\frac{1}{2}}$	
4356.180	1h	22949.46	−0.03	$b\ ^4G_{2\frac{1}{2}}$—$z\ ^2G^\circ_{3\frac{1}{2}}$	
4356.613	2	22947.18	0.00	$a\ ^2H_{5\frac{1}{2}}$—$x\ ^4H^\circ_{4\frac{1}{2}}$	
4359.640	2	22931.25	−0.02	$b\ ^4G_{3\frac{1}{2}}$—$z\ ^2G^\circ_{4\frac{1}{2}}$	
4359.815	8h	22930.33	0.06	$a\ ^2H_{5\frac{1}{2}}$—$w\ ^4F^\circ_{4\frac{1}{2}}$	
4366.078	1	22897.44	0.03	$b\ ^4P_{1\frac{1}{2}}$—$v\ ^4P^\circ_{1\frac{1}{2}}$	
4368.881	50	22882.75	−0.03	$a\ ^2H_{5\frac{1}{2}}$—$x\ ^4H^\circ_{6\frac{1}{2}}$	
4370.881	8	22872.29	0.00	$z\ ^8P^\circ_{3\frac{1}{2}}$—$e\ ^6S_{2\frac{1}{2}}$	
4374.952	50	22851.00	−0.16 0.00	$a\ ^4P_{1\frac{1}{2}}$—$v\ ^6P^\circ_{1\frac{1}{2}}$ $a\ ^2F_{2\frac{1}{2}}$—$y\ ^2G^\circ_{3\frac{1}{2}}$	7b
4381.700	50	22815.80	0.06	$a\ ^2F_{3\frac{1}{2}}$—$w\ ^4G^\circ_{4\frac{1}{2}}$	4
4382.135	1	22813.54	−0.01	$a\ ^2H_{4\frac{1}{2}}$—$x\ ^4H^\circ_{5\frac{1}{2}}$	
4382.620	40H	22811.01	0.02 0.01	$a\ ^4P_{2\frac{1}{2}}$—$v\ ^6P^\circ_{2\frac{1}{2}}$ $a\ ^2F_{3\frac{1}{2}}$—$w\ ^4G^\circ_{3\frac{1}{2}}$	6, 7b
4384.410	2h	22801.70	0.07	$a\ ^2F_{3\frac{1}{2}}$—$w\ ^4G^\circ_{2\frac{1}{2}}$	
4386.176	2h	22792.52	0.00	$a\ ^2F_{2\frac{1}{2}}$—$z\ ^2F^\circ_{2\frac{1}{2}}$	
4388.092	10	22782.57	−0.05	$a\ ^2H_{4\frac{1}{2}}$—$w\ ^4F^\circ_{5\frac{1}{2}}$	
4389.377	1h	22775.90	−0.14	$a\ ^2F_{2\frac{1}{2}}$—$z\ ^2F^\circ_{3\frac{1}{2}}$	
4390.540	2h	22769.87	−0.01	$b\ ^4D_{3\frac{1}{2}}$—$y\ ^4D^\circ_{3\frac{1}{2}}$	
4393.413	8	22754.96	−0.04	$b\ ^4D_{3\frac{1}{2}}$—$y\ ^4D^\circ_{2\frac{1}{2}}$	
4408.083	5s	22679.25	0.03	$a\ ^2I_{5\frac{1}{2}}$—$z\ ^2I^\circ_{5\frac{1}{2}}$	6
4410.493	2	22666.86	−0.04	$b\ ^4P_{0\frac{1}{2}}$—$y\ ^4S^\circ_{1\frac{1}{2}}$	
4411.874	10	22659.77	−0.02	$a\ ^2H_{5\frac{1}{2}}$—$z\ ^2G^\circ_{4\frac{1}{2}}$	4
4414.887	40	22644.30	0.04	$a\ ^4D_{3\frac{1}{2}}$—$z\ ^4D^\circ_{3\frac{1}{2}}$	5
4419.769	10	22619.29	0.05	$a\ ^2H_{4\frac{1}{2}}$—$z\ ^2G^\circ_{3\frac{1}{2}}$	4
4433.720	1s	22548.12	−0.19	$a\ ^2H_{4\frac{1}{2}}$—$z\ ^2G^\circ_{4\frac{1}{2}}$	
4434.139	2	22545.98	0.32	$a\ ^2F_{2\frac{1}{2}}$—$w\ ^4G^\circ_{3\frac{1}{2}}$	
4436.061	6h	22536.22	−0.07	$a\ ^2F_{3\frac{1}{2}}$—$w\ ^4G^\circ_{2\frac{1}{2}}$	
4436.358	80	22534.70	0.01	$a\ ^4D_{2\frac{1}{2}}$—$z\ ^4D^\circ_{1\frac{1}{2}}$	5
4439.873	0	22516.87	−0.14	$a\ ^2G_{4\frac{1}{2}}$—$z^2H^\circ_{4\frac{1}{2}}$	
4451.575	100	22457.66	0.06	$a\ ^4D_{3\frac{1}{2}}$—$z\ ^4D^\circ_{3\frac{1}{2}}$	6, 7b
4452.525	7s	22452.88	0.01	$a\ ^2I_{6\frac{1}{2}}$—$z\ ^2I^\circ_{6\frac{1}{2}}$	
4453.013	50	22450.42	0.01	$a\ ^4D_{1\frac{1}{2}}$—$z\ ^4D^\circ_{0\frac{1}{2}}$	5
4455.019	25	22440.32	0.00	$z\ ^6P^\circ_{1\frac{1}{2}}$—$e\ ^6D_{0\frac{1}{2}}$	
4455.320	25	22438.80	−0.03	$z\ ^6P^\circ_{1\frac{1}{2}}$—$e\ ^6D_{1\frac{1}{2}}$	
4455.820	25	22436.29	0.00	$z\ ^6P^\circ_{1\frac{1}{2}}$—$e\ ^6D_{2\frac{1}{2}}$	
4457.041	20	22430.14	0.04	$z\ ^6P^\circ_{2\frac{1}{2}}$—$e\ ^6D_{1\frac{1}{2}}$	
4457.553	20	22427.56	0.00	$z\ ^6P^\circ_{2\frac{1}{2}}$—$e\ ^6D_{2\frac{1}{2}}$	
4458.263	25	22423.99	−0.02	$z\ ^6P^\circ_{2\frac{1}{2}}$—$e\ ^6D_{3\frac{1}{2}}$	
4460.376	20	22413.37	0.01	$z\ ^6P^\circ_{3\frac{1}{2}}$—$e\ ^6D_{2\frac{1}{2}}$	
4461.089	30	22409.84	0.03	$z\ ^6P^\circ_{3\frac{1}{2}}$—$e\ ^6D_{3\frac{1}{2}}$	
4462.033	150	22405.05	0.02	$z\ ^6P^\circ_{3\frac{1}{2}}$—$e\ ^6D_{4\frac{1}{2}}$	

TABLE 1. Mn I—*Classified lines*—Continued

1	2	3	4	5	6
λ	Int.	σ	o−c	Term designation	Zeeman type
Å Air		*K*	*K*		
4464.679	80	22391.76	0.03	$a\ ^4D_{2\frac{1}{2}}$—$z\ ^4D^\circ_{2\frac{1}{2}}$	6, 7*b*
4470.142	60	22364.40	0.03	$a\ ^4D_{1\frac{1}{2}}$—$z\ ^4D^\circ_{1\frac{1}{2}}$	6, 7*b*
4472.793	100	22351.14	0.08	$a\ ^4D_{0\frac{1}{2}}$—$z\ ^4D^\circ_{0\frac{1}{2}}$	6, 0
4473.52	2	22347.2	0.1	$a\ ^4F_{1\frac{1}{2}}$—$y\ ^4S^\circ_{1\frac{1}{2}}$	
4479.399	10*s*	22318.18	−0.01	$a\ ^2G_{3\frac{1}{2}}$—$z\ ^2H^\circ_{4\frac{1}{2}}$	5
4489.23	2	22269.3	−0.1	$a\ ^2F_{3\frac{1}{2}}$—$w\ ^4F^\circ_{4\frac{1}{2}}$	
4490.078	30	22265.10	0.08	$a\ ^4D_{0\frac{1}{2}}$—$z\ ^4D^\circ_{1\frac{1}{2}}$	5
4491.652	10*s*	22257.30	0.00 0.00	$a\ ^2G_{4\frac{1}{2}}$—$z\ ^2H^\circ_{5\frac{1}{2}}$ $a\ ^2G_{4\frac{1}{2}}$—$x\ ^2F^\circ_{3\frac{1}{2}}$	5
4496.638	8*s*	22232.62	−0.04	$b\ ^4G_{5\frac{1}{2}}$—$x\ ^4G^\circ_{5\frac{1}{2}}$	6
4498.897	20	22221.45	0.04	$a\ ^4D_{1\frac{1}{2}}$—$z\ ^4D^\circ_{2\frac{1}{2}}$	5
4502.223	30	22205.04	−0.03	$a\ ^4D_{2\frac{1}{2}}$—$z\ ^4D^\circ_{3\frac{1}{2}}$	5
4503.868	15	22196.93	0.05	$b\ ^4G_{5\frac{1}{2}}$—$z\ ^2I^\circ_{6\frac{1}{2}}$	4
4512.659	2	22153.69	0.00	$b\ ^4G_{4\frac{1}{2}}$—$x\ ^4G^\circ_{3\frac{1}{2}}$	
4520.016	1	22117.63	0.02	$a\ ^2G_{3\frac{1}{2}}$—$y\ ^2H^\circ_{4\frac{1}{2}}$	
4523.399	3*s*	22101.09	−0.23	$b\ ^4G_{4\frac{1}{2}}$—$x\ ^4G^\circ_{4\frac{1}{2}}$	6, 7*b*
4529.804	3*s*	22069.84	0.02	$a\ ^2F_{3\frac{1}{2}}$—$z\ ^2G^\circ_{3\frac{1}{2}}$	6
4534.481	2.5*s*	22047.08	−0.01	$b\ ^4G_{3\frac{1}{2}}$—$x\ ^4G^\circ_{3\frac{1}{2}}$	6, 7*b*
4538.475	2	22027.68	−0.09	$b\ ^4G_{2\frac{1}{2}}$—$x\ ^4G^\circ_{2\frac{1}{2}}$	
4541.26	2	22014.2	−0.1	$a\ ^2P_{1\frac{1}{2}}$—$w\ ^4D^\circ_{2\frac{1}{2}}$	
4544.423	5*s*	21998.85	−0.04	$a\ ^2F_{3\frac{1}{2}}$—$z\ ^2G^\circ_{4\frac{1}{2}}$	4
4546.32	12	21994.5	0.1 −0.2	$b\ ^4G_{2\frac{1}{2}}$—$x\ ^4G^\circ_{3\frac{1}{2}}$ $b\ ^4G_{3\frac{1}{2}}$—$x\ ^4G^\circ_{4\frac{1}{2}}$	
4561.13	2	21918.2	0.2	$z\ ^6P^\circ_{2\frac{1}{2}}$—$e\ ^8D_{1\frac{1}{2}}$	
4563.62	2	21906.4	0.3	$z\ ^6P^\circ_{3\frac{1}{2}}$—$e\ ^8D_{3\frac{1}{2}}$	
4564.0	2	21904.5	−0.3	$z\ ^6P^\circ_{3\frac{1}{2}}$—$e\ ^8D_{2\frac{1}{2}}$	
4565.77	10	21896.0	0.0	$y\ ^6P^\circ_{2\frac{1}{2}}$—$f\ ^4D_{1\frac{1}{2}}$	
4578.077	1	21837.13	−0.07	$b\ ^4G_{5\frac{1}{2}}$—$x\ ^4F^\circ_{4\frac{1}{2}}$	
4581.854	2	21819.13	−0.05	$a\ ^2H_{5\frac{1}{2}}$—$z\ ^2I^\circ_{5\frac{1}{2}}$	
4584.918	1	21804.56	0.08	$a\ ^2F_{2\frac{1}{2}}$—$z\ ^2G^\circ_{3\frac{1}{2}}$	
4586.114	(30*h*)	21798.04	−0.38	$a\ ^2P_{1\frac{1}{2}}$—$u\ ^4P^\circ_{1\frac{1}{2}}$	
4598.940	1	21738.08	0.12	$b\ ^4G_{2\frac{1}{2}}$—$v\ ^4D^\circ_{1\frac{1}{2}}$?	
4605.365	20	21707.75	0.05	$a\ ^2H_{4\frac{1}{2}}$—$z\ ^2I^\circ_{5\frac{1}{2}}$	5
4606.38	1	21702.9	0.0	$b\ ^4D_{1\frac{1}{2}}$—$u\ ^6P^\circ_{2\frac{1}{2}}$	
4607.61	7*s*	21697.2	0.0	$a\ ^4D_{3\frac{1}{2}}$—$x\ ^6P^\circ_{3\frac{1}{2}}$	
4614.12	1	21666.6	0.0	$b\ ^4P_{2\frac{1}{2}}$—$v\ ^6F^\circ_{3\frac{1}{2}}$?	
4615.65	8	21659.4	−0.2	$b\ ^4G_{4\frac{1}{2}}$—$x\ ^4F^\circ_{3\frac{1}{2}}$	
4620.21	5*h*	21638.0	0.0	$a\ ^2P_{0\frac{1}{2}}$—$w\ ^4D^\circ_{1\frac{1}{2}}$	
4622.74	8	21626.2	0.0	$b\ ^4G_{2\frac{1}{2}}$—$x\ ^4F^\circ_{1\frac{1}{2}}$	
4623.33	8	21623.4	−0.1	$b\ ^4G_{3\frac{1}{2}}$—$x\ ^4F^\circ_{2\frac{1}{2}}$	
4624.220	8	21619.22	0.29	$y\ ^6P^\circ_{3\frac{1}{2}}$—$e\ ^8P_{4\frac{1}{2}}$	
4626.544	25	21608.37	−0.05	$a\ ^2H_{5\frac{1}{2}}$—$z\ ^2I^\circ_{6\frac{1}{2}}$	4
4626.861	2	21606.89	−0.02	$a\ ^4D_{2\frac{1}{2}}$—$x\ ^6P^\circ_{2\frac{1}{2}}$	
4642.803	5*s*	21532.70	−0.02	$a\ ^2H_{4\frac{1}{2}}$—$x\ ^4G^\circ_{5\frac{1}{2}}$	
4658.42	12	21460.5	0.1	$b\ ^4P_{1\frac{1}{2}}$—55923$^2_{2\frac{1}{2}}$	
4661.93	2	21444.4	−0.3	$a\ ^4D_{2\frac{1}{2}}$—$x\ ^6P^\circ_{3\frac{1}{2}}$	
4663.638	2	21436.51	−0.08	$a\ ^4D_{1\frac{1}{2}}$—$x\ ^6P^\circ_{2\frac{1}{2}}$	
4671.688	10*s*	21399.57	−0.05	$a\ ^4D_{3\frac{1}{2}}$—$z\ ^4F^\circ_{4\frac{1}{2}}$	5
4697.52	2	21281.9	0.1	$b\ ^4P_{2\frac{1}{2}}$—$x\ ^4D^\circ_{3\frac{1}{2}}$	
4701.150	8*s*	21265.46	−0.07	$a\ ^4D_{2\frac{1}{2}}$—$z\ ^4F^\circ_{1\frac{1}{2}}$	
4709.710	40	21226.81	0.03	$a\ ^4D_{3\frac{1}{2}}$—$z\ ^4F^\circ_{3\frac{1}{2}}$	6
4712.02	5	21216.5	0.0	$a\ ^2P_{0\frac{1}{2}}$—$u\ ^4P^\circ_{0\frac{1}{2}}$	

TABLE 1. Mn I—*Classified lines*—Continued

1	2	3	4	5	6
λ	Int.	σ	o−c	Term designation	Zeeman type
Å Air		*K*	*K*		
4727. 462	30	21147. 10	0. 01	$a\ ^4D_{2\frac{1}{2}}$—$z\ ^4F^{\circ}_{2\frac{1}{2}}$	6
4728. 789	1	21141. 17	0. 13	$b\ ^4D_{0\frac{1}{2}}$—$x\ ^4P^{\circ}_{0\frac{1}{2}}$	
4731. 92	1	21127. 2	0. 1	$b\ ^4D_{1\frac{1}{2}}$—$x\ ^4P^{\circ}_{0\frac{1}{2}}$	
4739. 110	25	21095. 13	−0. 08	$a\ ^4D_{1\frac{1}{2}}$—$z\ ^4F^{\circ}_{1\frac{1}{2}}$	6
4754. 048	50H	21028. 85	0. 00	$z\ ^8P^{\circ}_{2\frac{1}{2}}$—$e\ ^8S_{3\frac{1}{2}}$	4
4761. 527	50	20995. 81	−0. 05	$a\ ^4D_{0\frac{1}{2}}$—$z\ ^4F^{\circ}_{1\frac{1}{2}}$	5
4762. 376	80	20992. 09	0. 00	$a\ ^4D_{3\frac{1}{2}}$—$z\ ^4F^{\circ}_{4\frac{1}{2}}$	4
4765. 856	60	20976. 71	−0. 06	$a\ ^4D_{1\frac{1}{2}}$—$z\ ^4F^{\circ}_{2\frac{1}{2}}$	4
4766. 426	70	20974. 25	0. 00	$a\ ^4D_{2\frac{1}{2}}$—$z\ ^4F^{\circ}_{3\frac{1}{2}}$	4
4771. 668	4*s*	20951. 18	−0. 02	$b\ ^4D_{3\frac{1}{2}}$—$x\ ^4P^{\circ}_{2\frac{1}{2}}$	
4779. 138	4	20918. 44	0. 01	$b\ ^4G_{5\frac{1}{2}}$—$y\ ^4H^{\circ}_{6\frac{1}{2}}$	
4783. 432	100	20899. 67	0. 00	$z\ ^8P^{\circ}_{3\frac{1}{2}}$—$e\ ^8S_{3\frac{1}{2}}$	6
4786. 867	3	20884. 67	−0. 01	$z\ ^6D^{\circ}_{0\frac{1}{2}}$—$e\ ^6F_{1\frac{1}{2}}$	
4793. 011	8	20857. 90	−0. 06	$a\ ^2H_{5\frac{1}{2}}$—$z\ ^4I^{\circ}_{4\frac{1}{2}}$	
4796. 055	3	20844. 62	−0. 10	$a\ ^2G_{3\frac{1}{2}}$—$y\ ^2F^{\circ}_{2\frac{1}{2}}$	
4796. 704	15	20841. 85	−0. 23	$y\ ^6P^{\circ}_{2\frac{1}{2}}$—$i\ ^6D_{1\frac{1}{2}}$	
4798. 324	1	20834. 81	0. 12	$a\ ^2H_{5\frac{1}{2}}$—$z\ ^4I^{\circ}_{5\frac{1}{2}}$	
4807. 170	3*s*	20796. 46	−0. 22	$b\ ^4G_{4\frac{1}{2}}$—$y\ ^4H^{\circ}_{5\frac{1}{2}}$	
4815. 109	15*h*	20762. 18	−0. 06	$z\ ^6D^{\circ}_{1\frac{1}{2}}$—$e\ ^6F_{2\frac{1}{2}}$	
4816. 909	1	20754. 42	−0. 04	$a\ ^2G_{4\frac{1}{2}}$—$y\ ^2G^{\circ}_{3\frac{1}{2}}$	
4818. 331	2*s*	20748. 29	−0. 01	$b\ ^4G_{3\frac{1}{2}}$—$y\ ^4H^{\circ}_{4\frac{1}{2}}$	
4822. 708	10*h*	20729. 46	−0. 51	$b\ ^4G_{2\frac{1}{2}}$—$y\ ^4H^{\circ}_{3\frac{1}{2}}$?	
4823. 528	150	20725. 94	0. 00	$z\ ^8P^{\circ}_{1\frac{1}{2}}$—$e\ ^8S_{3\frac{1}{2}}$	4
4825. 592	20	20717. 07	0. 00	$z\ ^4P^{\circ}_{2\frac{1}{2}}$—$e\ ^4P_{1\frac{1}{2}}$	4
4826. 890	10	20711. 50	0. 00	$z\ ^4P^{\circ}_{1\frac{1}{2}}$—$e\ ^4P_{0\frac{1}{2}}$	4
4838. 228	8	20662. 97	0. 00	$z\ ^4P^{\circ}_{0\frac{1}{2}}$—$e\ ^4P_{0\frac{1}{2}}$	
4840. 139	3	20654. 81	−0. 01	$b\ ^4G_{5\frac{1}{2}}$—$y\ ^4G^{\circ}_{5\frac{1}{2}}$	
4840. 21	2	20654. 51	0. 02	$b\ ^4P_{0\frac{1}{2}}$—$y\ ^8F^{\circ}_{1\frac{1}{2}}$	
4843. 188	4	20641. 81	0. 01	$z\ ^4P^{\circ}_{1\frac{1}{2}}$—$e\ ^4P_{1\frac{1}{2}}$	
4844. 312	20*s*	20637. 03	0. 01	$z\ ^4P^{\circ}_{2\frac{1}{2}}$—$e\ ^4P_{2\frac{1}{2}}$	6
4854. 610	10*s*	20593. 24	−0. 03	$z\ ^4P^{\circ}_{0\frac{1}{2}}$—$e\ ^4P_{1\frac{1}{2}}$	4
4862. 048	15*s*	20561. 74	−0. 01	$z\ ^4P^{\circ}_{1\frac{1}{2}}$—$e\ ^4P_{2\frac{1}{2}}$	4
4881. 578	3	20479. 47	−0. 15	$b\ ^4G_{4\frac{1}{2}}$—$y\ ^4G^{\circ}_{4\frac{1}{2}}$	
4888. 833	2	20449. 08	−0. 04	$a\ ^2G_{4\frac{1}{2}}$—$w\ ^4G^{\circ}_{3\frac{1}{2}}$	
4900. 719	2	20399. 47	0. 00	$b\ ^4G_{3\frac{1}{2}}$—$y\ ^4G^{\circ}_{3\frac{1}{2}}$	
4902. 202	1	20393. 32	0. 10	$b\ ^4P_{2\frac{1}{2}}$—$z\ ^4S^{\circ}_{1\frac{1}{2}}$	
4907. 868	2	20369. 77	−0. 03	$b\ ^4G_{2\frac{1}{2}}$—$y\ ^4G^{\circ}_{2\frac{1}{2}}$	
4917. 446	1	20330. 10	0. 13	$a\ ^2H_{5\frac{1}{2}}$—$y\ ^4H^{\circ}_{6\frac{1}{2}}$	
4939. 115	6*h*	20240. 91	−0. 02	$z\ ^6D^{\circ}_{2\frac{1}{2}}$—$e\ ^6F_{3\frac{1}{2}}$	
4942. 396	3	20227. 47	0. 06	$a\ ^4D_{3\frac{1}{2}}$—$z\ ^6F^{\circ}_{3\frac{1}{2}}$	
4956. 733	1*s*	20168. 97	0. 15	$a\ ^4F_{4\frac{1}{2}}$—$x\ ^4D^{\circ}_{3\frac{1}{2}}$	
4965. 856	30	20131. 91	0. 00	$a\ ^4D_{3\frac{1}{2}}$—$z\ ^6F^{\circ}_{4\frac{1}{2}}$	5
4974. 334	6*h*	20097. 60	0. 06	$z\ ^6D^{\circ}_{3\frac{1}{2}}$—$e\ ^6F_{4\frac{1}{2}}$	
4982. 067	1	20066. 41	0. 05	$a\ ^2H_{5\frac{1}{2}}$—$y\ ^4G^{\circ}_{5\frac{1}{2}}$	
4985. 734	10*s*	20051. 65	0. 36	$a\ ^4P_{1\frac{1}{2}}$—$y\ ^4P^{\circ}_{0\frac{1}{2}}$	
4987. 066	2*s*	20046. 29	−0. 01	$a\ ^4D_{2\frac{1}{2}}$—$z\ ^6F^{\circ}_{2\frac{1}{2}}$	
4994. 213	3*s*	20017. 61	0. 17	$a\ ^4P_{0\frac{1}{2}}$—$y\ ^4P^{\circ}_{0\frac{1}{2}}$	
5004. 891	20*s*	19974. 90	0. 02	$a\ ^4D_{2\frac{1}{2}}$—$z\ ^6F^{\circ}_{3\frac{1}{2}}$	
5010. 349	8*s*	19953. 14	0. 17	$a\ ^4P_{2\frac{1}{2}}$—$y\ ^4P^{\circ}_{1\frac{1}{2}}$	
5017. 612	20*h*	19924. 26	0. 12	$z\ ^6D^{\circ}_{4\frac{1}{2}}$—$e\ ^6F_{5\frac{1}{2}}$	
5022. 004	5*s*	19906. 33	0. 32	$a\ ^4P_{1\frac{1}{2}}$—$y\ ^4P^{\circ}_{1\frac{1}{2}}$	
5029. 779	10*s*	19876. 06	0. 08	$a\ ^4D_{1\frac{1}{2}}$—$z\ ^6F^{\circ}_{2\frac{1}{2}}$	
5030. 623	5*s*	19872. 73	0. 07	$a\ ^4P_{0\frac{1}{2}}$—$y\ ^4P^{\circ}_{1\frac{1}{2}}$	
5042. 567	4*s*	19825. 55	−0. 03	$a\ ^4D_{0\frac{1}{2}}$—$z\ ^6F^{\circ}_{1\frac{1}{2}}$	
5074. 805	15	19699. 72	0. 13	$a\ ^4P_{2\frac{1}{2}}$—$y\ ^4P^{\circ}_{2\frac{1}{2}}$	

TABLE 1. Mn I—*Classified lines*—Continued

1	2	3	4	5	6
λ	Int.	σ	o−c	Term designation	Zeeman type
Å Air		K	K		
5086.884	10*s*	19652.94	−0.19	$a\ ^4P_{1\frac{1}{2}}$—$y\ ^4P^o_{2\frac{1}{2}}$	
5091.018	1*s*	19636.98	−0.03	$a\ ^2G_{4\frac{1}{2}}$—$z\ ^2G^o_{4\frac{1}{2}}$	
5117.935	20*s*	19533.70	0.01	$a\ ^4G_{2\frac{1}{2}}$—$z\ ^4F^o_{1\frac{1}{2}}$	P—B
5142.919	15*s*	19438.81	0.02	$z\ ^6F^o_{1\frac{1}{2}}$—$e\ ^6F_{1\frac{1}{2}}$	
5149.155	50	19415.27	0.02	$a\ ^4G_{2\frac{1}{2}}$—$z\ ^4F^o_{2\frac{1}{2}}$	
5150.937	30*s*	19408.55	0.00	$a\ ^4G_{3\frac{1}{2}}$—$z\ ^4F^o_{2\frac{1}{2}}$	
5177.077	2	19310.55	0.24	$z\ ^6F^o_{2\frac{1}{2}}$—$e\ ^6F_{2\frac{1}{2}}$	
5180.298	2*s*	19298.55	−0.05	$b\ ^4P_{2\frac{1}{2}}$—$y\ ^4D^o_{3\frac{1}{2}}$	
5190.02	6*h*	19262.40	−0.64	$y\ ^6P^o_{1\frac{1}{2}}$—$g\ ^6D_{1\frac{1}{2}}$	
5190.69	6*h*	19259.91	−0.01	$y\ ^6P^o_{1\frac{1}{2}}$—$g\ ^6D_{0\frac{1}{2}}$	
5196.603	30*s*	19238.00	−0.02	$a\ ^4G_{4\frac{1}{2}}$—$z\ ^4F^o_{3\frac{1}{2}}$	
5197.229	10	19235.68	−0.03	$a\ ^4G_{3\frac{1}{2}}$—$z\ ^4F^o_{3\frac{1}{2}}$	
5199.51	3	19227.24	0.07	$y\ ^6P^o_{2\frac{1}{2}}$—$g\ ^6D_{1\frac{1}{2}}$	
5200.18	5	19224.77	−0.04	$y\ ^6P^o_{2\frac{1}{2}}$—$g\ ^6D_{2\frac{1}{2}}$	
5201.440	2H	19220.11	−0.13	$y\ ^6P^o_{2\frac{1}{2}}$—$g\ ^6D_{3\frac{1}{2}}$	
5213.34	8	19176.24	0.12	$y\ ^6P^o_{3\frac{1}{2}}$—$g\ ^6D_{3\frac{1}{2}}$	
5215.434	5H	19168.54	−0.05	$y\ ^6P^o_{3\frac{1}{2}}$—$g\ ^6D_{4\frac{1}{2}}$	
5249.371	2	19044.60	−0.01	$b\ ^4P_{2\frac{1}{2}}$—$x\ ^6D^o_{3\frac{1}{2}}$	
5255.330	30	19023.02	0.00	$a\ ^4G_{5\frac{1}{2}}$—$z\ ^4F^o_{4\frac{1}{2}}$	4
5260.771	8*s*	19003.34	0.01	$a\ ^4G_{4\frac{1}{2}}$—$z\ ^4F^o_{4\frac{1}{2}}$	
5274.206	2	18954.94	−0.02	$z\ ^6F^o_{3\frac{1}{2}}$—$e\ ^6G_{4\frac{1}{2}}$	
5277.54	8H	18942.96	0.29	$z\ ^4F^o_{4\frac{1}{2}}$—$e\ ^4F_{4\frac{1}{2}}$	
5284.196	6H	18919.10	0.01	$z\ ^6F^o_{2\frac{1}{2}}$—$e\ ^6G_{2\frac{1}{2}}$?	
5289.495	5*h*	18900.15	−0.30 −0.40	$z\ ^6F^o_{0\frac{1}{2}}$—$e\ ^6G_{1\frac{1}{2}}$ $z\ ^4F^o_{3\frac{1}{2}}$—$e\ ^4F_{3\frac{1}{2}}$	
5292.869	1	18888.10	0.02	$a\ ^4P_{0\frac{1}{2}}$—$z\ ^4D^o_{0\frac{1}{2}}$	
5297.920	3*hd*	18870.10	−0.04	$z\ ^6F^o_{1\frac{1}{2}}$—$e\ ^6G_{2\frac{1}{2}}$	
5298.84	7*s*	18866.82	0.04	$z\ ^6F^o_{4\frac{1}{2}}$—$e\ ^4G_{5\frac{1}{2}}$	
5308.92	15*h*	18831.00	0.02	$z\ ^6F^o_{2\frac{1}{2}}$—$e\ ^6G_{3\frac{1}{2}}$	
5317.082	8*s*	18802.09	0.05	$a\ ^4P_{0\frac{1}{2}}$—$z\ ^4D^o_{1\frac{1}{2}}$	
5324.317	20*h*	18776.54	−0.01	$z\ ^6F^o_{3\frac{1}{2}}$—$e\ ^6G_{4\frac{1}{2}}$	
5325.999	5*h*	18770.61	0.03	$z\ ^6F^o_{3\frac{1}{2}}$—$e\ ^6F_{3\frac{1}{2}}$	
5334.872	5*s*	18739.39	0.00	$a\ ^4P_{2\frac{1}{2}}$—$z\ ^4D^o_{3\frac{1}{2}}$	
5341.065	250	18717.66	−0.02	$a\ ^6D_{4\frac{1}{2}}$—$y\ ^6P^o_{3\frac{1}{2}}$	4
5344.438	50H	18705.85	−0.02	$z\ ^6F^o_{4\frac{1}{2}}$—$e\ ^6G^o_{5\frac{1}{2}}$	
5348.078	20*s*	18693.12	0.19	$a\ ^4P_{1\frac{1}{2}}$—$z\ ^4D^o_{2\frac{1}{2}}$	
5349.878	80H	18686.83	−0.03	$z\ ^6F^o_{5\frac{1}{2}}$—$e\ ^6G_{6\frac{1}{2}}$	
5361.631	1	18645.86	0.02	$b\ ^4P_{1\frac{1}{2}}$—$y\ ^4D^o_{2\frac{1}{2}}$	
5364.488	5	18635.94	−0.03	$a\ ^4D_{3\frac{1}{2}}$—$z\ ^6D^o_{3\frac{1}{2}}$	
5374.39	1*h*	18601.60	0.00	$z\ ^6F^o_{4\frac{1}{2}}$—$e\ ^6F_{4\frac{1}{2}}$	
5375.306	2	18598.42	0.00	$z\ ^4H^o_{6\frac{1}{2}}$—$f\ ^4G_{5\frac{1}{2}}$?	
5377.634	100	18590.38	0.02	$z\ ^4P^o_{2\frac{1}{2}}$—$e\ ^4S_{1\frac{1}{2}}$	4
5388.538	15*s*	18552.80	0.07	$a\ ^4P_{2\frac{1}{2}}$—$z\ ^4D^o_{3\frac{1}{2}}$	
5394.677	30	18531.65	0.01	$a\ ^6S_{2\frac{1}{2}}$—$z\ ^6P^o_{3\frac{1}{2}}$	4
5399.506	30	18515.08	−0.01	$z\ ^4P_{1\frac{1}{2}}$—$e\ ^4S^o_{1\frac{1}{2}}$	6
5402.608	1	18504.45	−0.08	$a\ ^4D_{2\frac{1}{2}}$—$z\ ^6D^o_{2\frac{1}{2}}$	
5406.014	5	18492.79	−0.02	$a\ ^4D_{3\frac{1}{2}}$—$z\ ^6D^o_{4\frac{1}{2}}$	
5407.432	50*c*	18487.97	0.00	$a\ ^6D_{3\frac{1}{2}}$—$y\ ^6P^o_{3\frac{1}{2}}$	6
5413.696	30	18466.55	−0.01	$z\ ^4P^o_{0\frac{1}{2}}$—$e\ ^4S_{1\frac{1}{2}}$	4
5420.368	100*c*	18443.82	−0.03	$a\ ^6D_{3\frac{1}{2}}$—$y\ ^6P^o_{2\frac{1}{2}}$	4
5426.192	2	18424.03	−0.02	$a\ ^4D_{1\frac{1}{2}}$—$z\ ^6D^o_{1\frac{1}{2}}$	
5427.184	1*h*	18420.66	0.16	$b\ ^4P_{1\frac{1}{2}}$—$x\ ^6D^o_{1\frac{1}{2},\ 2\frac{1}{2}}$	
5432.555	60	18402.45	−0.01	$a\ ^6S_{2\frac{1}{2}}$—$z\ ^8P^o_{2\frac{1}{2}}$	
5433.422	100*wc*	18399.50	0.11	$z\ ^6F^o_{5\frac{1}{2}}$—$e\ ^6F_{5\frac{1}{2}}$	
5439.290	0	18379.66	−0.03	$a\ ^4D_{0\frac{1}{2}}$—$z\ ^6D^o_{0\frac{1}{2}}$	
5444.094	1*h*	18363.44	0.03	$a\ ^4G_{2\frac{1}{2}}$—$z\ ^6F^o_{1\frac{1}{2}}$	

TABLE 1. Mn I—*Classified lines*—Continued

1	2	3	4	5	6
λ	Int.	σ	o−c	Term designation	Zeeman type
Å Air		*K*	*K*		
5445. 99	1*h*	18357. 04	0. 10	*y* $^4F^o_{3½}$—*f* $^4G_{4½}$	
5447. 576	1*h*	18351. 70	−0. 02	*y* $^4F^o_{4½}$—*f* $^4G_{5½}$	
5457. 468	30	18318. 44	−0. 01	*a* $^6D_{2½}$—*y* $^6P^o_{3½}$	
5460. 645	1	18307. 78	0. 02	*a* $^4G_{3½}$—*z* $^6F^o_{2½}$	
5470. 640	100	18274. 33	0. 00	*a* $^6D_{2½}$—*y* $^6P^o_{2½}$	6
5481. 345	100	18238. 48	0. 02	*a* $^6D_{2½}$—*y* $^6P^o_{1½}$	
5495. 913	1	18190. 30	0. 02	*z* $^4F^o_{4½}$—*e* $^4G_{4½}$	
5497. 374	10*h*	18185. 47	0. 08	*a* $^4F_{4½}$—*y* $^4D^o_{3½}$	
5504. 224	15	18162. 83	−0. 01	*a* $^4G_{5½}$—*z* $^6F^o_{4½}$	
5505. 877	50	18157. 38	0. 01	*a* $^6D_{1½}$—*y* $^6P^o_{2½}$	
5510. 190	1	18143. 16	0. 01	*a* $^4G_{4½}$—*z* $^6F^o_{4½}$	
5516. 777	100	18121. 50	0. 00	*a* $^6D_{1½}$—*y* $^6P^o_{1½}$	6
5520. 496	10*h*	18109. 29	−0. 03	*z* $^4F^o_{3½}$—*e* $^4G_{3½}$	
5533. 156	5*s*	18067. 86	0. 02	*a* $^4F_{3½}$—*y* $^4D^o_{2½}$	
5536. 471	8*h*	18057. 04	−0. 04	*z* $^4F^o_{2½}$—*e* $^4G_{2½}$	
5537. 749	100	18052. 88	0. 05	*a* $^6D_{0½}$—*y* $^6P^o_{1½}$	4
5551. 978	80*w*	18006. 60	0. 00	*z* $^4F^o_{5½}$—*e* $^4G_{5½}$	
5555. 782	3*s*	17994. 29	0. 06	*a* $^4F_{2½}$—*y* $^4D^o_{2½}$	
5567. 764	50	17955. 55	−0. 04	*z* $^4F^o_{3½}$—*e* $^4G_{4½}$	
5573. 010	30	17938. 67	0. 03	*z* $^4F^o_{1½}$—*e* $^4G_{2½}$	
5573. 690	40	17936. 48	0. 00	*z* $^4F^o_{2½}$—*e* $^4G_{3½}$	
5575. 242	1	17931. 46	0. 06	*a* $^4F_{4½}$—*x* $^6D^o_{3½}$	
5602. 046	5	17845. 68	−0. 01	*z* $^4F^o_{4½}$—*e* $^6G_{5½}$	
5603. 08	1	17842. 38	−0. 12	*a* $^4F_{3½}$—*x* $^6D^o_{2½}$	
5607. 355	1	17828. 78	0. 05	*a* $^4F_{3½}$—*x* $^6D^o_{3½}$	
5626. 247	3	17768. 93	0. 04	*a* $^4F_{2½}$—*x* $^6D^o_{1½, 2½}$	
5642. 394	1	17718. 07	0. 02	*a* $^4F_{1½}$—*x* $^6D^o_{0½}$	
5658. 395	1	17667. 97	0. 05	*b* $^4G_{3½}$—*w* $^4P^o_{2½}$	
5687. 133	1	17578. 68	−0. 05	*b* $^4G_{2½}$—w $^4P^o_{1½}$	
5718. 236	2*h*	17483. 07	0. 00	*z* $^4D^o_{2½}$—*e* $^4F_{3½}$	
5720. 233	2*h*	17476. 97	−0. 19	*z* $^4D^o_{3½}$—*e* $^4F_{4½}$	
5738. 286	30	17422. 00	−0. 05	*a* $^4H_{6½}$—*z* $^4G^o_{5½}$	
5780. 173	25	17295. 74	−0. 01	*a* $^4H_{5½}$—*z* $^4G^o_{4½}$	
5782. 307	1*h*	17289. 34	−0. 26	*a* $^2G_{3½}$—*y* $^4H^o_{3½}$	
5816. 840	20	17186. 71	0. 00	*a* $^4H_{4½}$—*z* $^4G^o_{3½}$	
5822. 55	3	17169. 86	−0. 09	*z* $^4G^o_{4½}$—*f* $^4G_{4½}$	
5835. 372	5	17132. 12	0. 03	*z* $^4G^o_{5½}$—*f* $^4G_{5½}$	
5848. 950	15	17092. 36	0. 00	*a* $^4H_{3½}$—*z* $^4G^o_{2½}$	
5868. 18	2	17036. 35	0. 09	*x* $^6P^o_{3½}$—*e* $^6F_{4½}$	
5879. 18	2	17004. 47	−0. 09	*y* $^6P^o_{2½}$—*f* $^6D_{3½}$	
5973. 867	2	16734. 95	0. 05	*b* $^4D_{2½}$—*y* $^4P^o_{1½}$	
6013. 484	100	16624. 70	0. 09	*z* $^6P^o_{1½}$—*e* $^6S_{2½}$	4
6014. 385	20*s*	16622. 21	−0. 02	*a* $^4F_{4½}$—*z* $^4G^o_{5½}$	
6016. 697	150	16615. 82	−0. 06	*z* $^6P^o_{2½}$—*e* $^6S_{2½}$	6
6021. 787	200	16601. 78	0. 10	*z* $^6P^o_{3½}$—*e* $S_{2½}$	4
6041. 730	8*s*	16546. 98	0. 06	*b* $^4D_{3½}$—*y* $^4P^o_{2½}$	
6057. 120	15*s*	16504. 94	0. 04	*a* $^4F_{3½}$—*z* $^4G^o_{4½}$	
6062. 885	3*s*	16489. 24	0. 00	*a* $^4F_{3½}$—*z* $^4G^o_{3½}$	
6090. 080	10*s*	16415. 61	−0. 02	*a* $^4F_{2½}$—*z* $^4G^o_{3½}$	
6095–656	2*s*	16400. 60	−0. 05	*a* $^4F_{2½}$—*z* $^4G^o_{2½}$	
6114. 324	8*s*	16350. 52	−0. 06	*a* $^4F_{1½}$—*z* $^4G^o_{2½}$	
6177. 5	2	16183. 31	−0. 08	*e* $^6D_{3½}$—*w* $^4H^o_{3½}$	
6265. 627	10*s*	15955. 69	−0. 03	*a* $^4H_{6½}$—*z* $^4H^o_{6½}$	
6315. 064	10*s*	15830. 78	−0. 01	*a* $^4H_{5½}$—*z* $^4H^o_{5½}$	
6344. 133	30	15758. 23	0. 04	*b* $^4D_{0½}$—*z* $^4D^o_{0½}$	

TABLE 1. Mn I—*Classified lines*—Continued

1	2	3	4	5	6
λ	Int.	σ	o−c	Term designation	Zeeman type
Å Air		K	K		
6349.795	15	15744.19	−0.03	$b\ ^4D_{1\frac{1}{2}}$—$z\ ^4D^\circ_{0\frac{1}{2}}$	
6356.095	8*s*	15728.59	−0.10	$a\ ^4H_{4\frac{1}{2}}$—$z\ ^4H^\circ_{4\frac{1}{2}}$	
6378.969	20	15672.19	0.04	$b\ ^4D_{0\frac{1}{2}}$—$z\ ^4D^\circ_{1\frac{1}{2}}$	
6382.195	25	15664.27	−0.01	$b\ ^4D_{2\frac{1}{2}}$—$z\ ^4D^\circ_{1\frac{1}{2}}$	
6384.686	30	15658.16	−0.02	$b\ ^4D_{1\frac{1}{2}}$—$z\ ^4D^\circ_{1\frac{1}{2}}$	
6391.248	7*s*	15642.08	−0.11	$a\ ^4H_{3\frac{1}{2}}$—$z\ ^4H^\circ_{3\frac{1}{2}}$	
6413.947	2	15586.72	0.00	$b\ ^4D_{3\frac{1}{2}}$—$z\ ^4D^\circ_{2\frac{1}{2}}$	
6440.973	50	15521.32	0.00	$b\ ^4D_{2\frac{1}{2}}$—$z\ ^4D^\circ_{2\frac{1}{2}}$	
6443.511	20	15515.21	−0.01	$b\ ^4D_{1\frac{1}{2}}$—$z\ ^4D^\circ_{2\frac{1}{2}}$	
6483.061	2*s*	15420.56	−0.02	$a\ ^4F_{4\frac{1}{2}}$—$y\ ^4F^\circ_{3\frac{1}{2}}$	
6590.61	3	15402.62	0.02	$a\ ^4F_{4\frac{1}{2}}$—$y\ ^4F^\circ_{4\frac{1}{2}}$	
6491.697	50	15400.04	−0.02	$b\ ^4D_{3\frac{1}{2}}$—$z\ ^4D^\circ_{3\frac{1}{2}}$	
6519.381	20	15334.65	−0.01	$b\ ^4D_{2\frac{1}{2}}$—$z\ ^4D^\circ_{3\frac{1}{2}}$	
6520.548	2*h*	15331.90	0.04	$a\ ^4F_{3\frac{1}{2}}$—$y\ ^4F^\circ_{2\frac{1}{2}}$	
6526.528	8	15317.86	−0.05	$a\ ^4F_{3\frac{1}{2}}$—$y\ ^4F^\circ_{3\frac{1}{2}}$	
6534.103	6HH	15300.10	0.17	$a\ ^4F_{3\frac{1}{2}}$—$y\ ^4F^\circ_{4\frac{1}{2}}$	
6547.715	2*h*	15268.29	0.00	$a\ ^4F_{2\frac{1}{2}}$—$y\ ^4F^\circ_{1\frac{1}{2}}$	
6552.035	5	15258.23	−0.02	$a\ ^4F_{2\frac{1}{2}}$—$y\ ^4F^\circ_{2\frac{1}{2}}$	
6558.016	2*h*	15244.31	0.01	$a\ ^4F_{2\frac{1}{2}}$—$y\ ^4F^\circ_{3\frac{1}{2}}$	
6569.267	5	15218.20	−0.02	$a\ ^4F_{1\frac{1}{2}}$—$y\ ^4F^\circ_{1\frac{1}{2}}$	
6570.807	7HH	15214.64	−0.06	$y\ ^6P^\circ_{1\frac{1}{2}}$—$g\ ^6S_{2\frac{1}{2}}$	
6572.936	2*s*	15209.71	−0.29	$y\ ^6F^\circ_{3\frac{1}{2}}$—$e\ ^4F_{4\frac{1}{2}}$?	
6573.589	1*h*	15208.20	0.02	$a\ ^4F_{1\frac{1}{2}}$—$y\ ^4F^\circ_{2\frac{1}{2}}$	
6586.316	8HH	15178.81	−0.02	$y\ ^6P^\circ_{2\frac{1}{2}}$—$g\ ^6S_{2\frac{1}{2}}$	
6605.549	10HH	15134.62	−0.09	$y\ ^6P^\circ_{3\frac{1}{2}}$—$g\ ^6S_{2\frac{1}{2}}$	
6827.161	3*h*	14643.34	0.08	$z\ ^6P^\circ_{2\frac{1}{2}}$—$e\ ^8S_{3\frac{1}{2}}$	
6833.793	5*h*	14629.13	−0.18	$z\ ^6D^\circ_{3\frac{1}{2}}$—$e\ ^4D_{2\frac{1}{2}}$	
6833.936	10*h*	14628.83	−0.23	$z\ ^6P^\circ_{3\frac{1}{2}}$—$e\ ^8S_{3\frac{1}{2}}$	
6863.08	4H	14566.71	−0.02	$z\ ^6D^\circ_{4\frac{1}{2}}$—$i\ ^6D_{3\frac{1}{2}}$	
6867.18	3HH	14558.01	−0.14	$z\ ^6D^\circ_{3\frac{1}{2}}$—$i\ ^6D_{2\frac{1}{2}}$	
6880.64	5H	14529.53	0.09	$z\ ^6D^\circ_{3\frac{1}{2}}$—$e\ ^4D_{3\frac{1}{2}}$	
6887.73	15*s*	14514.57	0.37	$z\ ^6D^\circ_{2\frac{1}{2}}$—$i\ ^6D^1_{1\frac{1}{2}}$	
6890.764	1HHH	14508.18	−0.04	$z\ ^6D^\circ_{2\frac{1}{2}}$—$e\ ^4D_{2\frac{1}{2}}$	
6924.690	3H	14437.10	0.04	$z\ ^6D^\circ_{2\frac{1}{2}}$—$i\ ^6D_{2\frac{1}{2}}$	
6931.165	10H	14423.62	0.05	$z\ ^6D^\circ_{3\frac{1}{2}}$—$i\ ^6D_{3\frac{1}{2}}$	
6933.654	3HH	14418.44	0.06	$z\ ^6D^\circ_{1\frac{1}{2}}$—$e\ ^4D_{2\frac{1}{2}}$	
6938.486	4H	14408.40	0.05	$z\ ^6D^\circ_{2\frac{1}{2}}$—$e\ ^4D_{3\frac{1}{2}}$	
6941.045	2H	14403.09	0.10 0.02	$b\ ^4D_{0\frac{1}{2}}$—$z\ ^4F^\circ_{1\frac{1}{2}}$ $z\ ^6D^\circ_{0\frac{1}{2}}$—$e\ ^4D_{1\frac{1}{2}}$	
6942.538	20H	14399.99	0.02	$z\ ^6D^\circ_{4\frac{1}{2}}$—$i\ ^6D_{4\frac{1}{2}}$	
6947.828	1	14389.02	0.00	$b\ ^4D_{1\frac{1}{2}}$—$z\ ^4F^\circ_{1\frac{1}{2}}$	
6957.328	1*h*	14369.37	0.00	$z\ ^6D^\circ_{0\frac{1}{2}}$—$i\ ^6D_{1\frac{1}{2}}$	
6960.942	1*h*	14361.91	0.05	$y\ ^6F^\circ_{2\frac{1}{2}}$—$e\ ^4G_{3\frac{1}{2}}$	
6968.062	3HH	14347.24	0.02	$z\ ^6D^\circ_{1\frac{1}{2}}$—$i\ ^6D_{2\frac{1}{2}}$	
6970.567	1	14342.09	0.01	$b\ ^4D_{3\frac{1}{2}}$—$z\ ^4F^\circ_{2\frac{1}{2}}$	
6989.914	15*h*	14302.39	−0.09	$z\ ^6D^\circ_{2\frac{1}{2}}$—$i\ ^6D_{3\frac{1}{2}}$	
7002.50	4*s*	14276.68	0.00	$b\ ^4D_{2\frac{1}{2}}$—$z\ ^4F^\circ_{2\frac{1}{2}}$	
7005.500	2*s*	14270.57	−0.01	$b\ ^4D_{1\frac{1}{2}}$—$z\ ^4F^\circ_{2\frac{1}{2}}$	
7012.256	10H	14256.82	0.01	$z\ ^6D^\circ_{3\frac{1}{2}}$—$i\ ^6D_{4\frac{1}{2}}$	
7013.15	2H	14255.00	0.01	$y\ ^6F^\circ_{5\frac{1}{2}}$—$e\ ^6G_{1\frac{1}{2}}$	
7014.09	1H	14253.09	0.04	$y\ ^6F^\circ_{3\frac{1}{2}}$—$e\ ^4G_{4\frac{1}{2}}$	

TABLE 1. Mn I—*Classified lines*—Continued

1	2	3	4	5	6
λ	Int.	σ	o−c	Term designation	Zeeman type
Å Air		K	K		
7033. 555	1HHH	14213. 65	0. 04	$y\ {}^6F^\circ_{1\frac{1}{2}}$—$e\ {}^6G_{2\frac{1}{2}}$	
7055. 583	4s	14169. 27	0. 03	$b\ {}^4D_{3\frac{1}{2}}$—$z\ {}^4F^\circ_{3\frac{1}{2}}$	
7062. 42	1HH	14155. 55	−0. 02	$y\ {}^6F^\circ_{2\frac{1}{2}}$—$e\ {}^6G_{3\frac{1}{2}}$	
7069. 834	20s	14140. 71	0. 02	$b\ {}^4G_{5\frac{1}{2}}$—$z\ {}^4G^\circ_{5\frac{1}{2}}$	
7076. 553	2H	14127. 28	−0. 07	$y\ {}^6F^\circ_{4\frac{1}{2}}$—$e\ {}^4G_{3\frac{1}{2}}$	
7077. 145	1	14126. 10	0. 07	$b\ {}^4G_{5\frac{1}{2}}$—$z\ {}^4G^\circ_{4\frac{1}{2}}$	
7088. 288	3s	14103. 89	0. 05	$b\ {}^4D_{2\frac{1}{2}}$—$z\ {}^4F^\circ_{3\frac{1}{2}}$	
7103. 010	2HH	14074. 66	0. 02	$y\ {}^6F^\circ_{3\frac{1}{2}}$—$e\ {}^6G_{4\frac{1}{2}}$	
7151. 267	5HH	13979. 69	0. 03	$y\ {}^6F^\circ_{5\frac{1}{2}}$—$e\ {}^6G_{6\frac{1}{2}}$	
7158. 039	2HH	13966. 46	0. 02	$y\ {}^6F^\circ_{4\frac{1}{2}}$—$e\ {}^6G_{5\frac{1}{2}}$	
7174. 420	4s	13934. 57	0. 02	$b\ {}^4D_{3\frac{1}{2}}$—$z\ {}^4F^\circ_{4\frac{1}{2}}$	
7176. 705	2h	13930. 14	−0. 17	$b\ {}^4G_{4\frac{1}{2}}$—$z\ {}^4G^\circ_{5\frac{1}{2}}$	
7184. 29	15s	13915. 43	−0. 22	$b\ {}^4G_{4\frac{1}{2}}$—$z\ {}^4G^\circ_{4\frac{1}{2}}$	
7192. 363	1h	13899. 81	−0. 18	$b\ {}^4G_{4\frac{1}{2}}$—$z\ {}^4G^\circ_{3\frac{1}{2}}$	
7211. 93	2	13862. 17	0. 00	$y\ {}^6F^\circ_{4\frac{1}{2}}$—$e\ {}^6F_{4\frac{1}{2}}$	
7239. 600	3s	13809. 02	−0. 03	$b\ {}^4G_{3\frac{1}{2}}$—$z\ {}^4G^\circ_{4\frac{1}{2}}$	
7247. 821	10s	13793. 45	0. 06	$b\ {}^4G_{3\frac{1}{2}}$—$z\ {}^4G^\circ_{3\frac{1}{2}}$	
7275. 690	1	13740. 62	−0. 06	$b\ {}^4G_{2\frac{1}{2}}$—$z\ {}^4G^\circ_{3\frac{1}{2}}$	
7283. 80	100	13725. 32	−0. 05	$y\ {}^6P^\circ_{1\frac{1}{2}}$—$f\ {}^6S_{2\frac{1}{2}}$	
7287. 10	1HH	13719. 10	−0. 05	$a\ {}^6D_{3\frac{1}{2}}$—$z\ {}^4P^\circ_{2\frac{1}{2}}$	
7301. 38	1HH	13692. 27	0. 08	$y\ {}^6F^\circ_{5\frac{1}{2}}$—$e\ {}^6F_{5\frac{1}{2}}$	
7302. 89	300	13689. 44	−0. 06	$y\ {}^6P^\circ_{2\frac{1}{2}}$—$f\ {}^6S_{2\frac{1}{2}}$	
7322. 205	1	13653. 34	0. 06	$a\ {}^4H_{3\frac{1}{2}}$—$y\ {}^6D^\circ_{4\frac{1}{2}}$	
7326. 500	400	13645. 33	−0. 05	$y\ {}^6P^\circ_{3\frac{1}{2}}$—$f\ {}^6S_{2\frac{1}{2}}$	
7376. 85	3	13552. 19	−0. 04	$a\ {}^2H_{5\frac{1}{2}}$—$z\ {}^4G^\circ_{5\frac{1}{2}}$	
7378. 98	1	13548. 28	−0. 05	$z\ {}^6D^\circ_{1\frac{1}{2}}$—$h\ {}^6D_{1\frac{1}{2}}$?	
7443. 50	1	13430. 85	0. 23	$a\ {}^4H_{4\frac{1}{2}}$—$y\ {}^6D^\circ_{3\frac{1}{2}}$	
7446. 16	1	13426. 05	−0. 04	$a\ {}^2H_{4\frac{1}{2}}$—$z\ {}^4G^\circ_{4\frac{1}{2}}$	
7667. 89	1H	13037. 81	−0. 06	$z\ {}^6F^\circ_{5\frac{1}{2}}$—$e\ {}^4D_{2\frac{1}{2}}$	
7670. 42	2H	13033. 51	0. 01	$z\ {}^6F^\circ_{4\frac{1}{2}}$—$e\ {}^4D_{3\frac{1}{2}}$	
7677. 46	2Hl	13021. 56	−0. 05	$z\ {}^6F^\circ_{1\frac{1}{2}}$—$i\ {}^6D_{0\frac{1}{2}}$	
7680. 22	50H	13016. 88	0. 02	$z\ {}^4F^\circ_{4\frac{1}{2}}$—$f\ {}^4D_{3\frac{1}{2}}$	
7706. 52	1HHH	12972. 46	0. 03	$z\ {}^6F^\circ_{2\frac{1}{2}}$—$i\ {}^6D_{1\frac{1}{2}}$	
7709. 98	3HHH	12966. 64	0. 19 −0. 07	$z\ {}^6F^\circ_{2\frac{1}{2}}$—$e\ {}^4D_{2\frac{1}{2}}$ $z\ {}^6F^\circ_{3\frac{1}{2}}$—$i\ {}^6D_{2\frac{1}{2}}$	
7712. 42	10H	12962. 54	0. 02	$z\ {}^4F^\circ_{3\frac{1}{2}}$—$f\ {}^4D_{2\frac{1}{2}}$	
7727. 07	1H	12937. 96	−0. 04	$z\ {}^6F^\circ_{3\frac{1}{2}}$—$e\ {}^4D_{3\frac{1}{2}}$	
7733. 24	10H	12927. 64	0. 01	$z\ {}^6F^\circ_{4\frac{1}{2}}$—$i\ {}^6D_{3\frac{1}{2}}$	
7734. 43	5H	12925. 66	0. 05	$z\ {}^4F^\circ_{2\frac{1}{2}}$—$f\ {}^4D_{1\frac{1}{2}}$	
7735. 77	1H	12923. 41	−0. 07	$z\ {}^6F^\circ_{1\frac{1}{2}}$—$i\ {}^6D_{1\frac{1}{2}}$	
7737. 16	3s	12921. 09	0. 03	$b\ {}^4G_{5\frac{1}{2}}$—$y\ {}^4F^\circ_{4\frac{1}{2}}$	
7752. 67	1HH	12895. 24	−0. 03 −0. 05	$z\ {}^6F^\circ_{0\frac{1}{2}}$—$i\ {}^6D_{1\frac{1}{2}}$ $z\ {}^6F^\circ_{2\frac{1}{2}}$—$i\ {}^6D_{2\frac{1}{2}}$	
7755. 15	3HHH	12891. 11	0. 01	$z\ {}^4F^\circ_{1\frac{1}{2}}$—$f\ {}^4D_{0\frac{1}{2}}$	
7764. 72	50H	12875. 23	0. 01	$z\ {}^6F^\circ_{5\frac{1}{2}}$—$i\ {}^6D_{4\frac{1}{2}}$	
7782. 2	1h	12846. 3	0. 0	$z\ {}^6F^\circ_{1\frac{1}{2}}$—$i\ {}^6D_{2\frac{1}{2}}$	
7790. 82	3H	12832. 10	−0. 03	$z\ {}^6F^\circ_{3\frac{1}{2}}$—$i\ {}^6D_{3\frac{1}{2}}$	
7806. 00	1HHH	12807. 14	−0. 03	$z\ {}^4F^\circ_{1\frac{1}{2}}$—$f\ {}^4D_{1\frac{1}{2}}$	
7816. 61	3H	12789. 76	0. 08	$z\ {}^4F^\circ_{2\frac{1}{2}}$—$f\ {}^4D_{2\frac{1}{2}}$	
7821. 25	3H	12782. 17	0. 00	$z\ {}^4F^\circ_{3\frac{1}{2}}$—$f\ {}^4D_{3\frac{1}{2}}$	
7834. 34	10h	12760. 81	0. 10 −0. 06	$z\ {}^6F^\circ_{2\frac{1}{2}}$—$i\ {}^6D_{3\frac{1}{2}}$ $z\ {}^6F^\circ_{4\frac{1}{2}}$—$i\ {}^6D_{4\frac{1}{2}}$	
7854. 24	3	12728. 48	−0. 18	$b\ {}^4G_{4\frac{1}{2}}$—$y\ {}^4F^\circ_{3\frac{1}{2}}$	

TABLE 1. Mn I—*Classified lines*—Continued

1	2	3	4	5	6
λ	Int.	σ	o − c	Term designation	Zeeman type
Å Air		K	K		
7865. 36	2	12710. 48	−0. 20	$b\ {}^4G_{4½}$—$y\ {}^4F^\circ_{4½}$	
7889. 61	1*h*	12671. 42	0. 18	$z\ {}^4F^\circ_{1½}$—$f\ {}^4D_{2½}$	
7911. 68	2	12636. 07	0. 06	$b\ {}^4G_{3½}$—$y\ {}^4F^\circ_{2½}$	
7920. 44	2	12622. 10	0. 04	$b\ {}^4G_{3½}$—$y\ {}^4F^\circ_{3½}$	
7928. 45	4	12609. 34	0. 01	$z\ {}^4F^\circ_{2½}$—$f\ {}^4D_{3½}$	
7938. 52	2	12593. 35	0. 01	$b\ {}^4G_{2½}$—$y\ {}^4F^\circ_{1½}$	
8043. 37	8	12429. 18	0. 00	$a\ {}^4D_{3½}$—$y\ {}^6P^\circ_{2½}$	
8194. 06	1	12200. 61	−0. 15	$z\ {}^4H^\circ_{6½}$—$e\ {}^4G_{5½}$	
8210. 16	2	12176. 69	0. 04	$a\ {}^4D_{2½}$—$y\ {}^6P^\circ_{2½}$	
8212. 43	40*hl*	12173. 32	0. 00	$z\ {}^4F^\circ_{4½}$—$e\ {}^4D_{3½}$	
8234. 43	1	12140. 80	0. 02	$a\ {}^4D_{2½}$—$y\ {}^6P^\circ_{1½}$	
8251. 64	5*h*	12115. 48	0. 04	$b\ {}^4P_{2½}$—$z\ {}^4D^\circ_{2½}$	
8284. 48	4*h*	12067. 45	0. 00	$z\ {}^4F^\circ_{4½}$—$i\ {}^6D_{3½}$	
8304. 42	5H*l*	12038. 48	−0. 02	$z\ {}^4F^\circ_{3½}$—$e\ {}^4D_{2½}$	
8353. 79	2H	11967. 33	−0. 01	$z\ {}^4F^\circ_{3½}$—$i\ {}^6D_{2½}$	
8373. 93	4*h*	11938. 54	−0. 09	$z\ {}^4F^\circ_{3½}$—$e\ {}^4D_{3½}$	
8380. 77	40	11928. 80	0. 02	$b\ {}^4P_{2½}$—$z\ {}^4D^\circ_{3½}$	
8395. 87	10H	11907. 35	−0. 09	$e\ {}^6S_{2½}$—$t\ {}^6P^\circ_{1½}$	
8409. 88	15H	11887. 51	−0. 14	$e\ {}^6S_{2½}$—$t\ {}^6P^\circ_{3½}$	
8421. 12	2H	11871. 65	0. 01	$z\ {}^4F^\circ_{2½}$—$i\ {}^6D_{1½}$	
8431. 20	20H	11857. 45	−0. 04	$e\ {}^6S_{2½}$—$t\ {}^6P^\circ_{3½}$	
8476. 3	1H	11794. 4	−0. 1	$z\ {}^4F^\circ_{3½}$—$i\ {}^6D_{2½}$	
8481. 70	3	11786. 85	−0. 05	$z\ {}^4F^\circ_{1½}$—$e\ {}^4D_{1½}$	
8506. 0	1H	11753. 18	−0. 02	$z\ {}^4F^\circ_{1½}$—$i\ {}^6D_{1½}$	
8521. 57	10*h*	11731. 71	0. 01	$z\ {}^4D^\circ_{3½}$—$f\ {}^4D_{2½}$	
8558. 63	8*h*	11680. 91	−0. 06	$z\ {}^4D^\circ_{2½}$—$f\ {}^4D_{1½}$	
8600. 34	5H	11624. 26	−0. 07	$z\ {}^6F^\circ_{5½}$—$g\ {}^6D_{4½}$	
8602. 1	2H	11621. 9	0. 0	$z\ {}^4D^\circ_{1½}$—$f\ {}^4D_{0½}$	
8603. 03	5	11620. 62	0. 10	$b\ {}^4P_{1½}$—$z\ {}^4D^\circ_{1½}$	
8654. 63	40*h*	11551. 34	−0. 01	$z\ {}^4D^\circ_{3½}$—$f\ {}^4D_{3½}$	
8659. 38	10*h*	11545. 00	−0. 04	$z\ {}^4D^\circ_{2½}$—$f\ {}^4D_{2½}$	
8664. 6	2*h*	11538. 0	0. 0	$z\ {}^4D^\circ_{1½}$—$f\ {}^4D_{1½}$	
8666. 3	2*h*	11535. 8	−0. 1	$z\ {}^4D^\circ_{0½}$—$f\ {}^4D_{0½}$	
8670. 92	200*c*	11529. 74	0. 08	$y\ {}^6P^\circ_{1½}$—$e\ {}^6D_{0½}$	
8672. 06	300*c*	11528. 12	−0. 05	$y\ {}^6P^\circ_{1½}$—$e\ {}^6D_{1½}$	
8673. 97	200*c*	11525. 58	−0. 05	$y\ {}^6P^\circ_{1½}$—$e\ {}^6D_{2½}$	
8680. 24	2*h*	11517. 26	−0. 25	$z\ {}^6F^\circ_{4½}$—$g\ {}^6D_{3½}$	
8699. 13	100*c*	11492. 25	−0. 05	$y\ {}^6P^\circ_{2½}$—$e\ {}^6D_{1½}$	
8701. 05	300*c*	11489. 71	−0. 05	$y\ {}^6P^\circ_{2½}$—$e\ {}^6D_{2½}$	
8703. 76	500*cw*	11486. 14	−0. 07	$y\ {}^6P^\circ_{2½}$—$e\ {}^6D_{3½}$	
8710. 21	10	11477. 63	0. 07	$b\ {}^4P_{1½}$—$z\ {}^4D^\circ_{2½}$	
8717. 29	2*h*	11468. 31	0. 15	$x\ {}^6P^\circ_{3½}$—$e\ {}^4D_{3½}$	
8729. 80	2*h*	11451. 80	−0. 17	$z\ {}^4D^\circ_{0½}$—$f\ {}^4D_{1½}$	
8734. 60	30*c*	11445. 58	−0. 06	$y\ {}^6P^\circ_{3½}$—$e\ {}^6D_{2½}$	
8737. 32	300*c*	11442. 02	−0. 07	$y\ {}^6P^\circ_{3½}$—$e\ {}^6D_{3½}$	
8740. 93	1000*cw*	11437. 29	−0. 02	$y\ {}^6P^\circ_{3½}$—$e\ {}^6D_{4½}$	
8767. 96	5*h*	11402. 03	−0. 05	$z\ {}^4D^\circ_{1½}$—$f\ {}^4D_{2½}$	
8796. 83	6*h*	11364. 61	−0. 08	$z\ {}^4D^\circ_{2½}$—$f\ {}^4D_{3½}$	
8798. 66	3*h*	11362. 25	−0. 04 0. 10	$x\ {}^6P^\circ_{3½}$—$i\ {}^6D_{3½}$ $y\ {}^8P^\circ_{4½}$—$e\ {}^8P_{4½}$	
8820. 26	4*h*	11334. 43	−0. 25	$x\ {}^6P^\circ_{2½}$—$i\ {}^6D_{2½}$	
8827. 83	3	11324. 70	0. 03	$b\ {}^4P_{0½}$—$z\ {}^4D^\circ_{0½}$	
8842. 48	3*h*	11305. 94	−0. 03	$x\ {}^6P^\circ_{2½}$—$e\ {}^4D_{3½}$	
8895. 9	4	11238. 72	0. 09	$b\ {}^4P_{0½}$—$z\ {}^4D^\circ_{1½}$	
8901. 0	2*p*	11231. 6	0. 0	$x\ {}^6P^\circ_{1½}$—$i\ {}^6D_{2½}$	
8926. 06	15*h*	11200. 08	−0. 02	$x\ {}^6P^\circ_{2½}$—$i\ {}^6D_{3½}$	

TABLE 1. Mn I—*Classified lines*—Continued

1	2	3	4	5	6
λ	Int.	σ	o−c	Term designation	Zeeman type
Å Air		K	K		
8929. 72	60*h*	11195. 49	−0. 04	$x\ ^6P^o_{3½}$—$i\ ^6D_{4½}$	
8932. 96	2	11191. 43	0. 03	$y\ ^8P^o_{4½}$—$e\ ^8P_{3½}$	
9084. 29	30	11005. 00	0. 12	$a\ ^4F_{1½}$—$z\ ^4D^o_{0½}$	
9101. 2	3*hw*	10984. 6	0. 0	$e\ ^8D_{5½}$—$t\ ^6F°$	
9114. 02	50	10969. 10	0. 19	$a\ ^4F_{2½}$—$z\ ^4D^o_{1½}$	
9155 ±3	5	10918. 98	0. 14	$a\ ^4F_{1½}$—$z\ ^4D^o_{1½}$	
9172. 09	100	10899. 66	0. 10	$a\ ^4F_{2½}$—$z\ ^4D^o_{2½}$	
9234. 40	10	10826. 11	0. 16	$a\ ^4F_{2½}$—$z\ ^4D^o_{2½}$	
9243. 29	150	10815. 69	0. 12	$a\ ^4F_{4½}$—$z\ ^4D^o_{3½}$	
9325. 16	5	10720. 74	−0. 03	$y\ ^4P^o_{2½}$—$f\ ^4D_{1½}$	
9331. 90	20*h*	10712. 99	0. 09	$a\ ^4F_{3½}$—$z\ ^4D^o_{3½}$	
9336. 47	40*h*	10707. 75	−0. 06	$z\ ^4D^o_{3½}$—$e\ ^4D_{3½}$	
9412. 78	10*h*	10620. 94	−0. 08	$z\ ^4D^o_{2½}$—$e\ ^4D_{2½}$	
9429. 58	30*h*	10602. 02	0. 08	$z\ ^4D^o_{3½}$—$i\ ^6D_{3½}$	
9444. 90	40	10584. 82	−0. 02	$y\ ^4P^o_{2½}$—$f\ ^4D_{2½}$	
9474. 9	2	10551. 3	0. 0	$y\ ^4P^o_{1½}$—$f\ ^4D_{0½}$	
9476. 57	4*h*	10549. 45	−0. 41	$z\ ^4D^o_{2½}$—$i\ ^6D_{2½}$?	
9502. 12	6*h*	10521. 08	−0. 07	$z\ ^4D^o_{2½}$—$e\ ^4D_{3½}$	
9335. 72	5*h*	10484. 01	−0. 03	$z\ ^4D^o_{1½}$—$i\ ^6D_{1½}$	
9550. 80	20*h*	10467. 46	0. 07	$y\ ^4P^o_{1½}$—$f\ ^4D_{1½}$	
9584. 0	10*h*	10431. 2	−0. 5	$z\ ^4D^o_{0½}$—$e\ ^4D_{1½}$	
9598. 7	3	10415. 2	−0. 1	$z\ ^4D^o_{2½}$—$i\ ^6D_{3½}$	
9606. 71	5*h*	10406. 54	0. 00	$y\ ^4P^o_{0½}$—$f\ ^4D_{0½}$	
9608. 56	100*h*	10404. 54	0. 05	$y\ ^4P^o_{2½}$—$f\ ^4D_{2½}$	
9676. 50	40	10331. 49	0. 03	$y\ ^4P^o_{1½}$—$f\ ^4D_{2½}$	
9684. 9	15	10322. 5	−0. 1	$y\ ^4P^o_{0½}$—$f\ ^4D_{1½}$	
9845. 1	5H	10154. 54	0. 0	$e\ ^8D_{5½}$—$u\ ^6F°$	
10045. 4	4H	9952. 08	−0. 09	$x\ ^6P^o_{3½}$—$g\ ^6D_{3½}$	
10053. 1	10H	9944. 46	−0. 18	$x\ ^6P^o_{3½}$—$g\ ^6D_{4½}$	
10164. 9	2*h*	9835. 08	−0. 15	$b\ ^2I_{5½}$—$z\ ^8F°$?	
10204. 9	1H	9796. 53	−0. 38	$x\ ^6P^o_{2½}$—$g\ ^6D_{1½}$	
10208. 2	2H	9793. 36	−1. 19	$x\ ^6P^o_{2½}$—$g\ ^6D_{2½}$?	
10212. 3	5H	9789. 43	−0. 55	$x\ ^6P^o_{2½}$—$g\ ^6D_{3½}$	
10300. 7	5*h*	9705. 42	−0. 11	$z\ ^6D^o_{3½}$—$e\ ^4P_{2½}$	
10313. 35	2*h*	9693. 51	−0. 34	$x\ ^6P^o_{1½}$—$g\ ^6D_{1½}$	
10316. 05	5*h*	9690. 97	0. 24	$x\ ^6P^o_{1½}$—$g\ ^6D_{0½}$	
10349. 3	2H	9659. 84	0. 0	$e\ ^6D_{4½}$—$u\ ^6F°$	
10456. 60	3	9560. 72	−0. 23	$y\ ^4P^o_{2½}$—$e\ ^4D_{3½}$	
10561. 2	6*h*	9465. 94	−0. 44	$x\ ^6P^o_{3½}$—$h\ ^6S_{2½}$?	
10621. 9	6	9411. 93	−0. 23	$z\ ^6F^o_{5½}$—$f\ ^6D_{4½}$	
10643. 0	10H	9393. 26	−0. 06	$y\ ^8P^o_{2½}$—$g\ ^8D_{3½}$	
10664. 1	15H	9374. 69	−0. 24	$y\ ^8P^o_{3½}$—$g\ ^8D_{4½}$	
10686. 8	2	9354. 78	−0. 17	$y\ ^4D^o_{5½}$—$e\ ^4G_{4½}$	
10692. 2	20H	9350. 05	0. 10	$y\ ^8P^o_{4½}$—$g\ ^8D_{5½}$	
10745. 32	6*h*	9303. 83	−0. 36	$x\ ^6P^o_{2½}$—$h\ ^6S_{2½}$	
10856. 08	2*h*	9208. 91	−0. 23	$z\ ^6F^o_{3½}$—$f\ ^6D_{2½}$	
10865. 85	2*h*	9200. 63	−0. 50	$x\ ^6P^o_{1½}$—$h\ ^6S_{2½}$	
10938. 65	3*h*	9139. 40	−0. 11	$z\ ^6F^o_{2½}$—$f\ ^6D_{1½}$	
11163. 3	2	8955. 47	−0. 04	$x\ ^6D^o_{4½}$—$e\ ^6F_{5½}$	
11378. 8	100*w*	8785. 89	0. 0	$e\ ^8D_{5½}$—$y\ ^8F^o_{6½}$	
11497. 61	40	8695. 08	−0. 15	$e\ ^6S_{2½}$—$v\ ^6P^o_{1½}$	
11613. 24	50	8608. 50	−0. 10	$e\ ^6S_{2½}$—$v\ ^6P^o_{2½}$	
11644. 84	3	8585. 14	−0. 24	$a\ ^4F_{4½}$—$z\ ^6F^o_{5½}$	
11783. 58	60	8484. 07	−0. 08	$e\ ^6S_{2½}$—$v\ ^6P^o_{3½}$	
12899. 7	80	7750. 0	0. 0	$a\ ^6D_{4½}$—$z\ ^6P^o_{3½}$	

TABLE 1. Mn I—*Classified lines*—Continued

1	2	3	4	5	6
λ	Int.	σ	o−c	Term designation	Zeeman type
Å Air		K	K		
12975.9	40	7704.5	0.0	$a\ ^4D_{3\frac{1}{2}}$—$z\ ^4P^\circ_{2\frac{1}{2}}$	
13294.1	50	7520.1	−0.1	$a\ ^6D_{3\frac{1}{2}}$—$z\ ^6P^\circ_{3\frac{1}{2}}$	
13317.9	30	7506.7	0.7	$a\ ^6D_{3\frac{1}{2}}$—$z\ ^6P^\circ_{2\frac{1}{2}}$	
13415.9	80	7451.8	−0.2	$a\ ^4D_{2\frac{1}{2}}$—$z\ ^4P^\circ_{2\frac{1}{2}}$	
13500.1	100	7405.4	0.0	$a\ ^4D_{1\frac{1}{2}}$—$z\ ^4P^\circ_{0\frac{1}{2}}$	
13625.7	200	7337.1	0.6	$a\ ^6D_{2\frac{1}{2}}$—$z\ ^6P^\circ_{2\frac{1}{2}}$	
13684.6	80	7305.5	−0.6	$a\ ^4D_{0\frac{1}{2}}$—$z\ ^4P^\circ_{0\frac{1}{2}}$	
13863.8	100	7211.1	0.3	$a\ ^6D_{1\frac{1}{2}}$—$z\ ^6P^\circ_{1\frac{1}{2}}$	
13997.0	120	7142.4	0.2	$a\ ^6D_{0\frac{1}{2}}$—$z\ ^6P^\circ_{1\frac{1}{2}}$	
14969.9	30	6678.2	−0.3	$y\ ^8P^\circ_{4\frac{1}{2}}$—$f\ ^8D_{5\frac{1}{2}}$	
15217.9	80	6569.4	−0.1	$e\ ^8S_{3\frac{1}{2}}$—$y\ ^8P^\circ_{3\frac{1}{2}}$	
15263.1	200	6550.0	−0.1	$e\ ^8S_{3\frac{1}{2}}$—$y\ ^8P^\circ_{2\frac{1}{2}}$	
15964.9	200	6262.1	0.2	$e\ ^8D_{3\frac{1}{2}}$—$z\ ^8F^\circ$	
17335.2	80	5767.0	−0.2	$e\ ^6D_{4\frac{1}{2}}$—$z\ ^8F^\circ$	
17607.5	20	5677.9	−0.2	$e\ ^6S_{2\frac{1}{2}}$—$y\ ^6P^\circ_{2\frac{1}{2}}$	

TABLE 2. *Even terms of* Mn I

Config.	Desig.	J	Level	Interval	Obs. g
$3d^5\ 4s^2$	$a\ ^6S$	$2\frac{1}{2}$	0.00		1.999
$3d^6(a\ ^5D)4s$	$a\ ^6D$	$4\frac{1}{2}$	17052.29		1.559
		$3\frac{1}{2}$	17282.00	−229.71	1.584
		$2\frac{1}{2}$	17451.52	−169.52	1.657
		$1\frac{1}{2}$	17568.48	−116.96	1.866
		$0\frac{1}{2}$	17637.15	−68.67	3.327
$3d^6(a\ ^5D)4s$	$a\ ^4D$	$3\frac{1}{2}$	23296.67		1.427
		$2\frac{1}{2}$	23549.20	−252.53	1.368
		$1\frac{1}{2}$	23719.52	−170.32	1.198
		$0\frac{1}{2}$	23818.87	−99.35	0.000
$3d^5\ 4s^2$	$a\ ^4G$	$5\frac{1}{2}$	25265.74		1.270
		$4\frac{1}{2}$	25285.43	−19.69	1.173
		$3\frac{1}{2}$	25287.74	−2.31	
		$2\frac{1}{2}$	25281.04	6.70	
$3d^5\ 4s^2$	$a\ ^4P$	$2\frac{1}{2}$	27201.54		1.597
		$1\frac{1}{2}$	27248.00	−46.46	1.730
		$0\frac{1}{2}$	27281.85	−33.85	2.666
$3d^5\ 4s^2$	$b\ ^4D$	$3\frac{1}{2}$	30354.21		1.425
		$2\frac{1}{2}$	30419.61	−65.40	1.38
		$1\frac{1}{2}$	30425.71	−6.10	
		$0\frac{1}{2}$	30411.74	13.97	0.111
$3d^6(a\ ^3P)4s$	$b\ ^4P$	$2\frac{1}{2}$	33825.49		1.602
		$1\frac{1}{2}$	34463.37	−637.88	1.730
		$0\frac{1}{2}$	34845.26	−381.89	2.655
$3d^6(a^3H)4s$	$a\ ^4H$	$6\frac{1}{2}$	34138.88		1.231
		$5\frac{1}{2}$	34250.52	−111.64	1.135
		$4\frac{1}{2}$	34343.90	−93.38	0.971
		$3\frac{1}{2}$	34423.27	−79.37	0.665

TABLE 2. *Even terms of* Mn I—Continued

Config.	Desig.	J	Level	Interval	Obs. g
$3d^6(a\ ^3F)4s$	$a\ ^4F$	$4\frac{1}{2}$	34938. 70		1. 328
		$3\frac{1}{2}$	35041. 37	−102. 67	1. 238
		$2\frac{1}{2}$	35114. 98	−73. 61	1. 024
		$1\frac{1}{2}$	35165. 05	−50. 07	0. 430
$3d^5\ 4s^2$	$a\ ^2I$	$5\frac{1}{2}$	37148. 66		0. 94
		$6\frac{1}{2}$	37164. 25	15. 59	
$3d^6(a\ ^3G)4s$	$b\ ^4G$	$5\frac{1}{2}$	37420. 24		1. 263
		$4\frac{1}{2}$	37630. 62	−210. 58	1. 163
		$3\frac{1}{2}$	37737. 22	−106. 40	0. 989
		$2\frac{1}{2}$	37789. 93	−52. 71	0. 59
$3d^6(^3P)4s$	$a\ ^2P$	$1\frac{1}{2}$	37586. 03		
		$0\frac{1}{2}$	38351. 78	−765. 75	0. 675
$3d^6(a\ ^3H)4s$	$a\ ^2H$	$5\frac{1}{2}$	38008. 70		1. 098
		$4\frac{1}{2}$	38120. 18	−111. 48	0. 914
$3d^6(a\ ^3F)4s$	$a\ ^2F$	$3\frac{1}{2}$	38669. 60		1. 128
		$2\frac{1}{2}$	38934. 94	−265. 34	
$3d^5\ 4s(a\ ^7S)5s$	$e\ ^8S$	$3\frac{1}{2}$	39431. 31		2. 000
$3d^6(^3G)4s$	$a\ ^2G$	$4\frac{1}{2}$	41031. 48		1. 118
		$3\frac{1}{2}$	41230. 30	−198. 86	0. 88
$3d^5\ 4s(a\ ^7S)5s$	$e\ ^6S$	$2\frac{1}{2}$	41403. 93		1. 997
	$b\ ^2I$	$6\frac{1}{2}$	43053. 30		1. 07
		$5\frac{1}{2}$	43139. 27	−85. 97	0. 924
$3d^5\ 4s(a\ ^7S)4d$	$e\ ^8D$	$1\frac{1}{2}$	46706. 09		
		$2\frac{1}{2}$	46707. 03	0. 94	
		$3\frac{1}{2}$	46708. 33	1. 30	
		$4\frac{1}{2}$	46710. 15	1. 82	
		$5\frac{1}{2}$	46712. 58	2. 43	
$3d^5\ 4s(a\ ^7S)4d$	$e\ ^6D$	$4\frac{1}{2}$	47207. 28		1. 554
		$3\frac{1}{2}$	47212. 06	−4. 78	1. 581
		$2\frac{1}{2}$	47215. 61	−3. 55	1. 634
		$1\frac{1}{2}$	47218. 15	−2. 54	1. 759
		$0\frac{1}{2}$	47219. 64	−1. 49	3. 934
$3d^5\ 4s(a\ ^5S)5s$	$f\ ^6S$	$2\frac{1}{2}$	49415. 35		2. 00
$3d^54s(a\ ^5S)5s$	$e\ ^4S$	$1\frac{1}{2}$	49591. 51		1. 998
$3d^54s(a\ ^7S)6s$	$f\ ^8S$	$3\frac{1}{2}$	50157. 63		1. 995
$3d^54s(a\ ^7S)6s$	$g\ ^6S$	$2\frac{1}{2}$	50904. 68		
$3d^7$	$e\ ^4P$	$2\frac{1}{2}$	51638. 17		1. 601
		$1\frac{1}{2}$	51718. 22	−80. 05	1. 733
		$0\frac{1}{2}$	51787. 92	−69. 70	2. 65
$3d^54s(a\ ^7S)5d$	$f\ ^8D$	$1\frac{1}{2}$			
		$2\frac{1}{2}$	52702. 48?		
		$3\frac{1}{2}$			
		$4\frac{1}{2}$	52703. 1	0. 6	
		$5\frac{1}{2}$	52705. 23	2. 1	
$3d^54s(a\ ^7S)5d$	$f\ ^6D$	$4\frac{1}{2}$	52726. 39		
		$3\frac{1}{2}$	52730. 41	−4. 02	
		$2\frac{1}{2}$	52733. 22	−2. 81	
		$1\frac{1}{2}$	52735. 01	−1. 79	
		$0\frac{1}{2}$	52735. 83	−0. 82	
$3d^54s(a\ ^7S)7s$	$h\ ^6S$	$2\frac{1}{2}$	54460. 30		

TABLE 2. *Even terms of* Mn I—Continued

Config.	Desig.	J	Level	Interval	Obs. g
$3d^5 4s(a\ ^5S)4d$	$g\ ^6D$	4½	54938. 56		
		3½	54946. 09	−7. 53	
		2½	54950. 66	−4. 57	
		1½	54953. 02	−2. 36	
		½	54949. 90	3. 12	
$3d^5 4s(a\ ^7S)6d$	$g\ ^8D$	1½			
		2½			
		3½	55374. 76		
		4½	55375. 70	0. 94	
		5½	55376. 70	1. 00	
$3d^5 4s(a\ ^7S)6d$	$h\ ^6D$	4½	55681. 90		
		3½	55688. 10	−6. 20	
		2½	55690. 80	−2. 70	
		1½	55691. 90	−1. 10	
		½	55692. 40	−0. 50	
$3d^5 4s(a\ ^7S)8s$	$g\ ^8S$	3½	56144. 16		
$3d^6(a\ ^5D)5s$	$i\ ^6D$	4½	56189. 45		
		3½	56356. 21	−166. 76	1. 57
		2½	56490. 79	−134. 58	
		1½	56567. 93	−77. 14	
		½	56666. 06	−98. 13	
	$e\ ^4D$	3½	56462. 08		
		2½	56561. 95	−99. 87	
		1½	56601. 63	−39. 68	
		½			
$3d^5 4s(a\ ^7S)7d$	$h\ ^8D$	1½ to 5½	56801. 4?		
$3d^5 4p^2$	$e\ ^8P$	2½	57086. 33		2. 27
		3½	57218. 15	131. 82	
		4½	57388. 90	170. 75	1. 767
$3d^6(a\ ^5D)5s$	$f\ ^4D$	3½	57305. 62		
		2½	57485. 97	−180. 35	1. 372
		1½	57621. 90	−135. 93	
		½	57705. 83	−83. 93	
Mn II ($^7S_3$)	***Limit***		**59970**		
$3d^5(a\ ^5D)5d$	$e\ ^6F$	5½	61713. 62		
		4½	62030. 18	−316. 56	
		3½	62294. 66	−264. 48	
		2½	62905. 81	−611. 15	
		1½	63083. 24	−177. 43	
		½			
$3d^6(a\ ^5D)4d$	$e\ ^6G$	6½	62001. 09		
		5½	62134. 45	−133. 36	
		4½	62300. 63	−166. 18	
		3½	62426. 48	−125. 85	
		2½	62514. 59	−88. 11	
		1½	62573. 11	−58. 52	
$3d^6(a\ ^5D)4d$	$e\ ^4G$	5½	62295. 36		
		4½	62479. 04	−183. 68	
		3½	62632. 77	−153. 73	
		2½	62753. 37	−120. 60	
$3d^6(a\ ^5D)4d$	$e\ ^4F$	4½	63231. 43		
		3½	63424. 00	−192. 57	
		2½			
		1½			
$3d^5 4s(a\ ^5G)5s$	$f\ ^4G$	5½	68693. 02		
		4½	68716. 22	−23. 20	1. 17
		3½			
		2½			

TABLE 2. *Odd Terms of* Mn I

Config.	Desig.	J	Level	Interval	Obs. g
$3d^5\ 4s(a\ ^7S)4p$	$z\ ^8P^\circ$	$2\frac{1}{2}$	18402. 46		2. 284
		$3\frac{1}{2}$	18531. 64	129. 18	1. 938
		$4\frac{1}{2}$	18705. 37	173. 73	1. 779
$3d^5\ 4s(a\ ^7S)4p$	$z\ ^6P^\circ$	$1\frac{1}{2}$	24779. 32		2. 364
		$2\frac{1}{2}$	24788. 05	8. 73	1. 875
		$3\frac{1}{2}$	24802. 25	14. 20	1. 714
$3d^5\ 4s(a\ ^5S)4p$	$z\ ^4P^\circ$	$2\frac{1}{2}$	31001. 15		1. 60
		$1\frac{1}{2}$	31076. 42	−75. 27	1. 732
		$0\frac{1}{2}$	31124. 95	−48. 53	2. 668
$3d^5\ 4s(a\ ^5S)4p$	$y\ ^6P^\circ$	$1\frac{1}{2}$	35689. 98		2. 400
		$2\frac{1}{2}$	35725. 85	35. 87	1. 886
		$3\frac{1}{2}$	35769. 97	44. 12	1. 712
$3d^6(a\ ^5D)4p$	$z\ ^6D^\circ$	$4\frac{1}{2}$	41789. 48		1. 556
		$3\frac{1}{2}$	41932. 64	−143. 16	1. 587
		$2\frac{1}{2}$	42053. 73	−121. 09	1. 653
		$1\frac{1}{2}$	42143. 57	−89. 84	1. 867
		$0\frac{1}{2}$	42198. 56	−54. 99	3. 317
$3d^6(a\ ^5D)4p$	$z\ ^6F^\circ$	$5\frac{1}{2}$	43314. 23		1. 464
		$4\frac{1}{2}$	43428. 58	−114. 35	1. 431
		$3\frac{1}{2}$	43524. 08	−95. 50	1. 395
		$2\frac{1}{2}$	43595. 50	−71. 42	1. 310
		$1\frac{1}{2}$	43644. 45	−48. 95	1. 068
		$0\frac{1}{2}$	43672. 66	−28. 21	−0. 602
$3d^6(a\ ^5D)4p$	$z\ ^4F^\circ$	$4\frac{1}{2}$	44288. 76		1. 317
		$3\frac{1}{2}$	44523. 45	−234. 69	1. 240
		$2\frac{1}{2}$	44696. 29	−172. 84	1. 030
		$1\frac{1}{2}$	44814. 73	−118. 44	0. 400
$3d^6(a\ ^5D)4p$	$x\ ^6P^\circ$	$3\frac{1}{2}$	44993. 92		1. 717
		$2\frac{1}{2}$	45156. 11	−162. 19	1. 885
		$1\frac{1}{2}$	45259. 17	−103. 06	2. 399
$3d^6(a\ ^5D)4p$	$z\ ^4D^\circ$	$3\frac{1}{2}$	45754. 27		1. 427
		$2\frac{1}{2}$	45940. 93	−186. 66	1. 372
		$1\frac{1}{2}$	46083. 89	−142. 96	1. 200
		$0\frac{1}{2}$	46169. 93	−86. 04	0. 000
$3d^5\ 4s(a\ ^7S)5p$	$y\ ^8P^\circ$	$2\frac{1}{2}$	45981. 44		
		$3\frac{1}{2}$	46000. 77	19. 33	
		$4\frac{1}{2}$	46026. 75	25. 98	
$3d^6(a\ ^5D)4p$	$y\ ^4P^\circ$	$2\frac{1}{2}$	46901. 13		1. 595
		$1\frac{1}{2}$	47154. 51	−253. 38	1. 732
		$0\frac{1}{2}$	47299. 29	−144. 78	2. 666
$3d^5\ 4s(a\ ^7S)5p$	$w\ ^8P^\circ$	$3\frac{1}{2}$	47387. 62		1. 713
		$2\frac{1}{2}$	47659. 52	−271. 90	1. 952
		$1\frac{1}{2}$	47782. 43	−122. 91	2. 666
$3d^5\ 4s(a\ ^5P)4p$	$y\ ^6D^\circ$	$0\frac{1}{2}$	47452. 16		3. 174
		$1\frac{1}{2}$	47466. 66	14. 50	
		$2\frac{1}{2}$	47753. 99	287. 33	1. 820
		$3\frac{1}{2}$	47774. 52	20. 53	1. 594
		$4\frac{1}{2}$	47903. 80	129. 28	1. 540
$3d^5\ 4s(a\ ^5G)4p$	$y\ ^6F^\circ$	$5\frac{1}{2}$	48021. 43		1. 460
		$4\frac{1}{2}$	48168. 01	−146. 58	1. 432
		$3\frac{1}{2}$	48225. 99	−57. 98	1. 043
		$2\frac{1}{2}$	48270. 91	−44. 92	1. 319
		$1\frac{1}{2}$	48300. 98	−30. 07	1. 068
		$0\frac{1}{2}$	48318. 12	−17. 14	−0. 496

TABLE 2. *Odd Terms of* Mn I—Continued

Config.	Desig.	J	Level	Interval	Obs. g
$3d^5\ 4s(a\ ^5P)4p$	$v\ ^6P°$	$3\frac{1}{2}$	49888. 08		1. 711
		$2\frac{1}{2}$	50012. 53	−124. 45	1. 888
		$1\frac{1}{2}$	50099. 16	−86. 63	2. 398
$3d^5\ 4s(a\ ^5G)4p$	$z\ ^4H°$	$3\frac{1}{2}$	50065. 46		
		$4\frac{1}{2}$	50072. 59	7. 13	
		$5\frac{1}{2}$	50081. 31	8. 72	
		$6\frac{1}{2}$	50094. 60	13. 29	1. 22
$3d^5\ 4s(a\ ^5G)4p$	$y\ ^4F°$	$4\frac{1}{2}$	50341. 30		1. 318
		$3\frac{1}{2}$	50359. 28	−17. 98	1. 242
		$2\frac{1}{2}$	50373. 23	−13. 95	1. 03
		$1\frac{1}{2}$	50383. 27	−10. 04	
$3d^5\ 4s(b\ ^5D)4p$	$x\ ^6F°$	$0\frac{1}{2}$	50818. 64		−0. 62
		$1\frac{1}{2}$	50863. 05	44. 41	1. 07
		$2\frac{1}{2}$	50931. 42	68. 37	1. 316
		$3\frac{1}{2}$	51014. 95	83. 53	
		$4\frac{1}{2}$	51100. 49	85. 54	
		$5\frac{1}{2}$	51169. 18	68. 69	
$3d^5\ 4s(a\ ^5P)4p$	$x\ ^4P°$	$2\frac{1}{2}$	51305. 41		1. 591
		$1\frac{1}{2}$	51445. 65	−140. 24	1. 728
		$0\frac{1}{2}$	51552. 78	−107. 13	2. 664
$3d^5\ 4s(a\ ^5G)4p$	$z\ ^4G°$	$2\frac{1}{2}$	51515. 63		
		$3\frac{1}{2}$	51530. 61	14. 98	
		$4\frac{1}{2}$	51546. 27	15. 66	
		$5\frac{1}{2}$	51560. 93	14. 66	1. 273
$3d^5\ 4s(b\ ^5D)4p$	$u\ ^6P°$	$1\frac{1}{2}$	52015. 00		
		$2\frac{1}{2}$	52128. 65	113. 65	
		$3\frac{1}{2}$	52253. 24	124. 59	1. 71
$3d^5\ 4s(b\ ^5D)4p$	$x\ ^6D°$	$4\frac{1}{2}$	52758. 11		1. 552
		$3\frac{1}{2}$	52870. 10	−111. 99	1. 57
		$2\frac{1}{2}$	52883. 87	−13. 77	
		$1\frac{1}{2}$	52883. 87	0. 00	
		$0\frac{1}{2}$	52883. 10	0. 77	
$3d^5\ 4s(a\ ^7S)4f$	$z\ ^8F°$	$0\frac{1}{2}$ to $6\frac{1}{2}$	52974. 5?		
$3d^5\ 4s(a\ ^7S)4f$	$w\ ^6F°$	$0\frac{1}{2}$			
		$1\frac{1}{2}$	52977. 93		
		$2\frac{1}{2}$	52978. 03	0. 10	
		$3\frac{1}{2}$	52977. 82	−0. 21	
		$4\frac{1}{2}$	52977. 75	−0. 07	
		$5\frac{1}{2}$	52977. 89	0. 14	
$3d^5\ 4s(a\ ^5P)4p$	$y\ ^4D°$	$0\frac{1}{2}$	53101. 32		
		$1\frac{1}{2}$	53103. 19	1. 87	
		$2\frac{1}{2}$	53109. 21	6. 02	
		$3\frac{1}{2}$	53124. 09	14. 88	1. 423
$3d^5\ 4s(a\ ^7S)6p$	$t\ ^6P°$	$3\frac{1}{2}$	53261. 42		
		$2\frac{1}{2}$	53291. 58	−30. 16	
		$1\frac{1}{2}$	53311. 37	−19. 79	
$3d^5\ 4s(a\ ^5P)4p$	$z\ ^4S°$	$1\frac{1}{2}$	54218. 71		1. 770
$3d^5\ 4s(b\ ^5D)4p$	$x\ ^4D°$	$3\frac{1}{2}$	55107. 52		1. 407
		$2\frac{1}{2}$	55186. 17	−78. 65	1. 365
		$1\frac{1}{2}$	55279. 91	−93. 74	0. 826
		$0\frac{1}{2}$			
$3d^5\ 4s(b\ ^5D)4p$	$w\ ^4P°$	$2\frac{1}{2}$	55405. 14		
		$1\frac{1}{2}$	55368. 66	36. 48	
		$0\frac{1}{2}$	55457. 20	−88. 54	2. 28

TABLE 2. *Odd Terms of* Mn I—Continued

Config.	Desig.	J	Level	Interval	Obs. g
$3d^5\ 4s(a\ ^7S)5f$	$v\ ^6F°$	$0\frac{1}{2}$			
		$1\frac{1}{2}$	55491. 95		
		$2\frac{1}{2}$	55491. 57	−0. 38	
		$3\frac{1}{2}$	55492. 08	0. 15	
		$4\frac{1}{2}$	55492. 52	0. 44	
		$5\frac{1}{2}$	55492. 74	0. 22	
$3d^5\ 4s(a\ ^7S)5f$	$y\ ^8F°$	$6\frac{1}{2}$	55498. 5		
		$5\frac{1}{2}$	55499. 09	−0. 6	
		$4\frac{1}{2}$	55499. 09	0. 0	
		$3\frac{1}{2}$	55499. 5	−0. 4	
		$2\frac{1}{2}$	55499. 90	−0. 4	
		$1\frac{1}{2}$	55499. 75	0. 15	
		$0\frac{1}{2}$			
		$2\frac{1}{2}$	55923. 81		
$3d^5\ 4s(a\ ^5S)5p$	$s\ ^6P°?$	$1\frac{1}{2}$	55996. 62		
		$2\frac{1}{2}$	56007. 91	11. 29	
		$3\frac{1}{2}$	56012. 42	4. 51	
$3d^5\ 4s(a\ ^7S)6f$	$u\ ^6F°$	$0\frac{1}{2}$ to $6\frac{1}{2}$	56867. 1		
$3d^5\ 4s(b\ ^3P)4p$	$v\ ^4P°$	$0\frac{1}{2}$	57228. 30		2. 671
		$1\frac{1}{2}$	57360. 78	132. 48	1. 736
		$2\frac{1}{2}$	57487. 08	126. 30	1. 590
$3d^5\ 4s(b\ ^3P)4p$	$y\ ^4S°$	$1\frac{1}{2}$	57512. 16		2. 000
$3d^5\ 4s(a\ ^7S)7f$	$t\ ^6F°$	$0\frac{1}{2}$ to $6\frac{1}{2}$	57697. 2		
$3d^6(a\ ^3H)4p$	$y\ ^4G°$	$5\frac{1}{2}$	58075. 06		1. 269
		$4\frac{1}{2}$	58110. 24	−35. 18	1. 168
		$3\frac{1}{2}$	58136. 69	−26. 45	0. 980
		$2\frac{1}{2}$	58159. 73	−23. 04	0. 578
$3d^6(a\ ^3H)4p$	$y\ ^4H°$	$6\frac{1}{2}$	58338. 67		1. 228
		$5\frac{1}{2}$	58427. 30	−88. 63	1. 133
		$4\frac{1}{2}$	58485. 52	−58. 22	0. 968
		$3\frac{1}{2}$	58519. 90	−34. 38	0. 665
$3d^6(a\ ^3H)4p$	$z\ ^4I°$	$7\frac{1}{2}$	58852. 60		
		$6\frac{1}{2}$	58843. 39	9. 21	1. 09
		$5\frac{1}{2}$	58851. 49	−8. 10	
		$4\frac{1}{2}$	58866. 66	−15. 17	0. 73
$3d^6(a\ ^3P)4p$	$u\ ^4P°$	$2\frac{1}{2}$	59116. 60		1. 558
		$1\frac{1}{2}$	59384. 45	−267. 85	1. 608
		$0\frac{1}{2}$	59568. 29	−183. 84	1. 94
$3d^6(a\ ^3F)4p$	$x\ ^4F°$	$4\frac{1}{2}$	59257. 44		1. 327
		$3\frac{1}{2}$	59290. 23	−32. 79	1. 325
		$2\frac{1}{2}$	59360. 72	−70. 49	1. 11
		$1\frac{1}{2}$	59416. 15	−55. 43	0. 39
$3d^6(a\ ^2P)4p$	$w\ ^4D°$	$3\frac{1}{2}$	59339. 55		1. 362
		$2\frac{1}{2}$	59600. 35	−260. 86	1. 277
		$1\frac{1}{2}$	59989. 77	−389. 42	1. 194
		$0\frac{1}{2}$	60141. 98	−152. 21	0. 17
$3d^6(a\ ^3F)4p$	$v\ ^4D°$	$3\frac{1}{2}$	59470. 14		1. 386
		$2\frac{1}{2}$	59480. 80	−10. 66	1. 281
		$1\frac{1}{2}$	59527. 89	−47. 09	
		$0\frac{1}{2}$	59527. 36	0. 53	
$3d^6(a\ ^3H)4p$	$z\ ^2I°$	$6\frac{1}{2}$	59617. 12		1. 074
		$5\frac{1}{2}$	59827. 88	−210. 76	0. 93

TABLE 2. *Odd Terms of* Mn I—Continued

Config.	Desig.	*J*	Level	Interval	Obs. g
$3d^6(a\ ^3F)4p$	$x\ ^4G°$	$5\frac{1}{2}$	59652. 90	−79. 04	1. 239
		$4\frac{1}{2}$	59731. 94	−52. 37	1. 169
		$3\frac{1}{2}$	59784. 31	−33. 39	0. 990
		$2\frac{1}{2}$	59817. 70		0. 584
Mn II($^7S_3$)	***Limit***	----------	**59970**		
$3d^6(^3P)4p$	$z\ ^2D°$	$2\frac{1}{2}$	60101. 65	−293. 99	1. 31
		$1\frac{1}{2}$	60395. 64		0. 91
$3d^6(a\ ^3H)4p$	$z\ ^2G°$	$4\frac{1}{2}$	60668. 49	−70. 93	1. 112
		$3\frac{1}{2}$	60739. 42		
	$w\ ^4F°$	$1\frac{1}{2}$	60760. 87		
		$2\frac{1}{2}$	60820. 35	59. 48	
		$3\frac{1}{2}$	60902. 80	82. 45	
		$4\frac{1}{2}$	60938. 97	36. 17	
$3d^5\ 4s(^3I)4p$	$x\ ^4H°$	$6\frac{1}{2}$	60891. 48	−42. 25	1. 228
		$5\frac{1}{2}$	60933. 73	−22. 15	1. 134
		$4\frac{1}{2}$	60955. 88	−1. 33	
		$3\frac{1}{2}$	60957. 21		
$3d^5\ 4s(^3I)4p$	$y\ ^4I°$	$7\frac{1}{2}$	61204. 54	−21. 01	1. 20
		$6\frac{1}{2}$	61225. 55	−0. 22	
		$5\frac{1}{2}$	61225. 77	14. 34	
		$4\frac{1}{2}$	61211. 43		0. 75
	$w\ ^4G°$	$5\frac{1}{2}$	61469. 21	−16. 13	1. 164
		$4\frac{1}{2}$	61485. 34	4. 74	1. 020
		$3\frac{1}{2}$	61480. 60	9. 37	1. 13
		$2\frac{1}{2}$	61471. 23		
	$z\ ^2F°$	$3\frac{1}{2}$	61710. 98	−16. 48	
		$2\frac{1}{2}$	61727. 46		
	$y\ ^2G°$	$4\frac{1}{2}$	61714. 52	−71. 42	0. 93
		$3\frac{1}{2}$	61785. 94		
		$5\frac{1}{2}$	61744. 04		
	$y\ ^2I°$	$5\frac{1}{2}$	61819. 07	93. 50	
		$6\frac{1}{2}$	61912. 57		
	$y\ ^2F°$	$3\frac{1}{2}$	62034. 04	−40. 98	0. 58
		$2\frac{1}{2}$	62075. 02		
$3d^6(^3P)4p$	$z\ ^2P°$	$1\frac{1}{2}$	62354. 76	−36. 29	1. 24
		$0\frac{1}{2}$	62391. 05		0. 81
$3d^6(a^3G)4p$	$v\ ^4F°$	$1\frac{1}{2}$	62390. 20	97. 16	
		$2\frac{1}{2}$	62487. 36	17. 93	
		$3\frac{1}{2}$	62505. 29	−112. 47	
		$4\frac{1}{2}$	62392. 82		1. 35
$3d^5\ 4s(a\ ^5F)4p$	$w\ ^6D°$	$4\frac{1}{2}$	62670. 81	−180. 66	
		$3\frac{1}{2}$	62851. 47	90. 14	
		$2\frac{1}{2}$	62761. 33	−26. 30	
		$1\frac{1}{2}$	62787. 63	19. 47	
		$0\frac{1}{2}$	62768. 16		
	$y\ ^2D°$	$2\frac{1}{2}$	63081. 28	−32. 83	1. 24
		$1\frac{1}{2}$	63114. 11		0. 758
	$x\ ^2F°$	$2\frac{1}{2}$	63139. 70	149. 08	
		$3\frac{1}{2}$	63288. 78		
$3d^6(^3H?)4p$	$z\ ^2H°$	$5\frac{1}{2}$	63288. 78	−259. 71	1. 127
		$4\frac{1}{2}$	63548. 49		0. 92

TABLE 2. *Odd Terms of* Mn I—Continued

Config.	Desig.	J	Level	Interval	Obs g
		3½	63319. 85?		
	$y\ ^2H°$	4½	63347. 91	101. 22	
		5½	63449. 13		
$3d^6(^3G)4p$	$w\ ^4H°$	6½	63363. 54	−94. 31	1. 231
		5½	63457. 85	13. 24	1. 14
		4½	63444. 61	49. 16	
		3½	63395. 45		0. 70
		2½	63371. 56		
		4½	63374. 53		
		2½	63523. 82		
		3½	63546. 30		
		1½, 2½	63583. 84		
	$x\ ^2D°$	2½	63764. 90	−80. 42	
		1½	63845. 32		
	$x\ ^2H°$	5½	64051. 91	−3. 46	
		4½	64055. 37		
	$u\ ^4D°$	3½	64409. 69	−303. 25	1. 42
		2½	64712. 94	28. 99	
		1½	64683. 95	45. 27	1. 22
		0½	64638. 68		0. 22
	$x\ ^2G°$	4½	64585. 44	−63. 76	1. 307
		3½	64649. 20		
	$v\ ^4H°$	6½	64731. 88	−87. 65	1. 236
		5½	64819. 53	−68. 47	1. 137
		4½	64888. 00	−32. 33	0. 974
		3½	64920. 33		
	$w\ ^2F°$	2½	64823. 21	165. 01	
		3½	64988. 22		
	$w\ ^2G°$	4½	65262. 28	−42. 85	1. 13
		3½	65305. 13		
	$v\ ^2F°$	3½	65617. 37	−31. 76	1. 015
		2½	65649. 13?		
		4½	65768. 81		1. 12
	$v\ ^4G°$	2½	65873. 40	2. 94	
		3½	65876. 34	32. 58	
		4½	65908. 92	−21. 61	1. 160
		5½	65887. 31		1. 259
	$w\ ^2D°$	2½	65946. 87	−15. 03	1. 30
		1½	65961. 90		
	$u\ ^2F°$	2½	66020. 63	128. 47	
		3½	66149. 10		1. 14
	$u\ ^4H°$	3½	66334. 47	21. 93	0. 764
		4½	66356. 40	62. 15	1. 022
		5½	66418. 55	150. 03	
		6½	66568. 58		1. 23
	$u\ ^4G°$	2½	66395. 19	59. 08	0. 611
		3½	66454. 27	68. 35	0. 932
		4½	66522. 62	50. 98	1. 13
		5½	66573. 60		1. 24

TABLE 2. *Odd Terms of* Mn I—Continued

Config.	Desig.	J	Level	Interval	Obs. g
		1½	66504. 21		
		3½	66600. 17		
	$v\ ^2G°$	4½	66630. 92	−106. 90	1. 13
		3½	66737. 82		0. 46
		2½	66654. 65?		
	$u\ ^4F°$	1½	66843. 79	−6. 15	0. 46
		2½	66837. 64	−54. 59	
		3½	66783. 05	71. 95	1. 21
		4½	66855. 00		1. 33
		2½?	66910. 02		
		3½	66981. 30		1. 33
		2½	67008. 54		
	$w\ ^2H°$	5½	67504. 90	−71. 94	1. 09
		4½	67576. 84		0. 90
	$t\ ^4G°$	5½	67752. 84	−66. 33	1. 266
		4½	67819. 17	−72. 19	
		3½	67891. 36	−73. 51	
		2½	67964. 87		
	$u\ ^2G°$	4½	68286. 44	−52. 15	1. 320
		3½	68338. 59		
$3d^6(^1I)4p$	$z\ ^2K°$	7½	68797. 56?	−44. 96	1. 07
		6½	68842. 52?		0. 93
$3d^6(^1I)4p$	$x\ ^2I°$	6½	69560. 88?	−68. 97	1. 07
		5½	69629. 85?		0. 924
$3d^6(^1I)4p$?	$v\ ^2H°$	4½	69663. 20?	59. 76	
		5½	69722. 96		1. 10

the average differences do not exceed 0.03 K, we have retained the older values.

In col. 2, some intensity numbers are accompanied by literal symbols for line character; these have the following meanings, c=complex, d=double, h=hazy, H=very hazy, l=shaded long ward, r=narrow self-reversal, R=wide self-reversal, s=shaded short ward, w=wide. Excepting self-reversals, the remaining symbols for line character frequently suggest unresolved hyperfine structure because the manganese nucleus has a spin of 5/2 ($h/2\pi$) and a magnetic moment of 3.5 nuclear magnetons.

Table 1 contains 2030 classified lines of Mn I, including 55 accepted double classifications for lack of adequate spectroscopic resolving power. The energy levels derived from these classified levels are symbolized in col. 5, and the difference between their numerical values and the vacuum wave number associated with the measured wavelength is shown in col. 4, O—C. The average O—C for all classified lines is 0.06 K.

The electron configurations, numerical values, and g-factors associated with the atomic-energy-level symbols in col. 5 of table 1, will be found in table 2.

In the last column of table 1 appear Zeeman-type numbers for 390 classified lines of Mn I according to the description of basic types of Zeeman patterns by Back and Landé [32, 34.] Briefly, types 4, 5, 6 are restricted to even multiplicities (doublets, quartets, sextets, octets) whose energy levels always have half-integral inner-quantum number (J-values). In type 4, the level with larger J has the smaller g, in type 5 the level with larger J also has the larger g and in type 6, the two combining levels have equal J but unequal g values. Type 7b is a special case of types 4, 5, 6 in which the g values of both combining levels are equal so that the observed pattern is a pseudo triplet with one p component and two n components. In the case of equal J and equal g, the type is represented by 6, 7b, and the displacement of the n components in Lorentz units expresses both g values.

The letter C attached to a dozen type numbers in col. 6 indicates the lines with asymmetrical patterns which Catalán [24] analysed in detail and for which he derived proper g values. Finally, instead of type numbers, the letters P—B appear for fifty lines; these are additional lines with Zeeman patterns that

exhibit partial Paschen-Back effects partially interpreted by Garcia-Riquelme et al. [28]. The Zeeman data were most helpful in this analysis of Mn I; they have confirmed our interpretation almost completely and have permitted the designation of many terms belonging to the doublet system which was the most difficult to establish. The available Zeeman data for Mn I [6, 21, 23, 24, 27, 28, 29] prove that most of the levels arising from low-energy configurations (d^5s^2, d^6s, d^5sp, d^6p) exhibit a remarkably pure LS coupling of electrons, and their g-factors are usually identical with the theoretical Landé values, within the error of measurement. Some of the upper levels of both the even and the odd configurations present anomalous g-values that may be explained by intermediate coupling or by incorrect grouping of levels in designated terms. Many more Zeeman patterns could be observed if a modern light source that promotes the emission of Mn I radiation were used.

The latest information on spectral terms derived from this analysis of Mn I is presented in table 2 where electron configurations (including series limits), spectral-term designations in standard notation for LS electron coupling, J-values, relative numerical values, intervals, and observed g-factors are shown in successive columns. The totals are 42 even terms with 125 levels and 60 g values, and 94 odd terms with 266 levels plus 13 miscellaneous and 164 g values. In 1952 [21] the totals were 36 even terms with 109 levels and 26 g values, and 66 odd terms with 214 levels plus 33 miscellaneous and 81 g values, not counting 12 abandoned levels. It is seen that the present analysis of the Mn I spectrum is a considerable improvement over any preceding, but, if a comparison is made of the presently recognized terms with the table of predicted terms [21, pp. XIV, XV], any claim that it is satisfactorily completed is unjustified. In order to show the progress that has rewarded this problem during the past 40 years, we briefly summarize in table 3 the number of classified Mn I lines and derived atomic energy levels at different times during this period.

TABLE 3. *Energy levels and classified lines of* Mn I

Year	Reference	Number of levels	Number of lines
1922	4	70	169
1926	9	91	257
1949	15	211	711
1952	21	356	1500
1962	This work	404	2030

The present analysis has effectively exhausted all available data on wavelengths, intensities, and Zeeman patterns of Mn I so that no further progress can be made with that material. But now we know that an arc between manganese electrodes at atmospheric pressure, with which all observations were made, is an inferior light source. Because manganese is a relatively light atom (A-55), and the arc has a high temperature (>5000 °C), it produces broad lines which are always very hazy and unsymmetrical when they involve high energy levels. All complex Mn I terms that converge to a^7S_3 or a^5S_2 limits in Mn II have very small intervals and are mostly unresolved because of the excessive line widths. Furthermore, the traditional arc in air always produces a strong background of molecular spectra that often masks atomic lines. All of these spectroscopic objections to an arc in air can now be avoided by using highly evacuated electrodeless (quartz tube) lamps containing a trace of metal or halide compound excited with ultrahigh frequency as demonstrated by Meggers and Westfall [33] for mercury and by Corliss and Meggers [34] for hafnium. At elevated temperatures (ca. 800 °C) such lamps favor spectra of neutral atoms, especially important for faint lines and for observing first spectra in strong magnetic fields; we mention this to aid anyone who becomes ambitious to make further progress in the description and quantum interpretation of the Mn I spectrum. That such progress is desirable becomes obvious when the now known spectral terms (table 2) are compared with the predicted ones [21]. Although many electron configurations and spectral terms have been identified, rarely is a configuration represented by all its terms and in some cases the terms themselves are fragmentary or even uncertain.

In 1922, Catalán derived, from spectral series of running s electrons, the absolute energy of the ground state of Mn I, and computed the first ionization potential to be 7.41 electron volts. Thirty years later Catalán and Velasco [35] systematically studied the first three ionization potentials of elements in the iron group; for Mn I they obtained an absolute value of 59960 K for the ground state, the equivalent 7.432 eV. These values were quoted in the second volume of Atomic Energy Levels [21]. A decade later, Garcia-Riquelme [36] applied a Ritz formula to a series of ^6F terms with four members (4f, 5f, 6f, 7f) and found the limit near 59979 K or 7.434 eV. We decided to adopt the average of the last two determinations resulting in a limit of 59970 K or ionization potential of 7.433 eV for normal manganese.

The surviving authors wish to thank R. Velasco for valuable assistance in the term analysis of the Mn I spectrum, especially with the measurement and interpretation of Zeeman patterns published elsewhere. We are also very grateful to Mrs. Charlotte Moore-Sitterly whose experience and judgment in spectral-term analyses were frequently consulted. We are deeply indebted to Mrs. Isabel Murray for making a square array of all possible combinations of Mn I energy levels, and for preparing the final tables; her work is unsurpassed in accuracy and neatness. Without the aids above, the publication of this paper as a token of our affection and esteem for the late Professor Catalán might have been indefinitely delayed.

4. References

[1] H. Kayser, Handbuch der Spectroscopie, **5,** 726–771; 1910.

[2] H. Kayser and H. Konen, Handbuch der Spectroscopie **7,** 1052–1108; 1934.

[3] H. Kayser and C. Runge, Über die Spectra von Zinn, Blei, Arsen, Antimon und Wismuth, Wiedem. Ann., **52,** 93–113; 1894.

[4] M. A. Catalán, Series and Other Regularities in the Spectrum of Manganese, Phil. Trans. Roy. Soc. London, **223,** A, 127–173; 1922.

[5] A. Sommerfeld, Über die Deutung verwickelter Spektren (Mangan, Chrom, usw.) nach der Methode der inneren Quantenzahlen. Ann. d. Physik, **70,** 32–62; 1923.

[6] E. Back, Der Zeeman effekt des Bogen-und Funkenspektrums von Mangan. Z. Physik, **15,** 206–243; 1923.

[7] A. Landé. Termstruktur und Zeeman effekt der Multiplets. Z. Physik, **15,** 189–205; 1923.

[8] M. A. Catalán. Los Espectros y la Clasificacion Periodica. Anales Soc. Españ. Fis. y Quim. **21,** 321–329; 1923.

[9] J. C. McLennan and A. B. McLay. On the Structure of the Arc Spectrum of Manganese. Trans. Roy. Soc. Can. **20,** 89–120, 1926.

[10] H. N. Russell. Series and Ionization Potentials of the Elements of the Iron Group. Astrophys. J., **66,** 233–255; 1927.

[11] M. A. Catalán. Notas sobre la estructura del espectro del Manganeso. Anales Soc. Españ. Fis. y Quim., **26,** 67–74; 1928.

[12] R. F. Bacher and S. Goudsmit. Atomic Energy States as derived from Analyses of Optical Spectra. pp. 278–281, McGraw-Hill Book Co., New York, 1932.

[13] T. Dunham, Jr., Unpublished multiplets of Mn I.

[14] W. F. Meggers. The infrared Arc Spectra of Manganese and Rhenium. J. Res. Nat. Bur. Std. **10,** 757–769; 1933.

[15] O. Garcia-Riquelme. Estructura y nuevos niveles energeticos del espectro arco del manganeso. Anales Soc. Españ. Fis. y Quim., **45A,** 435–448, 547–576; 1949.

[16] H. Slevogt. Über die Bogenspektren von Chrom, Mangan, Kobalt und Nickel im Rot und nahen Ultrarot. Z. Physik, **82,** 92–118; 1933.

[17] F. W. Paul. Absorption Spectra of Manganese and Silver in the Schumann Region. Phys. Rev., **52,** 923–929; 1937.

[18] A. G. Shenstone. The First Spark Spectrum of Platinum. Phil. Trans. Roy. Soc. London, **237,** 453–470; 1938.

[19] R. W. Wood. Recent Improvements in Diffraction Gratings and Replicas. Nature **140,** 723–724; 1937.

[20] H. M. Randall and E. F. Barker. The Infrared Arc Spectra of Cobalt, Nickel, Manganese and Chromium Astrophys. J., **49,** 59–63; 1919.

[21] C. E. Moore. Atomic Energy Levels as Derived from the Analyses of Optical Spectra. N.B.S. Cir. 467, vol. **2,** 27–31; 1952.

[22] G. R. Harrison and F. Bitter. Zeeman Effects in Complex Spectra at Fields up to 100,000 Gauss. Phys. Rev., **57,** 15–20; 1940.

[23] M. A. Catalán and R. Velasco. Changes in g-values in a Spectrum, for different Magnetic Fields. J. Opt. Soc. Am., **40,** 653–655; 1950.

[24] M. A. Catalán. Asymmetries of Zeeman Patterns and g-values for Neutral Manganese. J. Res. Nat. Bur. Std., **47,** 502–524; 1951.

[25] M. L. Espinosa. Estudio de Patrones de fuerte interaccion Paschen-Back. Anales Soc. Españ. Fis. y Quim., **48A,** 211–218; 1952.

[26] M. L. Espinosa. Interpretacion del Multiplete $a^6S-z^6P^0$ del Mn I en campo magnetico del orden de los 85,000 oersted. Anales Soc. Españ. Fis. y Quim. **48A,** 267–270; 1952.

[27] M. A. Catalán and O. Garcia-Riquelme. Medidas de efecto Zeeman en el espectro de Mn I. Anales Soc. Españ. Fis. y Quim. **47A,** 173–180; 1951.

[28] O. Garcia-Riquelme, R. Velasco, R. Oyarzun, and F. Veas. Nuevas interpretaciones en el efecto Zeeman de Mn I. Anales Soc. Españ. Fis. Quim. **56A,** 137–150; 1960.

[29] O. Garcia-Riquelme. Unpublished Zeeman data for Mn I. June 1962.

[30] H. Kayser. Tabelle der Schwingungszahlen. S. Hirzel, Leipzig, 1925.

[31] C. D. Coleman, W. R. Bozman, and W. F. Meggers. Table of Wave numbers. N.B.S. Monograph 3. Government Printing Office, Washington, 1960.

[32] E. Back and A. Landé. Zeemaneffekt und Multiplett struktur der Spektrallinien. pp. 168–169. Julius Springer, Berlin, 1925.

[33] W. F. Meggers and F. O. Westfall. Lamps and wavelengths of Mercury 198. J. Res. Nat. Bur. Std. **44,** 447–455; 1950.

[34] C. H. Corliss and W. F. Meggers. Improved Description of Hafnium Spectra. J. Res. Nat. Bur. Std. **61,** 269–324; 1958.

[35] M. A. Catalán and R. Velasco. Series y potenciales de, ionizacion en los espectros I, II, y III de los elementos del grupo del hierro. Anales Real Soc. Espan. Fis. Quim. **68A,** 247–266; 1952.

[36] O. Garcia-Riquelme, Unpublished material, 1962.

(Paper 68A1–252)

JOURNAL OF RESEARCH of the National Bureau of Standards—A. Physics and Chemistry
Vol. 68A, No. 1, January-February 1964

Transition Probabilities of Forbidden Lines

R. H. Garstang [1]

(October 2, 1963)

This paper describes calculations of the transition probabilities of forbidden lines (magnetic dipole and electric quadrupole radiation) of laboratory and astrophysical interest. Results are given for Ti III, Cr II, Cr IV, Mn V, Mn VI, Fe VI, Fe VII, Ni I, Cu II, Ga I, Ge I, Ge II, As I, As III, Se I, Br I, Br II, Kr II, Kr III, Rb III, In I, Sn I, Sn II, Sb I, Sb III, Te I, I I, I II, Xe II, Xe III, Cs III, Hg II, Tl I, Pb I, Pb II, Bi I, Bi II, Bi III, Po I, and Rn II.

1. Introduction

This paper presents the results of calculations of the transition probabilities of forbidden lines for a number of atoms and ions of astrophysical or laboratory interest. Much work has been done in the past on atoms in the first two short periods and their isoelectronic sequences, and selected ions in the iron group have also been studied. A few additional ions in the iron group need study, chiefly with a view to astrophysical applications. These form the subject of sections 2 through 4 of the present paper. There have been few calculations on forbidden lines of heavier elements. Only a few are of possible astrophysical interest; a number have been observed in the laboratory. Calculations of their transition probabilities are not difficult, and have been carried out for many atoms and ions, the results being given in section 5 of this paper. They include, it is thought, every case in which one or more forbidden lines in an atom has been observed in laboratory sources, and for which transition probabilities have not previously been computed.

A comprehensive survey of this subject has recently been given [1],[2] and in this paper we shall only give such details as are immediately relevant to the individual atoms being considered. Unless otherwise mentioned all observed atomic energy levels have been taken from [2]. The procedure, now well established, is to take the quantum mechanical energy matrices including spin-orbit interaction (and, where necessary, configuration interaction) and determine the parameters (radial integrals) in these matrices so that the eigenvalues of the matrices reproduce the observed energies as accurately as possible. The eigenvectors provide the transformation from *LS*-coupling to intermediate coupling. The matrices of the square roots of line strengths are set up, the transformation to intermediate coupling carried out, and the final line strengths converted to transition probabilities. The total transition probability for a line is the sum of the magnetic dipole transition probability (A_m) and the electric quadrupole transition probability (A_q).

2. Lines of Ti III, Mn VI, Fe VII, Cr IV, Mn V, and Fe VI

In Ti III, Mn VI, and Fe VII the transitions take place within the $3d^2$ configuration. Fe VII was studied by Pasternack [3]; the other two ions do not appear to have been the subject of earlier forbidden line calculations. The spin-orbit matrix was taken from Condon and Shortley [4, p. 269]; the electrostatic energies were treated as arbitrary parameters. The parameters obtained by fitting the theory to the observed energies are given in table 1; E(^{1}S) was estimated using the theoretical formulas for electrostatic energies [5] including an $\alpha L(L+1)$ correction [6]. The resulting calculated energies are given in table 2. The only significant comparison with observation is for the ^{3}F and ^{3}P term intervals, for which the agreement is quite good, showing that the intermediate coupling theory provides a fair representation of the atomic fine structure. The line strength matrix for magnetic dipole radiation was obtained from formulae of Shortley [7], the electric quadrupole line strength matrix from Pasternack [3]

TABLE 1. *Parameters for the* $3d^2$ *configurations in* Ti III *and* Mn VI

(Units: s_q in atomic units, others in cm^{-1})

Parameter	Ti III	Mn VI
E(^{3}F)	243	974
E(^{1}D)	8482	15446
E(^{3}P)	10657	18274
E(^{1}G)	14398	25502
E(^{1}S)	(32881)	(57600)
ζ	118	465
s_q	2. 45	0. 979

[1] Normally at University of London Observatory, Mill Hill Park, London, N.W. 7, England, where part of this work was performed. The remainder was performed while the author was at the Atomic Physics Division, National Bureau of Standards, during 1961 and 1962, and is a part of project DEFENDER, sponsored by the Advanced Research Projects Agency, Department of Defense, through the Office of Naval Research.

[2] Figures in brackets indicate the literature references on page 71.

TABLE 2. *Energy levels in the* $3d^2$ *configurations in* Ti III *and* Mn VI

(Units: cm^{-1})

Level	Ti III			Mn VI		
	Obs.	Calc.	O−C	Obs.	Calc.	O−C
$^3F_2$	0	3	−3	0	10	−10
$^3F_3$	184	184	0	746	741	5
$^3F_4$	422	419	3	1669	1663	6
$^1D_2$	8473	8473	0	15336	15336	0
$^3P_0$	10536	10535	1	17782	17772	10
$^3P_1$	10604	10598	6	18057	18042	15
$^3P_2$	10721	10729	−8	18628	18652	−24
$^1G_4$	14399	14399	0	25511	25511	0
$^1S_0$	-------	(32885)	-------	-------	(57633)	------

TABLE 3. *Transition probabilities of* [Ti III] *and* [Mn VI]

(Units: sec^{-1})

Transition $3d^2$		Ti III		Mn VI	
		A_m	A_q	A_m	A_q
$^3F-{}^3F$	2–3	1.6×10^{-4}	1.4×10^{-12}	0.011	2.5×10^{-10}
	2–4	----------	3.4×10^{-12}	----------	4.8×10^{-10}
	3–4	2.7×10^{-4}	4.3×10^{-12}	0.016	6.0×10^{-10}
$^3F-{}^1D$	2–2	0.0049	9.0×10^{-6}	0.14	1.7×10^{-4}
	3–2	.0095	1.1×10^{-5}	.23	2.3×10^{-4}
	4–2	----------	5.4×10^{-5}	----------	9.0×10^{-4}
$^3F-{}^3P$	2–0	----------	0.039	----------	0.087
	2–1	2.7×10^{-6}	.014	3.8×10^{-4}	.031
	3–1	----------	.025	----------	.050
	2–2	1.9×10^{-5}	.0012	0.0035	.0028
	3–2	7.3×10^{-5}	.0079	.013	.017
	4–2	----------	.027	----------	.050
$^1D-{}^3P$	2–0	----------	5.5×10^{-8}	----------	1.6×10^{-7}
	2–1	0.0012	7.3×10^{-8}	0.020	2.8×10^{-7}
	2–2	.0026	2.8×10^{-9}	.060	2.6×10^{-8}
$^3P-{}^3P$	0–1	5.4×10^{-6}	----------	3.7×10^{-4}	----------
	0–2	----------	1.1×10^{-11}	----------	3.5×10^{-9}
	1–2	2.2×10^{-5}	2.6×10^{-12}	0.0024	1.1×10^{-9}
$^3F-{}^1G$	2–4	----------	1.9×10^{-5}	----------	2.5×10^{-4}
	3–4	0.0041	2.4×10^{-7}	0.12	3.2×10^{-6}
	4–4	.0064	8.9×10^{-6}	.17	1.1×10^{-4}
$^1D-{}^1G$	2–4	----------	4.5×10^{-4}	----------	0.0010
$^3P-{}^1G$	2–4	----------	3.2×10^{-7}	----------	8.5×10^{-6}
$^3F-{}^1S$	2–0	----------	0.0053	----------	0.063
$^1D-{}^1S$	2–0	----------	6.7	----------	16
$^3P-{}^1S$	1–0	0.098	----------	2.7	----------
	2–0	----------	0.028	----------	0.55

with corrections by Garstang [8], and the radial integrals

$$s_q=\int_0^\infty r^2P^2(3d)dr$$

were obtained from wave functions given by Watson [9]. The values of s_q used are listed in table 1. The intermediate coupling transformations and the final transition probabilities were computed in the usual way. The results are listed in table 3. A_m and A_q denote spontaneous emission transition probabilities in sec^{-1}; the total transition probability is A_m+A_q.

The results obtained for Mn VI may be compared with those obtained by Pasternack for Fe VII. The results show the usual trend of increasing transition probabilities along the isoelectronic sequence. Pasternack used $s_q=1.52$ for Fe VII, based on a rather crude estimate of certain screening constants. A better estimate of s_q can now be obtained from Watson's wave functions, based on an extrapolation of $s_q^{-1/2}$ along the isoelectronic sequence, Mn VI being the highest ion of this sequence for which wave functions were computed. The resulting estimate of s_q is given in table 4. The magnetic dipole transition probabilities obtained by Pasternack are unchanged on a change of s_q. The electric quadrupole strengths must be multiplied by the square of the ratio of the new s_q to the old s_q. The electric quadrupole transition probabilities must be multiplied by this same correction factor, which is given in table 4. Pasternack also performed calculations on Cr IV, Mn V, and Fe VI, for which the transitions take place within the $3d^3$ configuration. We have computed improved values of s_q for these three ions from the wave functions published by Watson. The values of s_q are given in table 4 together with correcting factors by which Pasternack's electric quadrupole transition probabilities are to be multiplied to take account of the revised s_q. As for Fe VII, the magnetic dipole transition probabilities are unaffected by the change in s_q.

Bowen [10] observed the transitions $^3F_2-{}^1D_2$ (λ6518.3), $^3F_4-{}^3P_2$(λ5894.0), and $^3F_3-{}^3P_1$(λ5776.4) of Mn VI in a planetary nebula. No forbidden lines of Ti III appear to have been observed.

TABLE 4. *Radial integrals and correction factors to be applied to certain transition probabilities*

(Units: s_q in atomic units)

Ion	s_q	Correction factor [a]
Fe VII [b]	0. 84	0. 30
Cr IV	1. 45	. 144
Mn V	1. 10	. 185
Fe VI	. 89	. 24

[a] To be applied to electric quadrupole transition probabilities published by Pasternack [3].

[b] New wave junctions computed by S. J. Czyzak of Wright-Patterson Air Force Base indicate $5_q=0.80$ for Fe VII, leading to a correction factor 0.28.

3. Lines of Cr II

A complete study of the forbidden lines of Cr II would necessitate a very long investigation which the astronomical importance of this ion is hardly sufficient to justify. It so happens that the one multiplet of most importance can be simply treated. This is the transition $3d^5\ {}^6S - 3d^4 4s\ {}^6D$. The four strongest lines of this multiplet were observed by Thackeray [11] in the infrared spectrum of η Carinae. ^6S and ^6D are the only sextet terms in their respective configurations, and consequently there are no large off-diagonal matrix elements connecting them with other terms. Experience (especially with Fe II [12]) has shown that in these circumstances, for a transition allowed in *LS*-coupling, magnetic dipole radiation is likely to be negligible and the *LS*-coupling approximation will give excellent values for the electric quadrupole transition probabilities. The total multiplet strength is given in the appendix to the present paper. The individual line strengths were obtained, and converted to transition probabilities. The radial integral

$$s_q = \int_0^\infty r^2 \mathrm{P}(3d)\mathrm{P}(4s)dr$$

was estimated by extrapolating $s_q^{-1/2}$ from the values previously obtained for Fe II [12] and Ni II [13]. We adopted $s_q = -3.5$. The results are listed in table 5.

TABLE 5. *Electric quadrupole transition probabilities for* Cr II $3d^5\ {}^6S - 3d^4 4s\ {}^6D$

(Units: sec^{-1})

Line	A_q
$^6S_{2\frac{1}{2}} - {}^6D_{1\frac{1}{2}}$	0.067
$- {}^6D_{1\frac{1}{2}}$	.069
$- {}^6D_{2\frac{1}{2}}$	.072
$- {}^6D_{3\frac{1}{2}}$	.077
$- {}^6D_{4\frac{1}{2}}$	.083

4. Lines of Ni I and Cu II

In connection with some intensity calculations on permitted transitions the writer undertook a study of Ni I, and part of that work may also be used in calculations on forbidden lines. The lower levels of Ni I arise from the configurations $3d^{10}$, $3d^9 4s$, and $3d^8 4s^2$. The energy levels have been fitted to the theory and parameters estimated in the usual way. The formulae for the electrostatic energies were obtained from [4, p. 299] and [5, eq (78)], an $\alpha L(L+1)$ correction [6] being added for the $3d^8 4s^2$ configuration. The configuration interaction matrix elements were obtained from [14, eqs (75) and (81)]. The spin-orbit interaction matrix elements were taken from [4, p. 269] with changes in the sign of ζ (for d^8 or d^9 instead of d^2 or d), and of the phase of ds (instead of sd). The adopted parameters are given in table 6. The configuration interaction parameter H_2 was neglected; a study by Racah and Shadmi [15] showed that H_2 is very small for Ni II, and presumably also for Ni I. Table 7 gives the observed energies and those calculated from the parameters in table 6. The Landé g-factors are also given. The overall agreement of observation and calculation is very satisfactory. The line strength matrices were obtained in the usual way [3, 7, 8, 16] and intermediate coupling transformations carried out to obtain the final line strengths and transition probabilities. The only problem which arose was the adoption of numerical values of the radial integrals

TABLE 6. *Adopted parameters in* Ni I

(Units: S_q in atomic units, others in cm^{-1})

$d^8 s^2$ ζ	650
α	75
A	8181
B	1010
C	4179
$d^9 s$ F_0	1992
G_2	1181
ζ'	604
d^{10} E_0	14928
$s_q(3d^{10})$	2.2
$s_q(3d^9 4s)$	1.6
$s_q(3d^8 4s^2)$	1.1
$s_q(3d^{10} - 3d^9 4s)$	−2.9
$s_q(3d^9 4s - 3d^8 4s^2)$	−2.2

TABLE 7. *Observed and calculated energy levels and Landé* g*-factors*

Term	J	Energy levels		Landé g-factors		
		Observed	Calculated	Observed	LS-coupling	Calculated
		cm^{-1}	cm^{-1}			
$3d^8 4s^2\ a^3F$	4	0	7	1.250	1.250	1.250
	3	1332^{-1332}	1326^{-1319}	1.083	1.083	1.083
	2	2217^{-885}	2214^{-888}	0.671	0.667	0.670
$3d^9 4s\ a^3D$	3	205	207	1.332	1.333	1.333
	2	880^{-675}	875^{-668}	1.149	1.167	1.151
	1	1713^{-833}	1717^{-842}	0.497	0.500	0.500
$3d^9 4s\ a^1D$	2	3410	3411	1.014	1.000	1.016
$3d^8 4s^2\ b^1D$	2	13521	13491	1.143	1.000	1.128
$3d^{10}\ a^1S$	0	14729	14729	-------	-------	------
$3d^8 4s^2\ a^3P$	2	15610	15632	1.356	1.500	1.370
	1	15734^{-124}	15726^{-94}	1.497	1.500	1.500
	0	16017^{-283}	15991^{-265}	-------	-------	------
$3d^8 4s^2\ a^1G$	4	22102	22098	0.99	1.000	1.000
$3d^8 4s^2\ {}^1S$	0	----------	51834	-------	-------	------

TABLE 8. *Transition probabilities of* [Ni I]

(Units: sec^{-1})

Transition		A_m	A_q
a^3F–a^3F	4–3	0. 062	6.0×10^{-9}
	4–2		3.6×10^{-9}
	3–2	. 025	1.1×10^{-9}
a^3F–a^3D	4–3		8.4×10^{-11}
	3–3		1.2×10^{-7}
	2–3		2.7×10^{-7}
	4–2		3.2×10^{-8}
	3–2		1.8×10^{-9}
	2–2		3.7×10^{-7}
	3–1		8.0×10^{-10}
	2–1		3.9×10^{-9}
a^3D–a^3D	3–2	0. 0070	4.1×10^{-9}
	3–1		3.0×10^{-8}
	2–1	. 021	1.7×10^{-8}
a^3F–a^1D	4–2		1.7×10^{-6}
	3–2		5.4×10^{-7}
	2–2		6.7×10^{-9}
a^3D–a^1D	3–2	0. 078	1.0×10^{-6}
	2–2	. 0062	1.8×10^{-7}
	1–2	. 011	3.6×10^{-8}
a^3F–b^1D (1F)	4–2		0. 0056
	3–2	0. 39	7.6×10^{-4}
	2–2	. 17	2.0×10^{-4}
a^3D–b^1D (4F)	3–2		0. 014
	2–2		. 017
	1–2		4.5×10^{-4}
a^1D–b^1D (6F)	2–2		0. 012
a^3F–a^1S	2–0		1.8×10^{-4}
a^3D–a^1S	2–0		0. 068
a^1D–a^1S (7F)	2–0		0. 31
b^1D–a^1S	2–0		2.9×10^{-4}
a^3F–a^3P (2F)	4–2		0. 032
	3–2	0. 15	. 0056
	2–2	. 039	3.98×10^{-4}
	3–1		0. 025
	2–1	. 0022	. 0090
	2–0		. 031
a^3D–a^3P (5F)	3–2		0. 074
	2–2		. 018
	1–2		. 0093
	3–1		. 092
	2–1		. 012
	1–1		. 053
	2–0		. 19
	1–0		
a^1D–a^3P (8F)	2–2		0. 024
	2–1		4.7×10^{-4}
	2–0		1.1×10^{-5}
b^1D–a^3P	2–2	0. 072	1.9×10^{-8}
	2–1	. 063	6.9×10^{-7}
	2–0		1.2×10^{-6}
a^1S–a^3P	0–2		1.3×10^{-12}
	0–1	1.4×10^{-4}	

TABLE 8. *Transition probabilities of* [Ni I]—Continued

Transition		A_m	A_q
a^3P–a^3P	2–1	3.2×10^{-5}	8.2×10^{-13}
	2–0		4.5×10^{-10}
	1–0	0. 0012	
a^3F–a^1G (3F)	4–4	0. 32	2.2×10^{-4}
	3–4	. 16	3.8×10^{-6}
	2–4		3.0×10^{-7}
a^3D–a^1G	3–4		7.9×10^{-4}
	2–4		. 080
a^1D–a^1G	2–4		0. 44
b^1D–a^1G	2–4		4.1×10^{-4}
a^3P–a^1G	2–4		4.3×10^{-5}
a^3F–(^1S)	2–0		0. 17
a^3D–(^1S)	2–0		8. 5
a^1D–(^1S)	2–0		84
b^1D–(^1S)	2–0		9. 9
a^3P–(^1S)	2–0		3. 0
	1–0	5. 4	

for electric quadrupole radiation. These were obtained by extrapolation of results for various stages of ionization of manganese, iron, and nickel which had been obtained in earlier work. The adopted radial integrals are listed in table 6 and the transition probabilities in table 8.

In Cu II we are only interested in the $3d^{10}$ and $3d^9 4s$ configurations, but the $3d^8 4s^2$ configuration must be included in the calculations. Cu II has been studied by Racah and Shadmi [15], and we have adopted the numerical values of the parameters which they obtained. The Ni I work was followed so far as necessary for Cu II. Examination showed that there are no magnetic dipole transitions between $3d^{10}$ and $3d^9 4s$. For electric quadrupole radiation $^1S_0$–$^3D_1$ and $^1S_0$–$^3D_3$ are strictly forbidden. The remaining transitions were computed in the same way as for Ni I. The radial integrals for electric quadrupole radiation were estimated by extrapolation of $s_q^{-1/5}$ from Fe II [12] and Ni II [13]. We adopted $s_q(d^{10}$–$d^9 s)=-2.0$, $s_q(d^9 s$–$d^8 s^2)=-1.5$, $s_q(d^9 s$–$d^9)=+1.0$. The resulting transition probabilities are given in table 9.

The transition probabilities of Cu II are of interest in connection with observations of the spectrum of η Carinae by Thackeray [17]. He observed the transition $3d^{10}\ ^1S_0$–$3d^9 4s\ ^1D_2$ at λ3806. Our results show that this line is indeed the strongest forbidden line of Cu II, and explain the absence of the $^1S_0$–$^3D_1$ line. The $^1S_0$–$^3D_2$ line might be observable under suitable conditions; but in η Carinae the relatively high densities of the gas (in comparison with planetary nebulae) would enhance the importance of collisional excitation and de-excitation relative to radiative processes, and the $^1S_0$–$^3D_2$ line would then be weaker than the $^1S_0$–$^1D_2$ line by an order of magnitude because of its lower transition probability.

TABLE 9. *Transition probabilities of* [Cu II]

(Units: sec^{-1})

Transition	A_m	A_q
$3d^{10}$ $^1S_0$–$3d^9 4s$ $^3D_2$	----------	0.12
$^1S_0$– $^3D_1$	----------	----------
$3d^{10}$ $^1S_0$–$3d^9 4s$ $^1D_2$	----------	1.9
$3d^9 4s$ $^3D_3$–$3d^9 4s$ $^3D_2$	0. 017	7.4×10^{-9}
$^3D_3$– $^3D_1$	----------	8.1×10^{-8}
$^3D_2$– $^3D_1$	. 055	3.4×10^{-8}
$3d^9 4s$ $^3D_3$–$3d^9 4s$ $^1D_2$	0. 23	2.1×10^{-6}
$^3D_2$– $^1D_2$	. 018	3.7×10^{-7}
$^3D_1$– $^1D_2$	. 031	7.4×10^{-8}

5. Forbidden Lines in Heavier Atoms ($Z>29$)

Transition probabilities are available for only a very few forbidden lines of atoms with $Z>29$. The remainder of this paper will be devoted to presenting some additional data on such transitions. The ^2D–^2S doublets in Rb I and Cs I have been discussed in detail [4, p. 256] and will not be further considered here. Results have previously been obtained also for Pb I [18], Br II [19], I II [20], Kr III [21], Rn II [22], Xe II [22], and Xe III [22].

5.1. np and np^5 Configurations

The only observation of the $^2P_{3/2}$–$^2P_{1/2}$ transition within an np configuration appears to be that in Pb II $6p$ at λ7099.8, first observed by Walters [23], and identified and studied by Cole [24]. The $^2P_{1/2}$–$^2P_{3/2}$ transition in the np^5 configuration has been observed in four cases: Xe II $5p^5$ at λ9487.8 and Rn II $6p^5$ at λ3235.8 by Edlén [22], I I $5p^5$ at λ13149 by Eshbach and Fisher [25] and Kiess and Corliss [26], and Br I $4p^5$ at λ27130 by J. C. Polanyi [private communication].

Transition probabilities have been calculated from the *LS*-coupling formulae for magnetic dipole line strengths given by Shortley [7] and for electric quadrupole line strengths by Garstang [8, eqs (3), (5), (6) and par. 5]. It is found that for np and np^5 configurations

$$S_m=\frac{4}{3} \qquad S_q=\frac{10}{3}s_q^2$$

where

$$s_q=\frac{2}{5}\int_0^\infty r^2 P^2(np)dr$$

and the factor (2/5) has been included in s_q for p electrons (cf s_q for d electrons) in accordance with custom [27]. $P(np)$ is the radial wave function for an np electron. The transition probabilities obtained are listed in tables 10 and 11, where we have included for completeness the two values calculated by Edlén [22]. The estimation of s_q is discussed below.

TABLE 10. *Transition probabilities for* np $^2P_{\frac{3}{2}}\rightarrow{}^2P_{\frac{1}{2}}$

(Units: sec^{-1})

Ion	Config.	A_m	A_q
Ga I	$4p$	0. 0050	1.6×10^{-6}
Ge II	$4p$	. 049	3.1×10^{-5}
As III	$4p$	. 23	1.9×10^{-4}
In I	$5p$	. 097	2.7×10^{-4}
Sn II	$5p$	. 68	0. 0035
Sb III	$5p$	2. 5	. 017
Tl I	$6p$	4. 2	. 11
Pb II	$6p$	25	1.3
Bi III	$6p$	80	5.9

TABLE 11. *Transition probabilities for* np^5 $^2P_{\frac{1}{2}}\rightarrow{}^2P_{\frac{3}{2}}$

(Units: sec^{-1})

Ion	Config.	A_m	A_q
Br I	$4p^5$	0. 89	8.3×10^{-4}
Kr II	$4p^5$	2. 8	0.0030
Rb III	$4p^5$	7. 2	.0094
I I	$5p^5$	7. 8	.055
Xe II	$5p^5$	[a] 21	.17
Cs III	$5p^5$	48	.45
Rn II	$6p^5$	[a] 530	34

[a] These values have been given previously by Edlén [22].

5.2. np^2, np^3, and np^4 Configurations

Observations of the forbidden line $^1S_0$–$^3P_1$ in Pb I $6p^2$ at λ4618 played an important part in the history of the subject, for it was by means of observations of the Zeeman effect on this line that Niewodniczanski [28] first demonstrated the occurrence of magnetic dipole radiation. The line $^1D_2$–$^3P_1$ (λ7330) was first observed by Walters [23], λ4618 by Gieseler and Grotrian [29], and by Sur [30], and $^1D_2$–$^3P_0$ (λ4659) and $^1S_0$–$^3P_2$ (λ5313) by Niewodniczanski [31], who also studied λ4618 and λ7330. Mrozowski [32] found $^1D_2$–$^3P_2$ (λ9250). Mrozowski studied the relative intensities I(4618): I(5313) and I(4659): I(7330): I(9250). The Zeeman effect of λ4618, λ4659, λ5313, and λ7330 was studied by Jenkins and Mrozowski [33]. Gerjuoy [18] gave a detailed discussion of the intensities, to be referred to again below.

Forbidden lines of Bi II $6p^2$ were observed by Cole and Mrozowski [34], and Cole [35], who obtained $^1S_0$–$^3P_1$ (λ3241), $^1S_0$–$^3P_2$(λ3683), $^1D_2$–$^3P_1$(λ4850), $^1D_2$–$^3P_2$(λ5914), and $^3P_1$–$^3P_0$(λ7503), and studied their hyperfine structure.

Forbidden lines of As I $4p^3$ $^2P_{3/2}$–$^4S_{3/2}$(λ5362) and $^2P_{1/2}$–$^4S_{3/2}$(λ5498) and of Sb I $5p^3$ $^2P_{3/2}$–$^4S_{3/2}$(λ5415) and $^2P_{1/2}$–$^4S_{3/2}$(λ6098) were observed by Hults and Mrozowski [36]. In Bi I $6p^3$ Toshniwal [37] found $^2D_{3/2}$–$^4S_{3/2}$(λ8755), $^2D_{5/2}$–$^4S_{3/2}$(λ6476), and $^2P_{1/2}$–$^4S_{3/2}$ (λ4615), and Mrozowski [38] made a study of these lines together with $^2P_{3/2}$–$^4S_{3/2}$(λ3014), $^2P_{3/2}$–$^2D_{3/2}$

(λ4597), and $^2P_{3/2}$–$^2D_{5/2}$(λ5640) which he found. Mrozowski made hyperfine structure observations which proved that all these Bi I transitions are predominantly magnetic dipole radiation. For λ6476, the best resolved line, electric quadrupole radiation was less than 0.15 of the total. Mrozowski also pointed out the need for more laboratory intensity measurements on the forbidden lines of Bi I and other atoms.

Ruedy and Gibbs [39] found the lines $^1S_0$–$^1D_2$ (λ7768) and $^1S_0$–$^3P_1$ (λ4887) in Se I $4p^4$. Niewodniczanski and Lipinski [40] found $^1S_0$–$^1D_2$ (λ7909), $^1S_0$–$^3P_1$ (λ5420), and $^1S_0$–$^3P_2$ (λ4309) in Te I $5p^4$, λ5420 being much stronger than the others. Mrozowski [41] observed $^1S_0$–$^3P_1$ (λ3862), $^1D_2$–$^3P_2$ (λ4611), and $^3P_1$–$^3P_2$ (λ5940) in Po I $6p^4$. Martin and Tech [19] found $^1S_0$–$^3P_1$ (λ4042) and $^1D_2$–$^3P_2$ (λ8270) in Br II $4p^4$. Martin and Corliss [20] found $^1S_0$–$^3P_1$ (λ4460) and $^1D_2$–$^3P_2$ (λ7283) in I II $5p^4$ and Edlén [22] found $^1D_2$–$^3P_2$ (λ5846.3) and $^3P_1$–$^3P_2$ (λ10206.5) in Xe III $5p^4$. Kr III $^1D_2$–$^3P_2$ (λ6827) may be present in spectra of RS Ophiuchi [54], but later work cast considerable doubt on the identification [61].

General formulae for line strengths and transition probabilities in p^2, p^3, and p^4 configurations were given by Shortley, Aller, Baker, and Menzel [27].

TABLE 12. *Parameters in* p^2 *configurations*

(Units: cm^{-1})

Parameter	Ge I	Sn I	Pb I	Bi II
	$4p^2$	$5p^2$	$6p^2$	$6p^2$
E(^{3}P)	1023	2839	11538	19275
E(^{1}D)	7050	8070	16930	25808
E(^{1}S)	16263	16554	25205	36618
ζ	921.5	2247	7355	11789

$$\Psi(^1D_2)=a\Phi(^1D_2)+b\Phi(^3P_2)$$
$$\Psi(^3P_2)=-b\Phi(^1D_2)+a\Phi(^3P_2)$$
$$\Psi(^3P_1)=\Phi(^3P_1)$$
$$\Psi(^3P_0)=c\Phi(^3P_0)+d\Phi(^1S_0)$$
$$\Psi(^1S_0)=-d\Phi(^3P_0)+c\Phi(^1S_0)$$

We have used their line strength formulae, but the parameters have been determined in the manner used by Garstang [e.g., 42]. The electrostatic parameters E(^{3}P), E(^{1}D) and E(^{1}S) (for p^2 and p^4 configurations) or E(^{4}S), E(^{2}D), and E(^{2}P) (for p^3 configurations) and the spin-orbit parameter ζ have been treated as adjustable. They have been determined by fitting the theory [4, p. 268] to the observed energy levels by trial and error followed by one or more least squares adjustments. The energies were taken from [2] except for I II [20] and Br II [19]. The adopted parameters are listed in tables 12, 17, and 21. The intermediate coupling wave functions are written in the form given by Shortley, Aller, Baker, and Menzel [27]:

for p^2 and p^4 configurations, and

$$\Psi(^2D_{5/2})=\Phi(^2D_{5/2})$$
$$\Psi(^2D_{3/2})=a\Phi(^2P_{3/2})+b\Phi(^4S_{3/2})+c\Phi(^2D_{3/2})$$
$$\Psi(^4S_{3/2})=a'\Phi(^2P_{3/2})+b'\Phi(^4S_{3/2})+c'\Phi(^2D_{3/2})$$
$$\Psi(^2P_{3/2})=a''\Phi(^2P_{3/2})+b''\Phi(^4S_{3/2})+c''\Phi(^2D_{3/2})$$
$$\Psi(^2P_{1/2})=\Phi(^2P_{1/2})$$

for p^3 configurations, where Φ and Ψ denote respectively the *LS*-coupling and intermediate coupling functions. The observed and calculated energies are listed in tables 13, 18, 22, 23, and 24, and the coefficients in the wave functions in tables 14 and 19. One check which can be applied in a few cases is to calculate the Landé *g*-values and compare them with observed values. This was done for Ge I, Sn I, and Pb I and the results are given in table 15. The general agreement of observed and calculated energy levels and Landé *g*-factors is very satisfactory, and lead us to think that the intermediate coupling theory provides a satisfactory representation of the atomic electron configurations. The radial integrals s_q (defined as above with the 2/5 factor) needed in the formulae of [27] for electric quadrupole radiation were estimated as discussed below. Then the transition probabilities were calculated, and are given in tables 16, 20, and 25.

It should be mentioned that a number of authors have attempted fitting theory to observation for p^n configurations, for example Te I, I II, and Xe III [20], Pb I [18, 43], Br II [19], Ge I [44], Sn I [45], and possibly others. Most assumed the Slater ratio between the term intervals, and thus had one fewer adjustable

TABLE 13. *Observed and calculated energy levels in* p^2 *configurations*

(Units: cm^{-1})

Level	Ge I ($4p^2$)			Sn I ($5p^2$)			Pb I ($6p^2$)			Bi II ($6p^2$)		
	O	C	O–C	O	C	O–C	O	C	O–C	O	C	O–C
$^3P_0$	0	−3	3	0	−17	17	0	−94	94	0	−87	87
$^3P_1$	557	562	−5	1692	1715	−23	7819	7860	−41	13324	13380	−56
$^3P_2$	1410	1408	2	3428	3420	8	10650	10802	−152	17030	17147	−117
$^1D_2$	7125	7125	0	8613	8613	0	21458	21344	114	33936	33831	107
$^1S_0$	16367	16367	0	17163	17163	0	29467	29482	−15	44173	44190	−17

TABLE 14. *Coefficients in intermediate coupling wave functions* (p^2 *and* p^4 *configurations*)

Ion		a	b	c	d
Ge I	$4p^2$	0. 9934	0. 1148	0. 9968	0. 0799
Sn I	$5p^2$	. 9463	. 3232	. 9821	. 1883
Pb I	$6p^2$	. 7624	. 6471	. 9249	. 3803
Bi II	$6p^2$	. 7206	. 6933	. 9106	. 4133
Se I	$4p^4$	. 9910	—. 1342	. 9916	—. 1297
Br II	$4p^4$	. 9863	—. 1652	. 9861	—. 1663
Kr III	$4p^4$	. 9807	—. 1953	. 9784	—. 2065
Te I	$5p^4$	. 9617	—. 2743	. 9471	—. 3211
I II	$5p^4$	. 9523	—. 3050	. 9277	—. 3732
Xe III	$5p^4$	. 9392	—. 3435	. 9039	—. 4277
Po I	$6p^4$	. 8921	—. 4519	. 7495	—. 6620

TABLE 15. *Landé g-factors in* p^2 *configurations*

Level	*LS* coupling	Ge I			Sn I			Pb I		
		Observed	Calculated	O–C	Observed	Calculated	O–C	Observed	Calculated	O–C
$^3P_1$	1. 500	1. 476	1. 500	−0. 024	1. 502	1. 500	0. 002	1. 501	1. 500	0. 001
$^3P_2$	1. 500	1. 514	1. 493	. 021	1. 452	1. 448	. 004	1. 269	1. 291	—. 022
$^1D_2$	1. 000	. 989	1. 007	—. 018	1. 052	1. 052	0	1. 230	1. 209	. 021

TABLE 16. *Transition probabilities for* p^2 *configurations*

(Units: sec^{-1})

Transition	Type	Ge I	Sn I	Pb I[a]	Bi II
$^1S_0$–$^1D_2$	A_q	1.1	0.95	0.48	1.1
$^1S_0$–$^3P_2$	A_q	0.068	0.57	10	47
$^1S_0$–$^3P_1$	A_m	1.0	7.0	78	270
$^1D_2$–$^3P_2$	A_m	0.097	0.52	12	48
	A_q	.0010	.0061	0.60	3.7
$^1D_2$–$^3P_1$	A_m	0.050	0.46	14	56
	A_q	3.0×10^{-4}	.0043	0.46	2.8
$^1D_2$–$^3P_0$	A_q	3.0×10^{-5}	8.1×10^{-5}	0.0017	0.039
$^3P_2$–$^3P_1$	A_m	0.0082	0.062	0.18	0.35
	A_q	8.3×10^{-7}	3.6×10^{-5}	2.5×10^{-4}	5.6×10^{-4}
$^3P_2$–$^3P_0$	A_q	4.6×10^{-6}	5.9×10^{-4}	0.21	1.6
$^3P_1$–$^3P_0$	A_m	0.0031	0.083	7.3	35

[a] In substantial agreement with Gerjuoy [18], allowing for difference in s_q.

TABLE 17. *Parameters in* p^3 *configurations*

(Units: cm^{-1})

Parameter	As I	Sb I	Bi I
	$4p^3$	$5p^3$	$6p^3$
E(^{4}S)	116	672	7493
E(^{2}D)	10919	9871	15348
E(^{2}P)	18193	16407	21747
ζ	1441	3183	10159

TABLE 18. *Observed and calculated energy levels in* p^3 *configurations*

(Units: cm^{-1})

Level	As I ($4p^3$)			Sb I ($5p^3$)			Bi I ($6p^3$)		
	O	C	O–C	O	C	O–C	O	C	O–C
$^4S_{3/2}$	0	0	0	0	2	−2	0	−129	129
$^2D_{3/2}$	10593	10587	6	8512	8495	17	11419	11652	−233
$^2D_{5/2}$	10915	10919	−4	9854	9871	−17	15438	15348	90
$^2P_{1/2}$	18186	18193	−7	16396	16407	−11	21661	21747	−86
$^2P_{3/2}$	18648	18641	7	18465	18453	12	33165	33064	101

TABLE 19. *Coefficients in intermediate coupling wave functions* (p^3 *configurations*)

	As I	Sb I	Bi I
	$4p^3$	$5p^3$	$6p^3$
a	−0.2021	−0.3572	−0.2466
b	−.0279	−.1453	−.6032
c	.9789	.9227	.7585
a'	−.0800	−.2053	−.5494
b'	.9968	.9759	.7318
c'	.0119	.0742	.4033
a''	.9761	.9113	.7984
b''	.0760	.1629	.3172
c''	.2038	.3781	.5118

TABLE 20. *Transition probabilities for* p^3 *configurations*

(Units: sec^{-1})

Transition	Type	As I	Sb I	Bi I
$^2P_{3/2}$–$^2P_{1/2}$	A_m	8.4×10^{-4}	0.065	8.6
	A_q	1.9×10^{-9}	2.0×10^{-5}	0.21
$^2P_{3/2}$–$^2D_{5/2}$	A_m	0.31	1.5	23
	A_q	.13	0.33	10
$^2P_{3/2}$–$^2D_{3/2}$	A_m	0.61	4.0	120
	A_q	.062	0.17	4.5
$^2P_{1/2}$–$^2D_{5/2}$	A_q	0.059	.058	0.050
$^2P_{1/2}$–$^2D_{3/2}$	A_m	.32	1.1	1.2
	A_q	.10	0.19	0.51
$^2P_{3/2}$–$^4S_{3/2}$	A_m	1.6	5.2	7.3
	A_q	1.0×10^{-4}	7.8×10^{-4}	0.27
$^2P_{1/2}$–$^4S_{3/2}$	A_m	0.69	3.3	55
	A_q	.0012	0.048	6.2
$^2D_{5/2}$–$^2D_{3/2}$	A_m	3.4×10^{-4}	.022	0.40
	A_q	4.7×10^{-10}	3.2×10^{-6}	4.0×10^{-4}
$^2D_{5/2}$–$^4S_{3/2}$	A_m	0.0020	0.056	6.4
	A_q	.0033	.022	1.6
$^2D_{3/2}$–$^4S_{3/2}$	A_m	0.073	1.1	31
	A_q	.0019	0.0075	0.21

TABLE 21. *Parameters in* p^4 *configurations*

(Units: cm^{-1})

Parameter	Se I	Br II	Kr III	Te I	I II	Xe III	Po I
	$4p^4$	$4p^4$	$4p^4$	$5p^4$	$5p^4$	$5p^4$	$6p^4$
E(^{3}P)	1075	1728	2549	2735	4133	5797	10611
E(^{1}D)	9402	11759	14084	9765	12453	15083	17250
E(^{1}S)	22112	27202	31890	21293	26310	32044	27295
ζ	1808	2785	3965	3954	5617	7906	12341

TABLE 22. *Observed and calculated energy levels in* $4p^4$ *configurations*

(Units: cm^{-1})

Level	Se I			Br II			Kr III		
	O	C	O–C	O	C	O–C	O	C	O–C
$^3P_2$	0	−3	3	0	6	−6	0	8	−8
$^3P_1$	1989	1979	10	3136	3120	16	4548	4531	17
$^3P_0$	2534	2549	−15	3838	3849	−11	5313	5330	−17
$^1D_2$	9576	9576	0	12089	12089	0	14644	14643	1
$^1S_0$	22446	22446	0	27867	27866	1	33079	33074	5

TABLE 23. *Observed and calculated energy levels in* $5p^4$ *configurations*

(Units: cm^{-1})

Level	Te I			I II			Xe III		
	O	C	O–C	O	C	O–C	O	C	O–C
$^3P_2$	0	−39	39	0	53	−53	0	−201	201
$^3P_1$	4751	4712	39	7087	6942	145	9795	9750	45
$^3P_0$	4707	4794	−87	6448	6555	−107	8131	8414	−283
$^1D_2$	10559	10562	−3	13727	13725	2	17100	17128	−28
$^1S_0$	23199	23188	11	29501	29505	−4	37398	37333	65

TABLE 24. *Observed and calculated energy levels in* Po I ($6p^4$)

(Units: cm^{-1})

Level	Observed	Calculated	O–C
$^3P_2$	0	13	−13
$^3P_1$	16831	16782	49
$^3P_0$	7514	7546	−32
$^1D_2$	21679	21671	8
$^1S_0$	42718	42710	8

TABLE 25. *Transition probabilities for* p^4 *configurations*

(Units: sec^{-1})

Transition	Type	Se I	Br II	Kr III	Te I	I II	Xe III	Po I
$^1S_0$–$^1D_2$	A_q	2. 3	4. 0	4. 5	3. 1	5. 5	13	42
$^1S_0$–$^3P_2$	A_q	0. 18	0. 43	0. 69	0. 79	1. 6	3. 9	4. 1
$^1S_0$–$^3P_1$	A_m	7. 7	[a] 23	53	37	[b] 84	210	410
$^1D_2$–$^3P_2$	A_m	0. 62	[a] 1. 9	[c] 4. 7	3. 3	[b] 8. 8	[d] 21	66
	A_q	. 0074	0. 022	0. 043	0. 077	0. 21	0. 52	9. 3
$^1D_2$–$^3P_1$	A_m	. 11	. 26	[c] 0. 53	. 20	. 36	[c] . 62	0. 31
	A_q	3.5×10^{-4}	7.2×10^{-4}	. 0010	6.0×10^{-4}	8.6×10^{-4}	. 0012	9.4×10^{-4}
$^1D_2$–$^3P_0$	A_q	9.2×10^{-5}	2.1×10^{-4}	3.7×10^{-4}	4.7×10^{-4}	0. 0012	. 0031	0. 31
[e] $^3P_0$–$^3P_1$	A_m	0. 0085	0. 018	0. 023	1.4×10^{-6}	. 0040	. 067	8. 1
$^3P_0$–$^3P_2$	A_q	1.8×10^{-4}	8.7×10^{-4}	. 0025	0. 0073	. 022	. 052	0. 15
$^3P_1$–$^3P_2$	A_m	0. 17	0. 67	2. 0	2. 2	7. 2	[d] 19	85
	A_q	3.9×10^{-5}	2.2×10^{-4}	7.6×10^{-4}	0. 0044	0. 020	0. 068	3. 1

[a] Given by Martin and Tech [19] with whom we agree.
[b] Given by Martin and Corliss [20], who obtained 99, 9.1, respectively.
[c] Given by Osterbrock [21] with whom we agree.
[d] Given by Edlén [22] and Osterbrock [21], with whom we agree.
[e] $^3P_0 \rightarrow {}^3P_1$ in Se I, Br II and Kr III, $^3P_1 \rightarrow {}^3P_0$ in Te I, I II, Xe III, and Po I.

parameters than we use. The writer has given reasons [46] for prefering to treat the term intervals as unconnected by a Slater relation whenever this is feasible (as it is for p^n configurations), and accordingly all the atoms have been treated in this way in the present work on p^n configurations. Our use of an extra adjustable parameter results in a closer fit of theory and observation. In the only case where earlier work is comparable with ours [43] our results agree closely.

5.3. Estimation of s_q

The most uncertain part of the calculations is the estimation of the radial integrals s_q. For Ga I, Ge I, As I, Se I, and Br I (and for Kr I and Rb II, which were needed for extrapolation purposes) the self-consistent field with exchange wave functions of Watson and Freeman [47] were used, and for Kr I as a check the wave function of Worsley [48]. For other $4p^n$ configurations we assumed that the Rb II *minus* Kr I difference in $s_q^{-1/2}$ (linear in atomic number) should be added to the values of $s_q^{-1/2}$ for the neutral atoms to get the values for the corresponding ions, and by repeating the process values were obtained for doubly ionized atoms. Values of s_q were collected for many atoms in the $3p^n$ [49, 52] and $2p^n$ [42, 50, 51] configurations. These were used with the values for $4p^n$ configurations to extrapolate $s_q^{-1/2}$ to the $5p^n$ and $6p^n$ configurations. In these very rough calculations consideration was given to the variation of the effective quantum numbers derived from the energies and from the values of s_q for $2p^n$, $3p^n$, and $4p^n$ configurations. Some smoothing was applied to the estimates within the $5p^n$ and $6p^n$ rows of atoms. The finally adopted values of s_q are listed in table 26. The values of s_q for the $4p^n$ configurations are thought to be reasonably reliable; the values for the $5p^n$ and $6p^n$ configurations are much less certain.

TABLE 26. *Adopted values of* $s_q = \frac{2}{5}\overline{r^2}$ *for* p^n *configurations*[a]

(s_q in atomic units)

		p	p^2	p^3	p^4	p^5
4	I	5. 54	3. 84	2. 95	2. 48	2. 09
	II	3. 58			1. 9	1. 58
	III	2. 51			1. 4	1. 24
5	I	6. 0	4. 5	3. 8	3. 1	2. 8
	II	4. 3			2. 4	2. 2
	III	3. 2			2. 0	1. 8
6	I	5. 3	4. 4	4. 0	3. 7	
	II	4. 1	3. 5			2. 1
	III	3. 3				

[a] 4, 5, 6 are the principal quantum numbers, I, II, III are spectrum numbers; e.g., $4p^5$ Kr II has s_q=1.58. Atomic units used.

5.4. Accuracy of Results

The magnetic dipole transition probabilities do not depend on the radial integral s_q, and they are therefore believed to be quite accurate, probably within 20 percent of the true values. It is very difficult to estimate the accuracy of our adopted values of s_q and hence of the electric quadrupole transition probabilities. Jenkins and Mrozowski [33] showed that the line Pb I $6p^2\ {}^1D_2$–$^3P_1$ λ7330 had 2.2 percent admixture of electric quadrupole radiation. According to our calculations the proportion is 3.3 percent, and 6.9 percent on combining the results of Gerjuoy [18] and Mrozowski [53]. This may suggest that the true s_q are rather smaller than the ones we have adopted, the work of Jenkins and Mrozowski being believed to be fairly reliable. The calculated intensity ratios are I (4618) : I(5313) = 9.0:1 and I(4659) : I(7330) : I(9250) = 0.0019 : 1 : 0.70, which may be compared with the observed values of Mrozowski [32] of 5.0:1 and 0.023:1:0.84. The discrepancy in I(4659) is not unduly disturbing because this line is rather sensitive to the parameters involved. The other calculated intensities are outside the probable errors given by Mrozowski, and the discrepancies cannot be explained by a reduction in s_q. Probably there were some undetected errors in the experimental intensities. In Bi I, for λ6476 ($^2D_{5/2}$–$^4S_{3/2}$) the percentage of the total intensity due to electric quadrupole radiation is 20 percent according to our calculations; according to the observations of Mrozowski [38] the percentage did not exceed 15 percent (upper limit). This discrepancy could be explained if our s_q were rather too large. The calculated percentage of electric quadrupole radiation in λ5640 ($^2P_{3/2}$–$^2D_{5/2}$) is about 30 percent; it does not exceed 10 percent for the other lines observed by Mrozowski. Our transition probabilities for Te I are in agreement with Niewodniczanski and Lipinski's [40] comment (mentioned above) that λ5420 is the strongest line from $^1S_0$. No other experimental results appear to be available. A new experimental determination of s_q from intensity measurements for one or more ions would be of interest.

5.5. $d^9s^2 + d^{10}s$ Configurations in Hg II

There is one other important group of forbidden lines in a heavy atom, those in Hg II. Déjardin [55] observed the line $^2D_{3/2}$–$^2S_{1/2}$(λ1978), Paschen [56] observed $^2D_{5/2}$–$^2S_{1/2}$(λ2815), and Naudé [57] observed $^2D_{3/2}$–$^2D_{5/2}$(λ6647). These transitions occur within the configurations $d^9s^2 + d^{10}s$. Later observations were made by Sambursky [58] and Mrozowski [59]. Mrozowski showed that λ2815 is due to electric quadrupole radiation.

The line strengths of the transitions were obtained from the work of Shortley [7] for magnetic dipole radiation and from that of Garstang [16] for electric quadrupole radiation. As usual it is difficult to estimate the radial integrals involved. The results involve the integral

$$s_q(s, d) = \int_0^\infty r^2 \mathrm{P}(6s)\,\mathrm{P}(5d)\,dr$$

where P(6s) is the radial wave function for the 6s electron in the $5d^9 6s^2$ configuration and P(5d) that for the 5d electron in the $5d^{10}6s$ configuration. For a heavy atom relativistic wave functions should be used, and then the d^{10} group subdivides into six d electrons and four $\overline{d}$ electrons, and the appropriate one must be used. The integral

$$s_q(d, \overline{d}) = \int_0^\infty r^2 \mathrm{P}(5d)\mathrm{P}(5\overline{d})dr$$

is also required for the transition $^2D_{3/2}$–$^2D_{5/2}$. Wave functions for Hg II do not appear to be available, but relativistic self-consistent field wave functions without exchange are available for neutral mercury, and we use the results of Mayers [60] for the $5d^{10}6s^2$ configuration. From his wave functions it is found that $s_q(s,d) = -4.05$, $s_q(s,\overline{d}) = -3.53$, and $s_q(d,\overline{d}) = +2.87$. Generally speaking the effect of exchange is to reduce the values of s_q, and increased ionization has the same effect. For the purposes of making rough numerical estimates we have taken for the 5/2−1/2 transition $s_q(s, d) = -2.7$, for the 3/2−1/2 transition $s_q(s, \overline{d}) = -2.4$, and for the 3/2−5/2 transition $s_q(d, \overline{d}) = +2.0$. These values have been used in deriving the transition probabilities listed in table 27. It must be recognized, however, that these values of s_q are only rough estimates. An accurate laboratory measurement of the ratio of λ1978 and λ6647 would be of exceptional interest.

TABLE 27. *Transition probabilities in* [Hg II]

(Units: sec^{-1})

Transition	A_m	A_q
$5d^9 6s^2\ ^2D_{3/2}$—$5d^9 6s^2\ ^2D_{5/2}$	54	0. 029
$5d^9 6s^2\ ^2D_{3/2}$—$5d^{10}6s\ ^2S_{1/2}$	------	42
$5d^9 6s^2\ ^2D_{5/2}$—$5d^{10}6s\ ^2S_{1/2}$	------	9. 5

I am indebted to L. M. Branscomb and K. G. Kessler for enabling me to work at the National Bureau of Standards in 1961, and again in 1962, and for their hospitality. I am indebted to C. W. Allen for encouragement during that part of the work performed in London. I am indebted to R. E. Watson for supplying me with a copy of his Report No. 12. Thanks are due to M. J. Price for computing assistance during one of his vacations. I am grateful to A. D. Thackeray, J. C. Polanyi, Mrs. C. M. Sitterly, and W. C. Martin for correspondence or discussions.

6. References

[1] R. H. Garstang, in Atomic and Molecular Processes, ed. D. R. Bates, ch. 1 (Academic Press, New York and London, 1962).
[2] C. E. Moore, Atomic energy levels, NBS Circ. **467,** Vol. I (1949); Vol. II (1952); Vol. III (1958).
[3] S. Pasternack, Astrophys. J. **92,** 129 (1940).
[4] E. U. Condon and G. H. Shortley The Theory of Atomic Spectra Cambridge University Press, London, England, 1951).
[5] G. Racah, Phys. Rev. **62,** 438 (1942).
[6] R. E. Trees, Phys. Rev. **85,** 382 (1952).
[7] G. H. Shortley, Phys. Rev. **57,** 225 (1940).
[8] R. H. Garstang, Proc. Cambridge Phil. Soc. **53,** 214 (1957).
[9] R. E. Watson, Tech. Report No. 12, Solid State and Molecular Theory Group, Mass. Inst. Technology, June 15, 1959.
[10] I. S. Bowen, Astrophys. J. **121,** 306 (1955).
[11] A. D. Thackeray, Monthly Notices Roy. Astron. Soc. **124,** 251 (1962).
[12] R. H. Garstang, Monthly Notices Roy. Astron. Soc. **124,** 321 (1962).
[13] R. H. Garstang, Monthly Notices Roy. Astron. Soc. **118,** 234 (1958).
[14] G. Racah, Phys. Rev. **63,** 367 (1943).
[15] G. Racah and Y. Shadmi, Bull. Res. Council Israel **8F,** 15 (1959).
[16] R. H. Garstang, Proc. Cambridge Phil. Soc. **54,** 383 (1958).
[17] A. D. Thackeray, Monthly Notices Roy. Astron. Soc. **113,** 211 (1953).
[18] E. Gerjuoy, Phys. Rev. **60,** 233 (1941).
[19] W. C. Martin and J. L. Tech, J. Opt. Soc. Am. **51,** 591 (1961).
[20] W. C. Martin and C. H. Corliss, J. Res. NBS, **64A** (Phys. and Chem.) No. 6 443 (1960).
[21] D. E. Osterbrock, Astrophys. J. **114,** 469 (1951).
[22] B. Edlén, Phys. Rev. **65,** 248 (1944).
[23] F. M. Walters, BS Sci. Pap., **17,** 161 (1922).
[24] C. D. Cole, Bull. Am. Phys. Soc. **6,** 74 (1961).
[25] F. E. Eshbach and R. A. Fisher, J. Opt. Soc. Am. **44,** 868 (1954).
[26] C. C. Kiess and C. H. Corliss, J. Res. NBS **63A** (Phys. and Chem.) No. 3, 1 (1959).
[27] G. H. Shortley, L. H. Aller, J. G. Baker, and D. H. Menzel, Astrophys J. **93,** 178 (1941).
[28] H. Niewodniczanski, Acta Phys. Polonica, **3,** 285 (1934).
[29] H. Gieseler and W. Grotrian, Zeit. Physik **34,** 374 (1925).
[30] N. K. Sur, Phil. Mag. **2,** 633 (1926).
[31] H. Niewodniczanski, Acta Phys. Polonica **2,** 375 (1933).
[32] S. Mrozowski, Phys. Rev. **58,** 1086 (1940).
[33] F. A. Jenkins and S. Mrozowski, Phys. Rev. **59,** 808, **60,** 225 (1941).
[34] C. D. Cole and S. Mrozowski, Phys. Rev. **93,** 933 (1954).
[35] C. D. Cole, Bull. Am. Phys. Soc. **5,** 412 (1960).
[36] M. Hults and S. Mrozowski, Phys. Rev. **86,** 587 (1952).
[37] G. R. Toshniwal, Phil. Mag. **4,** 774 (1927).
[38] S. Mrozowski, Phys. Rev. **69,** 169 (1946).
[39] J. E. Ruedy and R. C. Gibbs, Phys. Rev. **46,** 880 (1934).
[40] H. Niewodnicanski and F. Lipinski, Nature, **142,** 1160 (1938).
[41] S. Mrozowski, J. Opt. Soc. Am. **46,** 663 (1956).
[42] R. H. Garstang, Monthly Notices Roy. Astron. Soc. **111,** 115 (1951).
[43] T. M. Helliwell, Astrophys. J. **133,** 566 (1961).
[44] J. C. van den Bosch and P. F. A. Klinkenberg, Proc. Ned. Akad. Wetens. **44,** 556 (1941).
[45] S. Goudsmit, Phys. Rev. **35,** 1325 (1930).
[46] R. H. Garstang, Proc. Cambridge Phil. Soc. **52,** 107 (1956).
[47] R. E. Watson and A. J. Freeman, Phys. Rev. **124,** 1117 (1961).
[48] B. H. Worsley, Proc. Roy. Soc. **A247,** 390 (1958).
[49] S. J. Czyzak, Astrophys. J. Supp. **7,** 53 (1962).
[50] R. H. Garstang, Astrophys. J. **115,** 506 (1952).
[51] B. H. Worsley, Can. J. Phys. **36,** 289 (1958).
[52] D. R. Hartree and W. Hartree, Proc. Roy. Soc. **A166,** 450 (1938).
[53] S. Mrozowski, Reviews Mod. Phys. **16,** 153 (1944).
[54] A. H. Joy and P. Swings, Astrophys. J. **102,** 353 (1945).
[55] G. Déjardin, Ann. Phys. **8,** 424 (1927).
[56] F. Paschen, Ber. Preuss. Akad. Wiss. **32,** 536 (1928).
[57] S. M. Naudé, Ann. Physik, **3,** 1 (1929).
[58] S. Sambursky, Zeit. Physik **76,** 266 (1932).
[59] S. Mrozowski, Phys. Rev. **57,** 207 (1940).
[60] D. F. Mayers, Proc. Roy. Soc. **A241,** 93 (1957).
[61] A. H. Joy, Astrophys. J. **133,** 493 (1961).

7. Appendix. Electric Quadrupole Multiplet Strengths for the Transition Arrays $d^n - d^{n-1}s$

In an earlier paper Garstang [16] showed how to calculate electric quadrupole line strengths for many transitions involving s and d electrons. Among these were the transitions $d^n - d^{n-1}s$. Detailed results were given for $d^9 - d^8s$ and $d^7 - d^6s$. It was also shown that $S_q(d^n\alpha SL - d^{n-1}(\alpha_1 S_1 L_1)sSL_1) = S_q(d^{11-n}\alpha_1 S_1 L_1 - d^{10-n}(\alpha SL)sS_1L)$ so that values for the arrays $d^{11-n} - d^{10-n}s$ can be obtained from those for $d^n - d^{n-1}s$. The phases of the matrix elements for the former array are $(-1)^{S+S_1+L+L_1-\frac{1}{2}}$ times those of $d^n - d^{n-1}s$; an extra (-1) has to be introduced for $n=6$ if $\alpha_1 S_1 L_1$ has seniority 3. Thus the transitions $d^2 - ds$ and $d^4 - d^3s$ need not be listed. We list here results for $n=1$, 3, and 5. The tabulated quantities are $S_q(\alpha SL, \alpha' SL')$, as multiples of s_q^2 where

$$s_q = \int_0^\infty r^2 \mathrm{P}(d)\,\mathrm{P}(s)dr$$

involves the radial wave functions of the d electron in the d^n configuration and the s electron in the $d^{n-1}s$ configuration. As superscript prefixes to the strengths there have been inserted the signs of the square roots of the strengths (i.e., of the matrix elements $(\alpha SL \| T^{(2)} \| \alpha' SL')$) required in determining the phases for intermediate coupling calculations. Racah's seniority numbers are given as subscripts to the term symbols. The strengths of individual lines may be obtained (in LS-coupling) in cases where there is only one term of the same kind as each of the initial and final terms of the desired transition by a direct application of [8, eqs (3), (5), and (6)]. In cases where there are more than one term of the same kind in either or both of the initial and final states, much more elaborate calculations must be performed, as for example for Fe II [12].

TABLE 28. *Electric quadrupole multiplet strengths*

s

		^2S	
d	^2D	-4	$\times \frac{s_q^2}{3}$

d^2s

		^2S	^2P	^2D	^2F	^2G	
d^3	^2P	0	-294	-630	$+336$	0	$\times \frac{s_q^2}{525}$
	^2_1D	-560	$+315$	$+175$	$+735$	$+315$	
	^2_3D	0	$+735$	-675	-315	$+375$	
	^2F	0	-1176	$+420$	-294	$+1050$	
	^2G	0	0	$+900$	-1890	-990	
	^2H	0	0	0	$+2310$	-2310	

d^2s

		^4P	^4F	
d^3	^4P	$+64$	$+56$	$\times \frac{s_q^2}{25}$
	^4F	$+56$	-224	

d^4s

d^5	$(\frac{3}{2}P)^4P$	$(\frac{3}{4}P)^4P$	$(^3D)^4D$	$(^5D)^4D$	$(\frac{3}{2}F)^4F$	$(\frac{3}{4}F)^4F$	$(^3G)^4G$	$(^3H)^4H$
^4P	+896	−196	−490	+1050	+784	−784	0	0
^4D	0	−1260	+1350	+1750	0	+840	−1800	0
^4F	+784	+224	+210	+2450	−3136	−196	+1260	+1540
^4G	0	0	−750	+3150	0	+2100	+1980	−4620

$\times \frac{s_q^2}{525}$

d^4s

d^5	^6D
^6S	−4

$\times s_q^2$

d^4s

d^5	$(\frac{1}{0}S)^2S$	$(\frac{1}{4}S)^2S$	$(\frac{3}{2}P)^2P$	$(\frac{3}{4}P)^2P$	$(\frac{1}{2}D)^2D$	$(\frac{1}{4}D)^2D$	$(^3D)^2D$	$(^1F)^2F$
^2S	0	0	0	0	0	+12320	−18480	0
^2P	0	0	−8624	−15400	−18480	−9240	−6160	+9240
^2D	−18480	0	+27720	0	+15400	0	0	0
^2D	0	+6160	+21560	+6160	−19800	+4400	−26400	−15400
^2D	0	+12320	0	−27720	0	−19800	−13200	−7700
^2F	0	0	−34496	+15400	+12320	−13860	−9240	−8085
^2F	0	0	0	−27720	0	+7700	−46200	+40425
^2G	0	0	0	0	+26400	+3300	−19800	+231
^2G	0	0	0	0	0	−21780	−14520	+38115
^2H	0	0	0	0	0	0	0	−10164
^2I	0	0	0	0	0	0	0	0

$\times \frac{8 q^2}{23100}$

d^4s

d^5	$(\frac{3}{2}F)^2F$	$(\frac{3}{4}F)^2F$	$(\frac{1}{2}G)^2G$	$(\frac{1}{4}G)^2G$	$(^3G)^2G$	$(^3H)^2H$	$(^1I)^2I$
^2S	0	0	0	0	0	0	0
^2P	+9856	+15400	0	0	0	0	0
^2D	+64680	0	+27720	0	0	0	0
^2D	−9240	+9240	+11000	+4840	−19800	0	0
^2D	0	−41580	0	−21780	−9900	0	0
^2F	−8624	+13475	+30800	−21175	+31185	−16940	0
^2F	0	+24255	0	−38115	+693	+30492	0
^2G	−55440	−31185	−29040	−27885	−29403	−30492	+24024
^2G	0	−63525	0	+18225	+83655	+4620	+32760
^2H	+67760	−16940	−67760	+1540	+30492	−88088	−56056
^2I	0	0	0	+32760	−72072	−168168	+127400

$\times \frac{8 q^2}{23100}$

(Paper 68A1–253)

JOURNAL OF RESEARCH of the National Bureau of Standards—A. Physics and Chemistry
Vol. 68A, No. 1, January–February 1964

Franck-Condon Factors to High Vibrational Quantum Numbers III: CN

R. W. Nicholls*

(October 1, 1963)

Franck-Condon factor arrays have been computed numerically to high vibrational quantum numbers for the red ($A^2\Pi_i - X^2\Sigma^+$) and violet ($B^2\Sigma^+ - X^2\Sigma^+$) band systems of CN.

1. Introduction

The CN molecule is a significant contributor to the spectra of comets and stellar atmospheres. It also plays an important rôle in many aspects of combustion spectroscopy. The red and violet band systems are its two most important electronic transitions. Definitive vibrational assignments and molecular constants exist for them [Douglas and Routly 1954]. Intensity measurements have been made on both systems and interpreted in terms of electronic transition moment variation across them and of smoothed band strengths [Ornstein and Brinkmann 1931; Nicholls 1956; Dixon and Nicholls 1958; Ferguson 1963]. Franck-Condon factor arrays are necessary parameters for these studies. The purpose of this paper is to supplement the limited and approximate arrays of Franck-Condon factors previously available for the systems [Fraser, Jarmain, and Nicholls 1954; Nicholls, Fraser, and Jarmain 1959].

In previous papers of this series, the straightforward numerical method of computation for Morse molecules to high vibrational quantum numbers have been described. [Nicholls 1960, 1961] The method has since been used on a number of important band systems and excitation transitions (Nicholls 1962a, b, c, d).

The computations were performed upon the IBM 7090 computer of the National Bureau of Standards using a program written by Miss R. Zucker of the Computation Laboratory.

2. Basic Data

The input data for the program are ω_e, $\omega_e x_e$, r_e, μ_A and v_{max} for both states of the transition involved. These data were obtained from the work of Douglas and Routly and are listed in table 1.

TABLE 1. *Basic data*

State	ω_e (cm^{-1})	$\omega_e x_e$ (cm^{-1})	$r_e(A)$	μ_A	v_{max}
$X^2\Sigma^+$	2068.614	13.114	1.17198	6.46427	18
$A^2\Pi_i$	1812.33	12.61	1.2296	6.46427	19
$B^2\Sigma^+$	2163.9	20.2	1.1493	6.46427	19

*Department of Physics, University of Western Ontario, London, Ontario.

3. Results

The Franck-Condon factor arrays for the CN red and violet systems are displayed in tables 2 and 3. Franck-Condon factor surfaces of these arrays are shown in figures 1 and 2. The strongly developed Condon loci are clearly evident in both cases. The CN violet system, having a very small Δr_e ($\sim$0.02 Å), exhibits an almost diagonal primary Condon locus with some indications of subsidiary loci at high v′, v″. The CN red system having a somewhat larger Δr_e ($\sim$0.05 Å) exhibits more subsidiary loci at lower v', v''. In the tables, the power of 10 by which the entry is to be multiplied is indicated by the negative number at the end of each entry. The position of the CN "tail" bands of the violet system at the large values of v', v'' is clearly seen on the primary locus. The data for the CN red system agrees well with that of Wyller [1958] calculated on the basis of a Hulburt-Hischfelder potential.

4. Discussion

While the Morse model of molecular potential is admittedly an empirical expedient, the work of Jarmain [1963] on realistic Klein-Dunham potentials for the $X^2\Sigma^+$, $A^2\Pi$ and $B^2\Sigma^+$ states of CN shows that the departure from Morse potentials is small and thus that the tables 2 and 3 are probably acceptable. These Franck-Condon factors for the CN violet system have been used in conjunction with the lifetime measurements of Bennett and Dalby [1960], to determine absolute band strengths for important bands of the system [Nicholls 1964].

The great assistance to this work of Miss Zucker of the NBS Computational laboratory is gratefully acknowledged.

The work reported above has been supported in part by research grants from The Air Force Office of Scientific Research, The National Aeronautics and Space Administration, The National Research Council of Canada and The Ontario Research Foundation, and by contracts with the Air Force Cambridge Research Center and the Defence Research Board of Canada.

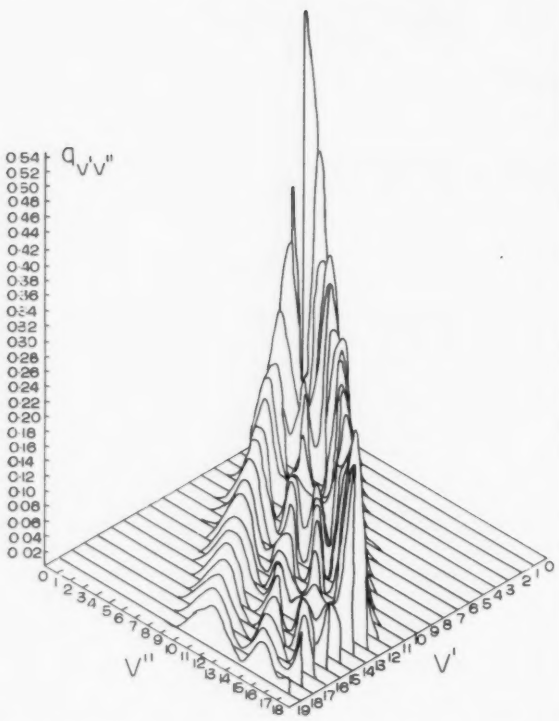

FIGURE 1. *Franck-Condon factor surface for the* CN *red system.*

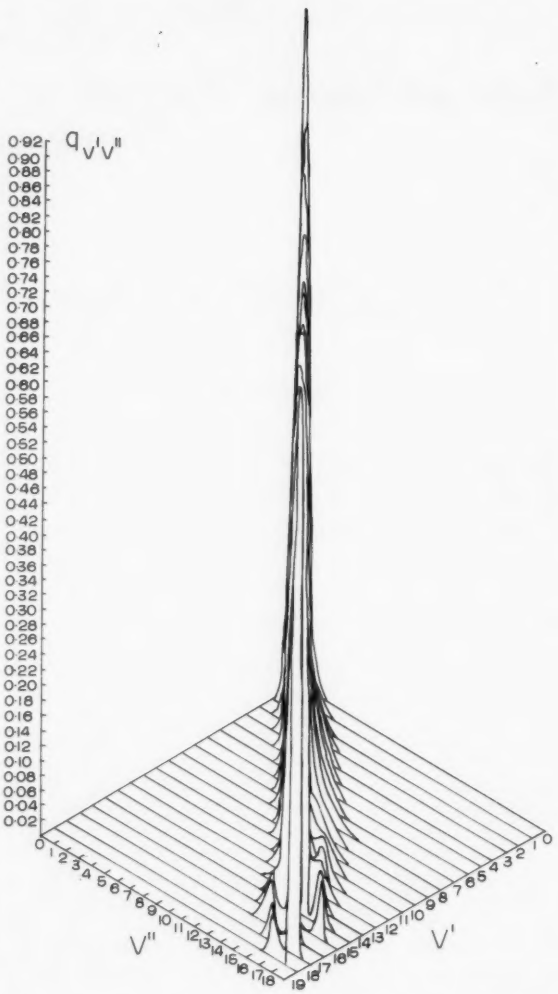

FIGURE 2. *Franck-Condon factor surface for the* CN *violet system.*

5. References

Bennett, R. G., and Dalby, F. W. (1960), J. Chem. Phys. **32,** 1716.

Dixon, R. N., and Nicholls, R. W. (1958), Can. J. Phys. **36,** 127.

Douglas, A. E., and Routly, P. M. (1954), Astrophys. J. Supp. **1,** 295.

Ferguson, H. I. S. (1963), private communication.

Fraser, P. A., Jarmain, W. R., and Nicholls, R. W. (1954), Astrophys. J. **119,** 286.

Ornstein, L. S., and Brinkman, H. (1931), Proc. Roy. Acad. Amsterdam **34,** 33.

Jarmain, W. R. (1963), private communication.

Nicholls, R. W. (1956), Proc. Phys. Soc. **A69,** 741; (1960) Can. J. Phys. **38,** 1705; (1961) J. Res. NBS **65A** (Phys. and Chem.) No. 5, 451; (1962a) J. Res. NBS **66A** (Phys. and Chem.) No. 3, 227; (1962b) Can. J. Phys. **40,** 523; (1962c) J. Quant. Spectr. Rad. Transfer **2,** 433; (1962d) Can. J. Phys. **40,** 1772; (1964) J. Quant. Spectr. Radiative Transfer (AGARDograph) (in press).

Nicholls, R. W., Fraser, P. A., and Jarmain, W. R. (1959), Combustion and Flame **3,** 13.

Wyller, A. (1958), Astrophys. J. **127,** 763.

TABLE 2. *Franck-Condon factors to high vibrational quantum numbers for the* CN *red* ($A^2\Pi_i - X^2\Sigma^+$) *system*

v' \ v''	0	1	2	3	4	5	6	7	8	9	10
0	*5.3757-1*	*3.5349-1*	9.4547.2	1.3294-2	1.0612-3	4.8473-5	1.2138-6	1.4932-8	7.0536-11	5.6474-14	6.0327-17
1	3.1160-1	7.6745-2	*3.6614-1*	1.9808-1	4.2582-2	4.5980-3	2.6517-4	8.0140-6	1.1506-7	6.1453-10	5.8270-13
2	1.0995-1	*2.6831-1*	1.5840-3	*2.5525-1*	*2.6968-1*	8.4473-2	1.1906-2	8.4458-4	3.0208-5	4.9874-7	2.9755-9
3	3.0917-2	1.8573-1	1.4030-1	5.9101-2	1.2855-1	*2.9670-1*	1.3272-1	2.3875-2	2.0455-3	8.5321-5	1.6002-6
4	7.6765-3	7.8903-2	*1.9523-1*	4.1744-2	1.2661-1	4.1349-2	*2.8285-1*	1.8045-1	4.0855-2	4.1713-3	2.0063-4
5	1.7727-3	2.6374-2	1.2139-1	*1.5531-1*	1.7048-3	*1.5852-1*	3.0781-	*2.3976-1*	*2.2154-1*	6.2617-2	7.5451-3
6	3.9235-4	7.6867-3	5.3102-2	1.4292-1	9.5944-2	9.5123-3	*1.5028-1*	5.6027-3	1.8144-1	*2.5148-1*	*8.8411-2*
7	8.4825-5	2.0608-3	1.9106-2	8.0911-2	*1.3913-1*	4.2513-2	4.1725-2	*1.1589-1*	3.3158-2	1.2078-1	2.6759-1
8	1.8140-5	5.2460-4	6.0988-3	3.5477-2	1.0231-1	*1.1478-1*	9.4069-3	7.6438-2	7.1121-2	6.9561-2	6.7741-2
9	3.8708-6	1.2939-4	1.8032-3	1.3328-2	5.4358-2	1.1197-1	7.9628-2	5.6759-5	*9.9305-2*	3.2356-2	*1.0201-1*
10	8.2929-7	3.1347.5	5.0732-4	4.5319-3	2.3859-2	7.2156-2	*1.0806-1*	4.4234-2	9.9830-3	*1.0456-1*	7.7358-3
11	1.7919-7	7.5314-6	1.3828-4	1.4422-3	9.2642-3	3.6871-2	8.5202-2	*9.2307-2*	1.6941-2	3.0679-2	*5.3289-2*
12	3.9187-8	1.8070-6	3.6973-5	4.3907-4	3.3133-3	1.6272-2	5.0687-2	9.0760-2	6.9020-2	2.3130-3	5.3066-2
13	8.6948-9	4.3515-7	9.7860-6	1.2985-4	1.1203-3	6.5098-3	2.5362-2	6.3117-2	*8.7701-2*	4.3691-2	9.1832-4
14	1.9606-9	1.0559-7	2.5810-6	3.7709-5	3.6460-4	2.4338-3	1.1313-2	3.5795-2	7.1952-2	*7.6715-2*	2.1553-2
15	4.4953-10	2.5890.8	6.8178-7	1.0842-5	1.1566-4	8.6806-4	4.6608-3	1.7769-2	4.6347-2	7.5492-2	6.0072-2
16	1.0480-10	6.4290-9	1.8105-7	3.1045-6	3.6104-5	2.9069-4	1.8159-3	8.0482-3	2.5594-2	5.5509-2	*7.2944-2*
17	2.4835-11	1.6193-9	4.8474-8	8.8960-7	1.1168-5	1.0122-4	6.8017-4	3.4168-3	1.2726-2	3.4139-2	6.1778-2
18	5.9886-12	4.1388-10	1.3115-8	2.5601-7	3.4419-6	3.3719-5	2.4788-4	1.3850-3	5.8764-3	1.8628-2	4.4444-2
19	1.4847-12	1.0731-10	3.5918-9	7.4199-8	1.0615-6	1.1146-5	8.8683-5	5.4329-4	2.5729-3	9.3449-3	2.5431-2

v' \ v''	11	12	13	14	15	16	17	18
0	1.8995-16	1.5948-16	3.0640-17	4.9182-16	1.7101-16	1.6302-16	7.1480-16	1.0901-16
1	1.5738-15	3.4200-17	5.6834-16	2.6135-17	1.9276-16	4.2348-17	6.8633-17	1.8084-17
2	2.8207-12	1.6150-15	1.3995-16	7.3001-18	5.3798-16	4.4321-17	4.9243-16	1.8682-16
3	1.0579-8	1.0711-11	6.6539-15	6.2089-16	3.5762-17	4.5407-17	6.9069-16	2.9542-16
4	4.2345-6	3.0765-8	3.1888-11	3.9175-14	6.9581-16	2.7820-15	3.0717-17	5.6938-16
5	4.1479-4	9.7748-6	7.7466-8	8.1963-11	8.1174-14	3.0691-16	1.8812-15	2.6983-16
6	1.2482-2	7.7879-4	2.0362-5	1.7507-7	1.9128-10	1.9412-13	2.2525-15	1.1570-15
7	1.1705-1	1.9265-2	1.3564-3	3.9138-5	3.6331-7	4.0722-10	4.3818-13	8.0260-15
8	*2.6911-1*	1.4707-1	2.8116-2	2.2239-3	7.0500-5	7.0357-7	8.0657-10	1.0900-12
9	2.8629-2	*2.5692-1*	1.7681-1	3.9180-2	3.4689-3	1.2036-4	1.2864-6	1.4842-9
10	*1.2255-1*	6.1753-3	*2.3317-1*	*2.0463-1*	5.2509-2	5.1887-3	1.9642-4	2.2406-6
11	4.1020-6	*1.2806-1*	6.5155-5	2.0090-1	*2.2897-1*	6.8051-2	7.4882-3	3.0842-4
12	*7.1283-2*	7.1603-3	*1.1932-1*	7.7315-3	1.6361-1	*2.4849-1*	8.5646-2	1.0477-2
13	6.9916-2	4.5342-2	2.4286-2	*9.9824-2*	2.5214-2	1.2483-1	*2.6215-1*	1.0503-1
14	1.0091-2	*7.7095-2*	2.2135-2	4.5364-2	*7.4405-2*	4.7974-2	8.7841-2	*2.6924-1*
15	6.4443-3	2.5233-2	*7.3755-2*	6.3297-3	6.4775-2	4.8100-2	7.1589-2	5.5390-2
16	4.1034-2	1.8308-4	4.1237-2	*6.1775-2*	9.6950-5	*7.8299-2*	2.5263-2	9.2280-2
17	*6.4626-2*	2.3101-2	2.4654-3	5.3708-2	4.4752-2	3.1795-3	*8.3620-2*	8.9971-3
18	6.3983-2	5.1914-2	9.2756-3	1.1233-2	*5.9788-2*	2.6884-2	1.3418-2	*8.0373-2*
19	4.9374-2	*6.1553-2*	3.6968-2	1.4930-3	2.3347-2	*5.8506-2*	1.1957-2	2.7528-2

TABLE 3. *Franck-Condon factors to high vibrational quantum numbers for the* CN *violet* ($B^2\Sigma^+ - X^2\Sigma^+$) *system*

v' \ v''	0	1	2	3	4	5	6	7	8	9	10
0	*9.0861-1*	8.3968-2	6.9510-3	4.4870-4	1.9898-5	2.7721-7	2.6248-8	2.7813-8	8.2117-9	1.5780-9	2.2678-10
1	8.9808-2	*7.5682-1*	1.3506-1	1.6796-2	1.4376-3	8.0435-5	1.4545-6	1.0223-7	1.6193-7	5.5089-8	1.1974-8
2	1.5782-3	1.5573-1	*6.4884-1*	1.6365-1	2.7137-2	2.8727-3	1.9375-4	4.3326-6	3.1869-7	5.3235-7	2.0531-7
3	7.8971-6	3.4362-3	2.0419-1	*6.7392-1*	1.7684-1	3.6660-2	4.5823-3	3.6058-4	9.5981-6	6.4476-7	1.3028-6
4	8.6112-7	5.1416-5	4.7889-3	2.3950-1	*5.2453-1*	1.7943-1	4.4743-2	6.3791-3	5.7143-4	1.7542-5	1.1125-6
5	1.1289-8	3.1220-6	1.8005-4	5.2344-3	2.6442-1	*4.9545-1*	1.7463-1	5.1190-2	8.0938-3	8.0971-4	2.7893-5
6	7.2137-10	1.0935-7	5.9244-6	4.5696-4	4.6839-3	2.8056-1	*4.8501-1*	1.6456-1	5.6067-2	9.5892-3	1.0555-3
7	1.0162-10	2.5942.9	5.2139-7	6.9330-6	9.4206-4	3.3282-3	2.8863-1	*4.8479-1*	1.5062-1	5.9592-2	1.0764-2
8	2.2048-12	9.0199-10	3.0495-9	1.6673-6	4.1392-6	1.6681-3	1.6228-3	2.8874-1	*4.9903-1*	1.3378-1	6.2069-2
9	2.1117-14	3.7404-11	4.0681-9	4.9483-11	4.0189-6	9.1838-8	2.6132-3	2.7056-4	2.8060.1	*5.2430-1*	1.1476-1
10	5.8414-15	6.9530-13	3.0099-10	1.2044-8	1.8076-8	7.6693-6	8.2223-6	3.6759-3	1.8061-4	2.6377-1	*5.5916-1*
11	4.2818-15	9.1614-14	9.2904-12	1.5548-9	2.5284-8	1.6872-7	1.1692-5	5.9422-5	4.6645-3	2.3775-3	2.3801-1
12	2.0230-15	5.1900-14	6.5811-13	7.8321-11	5.8540-9	3.6926-8	7.2502-7	1.3761-5	2.0506-4	5.3129-3	7.8393-3
13	8.5878-16	1.6294-14	3.1528-13	4.8529-12	4.5861-10	1.7078-8	3.1707-8	2.1227-6	1.1015-5	5.1087-4	5.3388-3
14	1.9348-16	3.8730-15	1.5327-13	1.4107-12	3.1444-11	2.0513-9	3.9504-8	5.6758-9	4.7351-6	3.4980-6	1.0360-3
15	6.4240-18	1.5402-15	4.9657-14	7.1185-13	6.2102-12	1.7368-10	7.2984-9	7.2291-8	2.5977-8	8.3072-6	1.0576-6
16	1.0932-16	1.2919-15	1.2348-14	3.0699-13	2.8671-12	2.6234-11	8.1219-10	2.1206-8	1.0035-7	3.2093-7	1.1244-5
17	4.2234-17	7.5678-16	4.0075-15	1.1304-13	1.3270-12	1.0021-11	1.1181-10	3.1849-9	5.0934-8	9.2597-8	1.3090-6
18	7.6386-18	1.1930-16	2.7265-15	3.9056-14	5.4181-13	4.9560-12	3.2952-11	4.6224-10	1.0564-8	1.0035-7	3.3415-8
19	1.4913-16	1.2611-17	2.3185-15	1.4397-14	2.1573-13	2.2311-12	1.5698-11	1.1152-10	1.7574-9	2.9753-8	1.5766-7

v' \ v''	11	12	13	14	15	16	17	18
0	2.3708-11	1.3796-12	1.8967-15	3.5222-14	2.3863-14	6.3210-15	9.6737-16	3.9930-16
1	1.9354-9	2.2979-10	1.6432-11	1.6721-13	2.3236-13	2.6470-13	1.2565-13	3.9558-14
2	4.9872-8	8.9924-9	1.2024-9	1.0079-10	1.8714-12	9.4542-13	1.4015-12	7.7329-13
3	5.6173-7	1.5076-7	2.9989-8	4.4674-9	4.3417-10	1.2589-11	2.6695-12	5.6301-12
4	2.6449-6	1.2589-6	3.6981-7	8.0445-8	1.3197-8	1.4568-9	5.9369-11	4.8901-12
5	1.7379-6	4.7150-6	2.4485-6	7.8033.7	1.8425-7	3.3041-8	4.0870-9	2.1537-10
6	3.9798-5	2.5507-6	7.6392-6	4.2813-6	1.4686-6	3.7366-7	7.2716-8	9.9852-9
7	1.2888-3	5.1942-5	3.6035-6	1.1507-5	6.8882-6	2.5250-6	6.8800-7	1.4426-7
8	1.1547-2	1.4927-3	6-2763-5	4.9771-6	1.6372-5	1.0365-5	4.0329-6	1.1702-6
9	6.3851-2	1.1897-2	1.6550-3	7.0697-5	6.7820-6	2.2257-5	1.4766-5	6.0589-6
10	9.4241-2	6.5324-2	1.1789-2	1.7698-3	7.4419-5	9.1587-6	2.9156-5	2.0092-5
11	*6.0182-1*	7.3017-2	6.6901-2	1.1219-2	1.8378-3	7.3035-5	1.2267-5	3.7042-5
12	2.0364-1	*6.4973-1*	5.2081-2	6.9023-2	1.0193-2	1.8665-3	6.6211.5	1.6264-5
13	1.7251-2	1.6199-1	*6.9989-1*	3.2712-2	7.2174-2	8.7397-3	1.8703-3	5.4272-5
14	4.5529-3	3.0684-2	1.1585-1	*7.4661-1*	1.6465-2	7.6894-2	6.9182-3	1.8704-3
15	1.7949-3	3.0119-3	4.7252-2	6.9762-2	*7.8246-1*	5.0559-3	8.3795-2	4.8435-3
16	3.2687-5	2.7084-3	1.1808-3	6.4849-2	3.0153-2	*8.0255-1*	1.0652-4	9.3565-2
17	1.0625-5	1.5344-4	3.5662-3	3.0855-5	8.0129-2	4.8684-3	*7.9831-1*	2.7309-3
18	3.3728-6	4.7289-6	4.3919-4	4.0374-3	9.6578-4	8.8941-2	2.0586-3	*7.6317-1*
19	9.2888-9	6.2080-6	1.4683-7	9.5701-4	3.7760-3	5.4660-3	8.7368-2	2.8251-2

(Paper 68A1–254)

JOURNAL OF RESEARCH of the National Bureau of Standards—A. Physics and Chemistry
Vol. 68A, No. 1, January–February 1964

Infrared Absorption Spectrum of Nitrous Oxide (N_2O) From 1830 cm^{-1} to 2270 cm^{-1}*

Earle K. Plyler, Eugene D. Tidwell, and Arthur G. Maki

(August 9, 1963)

The frequencies of the vibration-rotation spectrum of N_2O have been measured from 1830 cm^{-1} to 2270 cm^{-1}. A number of weak bands have been measured and assigned to "hot bands" and isotopic species in normal abundance. By using the Ritz principle and previously measured bands the bending frequency (ν_2) is calculated as 588.78_0 cm^{-1}. Frequencies are given for lines arising from the three principal transitions found in this region.

1. Introduction

Recently there has been considerable interest in obtaining accurate values for the vibration-rotation potential constants for small molecules. Pliva [1] [1] has measured the spectra of various isotopic species of nitrous oxide (N_2O) in the hope of obtaining more data with which to check the anharmonic terms of a potential function which he has devised [2]. Tidwell, Plyler, and Benedict [3] have reported measurements on a large number of vibrational-energy levels for N_2O and have derived a set of vibration-rotation constants.

Rank et al. [4] have reported the results of some very precise measurements on five absorption bands of N_2O. McCubbin, Grosso, and Mangus [5] have made some further precise measurements on N_2O which will be reported soon. While this work was in progress Fraley, Brim, and Rao [6] published results of measurements on the strongest absorption lines due to N_2O in the 5-μ region. The latter measurements are in essential agreement with those reported here.

2. Experimental Procedure

The spectra were measured on the NBS high-resolution infrared spectrometer described elsewhere [7]. Most of the measurements were made using a 7,500 lines/in. grating although some measurements were obtained with a 1,860 lines/in. grating. A liquid-nitrogen cooled PbSe detector was used. Calibration was achieved by the combination of accurately measured rare-gas spectra and a Fabry-Perot interferometer fringe system in the manner described in reference 8.

Spectra were obtained with pathlengths of 1.2, 4, and 24 m and pressures ranging from 1 to 200 mm Hg. Representative spectra are shown in figures 1 and 2. The 1.2 m cell could be either cooled to 220 °K or warmed to 400 °K; representative spectra obtained at these temperature extremes are shown in figures 3 and 4. In these figures it is evident that many lines which are weak at low temperatures have intensified with increase in temperature. These lines must be attributed to transitions originating from excited vibrational states and accordingly have been assigned as "hot band" lines.

3. Analysis of Data

The microwave measurements of Burrus and Gordy [9] have given very precise values for the ground-state rotational constant, B_0, and the l-doubling constant, q, of the molecule $N^{14}N^{14}O^{16}$. Coles and Hughes [10] and Coles, Good, and Lide [11] have made further measurements from which one can obtain B_0 for the isotopes $N^{14}N^{15}O^{16}$, $N^{15}N^{14}O^{16}$, and $N^{14}N^{14}O^{18}$. Combining the results of these workers with the velocity of light (taken as 299,793 km/s) we have calculated these constants in wavenumbers as given in table 1. Since these molecular constants are more accurate than could be obtained from the measurements reported here, the values given in table 1 were used wherever applicable for the calculation of the other molecular constants. For this same purpose the value of $D_0=17.6\times10^{-8}$ cm^{-1} given by Rank et al. [4] was used.

TABLE 1. *Accurately known molecular constants used in the analysis of the N_2O bands between 4.4 and 5.5 μ*

$B_{000}=$	0.419010_8 cm^{-1}
$D_{000}=$	17.6×10^{-8} cm^{-1}
q	$=79.17\times10^{-5}$ cm^{-1}
$B_{010}=$	0.419572_7 cm^{-1} (average of c and d levels)
$B_{000}(N^{14}N^{15}O^{16})=$	0.418982_1 cm^{-1}
$B_{000}(N^{15}N^{14}O^{16})=$	0.404856_4 cm^{-1}
$B_{000}(N^{14}N^{14}O^{18})=$	0.39557_7 cm^{-1}

Since the data for many of the bands reported here was rather fragmentary due to the high degree of overlapping, all of the absorption bands were analyzed by obtaining a least-squares fit to the polynomial

$$\nu_{obs}=\nu_0+(B'+B'')m+(B'-B'')m^2 -2(D'+D'')m^3-(D'-D'')m^4$$

where the terms have their usual significance.

*This work was supported in part by the Geophysic Research Directorate, Air Force Cambridge Research Laboratories.

[1] Figures in brackets indicate the literature references at the end of this paper.

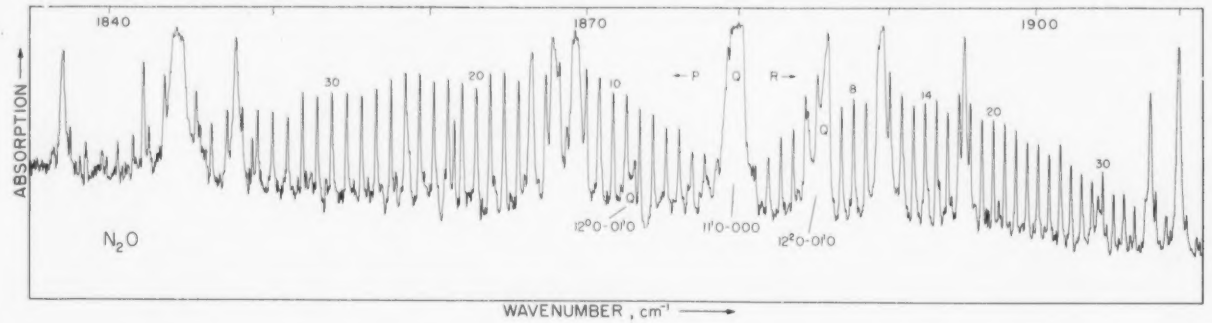

FIGURE 1. N_2O *absorption from 1840 to 1910* cm^{-1}.

Pathlength 1.2 m; pressure 28 cm Hg.

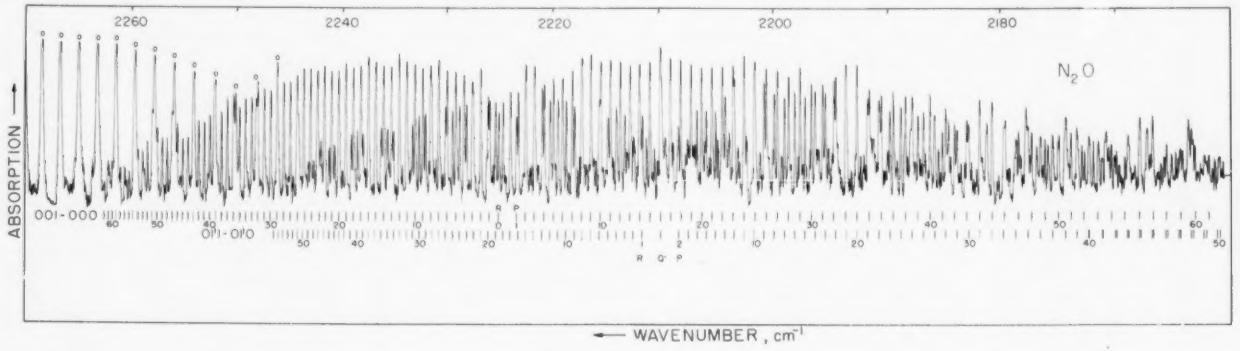

FIGURE 2. N_2O *absorption from 2270 to 2160* cm^{-1}.

Pathlength 4 m; pressure 1 mm Hg. Circle: indicates absorption lines due to atmospheric $C^{13}O_2^{16}$ in the optical path.

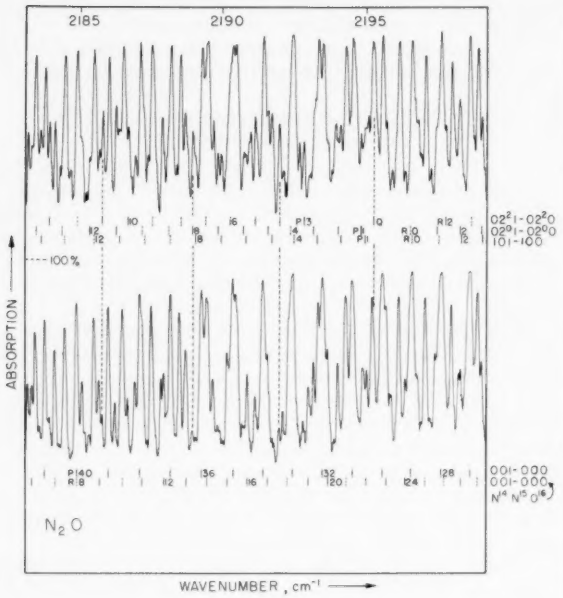

FIGURE 3. N_2O *absorption from 2184 to 2200* cm^{-1}.

Upper curve is for a temperature of 400 °K and lower curve is with cell cooled to about 220 °K. Pathlength is 1.2 m; pressure 1 mm Hg.

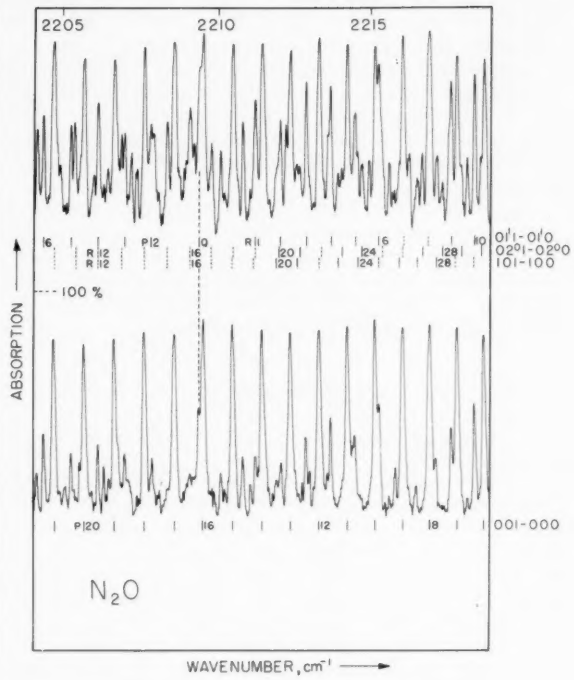

FIGURE 4. N_2O *absorption from 2204 to 2220* cm^{-1}.

Temperature of gas in upper curve is 400 °K, temperature of gas in lower curve is 220 °K. Pathlength is 1.2 m; pressure is 2 mm Hg.

TABLE 2. *Vibration-rotation constants describing the absorption bands of* N_2O *in the 2000* cm^{-1} *Region*

The limits of error given are standard deviations

Isotopic species	Assignment	ν_0	$\Delta B \times 10^{+5}$ cm^{-1}	$*D' \times 10^8$	$*D'' \times 10^8$	$\Delta D \times 10^{+8}$
$N^{14}N^{14}O^{16}$	12^00-01^1c0	1873. $20_6 \pm 0.009$	$-9_3 ** \pm 3$	23. 8	17. 6	
	$11^1c0-000$	1880. $271 \pm .003$	$-154._6 \pm 0.7$	17. 6	17. 6	-0.2 ± 0.3
	12^2c0-01^1c0	1886. $03_3 \pm .009$	$-9_6 \pm 3$	13. 1	17. 6	
	12^2d0-01^1d0			17. 6		
	$200-01^1c0$	1974. $571 \pm .003$	$-397._5 \pm 1.0$	16. 1	17. 6	-2.3 ± 0.6
	$200-01^1d0$					
	21^10-02^20	1988. $2 \pm .3$ — Q branch position				
	21^1d0-02^20	1997. $6_5 \pm .15$ — Q branch position				
	02^2c1-02^2c0	2195. $40_6 \pm .006$	$-340._3 \pm 1.2$	11. 6	11. 6	
	02^2d1-02^2d0			17. 6	17. 6	
	02^01-02^00	2195. $84_9 \pm .025$	-336 ± 2	23. 6	23. 6	0 ± 1.4
	101–100	2195. $9_3 \pm .04$	$-35_2 \pm 5$	17. 0	17. 4	
	01^11-01^10	2209. $52_7 \pm .004$	$-340._3 \pm 0.9$	17. 6	17. 6	0.4 ± 0.3
	001–000	2223. $76_4 \pm .003$	-345.6 ± 0.3	17. 4	17. 6	-0.26 ± 0.05
$N^{14}N^{15}O^{16}$	01^11-01^10	2164. $13 \pm .03$	$-31_5 \pm 15$	17. 5	17. 5	
$N^{14}N^{15}O^{16}$	001–000	2177. 659	$-33_0 \pm 3$	17. 5	17. 5	
$N^{15}N^{14}O^{16}$	001–000	2201. $60_4 \pm .015$	$-33_7 \pm 3$	16. 5	16. 5	
$N^{14}N^{14}O^{18}$	001–000	2219. $67_8 \pm .02$	$-41_1 \pm 10$	16. 5	16. 5	

*In all cases the values of D given were assumed in order to obtain the best possible values of ν_0, ΔB, and ΔD.
**This ΔB value is from the average of the c and d levels of the lower state.

The data were also analyzed using the method of combinations and differences. The results of both methods were comparable, but in many cases the fact that more lines could be used in fitting to the polynomial given above resulted in a reduction in the uncertainty of the various unknown constants when this method was used, especially since the lower state constants were in most cases very accurately known.

For those bands which are split into resolved c and d components the two bands were analyzed simultaneously to obtain a least-squares fit to the same band center and other constants were made compatible. A more detailed description is given for the individual bands in the next section.

4. Results

4.1. The Region From 1830 to 1925 cm^{-1}

In this region lines have been identified due to the three transitions 12^00–01^1c0, 12^20–01^10, and 11^1c0–000. For all these perpendicular bands the Q branches were observed, but the resolution was not good enough to measure any individual Q branch lines. The splitting of the $\Delta-\Pi$ band was observed for all but a few low J lines. The analysis of this $\Delta-\Pi$ band was carried out by analyzing the c and d components simultaneously. Since the data were quite fragmentary for these weak "hot bands," the best available estimates of the values of B_c'', B_d'', D'', D_c', and D_d' were used in order to obtain more accurate values of ν_0 and B'. For this purpose it was assumed that $B_c'=B_d'$. Since the c and d levels of the 12^20 state undergo l-type resonance with different levels, it was necessary to use different values of D for the c and d levels. The values of the constants used are given in table 2. Only the c component of the $\nu_1+\nu_2$ band was measured, therefore the value obtained for ΔB as given in table 2 is for the transition to the c level only.

The calculated and observed frequencies of absorption lines due to the transition 11^1c0–000 are given in table 3. Figure 1 shows the appearance of the absorption in this region.

4.2. Absorption Lines in the Region 1925 to 2000 cm^{-1}

The main band found in this region is a Σ–Π band due to the transition 200–01^10. In this case the Q branch was sufficiently well resolved so that measurements were obtained for both the c and d levels. Since microwave values for the lower state are quite good, these values were used in the analysis and transitions from both the c and d levels were analyzed simultaneously by a least-squares program in order to obtain the best values for ν_0 and B'.

Absorption in this region was very weak as might be expected from the transitions involved. The Q branches for the two "hot bands" 21^10–02^20 and 21^10–02^00 were also observed in this wavelength region, but they were not resolved. Nor were any lines of the P and R branches observed.

The calculated and observed frequencies of the lines for the 200–01^10 transition are given in table 3.

4.3. $N^{14}N^{14}O^{16}$ Absorption Between 2130 and 2270 cm^{-1}

The fundamental ν_3 and associated "hot bands" are located in this region. ν_3 is a rather strong absorption band, consequently with the pathlength and resolution available it was possible to obtain measurements on four "hot bands" and four isotopic bands.

The splitting of the first "hot band" was observed for high-J levels but overlapping with various other bands was rather severe. For this reason it was felt that more accurate band constants could be obtained by averaging the frequencies of the c and d components. Even though this procedure did not permit the use of measurements where only one component was observed, the resultant constants are believed to be more reliable than those found by analyzing each band individually.

Lines due to the $\Delta-\Delta$ transition 02^21–02^20 have been observed and the position of the Q, while overlapped, has been verified by observations at 220 °K and 400 °K. Figure 3 shows a few lines due to this transition and the manner in which the line intensities change with temperature. The Boltzman distribution predicts this transition will show an approximate six-fold increase in intensity in going from 220 °K to 400 °K.

Since the two $\Sigma-\Sigma$ transitions 101–100 and 02^01–02^00 are predicted to lie quite close to each other, some difficulty was anticipated in assigning the two series of lines which must be due to these transitions. The assignments of these lines are, however, considered to be reliable due to the rather large differences in the lower-state B values. Δ_2F'' plots for these two bands yield respective B'' values of 0.4175 and 0.4200 cm^{-1}. The B'' values expected from the data of reference 3 are 0.41725 and 0.41991, respectively. Many of the low-J lines are badly overlapped because the two band centers lie so close together. As a consequence the band centers calculated from the data may be in error by several hundredths of a wavenumber. The statistical treatment of the data resulted in a standard deviation for the ν_o values of 0.01 cm^{-1}, but inspection of the data leads us to believe that this is not a realistic number. Therefore table 2 contains a more subjective evaluation of the accuracy of the band centers for these two bands.

Table 4 lists the frequencies of the ν_3 band as observed in this laboratory and as reported by Fraley, Brim, and Rao. Columns 3 and 6 compare the calculated frequencies with those observed.

4.4. Isotopic Absorption Bands From 2100 to 2240 cm^{-1}

Within this region absorption bands due to N_2O molecules containing N^{15} or O^{18} are expected. Lines

TABLE 3. *Observed and calculated wavenumbers for the two strongest N_2O absorption bands between 1830 and 2000 cm^{-1}*

J''	11^{1c} 0–000				$200–01^{1c}$ 0				$200–01^{1d}$ 0	
	P		R		P		R		Q	
	Obs.	Calc.	Obs.	Calc.	Obs.	Calc.	Obs.	Calc.	Obs.	Calc.
0			1881. 095	. 106						
1			81. 929	. 937			[b] 1976. 222	. 227		
2	[b] 1878. 595	. 591	82. 751	. 766						
3	[b] 77. 766	. 747	83. 600	. 592			[b] 77. 832	. 853		
4	76. 894	. 900					[b] 78. 643	. 656		
5	76. 041	. 050								
6	75. 185	. 196					[b] 80. 253	. 239		
7			86. 865	. 863			81. 016	. 020		
8	[b] 73. 472	. 480					81. 790	. 794		
9					[b] 1966. 764	. 769	82. 559	. 561		
10					[b] 65. 880	. 867	83. 317	. 320		
11					64. 952	. 957	84. 081	. 073	1973. 995	. 995
12			[b] 90. 861	. 882	64. 034	. 040	84. 821	. 818		
13			[b] 91. 684	. 677	63. 127	. 117	85. 553	. 556	73. 784	. 777
14			[b] 92. 488	. 468	62. 181	. 186	86. 287	. 287	73. 636	. 655
15			93. 253	. 256			87. 030	. 010	73. 543	. 524
16			94. 054	. 041	60. 302	. 303	87. 723	. 727	73. 400	. 384
17	[b] 65. 590	. 607	[b] 94. 850	. 823	59. 351	. 351			73. 218	. 236
18	[b] 64. 720	. 717	[b] 95. 585	. 601	58. 399	. 392	89. 127	. 139	73. 088	. 079
19	[b] 63. 844	. 824			57. 422	. 426	89. 833	. 834	72. 920	. 914
20	[b] 62. 958	. 928	97. 150	. 149	56. 448	. 453	90. 521	. 522	72. 754	. 740
21			97. 910	. 918	55. 465	. 473			72. 560	. 557
22	61. 130	. 128	98. 674	. 684	54. 494	. 489			72. 381	. 366
23	60. 210	. 223	1899. 436	. 447	53. 490	. 493			72. 160	. 166
24	59. 315	. 315	[b] 1900. 190	. 207	52. 487	. 492	93. 222	. 202	[b] 71. 986	. 957
25			00. 964	. 963	51. 481	. 484	93. 859	. 855	71. 746	. 740
26	57. 496	. 491	01. 715	. 716	50. 469	. 470	94. 496	. 500	71. 518	. 514
27	56. 576	. 574	[b] 02. 493	. 466	[b] 49. 440	. 449	95. 138	. 138	[b] 71. 258	. 280
28	55. 662	. 654	03. 221	. 213	48. 423	. 420	95. 777	. 770	[b] 71. 032	. 037
29	54. 739	. 732	03. 960	. 957	47. 383	. 386	96. 389	. 394	70. 787	. 786
30	53. 808	. 806	04. 689	. 697					70. 518	. 526
31	52. 884	. 877	05. 425	. 435			[b] 97. 600	. 621	[b] 70. 270	. 258
32	51. 950	. 946	06. 154	. 169	44. 234	. 240	[b] 1998. 197	. 224	69. 987	. 981
33	51. 012	. 012	06. 883	. 900	[b] 43. 171	. 178			1969. 700	. 696
34	50. 062	. 074	[b] 07. 617	. 627						
35	49. 125	. 134	08. 348	. 352	41. 034	. 033				
36			09. 070	. 073	39. 938	. 951				
37	[b] 47. 256	. 245			38. 880	. 862				
38	[b] 46. 266	. 296	10. 517	. 506	[b] 37. 783	. 767				
39			11. 220	. 217	36. 680	. 665				
40			11. 931	. 926	35. 542	. 556				
41			12. 626	. 631	1934. 443	. 441				
42	[b] 42. 475	. 472	13. 345	. 333						
43	41. 518	. 509	14. 024	. 032						
44	40. 544	. 543	[b] 14. 720	. 727						
45	[b] 39. 591	. 574	1915. 421	. 420						
46	38. 604	. 602								
47										
48	36. 662	. 650								
49	35. 672	. 670								
50	34. 696	. 687								
51	33. 700	. 701								
52	32. 712	. 712								
53	[b] 1831. 720	. 721								

[b] Blended or weak lines.

TABLE 4. *Wavenumbers of absorption lines for the ν_1 band of N_2O*

J	P Branch			R Branch		
	Observed wavenumber NBS	Calc. NBS	Observed wavenumber ref. 6	Observed wavenumber NBS	Calc. NBS	Observed wavenumber ref. 6
0				2224. 59_3	2224. 59_5	2224. 59_4
1	[b] 2222. 90_0	2222. 92_6	2222. 94_0	[b] 25. 41_2	25. 41_9	25. 43_0
2	[b] 22. 06_5	22. 08_1	22. 08_5	[b] 26. 23_7	26. 23_6	26. 24_3
3	[b] 21. 25_3	21. 22_9	21. 27_3	[b]		27. 05_0
4	20. 36_1	20. 37_0	20. 38_2	27. 84_7	27. 85_0	27. 84_8
5	19. 51_4	19. 50_5	19. 51_6	28. 65_0	28. 64_7	28. 63_9
6	18. 63_8	18. 63_2	18. 64_1	[b] 29. 45_9	29. 43_6	29. 45_0
7	17. 74_5	17. 75_3	17. 75_6	[b] 30. 22_4	30. 21_9	30. 21_8
8	[b] 16. 83_3	16. 86_7	16. 84_0	[b] 30. 97_5	30. 99_5	30. 97_5
9	[b] 15. 97_5	15. 97_3	15. 98_3	31. 78_4	31. 76_3	31. 74_1
10	[b] 15. 10_9	15. 07_3	15. 08_8	32. 54_3	32. 52_5	32. 54_8
11	14. 17_5	14. 16_6	14. 17_3	[b]		33. 30_1
12	13. 24_4	13. 25_3	13. 26_9	[b] 34. 02_4	34. 02_8	34. 02_3
13	12. 30_4	12. 33_2	12. 33_0	34. 78_4	34. 76_9	34. 80_6
14	11. 40_4	11. 40_5	11. 42_0	35. 52_6	35. 50_3	35. 50_9
15	[b] 10. 46_9	10. 47_0	10. 47_8	[b] 36. 25_3	36. 22_9	36. 24_6
16	[b]		09. 52_3	[b] 36. 94_2	36. 95_0	36. 94_5
17	[b] 08. 58_2	08. 58_1	08. 59_0	[b] 37. 67_0	37. 66_3	37. 66_3
18	09. 62_5	07. 62_6	07. 62_2	38. 36_4	38. 36_9	38. 36_8
19	06. 66_9	06. 66_5	06. 66_8	[b] 39. 07_6	39. 06_8	39. 07_6
20	05. 68_1	05. 69_6	05. 68_7	[b] 39. 72_8	39. 76_0	39. 76_1
21	04. 71_9	04. 72_1	04. 71_7	40. 45_4	40. 44_3	40. 44_4
22	[b] 03. 73_7	03. 73_9	03. 73_5	41. 13_4	41. 12_3	41. 13_0
23	[b] 02. 73_6	02. 75_9	02. 74_1	41. 78_0	41. 79_4	41. 80_5
24	[b] 2201. 74_7	2201. 75_4	01. 75_2	42. 46_6	42. 45_8	42. 44_3
25			2200. 77_2	43. 12_2	43. 11_5	43. 12_0
26	2199. 72_0	2199. 74_2	2199. 73_5	43. 75_9	43. 76_5	43. 77_3
27	98. 72_6	98. 72_6	98. 73_5	44. 42_4	44. 40_9	44. 41_6
28	97. 70_7	97. 70_4	97. 69_6	45. 04_3	45. 04_5	45. 04_9
29	96. 67_7	96. 67_4	96. 66_7	[b] 45. 66_8	45. 67_4	45. 68_8
30	95. 64_5	95. 63_8	95. 63_1			46. 28_9
31	94. 60_0	94. 59_4	94. 60_2	46. 89_5	46. 91_1	46. 91_8
32	[b] 93. 52_6	93. 54_5	93. 52_8	47. 53_1	47. 51_9	47. 50_9
33	[b]		92. 42_8	48. 11_4	48. 12_0	48. 11_9
34	[b] 91. 43_2	91. 42_5	91. 43_3	48. 71_2	48. 71_4	48. 71_4
35	[b] 90. 34_5	90. 35_5	90. 34_9	49. 30_4	49. 30_1	49. 32_8
36	89. 26_4	89. 27_8	89. 28_0	49. 88_7	49. 88_1	49. 88_9
37	88. 18_4	88. 19_4	88. 18_9	50. 46_0	50. 45_4	50. 44_9
38	87. 13_1	87. 10_4	87. 10_6	51. 03_3	51. 02_9	51. 04_7
39	86. 00_2	86. 00_7	86. 00_4	[b]		
40	84. 91_1	84. 90_3	84. 89_0	52. 14_5	52. 13_1	52. 14_8
41	83. 79_4	83. 79_3	83. 79_0	52. 68_2	52. 67_6	52. 68_5
42	82. 66_6	82. 67_6	82. 66_7	53. 20_9	53. 21_4	53. 21_6
43	[b] 81. 56_9	81. 55_2	81. 54_5	[b]		
44	[b]		80. 38_0	54. 23_6	54. 26_8	54. 25_3
45	[b] 79. 30_3	79. 28_5	79. 29_3	54. 79_6	54. 78_5	2254. 79_9
46	[b]		78. 14_2	55. 31_8	55. 29_5	
47	76. 98_2	76. 99_1	76. 98_3	55. 79_6	55. 79_7	
48	75. 84_0	75. 83_4	75. 83_8	56. 28_7	56. 29_3	
49	74. 67_4	74. 67_0	74. 67_2	56. 76_2	56. 78_1	
50	73. 49_7	73. 50_0	73. 48_8	[b] 57. 30_0	57. 26_3	
51			72. 32_4	[b] 57. 70_7	57. 73_7	
52	71. 14_4	71. 13_9	71. 13_4	58. 21_2	58. 20_5	
53	[b] 69. 89_8		69. 89_1	58. 66_4	58. 66_5	
54	68. 75_1	68. 75_2	68. 75_9	59. 13_1	59. 11_9	

See note at end of table.

TABLE 4. *Wavenumbers of absorption lines for the ν_1 band of* N_2O—Continued

J	P Branch			R Branch		
	Observed wavenumber NBS	Calc. NBS	Observed wavenumber ref. 6	Observed wavenumber NBS	Calc. NBS	Observed wavenumber ref. 6
55	67.53$_6$	67.54$_9$	2167.57$_9$	[b]		
56	[b] 66.31$_8$	66.33$_9$		60.00$_1$	60.00$_4$	
57	[b]			60.41$_9$	60.43$_8$	
58	63.92$_6$	63.90$_0$		60.88$_2$	60.86$_2$	
59	62.69$_0$	62.67$_0$		[b] 61.28	61.28$_0$	
60	61.41$_8$	61.43$_4$		61.67$_5$	61.69$_1$	
61	60.21$_0$	60.19$_1$		62.08$_2$	62.09$_5$	
62	58.97$_9$			62.48$_9$	62.49$_2$	
63	57.69$_3$	57.68$_6$		[b]		
64	56.42$_2$	56.42$_4$				
65	55.16$_8$	55.15$_3$		63.63$_6$	63.64$_0$	
66	53.88$_3$	53.88$_0$		64.02$_0$	64.00$_9$	
67				64.36$_2$	64.37$_1$	
68	51.29$_5$	51.31$_5$		64.74$_1$	64.72$_5$	
69	[b] 49.97$_6$	50.01$_5$		[b]		
70	48.74$_0$	48.71$_4$		65.42$_9$	65.41$_4$	
71	47.36$_9$	47.40$_6$		[b]		
72	46.09$_7$	46.09$_7$		[b] 66.08	66.07$_4$	
73	44.73$_6$	44.77$_1$		[b] 66.40	66.39$_3$	
74	[b] 43.46	43.44$_4$		[b] 66.71$_3$	66.70$_5$	
75	[b]			[b]		
76	[b]			[b]		
77	[b] 39.43$_8$	39.42$_4$		[b] 2267.61$_2$	2267.60$_0$	
78	[b] 2138.08$_6$	2138.07$_2$				

[b] Blended or weak lines.

due to four transitions in such isotopically substituted molecules have been identified in this study.

The band at 2201.60 cm^{-1} due to $N^{15}N^{14}O^{16}$ has been previously measured by Pliva [1] but bands due to the molecules $N^{14}N^{15}O^{16}$ and $N^{14}N^{14}O^{18}$ found at 2164.13, 2177.66, and 2219.67 cm^{-1} have not been previously reported. The assignments for these latter three bands have been confirmed by determination of the values of B'' from the Δ_2F'' plots. In the case of the $\Pi-\Pi$ transition at 2164.13 cm^{-1} the sharp Q branch seems to be observable at 2164.128 cm^{-1}, thus providing greater confidence in the position of the band center. Since many of the lines for these isotopic molecules were weaker than or of comparable intensity with the "hot bands" of the most abundant molecule, the identification of the lines was greatly aided by spectra obtained at 220 °K. At this temperature the intensity of the "hot band" lines is very greatly diminished. This leaves the isotopic lines as the most outstanding of the weak lines at low temperatures.

4.5. Discussion of Results

By means of the Ritz principle the position of some of the low-lying vibrational levels may be obtained. The bending vibration, ν_2, may be obtained in four different ways. Using the precise measurements of reference 4 and the recent measurements of reference 5, we find

$$\nu_2^1=(12^00-000)-(12^00-01^10)$$
$$=2461.998-1873.206=588.792\ cm^{-1}$$
$$\nu_2^1=(200-000)-(200-01^10)$$
$$=2563.341-1974.571=588.770\ cm^{-1}$$
$$\nu_2^1=(11^10-000)-(11^10-01^10)$$
$$=1880.271-1291.496=588.775\ cm^{-1}$$

Taking the average of the values given for the 01^11-000 transition in references 1 and 3, one obtains

$$\nu_2^1=(01^11-000)-(01^11-01^10)$$
$$=2798.308-2209.527=588.781\ cm^{-1}.$$

TABLE 5. *Comparison of the results of measurements on N_2O in different laboratories*

	001–000		$01^11–01^10$		001–000 $N^{15}N^{14}O^{16}$	
	ν_0	$\Delta B\times10^5$	ν_0	$\Delta B\times10^5$	ν_0	$\Delta B\times10^5$
NBS (this work)	2223. 764	−345. 6	2209. 527	−340. 3	2201. 604	−337
Pliva (ref. 1)	2223. 754	−344. 7	2209. 521	−341. 2	2201. 605	−336. 0
Fraley, Brim, and Rao (ref. 6)	2223. 759	−344. 6	2209. 535			

The average of these four indirect determinations, 588.780 cm^{-1}, compares very favorably with the indirect measurement of Pliva [1] (588.767 cm^{-1}), the four indirect measurements of Tidwell et al. [3] (588.773 cm^{-1}), and the direct measurement of Lakshmi, Rao, and Nielsen [12] (588.78 cm^{-1}).

The Ritz principle may also be applied to determine the values of $2\nu_2^0$, $2\nu_2^2$, and ν_1 as follows:

$$2\nu_2^2=(02^21–000)-(02^21–02^20)$$
$$=3373.184-2195.406=1177.778\ cm^{-1}$$
$$2\nu_2^0=(02^01–000)-(02^01–02^00)$$
$$=3363.997-2195.85\ =1168.15\ cm^{-1}$$
$$\nu_1=(101–000)\ -(101–100)$$
$$=3480.854-2195.93\ =1284.92\ cm^{-1}$$

where the values for the vibration levels given by Pliva [1] and Tidwell et al. [3] are used. By using similar combinations Tidwell et al., have previously determined $2\nu_2^2=1177.78$ cm^{-1}. McCubbin et al. [5] have recently measured $2\nu_2^0$ and ν_1 at 1168.13_4 and 1284.90_7 cm^{-1}, respectively. These were direct measurements and should be more accurate than the indirectly obtained values given above.

The band centers for the transitions 001–000 and $01^11–01^10$ have now been measured quite carefully in three different laboratories. Some idea of the absolute accuracy of these measurements may be obtained by comparing the constants derived from the measurements. We may also compare the measurements of ν_3 for the $N^{15}N^{14}O^{16}$ molecule with those reported by Pliva [1]. Table 5 shows how closely these independent measurements agree. Although it is seen that Pliva and Fraley et al., agree on a slightly larger value for B_{001} than has been reported in this work, nevertheless it is felt that the values given here are probably more accurate. The present measurements extend to considerably higher values of J than previous measurements and as a consequence a more accurate determination of ΔB and ΔD is expected. On the other hand Fraley, Brim, and Rao probably have a more accurate value for ν_0 since their resolution was slightly better so that blending of low-J lines would have less tendency to cause errors in the derived ν_0. Since Pliva worked with an isotopically enriched sample, it is to be expected that his constants for $N^{15}N^{14}O^{16}$ are better than those reported here.

An attempt was made to compare the results of this work with the constants given by Tidwell et al., but, as noted by Pliva [1], the agreement is not entirely satisfactory. Perhaps the measurements given here will be of value in determining the accuracy of the revised constants which Pliva is calculating.

5. References

[1] Josef Pliva, International Symposium on Molecular Structure and Spectroscopy, Sept. 1962, Tokyo, Japan.
[2] Josef Pliva, Collection Czech. Chem. Communs. **23,** 777 (1958).
[3] E. D. Tidwell, E. K. Plyler, and W. S. Benedict, J. Opt. Soc. Am. **50,** 1243 (1960).
[4] D. H. Rank, D. P. Eastman, B. S. Rao, and T. A. Wiggins, J. Opt. Soc. Am. **51,** 929 (1961).
[5] T. K. McCubbin, R. Grosso, and J. Mangus, to be published.
[6] P. E. Fraley, W. W. Brim, and K. N. Rao, J. Mol. Spect. **9,** 487 (1962).
[7] E. K. Plyler and L. R. Blaine, J. Res. NBS **62,** (Phys. and Chem.) No. 1,7 (1959).
[8] E. K. Plyler, L. R. Blaine, and E. D. Tidwell, J. Res. NBS **55,** 279 (1955) RP2630.
[9] C. A. Burrus and W. Gordy, Phys. Rev. **101,** 599 (1956).
[10] D. K. Coles and R. H. Hughes, Phys. Rev. **76,** 178A (1949).
[11] P. Kislink and C. H. Townes, NBS Circ. 518 (1952).
[12] K. Lakshmi, K. N. Rao, and H. H. Nielsen, J. Chem. Phys. **24,** 811 (1956).

(Paper 68A1–255)

JOURNAL OF RESEARCH of the National Bureau of Standards—A. Physics and Chemistry
Vol. 68A, No. 1, January–February 1964

An Absolute Light Scattering Photometer: II. Direct Determination of Scattered Light From Solutions

Donald McIntyre

(August 9, 1963)

The light scattering photometer recently described in this journal by McIntyre and Doderer has been examined to determine its ability to measure the absolute scattering of liquids. The absolute scattering of polymer solutions was determined from transmission measurements and from two different transverse measurements. The experimental results are in good agreement. The variables of the photometric system were also analyzed and experimentally studied to determine its ability to measure absolute scattering of liquids under different geometrical arrangements.

1. Introduction

For the determination of the molecular weight of a solute by light scattering, the proportion of incident light that is dissipated as molecular scattering must be measured. This scattered light may be determined in either of two ways. First, the amount of light scattered at a given angle with respect to the incident beam of light may be experimentally determined when a given volume of illuminated solution is seen by a detector that has a well-defined angular acceptance. This method obviously requires that either a great number of dimensional details and optical constants be known or a comparison standard be available. Second, the amount of light scattered over all angles may be determined. The total scattered light may be determined by using an integrating sphere or by measuring the loss of light that occurs in the passage of a light beam through a given path of solution. The latter method of measuring total scattering requires that very precise transmission measurements be made, that extreme care be employed to eliminate secondary scattering in the experimental setup, and that materials be chosen that remove energy from the light beam only by molecular scattering and not by absorption or fluorescence. A molecular theory of light scattering is needed to relate the first experimental method, which measures the light scattered from a solution at a given angle, to the second method, which measures the total amount of light scattered at all angles.

The theories of Rayleigh [1, 2,][1] which apply to small isotropic particles, state that the intensity of scattering is proportional to the quantity $(1+\cos^2\theta)$ when the incident light is unpolarized and θ is the angle measured from the direction of the incident beam to the direction of observation. The radiant intensity of scattered light, J_θ, in the direction θ, from a volume, V, that is illuminated by an incident beam of irradiance H_0, can be described by a parameter called Rayleigh's ratio, R_θ, as shown in eq (1).

$$R_\theta=(J_\theta/H_0V). \tag{1}$$

If now the scattering is summed up over all angles, the fractional decrease in the flux of the incident light for a small length, dl, of solution can be calculated and is known as the turbidity, τ. It is usually expressed in the integrated form shown in eq (2). In those cases where the above angular function $(1+\cos^2\theta)$ applies, the integration of the scattering over all angles yields a simple relation between Rayleigh's ratio and the turbidity as shown in eq (3).

$$\tau=\frac{1}{l}\ln\frac{J}{J_0} \tag{2}$$

$$\tau=(16\pi/3)R_{90}. \tag{3}$$

By measuring both Rayleigh's ratio at 90° and turbidity of a solution of isotropic particles, a light scattering photometer can be tested for self-consistency solely on the basis of optical determinations.

The work of Carr and Zimm [3] on the absolute scattering of liquids is based upon this approach. Doty and Steiner [4], in a study aimed at using spectrophotometric techniques for determining molecular weights, made a similar though less complete comparison. In spite of these efforts there still is an uncertainty about the absolute values of scattering from pure liquids [5]. The present work does not attempt to answer this molecular problem of liquids because it is not necessary for the ultimate use of this absolute photometer in molecular weight determinations. This work attempts to assess the reliability of the light scattering photometer, described earlier [6] for the determination of absolute scattering from solutions by comparing results from various optical measurements.

In addition to the direct optical methods of checking the consistency of a light scattering photometer, there are also indirect ways which use molecular

[1] Figures in brackets indicate the literature references at the end of this paper.

theories to relate either the scattering of pure liquids to Avogadro's number, or the scattering of solutions to the known molecular weight of the solute. Both of these indirect measurements have been carried out with this photometer although the results are not given at this time because greater care must be given to the preparation of "pure" liquids. A comparison of the molecular weights of polystyrene fractions determined by equilibrium ultracentrifugation and by light scattering will be published later.

2. Photometric Analysis

2.1. General Discussion

a. Definitions

If a source of radiant energy is designated 1, and a point in space from which the flux is measured is designated 2, then the following photometric quantities may be defined in terms of the area A, solid angle $d\Omega$, and the angle α between the normal to the surface and the direction of irradiation:

radiant flux, P
radiant intensity, $J=dP/d\Omega$, flux per unit solid angle.
radiance, $N=dJ/dA\cos\alpha$, intensity of the area dA projected perpendicularly to the direction θ.
irradiance, $H=dP/dA_2$, flux incident on the small area dA_2.
radiant emittance, $W=dP/dA_1$, flux from the element of the surface dA_1.

The incident irradiance from the lamp to a secondary source is referred to as H_0. All other quantities without subscripts refer to the secondary source. Unfortunately two secondary sources need to be considered, a diffuser and a scattering solution, and accepted convention makes it necessary to talk about the directions from the source to the detector in different ways. For a plane diffuser the angle θ is measured from the normal to the surface of the diffuser. For a scattering solution the angle θ is measured from the forward direction of the beam.

b. Diffuser

Diffusing plates of magnesium oxide or magnesium carbonate are used frequently as attenuators in light scattering calibrations to provide a known fraction of the incident radiant flux. Since only the total diffuse reflectance has been determined for these diffusers, it is necessary to know that the particular diffuser used in the light scattering experiments redistributes the flux so that the radiance is equal in all directions. If this is true, it follows that the radiant intensity from the diffuser obeys Lambert's law (as stated in eq (4)) and that the radiant emittance may be described in terms of the radiance by eq (4a).

$$J_\theta=J_0\cos\theta \tag{4}$$

$$W=\pi N. \tag{4a}$$

In order to relate the radiance of the diffuser to the incident irradiance additional experiments are necessary. Several workers [7, 8, 9] have shown that magnesium oxide and magnesium carbonate are not perfect diffusers because they do not diffusedly scatter all of the incident radiant flux. However, they are almost perfect in the visible region where they have a reflectance very close to unity. The incident irradiance, H_0, on an ideal diffuser but imperfect reflector may be expressed as

$$r_f H_0\cos\alpha=\pi N, \tag{5}$$

where α is the angle between the direction of the incident beam and the normal to the diffuser surface and r_f is the reflection factor.

c. Photometric Detection

The radiation detectors commonly used in light scattering measurements are photomultiplier tubes. These detectors usually do not have uniform sensitivity over the photosensitive surface, and for this reason they will not respond properly to the irradiance from two different sources unless the geometry of viewing is identical for the two sources. In any determination of absolute scattering where measurement of the ratio of irradiances from two different types of secondary sources, it is necessary to ensure that the flux density is uniform over the irradiated area.

d. Rayleigh's Ratio

The scattering function, termed Rayleigh's ratio, is easily defined in terms of the small volume of scattering material, V, the distance of the detector from the scatterer, r, and the photometric quantities. Thus Rayleigh's ratio may be written in the form of eq (1) or its equivalent forms in eq (1a).

$$R_\theta=(H_\theta r^2)/(H_0V)=N_\theta A_1\cos\theta/(H_0V). \tag{1a}$$

Since the scattering volume can easily be arranged to be equal to the product of the area of the field stop and the width of the incident light beam w, and since the same field stop can be used for the measurement of the incident irradiance, the ratio may also be written as in eq (6).

$$R_\theta=N_\theta\cos\theta/H_0w. \tag{6}$$

The Rayleigh's ratio for a given isotropic material is generally considered to be the value at 90° to the incident beam where the cosine term becomes unity. Therefore, only the ratios, N_θ/H_0w, needs to be determined. To make this measurement accurately, the detector should be irradiated with nearly equal flux density from both incident and scattered beams. This may be accomplished by attenuation by absorption with calibrated filters, called in this work the direct method, or by attenuation by redistribution of the incident flux with a diffuser, referred to as the diffuser method.

To visualize more easily the different dimensions that are associated with the determination of the absolute scattering, figure 1 is drawn with the detector viewing a scattering solution at 90°. The image S_1' of the field stop S_1 at the center of the scattering volume has the dimensions $w'h'$. The incident beam of irradiance H_0 has the area w_0, h_0, and thus defines a scattering volume for the detector of $w_0\, w'h'$.

2.2. Diffuser Method

In this case, the diffuser is substituted for the scattering volume shown in figure 1 so that the detector can measure the irradiance from source H_0. Equation (5) may be substituted into eq (1a) when the detector is viewing the diffuser at 90° to give eq (7).

$$R_{90}=(N_{90}/N_{\mathrm{diff}})(r_f \cos \alpha/\pi)(A_{\mathrm{diff}}/V). \qquad (7)$$

In this method only the radiance of the scatterer and diffuser need to be measured.

Since the area of the field stop that is used for the diffuser measurements is also known, Rayleigh's ratio may be written as in eq (8).

$$R_{90}=(r_f \cos \alpha/\pi)(J_{90}/J_{\mathrm{diff}})(A_{\mathrm{diff}}/V). \qquad (8)$$

In the special case where the radiation incident on the diffuser has a projected area equal to the field stop in the diffuser measurement, Rayleigh's ratio can very simply be written as eq (8a).

$$R_{90}=(r_f \cos \alpha/\pi)(J_{90}/J_{\mathrm{diff}})(1/w). \qquad (8a)$$

For this case, the width of the field stop is the only geometrical factor that needs to be evaluated.

This experimental arrangement has been used frequently because the quantity w' is the only dimensional measurement needed, and it can easily be determined by placing a real stop just in front of the scattering volume. However, two additional factors must then be examined. If the field stop is changed between the measurement of the diffuser and scatterer, then a simple relation between the radiant intensities and phototube responses may not be valid. Even if the limiting area in front of the phototube is maintained by a second lens that magnifies the image of the scatterer or diffuser, it must be known that the aperture stop of the second system is not changing simultaneously. Otherwise, the solid angle of acceptance changes and does not allow eq (8a) to be used without modification.

It seems preferable, therefore, to determine the uniformity of the light beam and then to sample a portion of the beam with the same field stop that is used in the 90° scattering measurement. In this way eq (8b) is used to calculate the Rayleigh's ratio. The width of the incident beam is the only dimensional measurement that must be made, and this measurement can easily be made.

$$R_{90}=(r_f \cos \alpha/\pi)(N_{90}/N_{\mathrm{diff}})\left(\frac{1}{\omega_0}\right). \qquad (8b)$$

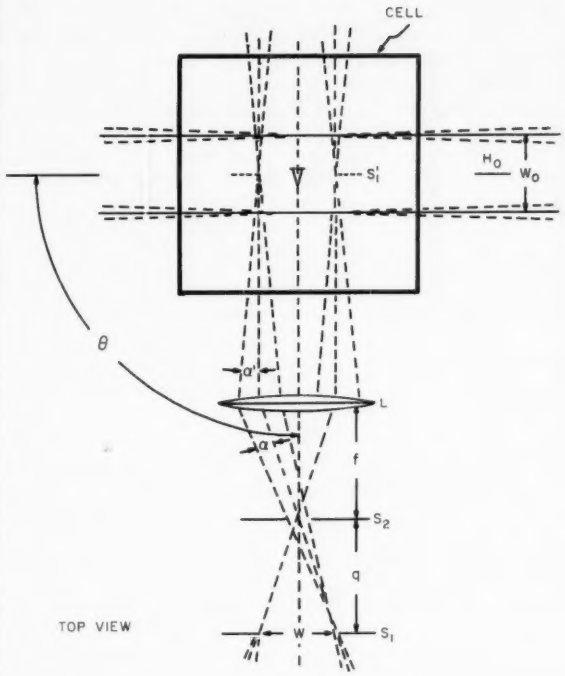

FIGURE 1. *Detailed geometry of viewing for absolute scattering at right angles to the incident beam.*

2.3. Direct Method

a. Flux Through Two Stops

To evaluate Rayleigh's ratio directly the radiant intensity of the light scattered from the solution must be determined so that eq (1) may be used. There have been two suggestions for the use of this method [10, 11]. One of these is a particularized solution of the other. Basically, one must calculate the flux passing through two apertures from a source that is located at one of the apertures. This is a very difficult problem to solve generally since it involves numerical approximations. However, the general outline of the problem can easily be seen, and the point at which approximations are introduced is easily recognized and the approximations evaluated.

If a lens is used, the stops either in image space or object space can be analyzed. Consider the system shown in figure 2, where S_1 and S_2 are parallel apertures (sometimes called stops) that are separated by a distance q, and the radiant source is located in the plane of one of the apertures S_1 and has a radiance N_θ in the direction of θ. The source is uniform over S_1 so that the radiance is constant over the area. The solid angle, $d\Omega$, from which the radiant flux is received at the second aperture is small enough so that the variation of the irradiance from the scattered light can be considered to be an average value equal to that at θ. Then the increment of radiant flux,

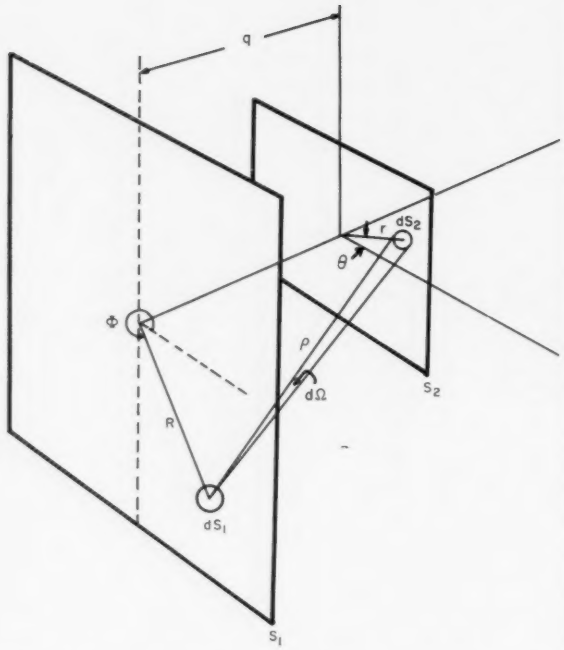

FIGURE 2. *Diagram for the calculation of the flux passing through two stops.*

dP, coming to the area dS_2 on aperture S_2, at a distance ρ from a small area dS_1 on aperture S_1, may be integrated to determine the total flux incident on S_2.

$$(P) \text{ at } dS_2, \text{ from } dS_1 = N_\theta dS_1(d\Omega) = J_\theta d\Omega = J_0 q \cdot \frac{dS_2}{\rho^3} \tag{9}$$

$$P = \int_{S_1}\int_{S_2} (J_0 q)\,\frac{dS_2 dS_1}{\rho^3}. \tag{10}$$

These equations lead to elliptic integrals and numerical integration for any stop system, circular or rectangular. However, an approximation may be easily made in circular coordinates that will be valid for circular stop systems. Equation (10) can then be written as eq (11).

$$P = J_\theta \int_{S_1} dS_1 \int_{S_2} \frac{qr dr d\theta}{[R^2 + r^2 + 2Rr\cos(\theta - \Phi) + q^2]^{3/2}}. \tag{11}$$

If the aperture stop in the optical system is small compared to the interstop distance and the field stop, then the above expression may be integrated and expanded in powers of the ratio of field stop radius to interstop distance as shown in eq (12).

$$P = J_{90}(S_1 S_2/q^2)[1 - 3/4(r/q)^2 + \ldots]. \tag{12}$$

For the setup used in these experiments, the approximation in eq (12) involves neglecting a term contributing less than ⅛ percent to the series before the first integration. Thus the use of the term (S_1S_2/q^2) J_{90} to measure the flux would indicate an error less than 1 percent from the true value.

R_{90} can be evaluated from eqs (12) and (1) by measuring the stop geometry, the irradiated volume and H_0. A special case of this general photometric analysis is the telecentric optical system. The irradiance from the source is accepted in such a way that the principal ray always passes through the principal point of the lens because the aperture stop is centered at this position. If the focal length of the lens is f, then the magnification, m, of the system according to Newton's formula is f/q, so that the viewed area will be $S_i(m)^2$. In this case the flux can be represented as shown in eq (13).

$$P = J_{90}(S_1 S_2/f^2). \tag{13}$$

Only the aperture stop and focal length must be known to determine the radiant intensity in such an optical system.

A scattering solution, however, occupies volume and may not be exactly centered in the plane of one of the stops. In this case the scattering surface can be considered to be moved toward or away from stop S_2. The angular acceptance of the system increases in the same proportion that the area of the source is decreased by the aperture stop provided that the movement of the surface is much less than the interstop distance.

b. Volume Correction

The total volume contributing to the scattering is not that defined by a principal ray but rather the volume that is defined by a pencil of rays over the entire aperture stop. If the ray that passes through the center of the aperture stop also passes through the focal plane, there is no volume correction because the zones in the field of view for which only a portion of the aperture is filled are equally compensated by those portions of the field that pass symmetrically on the other side of the aperture stop. If, on the other hand, the ray through the center of the aperture stop is not also the ray through the focal point, the scattering volume will be that defined by the rays through the center of the aperture stop.

c. Refraction Correction

Hermans and Levinson [12] have determined the effect of viewing a radiant source through a system of two stops when the source is located in a medium of refractive index n. They found that in all cases where the image of the field stop did not exceed the dimensions of the radiant source, the angular acceptance would be proportional to n^2. Their calculation was based upon an optical system that had the same dimensional restrictions as ours, but had the additional implicit restriction that the stops be much smaller in a linear dimension than the interstop distance.

d. Reflection Correction

The Fresnel formula for computing reflection at normal incidence allows a correction to be made easily for reflections from the glass-air interfaces in these experiments. The correction needs to be made only when the direct beam is being measured through a square cell. In this case, the additional scattering due to reflection of the scattered beam from the back surface of the cell and the reflection of the incident beam where it leaves the cell is subtracted from the 90° measurement of scattering. When the incident beam irradiance is measured without the cell in place, the loss of light in entering the cell and leaving the cell is just compensated by the back reflections discussed above. The Fresnel reflections from the liquids to the glass, when they are not isorefractive, are usually no more than 0.2 percent. For soft glass cells, the refractive index for the sodium D line is 1.516, and the calculated indexes for 436 mμ and 546 mμ are 1.524 and 1.517, respectively. The 90° light scattering measurements are thus decreased by factors of 0.915 and 0.913, respectively. For a Pyrex cell the reflectance is computed to increase by about a percent to 0.927 at 546 mμ if the refractive index of the Pyrex is 1.474.

3. Experimental Measurements

3.1 Materials

a. Cells

Several different types of light scattering cells were used. Two of them were 44 mm semi-octagonal cells. One cell was coated with a black absorbing paint on the back; the other was uncoated. Two other cells had cross sections 37 mm square. One was made of Pyrex glass; the other of lime glass. A fifth rectangular cell was used that could be tightly sealed. A seventh cell was a specially constructed cell made of Pyrex glass, measuring 55 × 10 × 10 mm, and had extreme close tolerances on angles and high clarity in the fused joints. A sixth cell was a Rayleigh horn which had 1-in. fused Pyrex circular entrance and exit windows and a total volume of 200 ml.

b. Solutions

The polystyrene samples used in these measurements were fractions that had been prepared for work on molecular weight determinations. The fraction used for the comparison of transverse scattering and transmission measurement had a molecular weight of 390,000. The fraction used for studies of the variables involved in low-level light scattering from solutions had a molecular weight of 150,000. Another fraction of 50,000 molecular weight was also studied. The strongly scattering solutions of colloidal silica were selected samples of Ludox.[2] Attempts to determine aggregation by the dissymmetry of the scattered light using four Ludox samples on hand showed little difference.

Reagent-grade cyclohexane was used. After a fractional distillation from a glass helix-packed column it had a refractive index n_D^{30} of 1.4205. Methyl ethyl ketone (Matheson) was also prepared by distillation from a glass helix-packed column; it had a refractive index n_D^{30} of 1.3738. Benzene and toluene were prepared from reagent grade (ACS) materials by fractionally distilling from a pot containing sodium. A spectroscopic-grade sample of carbon tetrachloride was measured without purification, then after a simple distillation, and again after a treatment with sodium hydroxide followed by drying and distillation.

All solutions of polystyrene in cyclohexane were handled in a large heated box.

c. Diffusers

Magnesium oxide diffusers were prepared in two ways. Magnesium oxide was obtained on an aluminum plaque 2 in. in diameter by burning magnesium turnings [13]. On several occasions a magnesium oxide cake was prepared from ACS reagent-grade magnesium oxide powder by packing it into a brass holder and then pressing it together lightly with a piece of glass.

Magnesium carbonate diffusers were surfaced by drawing a straight edge over the surface of magnesia blocks. In addition, a piece of white Vitrolite [14] was used as a reference diffuser after calibration with magnesium oxide in the light scattering photometer.

TABLE 1. *Angular variation of relative intensity from various magnesium oxide diffusers irradiated by a 1 mm beam*

(1)	(2)	(3)	(4)	(5)
α	Smoked MgO	Pressed MgO	cos α	Polarization ratio ρu (Smoked MgO)
−15	0.969	0.983	0.966	0.987
−5	.998	1.000	.996	.961
0	1.000	1.000	1.000	.952
5	0.996	0.994	0.996	.932
15	.955	.971	.966	.903
25	.889	.913	.906	.883
35	.799	.830	.819	.859
45	.686	.719	.707	.822
55	.559	.580	.574	.818
65	.410	.425	.423	.799
75	.352	.253	.259	.791

Table 1 shows the relative intensity as a function of viewing angle for a magnesium oxide diffusing surface irradiated by a 1 mm beam of light of wavelength 546 mμ incident at 45°.

The divergence of the incident beam was less than 0.1° in all directions and the angular acceptance of the receiver was 2.5°. Column 4 lists the function cos α which corresponds to the relative irradiance from a Lambertian diffuser. Column 5 lists the polarization ratio for the smoked oxide that is, the ratio of horizontally to vertically polarized scattered light. In view of the relatively good agreement of

[2] Trademark of E. I. du Pont de Nemours & Co., Inc.

cols. 2 and 3 with col. 4, the diffusers were considered to obey Lambert's law to a satisfactory degree.

Diffusers are illuminated by a relatively large beam, usually of the order of 10 mm in width, when they are used in light scattering calibration. Table 2 shows the results obtained with the above diffusers when they had a 9.9×12 mm rectangular light beam of wavelength 546 mμ incident upon them at 45°. The angular acceptance of the receiver was again 2.5°, and the field of view was 6×11 mm at all times. In this setup, measurements beyond 80° must be excluded since the projected area of the receiver field of view becomes larger than the width of the beam. The values have also been obtained for 436 mμ and are similar. Magnesium carbonate was studied in the same manner and the results are shown in table 3 for both the large and small beams.

TABLE 2. *Angular variation of radiance for MgO using a 9.9 mm beam, normalized to unity for α=0*

α	Smoked MgO	Pressed MgO	Polarization ratio ρu (smoked MgO)
−15	1.000	1.006	0.992
−10		1.005	
−5	1.000	1.005	
0	1.000	1.000	
5	1.000	0.996	.945
10		.993	
15		.993	
20		.992	
25	1.000	.992	
30		.993	
35		.994	
40	1.002	.989	
45	1.010	1.003	.827
50		1.007	
55	1.022	1.014	.807
60		1.021	
65			
70		1.007	

TABLE 3. *Angular variation of radiance for $MgCO_3$ diffusers, normalized to unity for α=0*

(1)	(2)	(3)	(4)	(5)	(6)
α	Diffuser 1			Diffuser 2	
	1 mm beam	10 mm beam	ρu	10 mm beam	ρu
−15	0.996	0.998		1.000	
−5	.997	.998			
0	1.000	1.000		1.000	0.996
5	1.002	1.001	0.869	0.999	
15	0.996	1.001		.995	
25	.998	1.008		1.000	
35	1.009	1.012		1.000	
45	1.006	1.028	.916	1.006	.877
55	1.002	1.047	.985	1.025	
65	0.998	1.073			
75	1.050	1.091	.957		

Table 4 shows the ratios obtained by direct comparison of the intensities from MgO and $MgCO_3$ as well as for Vitrolite and MgO under conditions of 45° incidence and normal viewing when using freshly smoked MgO and freshly scraped $MgCO_3$. In order to obtain more information about possible variations of these diffusers, a pressed MgO and a smoked MgO were compared directly with the Vitrolite. The

TABLE 4. *Scattering ratios for different types of diffusers*

Diffusing media	Scattering ratio for indicated wavelength	
	546 mμ	*436 mμ*
$MgCO_3$/MgO	0.995	0.990
Vitrolite/MgO	.850	.838

reflectance ratios at 546 mμ and 436 mμ, respectively, were 0.855 and 0.840 for the pressed sample, and 0.854 and 0.840 for the smoked.

Columns (5) and (6) of table 3 contain the radiance variations and polarization of another $MgCO_3$ diffuser which was used to obtain a constant luminance over a larger angular range. Both samples were measured for total reflectance relative to freshly smoked MgO and found to be within 1 percent in the green portion of the spectrum but different by about 5 percent in the blue. A similar slight decrease in the total reflectance at 436 mμ of the magnesia blocks was found later. The magnesium oxide did not show any appreciable reflectance changes with time.

The total reflectance of the magnesium oxide diffuser was determined several times under the same viewing conditions and also, as will be discussed later, several times under different viewing conditions. The total reflectance was determined from eq (5) in which the incident irradiance H_0 was determined by reference to neutral filters calibrated at the same time. The reflectances of Vitrolite, which does not have a fragile surface and can be assumed to have a greater permanence, were also determined at the same time. The measured Vitrolite reflectances were repeatable within 1.3 percent in the green and 0.8 percent in the blue over the course of several months. The MgO over the same period varied by 1.6 percent in the green and 1.3 percent in the blue. The reflection factor of the MgO diffuser was determined to be 0.967 in the green and 0.888 in the blue.

3.2. Transmission Measurements

Transmission measurements were made by using 5 cm or 10 cm Beckman cells. The transmission cell holder was built with a jacket so that water from a constant-temperature bath could circulate to keep constant temperatures in the cell at temperatures not too far from ambient temperature. The blackened thermostat was slightly longer than the cell to minimize the effect of ambient air on the cell ends. The experimental setup was very adaptable, and in view of Heller and Tabibian's work [15] it was decided to investigate any effects of secondary scattering photographically as well as photoelectrically. With a 2 mm incident beam, having an angular divergence of 0.3°, no difference could be detected in the photographs when a solution of 3 percent Ludox or a sample of ultracentrifuged water was inserted into the transmission cell and placed on the table. The camera was focused on the center of the cell with the aperture wide open

so as not to fail to detect any secondary scattering. A stray-light baffle did seem to help somewhat if it was placed about 4 in. on the source side of the cell center.

Measurements were made at 546 mμ for different dilutions of a high turbidity (0.123 cm^{-1}) Ludox solution in a 10 cm cell using a 2 mm beam of 0.07° divergence and a receiver allowing use of different fields of view and angular acceptance. With a 5.5×9.9 mm field of view and angular acceptances of both 0.5° and 4° the measured turbidity increased less than 2 percent. With a 2 mm diameter circular field of view and the same angular acceptances there was no change in the transmission measurements within experimental error.

The small amount of secondary scattering is unquestionably due to the very small size and angular divergence of the light beam used in these transmission measurements. The turbidity was obtained from transmission measurements using a 4 mm diameter circular field of view. Equation (2) was used to calculate the turbidity where J_0 and J are the radiant intensities of the incident and transmitted beams, respectively, after subtraction of any solvent absorption blank, and l is the solution path length in cm. The turbidity can be related to the transversely scattered light by eq (2) only in special cases. In general, a particle scattering factor is required, and it is different in transmission and transverse measurements.

3.3. Transverse Measurements

Since a wide variety of stop arrangements were available in the instrument, several experiments were conducted to test the applicability of eq (12) relating the radiant flux to the stop areas. In addition, tests were made to ascertain what effects the beam divergence and the volume of irradiated solution had on the measurement of the flux from the scattered light. Equation (12) states that if the radius of the receiver stop is less than $\frac{1}{10}$ of the interstop distance the radiant flux received will be directly proportional to the product of the stop areas to within 1 percent. With a fixed interstop distance and a fixed field stop in front of the phototube the ratio of the aperture stop area (proportional to diameter squared, D^2) to the phototube signal, G, should be a constant. Table 5 reports ratios of D^2/G obtained with two solutions of vastly different scattering intensities (polystyrene and Ludox) and also from a magnesium oxide diffuser. The low-molecular weight polystyrene fraction in cyclohexane had a turbidity of approximately 0.008 cm^{-1} while the Ludox solution had a turbidity of approximately 0.07 cm^{-1}. Table 5 lists the diameter of the aperture stop in col. (1) and its half angle in col. (2), that is, half of the conical apex angle defined by the circular aperture stop. The footnotes describe the size of the incident beam, its half angle of divergence, and also the size of the field stop. The linear dimensions of the image of the field stop seen by the phototube are magnified 1.1 times.

TABLE 5. *Ratio of aperture stop to phototube response for different viewing conditions*

(1) Aperture stop	(2) Half angle	(3) [a] D^2/G	(4) [b] D^2/G	(5) [c] D^2/G	(6) [d] D^2/G	(7) [e] D^2/G
Diameter, D, mm	*degrees*					
4.08	2.9	2.91	2.86	5.55	1.39	1.69
3.150	2.2	2.90				
2.479	1.8	2.84	2.87		1.40	1.71
1.326	0.936	2.93		5.51	1.44	
0.975	.689	2.88	2.87		1.55	
.772	.55	3.17		5.73	1.50	1.78

[a] Polystyrene solution: 10 mm beam, 0.07° divergence; 5.5×9.9 mm field stop.
[b] Polystyrene solution: 10 mm beam, 0.07° divergence; 5.04 mm diam. field stop.
[c] Ludox: 10 mm beam, 0.07° divergence; 5.04 mm diam. field stop.
[d] MgO: 10 mm beam, 0.07° divergence; 5.04 mm diam. field stop.
[e] MgO: 10 mm beam, approximately 0.3° divergence; 5.5×9.9 mm field stop.

The effect of the divergence of the incident beam on the scattering measurement from these weakly scattering solutions is shown to be quite small, though not negligible, in table 6.

TABLE 6. *Effect of divergence of incident beam on the measured scattering*

Wavelength	Scattering response	
	0.07° Div. vertical 0.07° Div. horizontal	3° Div. vertical 1° Div. horizontal
546 mμ	1.124	1.137
436 mμ	1.033	1.064

The analysis of this optical system indicated that the volume of scattering should be calculable from the field stop image and the width of the incident beam. To see if edge effects were actually important, a comparison was made on the above polystyrene solution with a 3 mm and also a 9 mm incident beam whose dimensions had been measured earlier [6]. At 546 mμ the ratio of the scattered flux intensities when using these two beam widths was 2.93 while the ratio calculated on the basis of the measured widths was 2.95.

Another conclusion of the previous photometric discussion is that the position of the field stop image with respect to the exact center of the secondary scattering source should not be critical in defining the scattering volume. Table 7 reports the experimental measurements on the polystyrene solution as well as on the magnesium oxide diffuser. Column 1 lists the distance of the field stop image from the center of the scattering, col. 2 lists the data for the polystyrene solution, and cols. 3 and 4 list the data for the magnesium oxide diffuser for two different acceptance angles, 2.9° and 1.8°, respectively. The above experiments examine the effects of not locating

TABLE 7. *Effect of distance between field stop image and the scattering volume center*

(1) Distance	(2) Polystyrene	(3) MgO	(4) MgO
cm		*2.9°*	*1.8°*
0	59.5	85.2	41.0
8.1	59.8	85.0	41.2

the image exactly in the center of the field stop and show very little difference.

The effects of the volume correction were also examined to determine if the edge effects in the volume had really been eliminated by assuming that the principal ray in this telecentric system did define the volume that was to be considered in Rayleigh's ratio. For this purpose several field stops were used to measure the scattering from the same solution irradiated by the same beam. The ratio of scattered to incident radiation was then determined. Table 8 shows that a doubling of the scattering volume has little effect on the measured scattering.

TABLE 8. *Effect of the field stop on the measured scattering*

Field stop dimensions	Scattering	
mm	*436 mμ*	*546 mμ*
3.0×7.3	1.68	6.44
5.04 dia	1.82	6.64
5.5×9.9	1.74	6.54

The scattering is almost constant. Since the results appear random, and since the incident beam is known to be uniform over its area [6], it appears that the scattering volume has been properly treated.

Another possible source of error in transverse measurements arises from a cell construction that allows stray light to interfere with low-level scattering measurements. An attempt was made to determine if cell construction had very much effect upon the determination of scattering from pure solvents like benzene and cyclohexane. Extraneous scattering from the cell walls should be most noticeable at these low levels of scattering. Although there is no easy way to explore the errors in cell design systematically, several quite different cells were examined with the same solvent to observe any large changes in scattering values. Table 9 shows the results obtained using benzene in the various cells described earlier, for both 546 mμ and 436 mμ light. The projected incident beam was 10 mm wide; it had an angular divergence of 0.5° in the horizontal direction and 1° in the vertical direction. The receiver accepted a 2.5° half angle and viewed an area 6×11 mm. The benzene was thermostatted at 25° C. The scattering from the Rayleigh horns were corrected for the loss of the back reflections by increasing the scattering ratio for the Fresnel reflections at two Pyrex surfaces. The ratio for the semi-octagonal cell that had been coated on its back surface with an absorbing paint was increased by the lime-glass correction for one reflection surface. The data given are for the ratio of the scattered beam signal to the incident beam signal. These different cells do not give as widely different values of absolute scattering as might have been assumed; however, the depolarization values vary considerably. In the case of carbon tetrachloride successive purification was necessary to reduce the depolarization apparently due to some fluorescing impurity.

TABLE 9. *Scattering from benzene in different cells*

	37mm×37mm square		44mm semi-octagonal		5.5×10mm×10mm	
	Soft glass	Pyrex	Soft unpainted	Soft back painted	Pyrex	Horn Pyrex
	546 mμ					
Scattering	0.566	0.563	0.552	0.552	0.553	0.552
Depolarization	.398	.410	.405	.413	.405	.411
	436 mμ					
Scattering	1.450	----	1.480	----	1.436	1.448
Depolarization	0.443	----	0.400	----	0.420	0.429

3.4. Comparative Transverse and Transmission Measurements

a. Polystyrene Solutions

Experiments were made on solutions of polystyrene to determine Rayleigh's ratio by transmission measurements as well as by two different transverse scattering measurements. The transverse measurements involved the use of eq (8b) when the diffuser was used, and eq (13) when the stop theory was used. In general, the transmission turbidity was determined by eq (2) only for solutions which scattered so strongly that extremely accurate transmission turbidities, better than the 0.2–0.3 percent available, were not needed. In one case, the scattering from the same solution was measured by two different types of photomultipliers, the 1P21 and the end-on type 5819 in order to ascertain the presence of any small differences due to the overshooting of the photosensitive surface by the incoming rays.

The solutions were cleaned by filtration through ultrafine filters and were measured in a semi-octagonal cell so that the high-angle dissymmetry of scattering was always easy to establish. In some

TABLE 10. *Comparison of transverse and transmission turbidities for polystyrene solutions*

Polystyrene (400,000 M W)	Solvent	Temp.	Photo-tube	Turbidities ($cm^{-1}\times10^3$) Transverse		Trans-mission
				Direct	Dif-fuser	
At 546 mμ						
conc (g/dl)						
0.94	cyclohexane	37°	1P21	14.3	14.4	14.4
			5819	14.2	14.3	14.0
1.10	do	37°	5819	15.44	15.2	15.08
0.90	butanone	room	5819	9.79	9.64	9.65
At 436 mμ						
0.94	cyclohexane	37°	1P21	38.7	35.4	38.60
			5819	38.1	37.8	38.60
1.10	do	37°	5819	41.1	39.5	40.5
0.90	butanone	room	5819	25.2	24.8	26.5

cases the solutions were first used in the semi-octagonal cells, then put into the transmission cell, and again introduced into the semi-octagonal cell to see if time and repeated handling perceptibly changed any of the scattering values. The values of the scattering always stayed the same within 0.5 percent. The results are listed in table 10. The 45°/135° dissymmetry of scattering for these strongly turbid solutions made up from the 390,000 molecular weight polystyrene fraction was about 1.1. The fraction used in this work was examined closely for depolarization and fluorescence effects. The depolarization ratio at 90° was always less than 0.01 and the fluorescence was less than 0.3 percent when it was present.

b. Ludox

A stock solution of Ludox about two years old was examined in order to check the consistency of the transmission turbidity and transverse scattering from water media at very high turbidities. It was realized that, in view of Goring's work [16], such comparisons might be in error because of the discrepancy which can occur between the transmission turbidity and the integrated transverse scattering when there is light absorption by the Ludox. The water used to dilute the Ludox was clarified by ultracentrifugation, and the Ludox was filtered through sintered glass filters. Solutions of 1, 2, 3, and 4 percent were prepared from a filtered stock solution of 6 percent. The angular dissymmetry (45°/135°) measurements throughout the experiments were about 1.05. This is not the ultimate cleanliness of the samples, but merely the level which allowed quick and easy filtration through fine sintered glass filters. At this level the scattering factor is low enough to make the corrections to both the transverse and transmission measurements negligible for the purposes of these measurements.

Since many people have used this particular technique to calibrate their photometers, it was of interest to us to find out how routine use of this method would agree with our other determinations of scattering. The experimental measurement of R_{90} and τ was similar to that described earlier for the polystyrene solutions. The ratio $(16\pi/3)\ R_{90}/\tau$ was plotted against concentration to give a curve which on extrapolation to zero concentration gave a value of 0.98 for light at 436 mμ and 0.97 at 546 mμ. Theoretically the intercept should be 1.000. The reason for this difference was not investigated further but could be due to a small amount of absorption by the solute. The slopes of the curves do give some measure of the amount of secondary scattering which, as is to be expected, is smaller for the 546 mμ light than the 436 mμ.

The increased secondary scattering at higher concentrations also causes the depolarization ratios to change from 0.033 and 0.012 for a 4 percent solution at 436 mμ and 546 mμ, respectively, to 0.008 and 0.008 at 0.5 percent.

4. Discussion

4.1. Agreement of the Different Scattering Methods

The data in table 10 demonstrate the very good agreement of the transverse scattering determined by the use of the diffuse reflector and the direct measurement of the incident beam intensity. These two scattering measurements are different from their respective forms in eqs (8) and (13) only in that a reflectance factor for the cell is calculated from the Fresnel equation and applied to the direct-beam measurement. The results for the 546 mμ wavelength light are consistent and make these transverse scattering measurements extremely reliable. However, a disturbing fact arises for the results at 436 mμ because the direct-beam measurements and diffuser measurements agree within a few percent even though the experimental determination of the absolute reflectance of the magnesium oxide is 0.88 rather than the literature value of 0.96 which was used to calculate R_{90}.

The agreement of the transmission turbidities and the transverse scattering are within ± 1.5 percent in all but one case. However, this particular run must have been in error since the results of the direct transverse measurement and the diffuser transverse measurement are also different. In both green and blue light, the agreement of the turbidities is equally good. It must be emphasized at this point that only impurities in the polymer sample could have an effect on the transmission since the solution transmission was always referred to the solvent. The transverse scattering measurements which were made in semi-octagonal cells are correct, even if the sample absorbs light, because the incident beam is measured after passage through the cell. The additional results with lower molecular weight samples indicate that even at very low turbidities, where the transmission results are subject to great errors, the two methods of transverse scattering agree. It should also be pointed out, as the data in table 10 indicate, that two different solvents were used. The turbidity level was correspondingly decreased at the same concentration so that any absorption effects would be expected to become more predominant. These data indicate that such an effect is not present. Since depolarization and fluorescence were shown to be small, the equating of the transmission turbidity to the transverse scattering by the simple eq (3) is valid. Any corrections due to the different Cabannes' depolarization factor for transverse scattering and integrated scattering would be insignificant.

The results of the Ludox experiments indicate that any calibration with such a highly scattering substance is bound to be difficult because of secondary scattering most pronounced in blue light. However, the agreement of the Ludox results with the polystyrene calibrations indicates that the refractive index correction for the square cell is correct for the small refractive index range 1.33 to 1.42.

4.2. Transverse Scattering Measurements

As the data in table 5 indicate, the flux is a linear function of the area of the stop for a half-angle acceptance range of 4° to less than 1°. The value for the half-angle of 0.55° is included even though it is not in line with the other results. Inspection of the 0.55° stop under a coordinate comparator showed that the hole had been drilled quite unevenly. The scattering from the isotropic polystyrene solution of low turbidity naturally gives the best results in this test of the instrument over its range of angular acceptance. The measurements of the angular acceptance using magnesium oxide as a scatterer are not as consistent as the results with scattering solutions.

The results indicate that the freshly prepared diffusers agree very well in relation to each other and with respect to the relative literature values for MgO and $MgCO_3$. The experimental value for the particular sample of Vitrolite agreed with that determined with an integrating sphere. Furthermore the agreement with Lambert's law was satisfactory in all of the samples used. It should be noted that making a MgO diffuser by packing MgO powder in a plaque did not at first yield good results, but gradually a technique was developed in which a Lambertian diffuser could be prepared at will.

The very good agreement mentioned earlier when comparing two different beam widths indicates that the calculations which predict no volume effects in scattering when using this type of receiver are correct. Similarly, the data in table 7 indicate that the calculation is correct in its prediction that the scattered flux is unchanged if the stop is imaged behind or in front of the center of the source. The results in table 8 also indicate that even when the field of view is halved the scattering ratio remains the same so that the volume correction is adequate.

The results with pure solvents in different types of cells is highly encouraging because it suggests that even at low turbidities the cells are not contributing stray light. The data in table 9 suggest that for our instrument the measured solvent scattering is not affected appreciably by cell design, although such effects can never be said to be absolutely eliminated. However, the high scattering value for benzene at 436 mμ in the semi-octagonal cell illustrates some of the dangers and problems in making low-level measurements. It also points out the value of making additional measurements of depolarization and fluorescence, especially at 436 mμ. At first, the apparent discrepancy in cells was difficult to understand. After many days of retesting and rinsing, it was discovered that this cell had been cleaned at one time with a detergent that had a strongly fluorescing material. Only after a lengthy treatment with strong acid did the scattering in this cell revert to the lower values obtained with the other cells. The values obtained at 546 mμ were at all times normal.

4.3. Transmission Measurements

The transmission values are very reproducible. The same values have been measured whatever variety of experimental arrangements has been used. At one time a diffuser was even inserted before the phototube to make certain that any possible geometrical changes in the positioning of the small beam used for transmission measurements were not producing erroneous results by allowing light to strike the photosensitive surface at different places. The results were the same with or without the diffuser.

5. Summary

A light-scattering photometer has been examined by two independent optical means, that is, by transmission and transverse scattering measurements, and the results shown to be in agreement. The results of this study indicate that the instrument is capable of a diversity of different arrangements which give reliable results. It should allow a more extensive investigation of the theory and practice of light scattering. The extension of these measurements to molecular weight determinations and other absolute liquid scattering should be a straightforward experimental procedure when clarification techniques become more reproducible.

6. References

[1] H. C. van de Hulst, Light scattering by small particles, John Wiley & Sons, Inc., New York, N.Y. (1957).
[2] B. H. Zimm, R. S. Stein, and P. Doty, Polymer Bull. **1,** 90 (1945).
[3] C. I. Carr and B. H. Zimm, J. Chem. Phys. **18,** 1616 (1950).
[4] P. Doty and R. F. Steiner, J. Chem. Phys. **18,** 1211 (1950).
[5] J. Cabannes, Ann. de Physique **13,** 858 (1956).
[6] D. McIntyre and G. C. Doderer, J. Res. NBS **62,** 153 (1959).
[7] F. Benford, G. P. Lloyd, and S. Schwartz, J. Opt. Soc. Am. **38,** 445 (1948).
[8] W. Middleton and C. Sanders, J. Opt. Soc. Am. **41,** 419 (1951).
[9] P. Tellex and J. Waldron, J. Opt. Soc. Am. **45,** 19 (1955).
[10] L. M. Kushner, Opt. Soc. **44,** 155 (1954).
[11] J. Kremens and J. Shapiro, J. Opt. Soc. Am. **44,** 500 (1954).
[12] J. Hermans and S. Levinson, J. Opt. Soc. Am. **41,** 460 (1951).
[13] National Bureau of Standards Letter Circular LC547, 1939.
[14] National Bureau of Standards Letter Circular LC1017, (1955).
[15] W. Heller and R. M. Tabibian, J. Colloid Sci. **12,** 25 (1957).
[16] D. A. I. Goring, M. Senez, G. Melanson, and M. M. Hugue, J. Colloid Sci. **12,** 412 (1957).

(Paper 68Al–256)

JOURNAL OF RESEARCH of the National Bureau of Standards—A. Physics and Chemistry
Vol. 68A, No. 1, January–February 1964

High Pressure Microscopy of the Silver and Cuprous Halides

A. Van Valkenburg

(October 9, 1963)

Using a diamond pressure cell and a polarizing microscope, visual observations were made on the transformations of silver and cuprous halides at calculated pressures up to 125 kilobars. A new birefringent phase was observed in silver iodide at 2400 bars. Four phases were observed in CuI and CuBr while CuCl appeared to have only three.

Using a diamond pressure cell previously described [1][1] and a polarizing microscope, visual observations were made on the transformations of silver and cuprous halides at calculated pressures up to 125 kilobars. The object of this investigation was to determine the nature and optical characteristics of new phases resulting from polymorphic changes that may occur in any one of these halides.

It has been previously demonstrated, that pressures in the diamond cell are greatest at the cell center and least at the edges. This gradient serves a very useful purpose in enabling one to observe several polymorphic phases occurring in the same field of view at the same time, the denser phases always occurring nearest the cell center. Phase changes occurring as a result of applied pressure were detected by observing changes in indices of refraction between adjoining phases using the well-known Becke line movement technique [2]. Under the microscope a thin white pencil line (Becke line) is observed moving towards the denser phase as the viewing tube is raised; the movement is reversed when the tube is lowered.

Phase changes were also observed by detecting birefringence changes between crossed nicols and by noting changes in absorption in both white and monochromatic light. The various optical effects were observed under the microscope at magnifications of 160 and 400 diam. Pressure values as used in this paper will be confined to the bar[2] which is defined as 10^6 dynes/cm^2.

Accurate pressure measurements are difficult to obtain in the diamond cell since friction and flow shear generate pressure gradients across the anvil faces. These gradients on a first compression may be very large especially when the sample is in a powdered form. An explanation for this is that, on the first compression, the movement of material is large compared with the movement for subsequent pressure cyclings. When the cell is newly charged with powdered material, there is a large volume of unoccupied interstitial space. On the first application of pressure, material is squeezed into these spaces and at the same time flows towards the cell edge. It is this movement at the beginning of compression that produces the greatest pressure at the center of the anvil. As compression is increased extrusion along the cell edge is prevented both by the internal friction of the material and the friction between it and the diamond surfaces. On the second and subsequent compressions the internal movement is relatively small, since the material has been previously compacted. Thus the pressure is distributed over a larger area and the buildup of very high pressure at the center is reduced. If pressures are calculated for the cell using the method in which the force is divided by cross-sectional area, one will obtain large errors, especially on the first compression of the material. The explanation for this is that the method assumes that pressure is equally distributed over the anvil surfaces whereas in practice gradients always exist. This point can be illustrated as follows: The maximum pressure calculated under this assumption for one of the diamond cells, was approximately 70 kilobars. A transition that occurs in AgI at 115 kilobars [4] was observed and photographed at a pressure of 60 kilobars calculated in this manner. These calculations were made on the first compression of the sample. On cycling the pressure, the transition did not appear at the maximum pressure of the cell, thus indicating the reduction of the highest pressure in the sample. By cycling the pressure in the cell, pressure measurement errors have been reduced to values of 5 percent or less in the range below 50 kilobars and to 10 percent in the higher pressure range.

Silver Halides

The silver halides, AgI, AgBr, and AgCl were obtained in powdered form from commercial sources, and samples were used directly from the bottle. When the powdered sample is squeezed, it forms a uniform transparent surface that is ideal for detecting optical changes. The stable forms of silver iodide at room temperature and pressure are the

[1] Figures in brackets indicate the literature references at the end of this paper.
[2] The author wishes to support the recommendation of the informal committee on high pressure measurements at the Lake George International Conference on High Pressures, 1960 [3], that the bar be universally used as a standard pressure measurement in high pressure work.

711-046—64——7

hexagonal or wurtzite type structure and the cubic or sphalerite type structure [5]. A microscopical examination of the sample indicated that both forms were present but it was estimated that the hexagonal form comprised 90 percent of the sample by volume. Both silver bromide and silver cholride have the sodium chloride type structure at room pressure and temperature [6, 7]. The latter two samples contained less than 0.5 percent impurities by volume.

Silver Iodide

The hexagonal silver iodide crystals when viewed under the microscope without the application of pressure are lath-shaped with an average grain size of 0.024 mm. The crystals are birefringent when viewed between crossed nicols. As pressure is applied to the cell, they are squeezed together, losing their individual identity. At a calculated pressure of 2400 bars the central portion of the sample begins to darken when observed in white light. With an increase in pressure of approximatley 300 bars the darkened area spreads out from the center. When the dark area is viewed in monochromatic light, using a grating type monochromator with a tungsten light source, it appears opaque. As pressure is increased to 2900 bars the center of the darkened area becomes transparent. In white transmitted light the transparent area has a light amber color and it is optically cubic with a sodium chloride structure [8]. When viewed in monochromatic light this center area begins to absorb strongly at approximately 514 mμ and it appears to be completely absorbing at 450 mμ. However, on careful examination at 450 mμ the area appeared to exhibit a dark reddish color that may be interpreted as a fluorescence phenomenon. Figure 1 shows the three phases of silver iodide photographed at approximately 4000 bars.

After standing for several hours the dark ring of material surrounding the amber area crystallized. When viewed in the polarizing microscope individual crystals measuring up to 100 microns in diameter were strongly briefringent and exhibited bright interference colors, see figure 2. The crystals have positive elongation and their long direction parallels the pressure gradient. In monochromatic light the crystals began to absorb at 473 mμ and total absorption occurred at 460 mμ. There was no indication of any fluorescence in these crystals. If the diamond cell was jarred or if the pressure was slightly modified the individual crystals readily broke up into smaller domains without any further regrowth. The refractive index of these crystals as detected by the Becke line movement was considerably higher than that of the low pressure phase, but lower than the amber colored area. Using Bridgman's compressive data to obtain the densities of the silver halides [9], the refractive indices of the polymorphic phases were calculated using Gladstone and Dale's equation of $\frac{n-1}{d}=K$, where n is the mean refractive index,

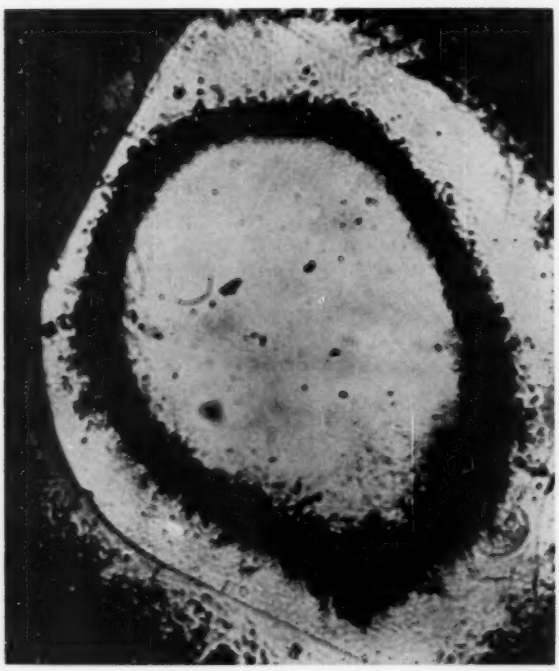

FIGURE 1. *Silver iodide showing the presence of three phases.* Pressure 4,000 bars. Magnification 160 ×.

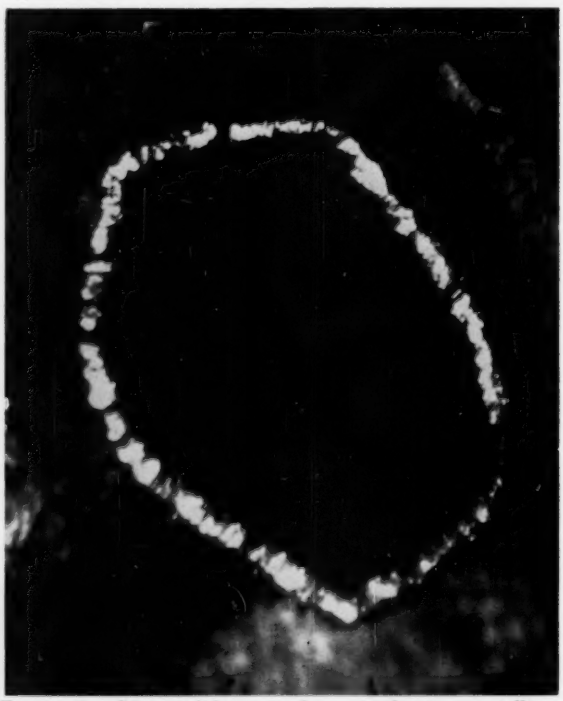

FIGURE 2. *Silver iodide as in figure 1, showing crystallization of dark ring; photographed between crossed nicols.* Mag nification 160 ×

d=density and K=specific refraction [10]. Table 1 gives the refractive index values of the polymorphic phases and their differences just before and after transition.

TABLE 1

Silver iodide		Silver bromide	Silver chloride
	N	N	N
High	[1] 2.430	2.442	2.239
Low sphalerite	2.232	2.429	2.221
Difference	0.198	0.013	0.018

[1] The sodium chloride or amber colored phase.

Since index differences >0.003 can be detected microscopically, the boundary between adjacent polymorphic phases can readily be observed in the silver halides. A third transition was observed in AgI using a diamond cell that could attain a calculated pressure of 125 kilobars. At a calculated value of 90 kilobars the sample center began to darken as observed in white light. With the pressure increased to about 100 kilobars a transition occurred with the emergence of a new phase (Drickamer places this transition at about 115 kilobars [4], see fig. 3). (Area in upper right hand section.) The Becke line moved quickly into the new phase when the viewing scope was raised indicating a large difference in the refractive indices of the two phases. It was estimated that the new phase had an index of refraction which was 0.06 greater than the adjacent phase. This would indicate a volume change in the order of 10 to 20 percent. As pressure was increased the central area of the new phase changed in appearance with the formation of a ridgelike surface, see figure 4. (Area in upper right hand section.) This photograph was taken at a later time using a fresh sample. The off-center position of the transition is caused by a misalinement of the diamond anvils, and the area in the lower portion of the photograph shows small fractures in one of the anvils. The average length of the ridges in the high pressure phase is about 10 μ. Between crossed nicols the area appeared to be birefringent with domains that had an apparent extinction. At these high pressures the diamonds showed strain birefringence but it was possible to distinguish this from the sample birefringence. In general, the strain birefringence of the diamond was wavy in character between crossed nicols while extinction in the birefringent crystals was sharp. There is also the possibility of strain birefringence in the sample itself at these ultra high pressures but this does not appear to be a significant effect. The boundary area between the birefringent phase and the adjacent phase is also well defined indicating the absence of strain. On releasing pressure the birefringent phase disappears; however, the darkened area adjacent to the birefringent phase does not disappear immediately but remains for several hours before it becomes clear and transparent. This absorbing or darkened area shows absorption throughout the visible spectrum. When pressure is totally released the sample transforms back to a cubic or sphalerite form. The hexagonal or wurtzite phase does not reappear.

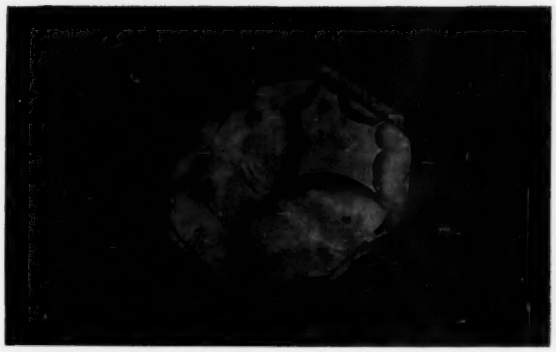

FIGURE 3. *Silver iodide transition at 115 kilobars.* Magnification 160 ×.

FIGURE 4. *Silver iodide showing ridge like surface.* Magnification 160 ×.

Silver Bromide

The sample has a very bright yellow color as taken from the bottle. When pressure was applied to the sample, a transition was observed at approximately 90 kilobars [9] with the familiar appearance of a small island surrounded by the familiar Becke line. When the high pressure phase first emerged the area was clear and transparent and it appeared to be optically isotropic, indicating that the material is cubic. As pressure increases the high pressure phase spreads out and the central area develops a ridgelike surface, similar to that observed in the silver iodide phase at 100 kilobars. This surface when viewed between crossed nicols appears to have a birefringent character. An apparent extinction was observed on a few small grains of about 4μ in size at a magnification of 400 diam. Although the evidence is not conclusive, the presence of birefringent particles would indicate that the high pressure phase is anisotropic in character. Bridgman [12] reports transitions in both AgCl and AgBr at 13 kilobars and ambient temperatures using shearing and volume change techniques. A microscopical examination of these two compounds, at pressure ranging from 5 to 20 kilobars did not indicate the presence of any transitions.

Silver Chloride

The material used in this experiment was obtained from a single crystal of silver chloride of optical grade quality by slicing an area from the crystal that was approximately 2 mm² by 0.5 mm thick. This was then placed between the diamond anvils and squeezed. The transition that occurs near 90 kilobars [9] is rather sluggish as compared with the transition in silver bromide. It was necessary to wait several minutes after a calculated pressure of 100 kilobars had been reached before the formation of the island with the characteristic Becke line was observed. In contrast to the high pressure phase in silver bromide, the high pressure phase of silver chloride, when observed at a magnification of 160 times, was clear and not ridgelike in appearance. Optically the high pressure phase appeared to be cubic and there was no detectable absorption or fluorescence in the visible spectra.

Silver chloride is used in many laboratories as a pressure transmitting medium, especially in the calibration of equipment that uses pyrophyllite or similar compounds for reaction chambers. At low pressures or at pressures under 50 kilobars silver chloride appears to undergo plastic deformation easily. It is interesting to note that the silver chloride transition observed in the diamond cell was obtained without the use of gasket material. There was no tendency for the silver chloride, which had an approximate thickness of 4μ to extrude or flow by plastic deformation even after a period of several hours. The friction between the diamond surfaces and the silver chloride, plus the internal friction of the silver chloride, was evidently sufficient to prevent extrusion.

Cuprous Halides

The cuprous halides, CuI, CuBr, and CuCl, were obtained from commercial sources and the material was used directly from the bottle. The impurity content of these compounds as observed under the microscope was estimated to be less than 1 percent by volume. The stable form of the cuprous halides at room pressure and temperature is the sphalerite or zinc blende structure in which the metal atoms are surrounded by four halogen atoms [11]. Under pressure the cuprous halides undergo phase transformations with differences in absorptions in the visible spectrum. The only previously reported cuprous halide transformation was that for CuI given by Bridgman [12]. He found a transition at 14,000 bars based on measurements obtained from shearing and volume changes. Since the cuprous halides are similar structurally it was believed that their polymorphic forms would also show similarities.

Cuprous Iodide

Cuprous iodide appears to have three transitions. At a calculated pressure of 4,000 bars the sphalerite form of cuprous iodide undergoes a transition to a phase which is optically birefringent. (See central area fig. 5 taken between crossed nicols.) The individual crystals have an average diameter of about 3 μ and their mean refractive index is estimated to be 0.008 higher than the zinc blende phase. The outer light areas segmented by the dark cross are the result of pressure birefringence in the diamonds as observed between nicols. As the pressure is increased by 1,000 bars the birefringent center moves outward and is replaced by a dark nonbirefringent center that suggest a phase transformation to a cubic modification (fig. 6). The refractive index difference between the two regions is small, estimated to be about 0.004, and it was difficult to see a Becke line. At a calculated pressure of approximately 15 kilobars a third transition takes place with the emergence of a phase with weak birefringence. This transition is believed to correspond to the transition reported by Bridgman. Figure 7 shows 3 transitions photographed in white light between uncrossed nicols. The boundary separating the two phases in the first transition can readily be seen but the boundary separating the two phases in the second transition has been sketched in by a dashed line. The third transition boundary is also readily visible and it will be noted that there is a lighter ring surrounding a dark inner area. The lighter ring contains the weakly birefringent phase and the inner dark area shows no birefringence. This area may represent another phase but the strong absorption prevents further identification. On releasing the pressure the transformations are reversible. However, the dark central area remains absorbing for several hours before returning to its normal transparency.

Cuprous Bromide

Cuprous bromide has three transitions, the first two occurring close to a calculated pressure of 47 kilobars, and the third occurring at a calculated pressure of 80 kilobars. Figure 8 taken at a calculated pressure of 50 kilobars shows the first and second transitions along with the darkening of the center. Phase number one is the white outer area of the photograph. Phase number two is shown by a darkened narrow zone line approximate 1 mm in width; phase number three a lighter region that has an amber color when viewed in white light. The dark central area does not appear to be a phase since it lacks a distinct boundary indicating a difference in refractive indices. This darkening is believed to be an absorption that occurs at all wavelengths in the visible spectrum. It was also observed that the absorption began just before the 47 kilobar transition when pressure was applied slowly. If pressure is applied quickly to the sample, going through the 47 kilobar transition to pressures of 60 kilobars or more, the central area does not develop an absorption area. As the zinc blende or original phase undergoes a transition at 47 kilobars one observes between crossed nicols the emergence of two phases at the same time;

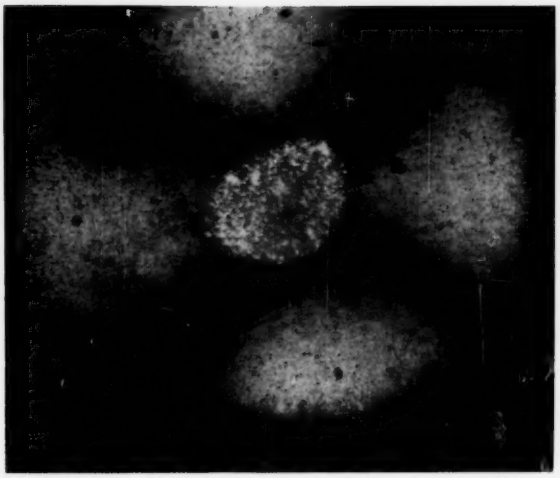

FIGURE 5. *Cuprous iodide showing birefringent phase between crossed nicols at 4,000 bars.*
Magnification 160 ×

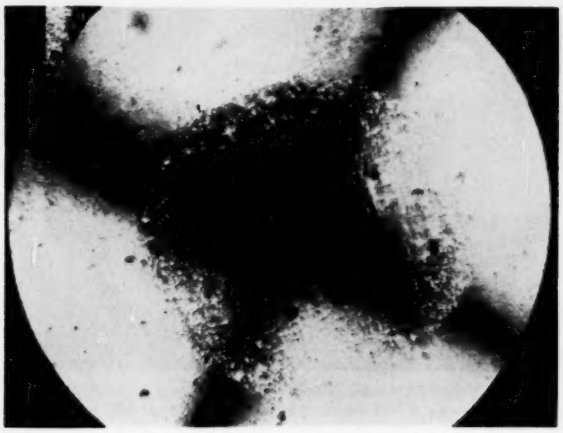

FIGURE 6. *Cuprous iodide showing outer birefringent phase with central cubic phase.*
Under crossed nicols at a pressure of 5,000 bars. Magnification 400 ×.

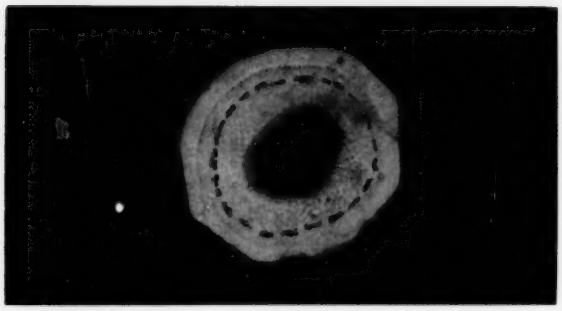

FIGURE 7. *Cuprous iodide showing three phases.*
Pressure 40 kilobars. Magnification 160 ×.

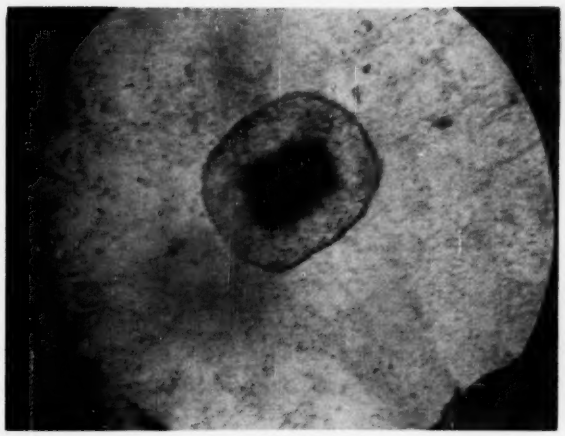

FIGURE 8. *Cuprous bromide showing emergence of initial phase and dark center.*
Pressure 50 kilobars. Magnification 400 ×.

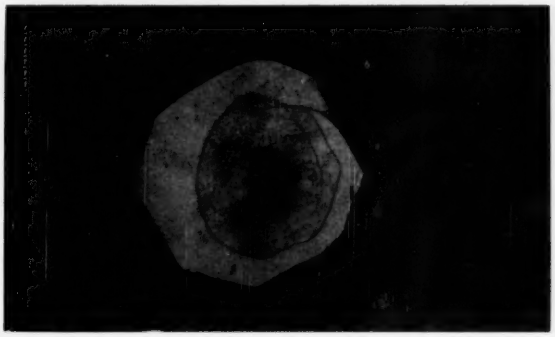

FIGURE 9. *Cuprous bromide shows the two transitions with the absorbing center.*
Pressure 90 kilobars. Magnification 160 ×.

one is birefringent and the second is cubic and colored amber. The crystals of the birefringent phase, form the thin outer band as observed in figure 8. The manner in which these crystals develop and form a thin line suggests that they are stable only in a very narrow pressure range of 100 bars or less. In monochromatic light the amber phase shows a strong absorption beginning at 520 mμ and a total absorption at 475 mμ. The third transition was evidenced by the appearance of a light area (phase number four) that appeared to be faintly birefringent. The Becke line movement between the amber and weakly birefringent phase was slow, indicating the relative refractive indices were small, with an estimated difference of 0.008. There was no apparent absorption of the light phase in the visible range using monochromatic light. Figure 9 shows the occurrences of the four phases. Figure 10 is a photograph of CuBr taken in monochromatic light at a wavelength of 505 mμ and at a pressure of approximately 90 kilobars. At this wavelength the four phases show very little absorption. In comparison figure 11 is a photo-

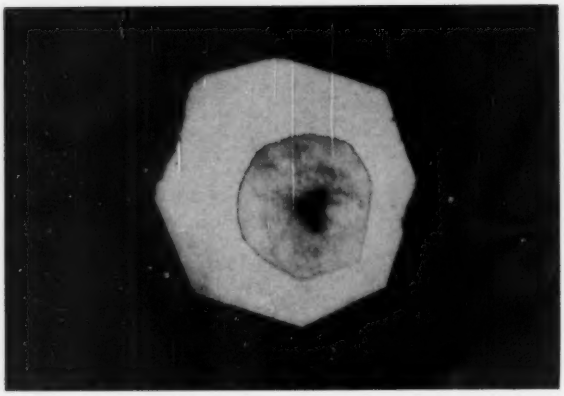

FIGURE 10. *Conditions as in Fig. 8, but photographed at a wavelength of 505μ*

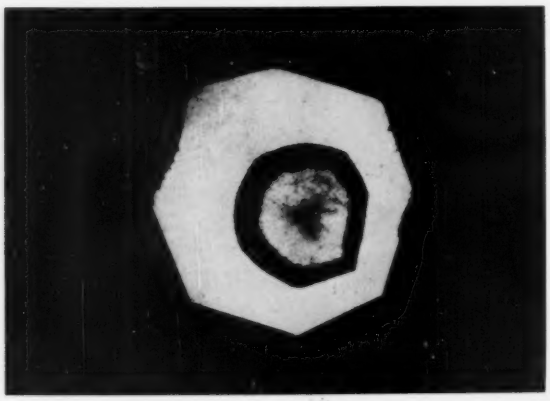

FIGURE 11. *Conditions as in figure 8, but photographed at a wavelength of 475 μ.*

graph of the same area taken at 475 mμ. Phase number three and possibly number two are totally absorbing at this wavelength while phase number four is transparent.

When pressure is released the transitions are reversible. The darkened central area, however, remains for several hours before it becomes transparent.

Cuprous Chloride

Two transformations were detected in cuprous chloride in the pressure range 0 to 100 kilobars. The first transition occurred at a calculated pressure of 42 kilobars, while a second occurred at approximately 55 kilobars. The second transition was very sluggish and it was almost missed. The initial zinc blende structure transformed to a weakly birefringent phase with crystals up to 30 μ in length. Between crossed nicols the crystals have an estimated birefringence of about 0.006 and their extinction positions were well-defined. See figure 12. The difference of the mean refractive index between the phases is estimated to be 0.015 as determined by the Becke line movement. The difference would give a

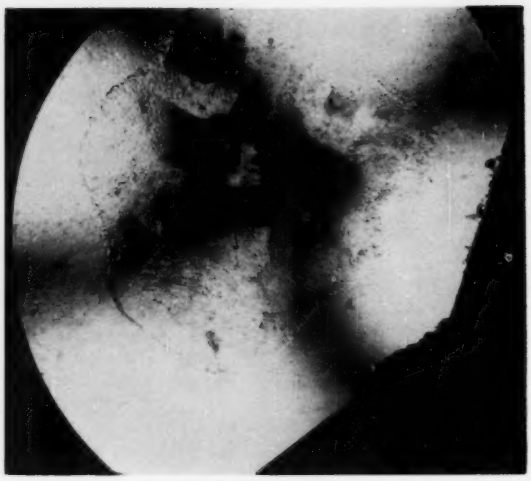

FIGURE 12. *Cuprous chloride showing birefringent character of crystals under crossed nicols.*
Pressure 45 kilobars. Magnification 400 ×.

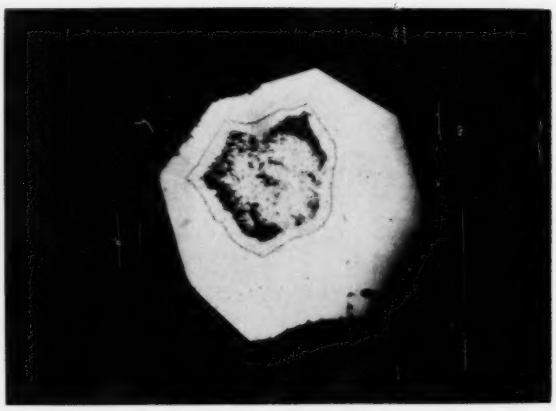

FIGURE 13. *Cuprous chloride.*
Dark opaque areas in white transmitted light. Pressure 45 kilobars. Magnification 160 ×.

FIGURE 14. *Cuprous chloride.*
Conditions as in figure 12, but photographed between crossed nicols.

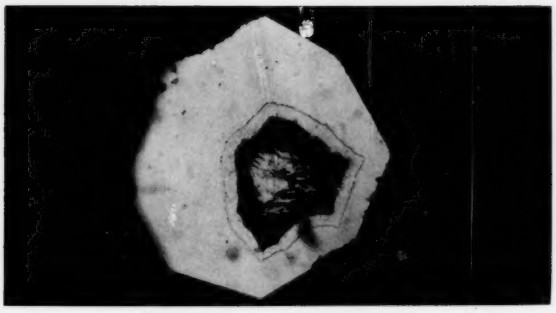

FIGURE 15. *Cuprous chloride.*
Conditions as in figure 12, but photographed 4 days later.

volume change in the range of 10 to 15 percent. After a period of 12 hr or longer at a pressure of 60 kilobars an area within the birefringent phase became opaque when observed in white transmitted light. The outside of the darkened area showed a definite boundary but the inner portions were irregular. See figure 13. Figure 14 is the same area taken between crossed nicols and one can observe the birefringent crystals similar to those observed in figure 12. Figure 15 shows the same area taken with uncrossed nicols four days later. As compared with figure 13, it can be seen that the opaque area has greatly increased in size and is completely absorbing in the visible spectrum. As pressure is decreased from 60 kilobars to approximately 30 kilobars the opaque areas transform to a transparent brown color in white light. Between crossed nicols at one bar pressure, the area formally opaque at 60 kilobars becomes granularly birefringent as shown in figure 16. This phase has refractive indices slightly higher than the cubic zinc blende structure. After a period of 24 hr the birefringent phase transforms back to a cubic material.

Summary of Cuprous Halides

In general the cuprous halides do not all have the same transition characteristics either with respect to their transition pressures or with respect to their transition phases. The initial transition of the cuprous halides is from a cubic zinc blende type structure to a birefringent phase. As is shown in table 2 these transformations do not all occur at the same pressure although the transition pressures of CuBr and CuCl are of the same order of magnitude. The pressures as given in table 2 are believed to be correct within a limit of 5 percent. In transition number 2 birefringent phases of CuI and CuBr appear to transform into a cubic phase whereas CuCl appears to transform into a second birefringent phase. The transformation of CuCl

TABLE 2. *Transition pressures*

	1	2	3
CuI	4,000 bars	5,000 bars	15,000 bars
CuBr	47,000 bars	47,000 bars	80,000 bars
CuCl	42,000 bars	55,000 bars	

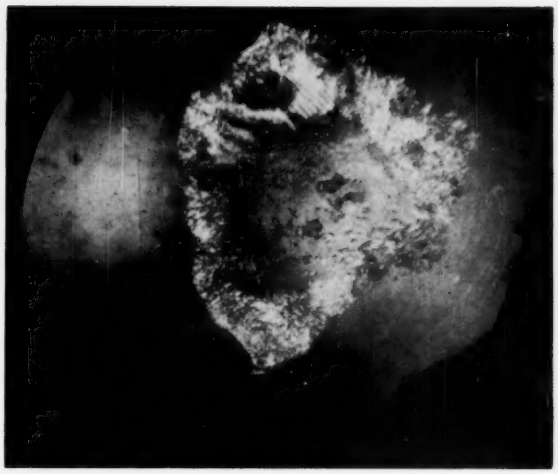

FIGURE 16. *Cuprous chloride between crossed nicols showing birefringent areas formally occupied by opaque areas.*
Pressure 1 bar. Magnification 400 diam.

into an opaque phase (fig. 13) is sluggish. This phase is considered to be anisotropic since at lower pressures the material becomes transparent and birefringent. It is quite possible, however, that the opaque area is cubic in character, its optical transmission being masked by the total absorption in the visible spectrum.

References

[1] C. E. Weir, A. Van Valkenburg, and E. R. Lippincott, Optical studies at high pressures using diamond anvils, Modern Very High Pressure Techniques, p. 51 (Butterworth, Inc., Washington, D.C., 1962).

[2] E. E. Wahlstrom, Optical Crystallography, 2d edition, p. 48 (John Wiley & Sons, Inc., New York, N.Y., 1951).

[3] G. C. Kennedy, Large pressure units, Progress in Very High Pressure Research ed., F. P. Bundy et al., p. 314. (John Wiley & Sons, Inc. New York, N.Y., 1961).

[4] H. G. Drickamer, Optical studies at high pressures, Progress in Very High Pressure Research ed., F. P. Bundy et al., p. 22. (John Wiley & Sons, Inc., New York, N.Y.)

[5] R. B. Wilsey, The crystalline structures of silver iodide, Phil. Mag. **46,** 487–496 (1923).

[6] R. B. Wilsey, The crystalline structure of silver bromide, Phil. Mag. **46,** 487–96, (1923).

[7] W. P. Davey, The absolute sizes of certain monovalent bivalent ions, Phys. Rev. **19,** 248–251 (1922).

[8] G. J. Piermarini and C. E. Weir, A diamond cell for X-ray diffraction studies at high pressures, J. Res. NBS, **66A** (Phys. and Chem.) No. 4, 325 (1962).

[9] P. W. Bridgman, The compression of twenty-one halogen compunds and eleven other simple substances to 100,000 kg/cm². Proceedings of the American Academy of Arts and Sciences, Vol. **76,** No. 1. pp. 1–24 (Feb. 1945).

[10] E. S. Larsen and Harry Berman, The microscopic determinations of the nonopaque minerals, Bulletin 848, U.S. Dept. of the Interior, Geol. Survey 1934, p. 30.

[11] R. W. G. Wyckoff and E. Posnjak, Crystal structures of the cuprous halides, J. Am. Chem. Soc. **44,** 30–36 (1922).

[12] P. W. Bridgman, Polymorphic transitions of 35 substances to 50,000 kg/cm², Proceedings of the American Academy of Arts and Sciences, Vol. **72,** No. 2, pp. 63–65 (July 1937).

(Paper 68A1–257)

JOURNAL OF RESEARCH of the National Bureau of Standards—A. Physics and Chemistry
Vol. 68A, No. 1, January–February 1964

Lattice Parameters and Lattice Energies of High-Pressure Polymorphs of Some Alkali Halides

C. E. Weir and G. J. Piermarini

(September 18, 1963)

Lattice parameters of the high-pressure forms of the alkali halides were determined. The lattice parameters were used to compare the lattice energies of the NaCl and CsCl type structures at the transition pressure. An analysis of the effect of experimental uncertainties on the calculated lattice energies showed that in almost every instance the Born-Mayer theory adequately accounts for the lattice energy of the high-pressure structure.

1. Introduction

A continuing widespread interest in the alkali halides arises, at least in part, from the early success of Born and Mayer [1][1] in calculating the lattice energies of the ionic crystals and the subsequent experimental verification of the calculated values by means of the Born-Haber cycle [2]. The success of the Born-Mayer model applies to the normal structures of the alkali halides, i.e., NaCl type or face-centered cubic structure (fcc) for all alkali halides except CsCl, CsBr, and CsI which assume the CsCl type or simple cubic structure (sc). Certain alkali halides normally in the fcc structure undergo a polymorphic transition to the denser sc structure at elevated pressures and until recently the Born-Mayer model had been unable to account for the relative stability of the two structure types. In a recent report Tosi and Fumi [3] have shown that earlier treatments of the equilibrium between the two structure types were subject to errors arising principally from an incorrect evaluation of the repulsive energy at the elevated pressures. On reevaluating the repulsive energy they demonstrated that the lattice energies of the two polymorphs at the transition pressure differed by not much more than the $P\Delta V$ energy reported for the transition. It should be noted that on the basis of Bridgman's data [4, 5] it has been concluded that the thermal energy involved in the transition is negligible on the scale of energies of present concern in the lattice energies. Therefore from the treatment of Tosi and Fumi it appears that the transition occurs between structures which are very nearly equivalent energetically. Of additional interest is the fact that according to Tosi and Fumi [3] the repulsive energy in the denser CsCl type structure is less than that of the corresponding NaCl type structure.

Tosi and Fumi employed lattice parameters derived from Bridgman's P–V data on the alkali halides [6] for their calculations. Inasmuch as the lattice energies are very sensitive to the lattice constants, it was considered desirable to obtain direct experimental values for these constants to permit a more accurate evaluation of the lattice energies of the two structures. This report presents experimental values for the lattice constants of the high-pressure forms of nine of the alkali halides. The high-pressure transitions of CsF and KF are being reported for the first time. The corresponding transition in RbF, which apparently represented the first transition observed in an alkali fluoride, was reported recently [7]. From the measured lattice parameters of the high-pressure forms the lattice energies are then calculated by the method described by Tosi and Fumi [3].

Polymorphism in the alkali halides at elevated pressures was discovered by Slater [8] in RbBr and RbI. Bridgman subsequently studied these transitions in some detail [4] and observed the corresponding transition in RbCl. Later, Bridgman located transitions in KCl, KBr, and KI and reported the thermodynamic constants of the transitions [5]. The transition pressures are of the order of 5 kb for the rubidium halides and 20kb for the potassium halides with only a small variation in pressure with type of anion. Although it had been suspected that the transition involved transformation from the NaCl type to the CsCl type structure this was not confirmed until Jacobs [9] determined the structure of the high-pressure form of RbI by X-ray diffraction. Much later Jamieson [10] reported that the high-pressure form of KI was also the CsCl type structure. This was confirmed recently in this laboratory [11]. Vereschagin and Kabalkina [12] and Adams and Davis [13] have reported the parameters of high-pressure forms of RbCl and RbI. The lattice parameter of a high-pressure form of RbF has also been reported [7].

[1] Figures in brackets indicate the literature references at the end of this paper.

2. Experimental Method and Materials

The apparatus and experimental technique developed here for X-ray studies at high pressures have been described in detail [11] and will be outlined very briefly here. A collimated beam of Mo K_α X-rays is diffracted by a thin layer of the material under study that is squeezed between flat parallel surfaces of two diamonds. The diffraction rings are recorded photographically and their diameters are measured on the film. The specimen-to-film distance is obtained from the measured diameters of the rings at 1 bar and the known X-ray diffraction patterns [14, 15]. The pressure on the material is calculated from the applied load divided by the smaller of the two diamond pressure areas.

During these experiments the camera [11] was modified by inserting a fixed diaphragm which permitted simultaneous exposure of opposite quadrants of the film. The filmholder was then rotated 90° and the other pair of quadrants exposed. In these studies the diffraction patterns of the high-pressure forms were obtained first and then the corresponding patterns at 1 bar were photographed in the adjacent quadrants. The two patterns appeared on the same film for comparison purposes. The order of the experiments was adopted because of the hygroscopicity of the alkali fluorides and it was considered necessary to verify the fact that the fluorides remained anhydrous during the experiment.

Both Bridgman [4, 5] and Jacobs [9] have emphasized the difficulties arising from hysteresis, sluggishness, etc., in the transitions of the alkali halides. For these reasons no effort was made to undertake measurements at the reported transition pressures. All data were obtained at fixed pressures at least 1 kb above the reported transition pressures. In the fluorides where transition points have not been reported previously, no attempt was made to locate the transition within narrow limits.

Most of the alkali halides studied were reagent grade materials of commercial origin. RbI, however, was prepared from Rb_2CO_3 with freshly distilled HI. The fluorides were formed from the carbonates or nitrates by successive treatments with HF. In addition, commercially available specimens of the fluorides were also used. The fluorides were so hygroscopic that it was found necessary to introduce the hot, freshly fused salt into the X-ray cell. This procedure was successful in eliminating problems arising from absorption of moisture as demonstrated by the fact that the X-ray diffraction patterns of the anhydrous fluorides were obtained at least 8 hr after introducing the material into the cell. The known X-ray diffraction patterns [14, 15] served to verify the identity and purity of these materials.

3. X-ray Diffraction Data

The results of the X-ray diffraction measurements on the high-pressure phases are given in table 1, which gives the observed *d*-spacings, the assigned indices, and the lattice constant for each material studied. The average lattice constant and the pressure to which the data apply are given for each material.

Each *d*-spacing of table 1 represents the average of at least five independent measurements on the same film. Additional experiments performed on each material yielded essentially the same *d*-spacings. The data tabulated pertain to a film selected for sharpness of lines, number of lines, etc. The average lattice spacings represent the numerical averages of the tabular data to three significant figures although in some instances somewhat greater precision is indicated by the data.

The *d*-spacing for every observed diffraction ring is reported in table 1, and it will be noted that the stronger diffraction rings of the fcc phases, i.e., the 200 and 220 reflections, generally persist at the higher pressures. The persistence of the low-pressure phases may be attributed to sluggishness in the transitions or to pressure gradients in the specimen.

As shown in table 1 all observed spacings not attributable to the fcc phase are readily indexed on the basis of the sc structure. In some instances, the lattice parameters are deduced from two diffraction rings only. It is believed that sufficient data are available, however, to eliminate any uncertainties in the expected structure of the high pressure polymorphs of the alkali halides and that the lattice parameters so determined are as reliable as the other data. The lattice parameters agree reasonably well with previously reported values [9, 12, 13] with one notable exception. The lattice parameter for the sc form of KI is somewhat smaller than the values reported by Jamieson [10] and in the preliminary report on the instrument used here [11]. Since construction of the camera, refinements have been made to improve the precision, and the present value is considered to be more reliable than the earlier one. Several independent experiments have been made with two different cameras which reproduce the present value within the experimental error.

These data appear to represent the first reported observation of the high-pressure CsCl type structure for KF and CsF. In each case, several independent experiments were performed on salts of different origin to check the transition as well as the lattice parameters. The appearance of the high-pressure form was also verified in all three fluorides by a microscopic method [16]. The transition pressures reported for the fluorides (see table 2) are considered to be only estimates because of uncertainties in the pressure calibration and strong evidence for sluggishness in the transitions. It will be noted that the diffraction data for KF and CsF are reported at 35 kb and 48 kb respectively while the transition pressures are estimated to be only 20 kb. In both cases the higher pressure was required to produce a sufficiently strong diffraction pattern for satisfactory measurement; the transition pressure was estimated to be 20 kb because the strongest ring of the high

TABLE 1. *X-ray diffraction data on the alkali halides at high pressures*

Index	KI (P≈19 kb)		KBr (P≈22 kb)		KCl (P≈22 kb)		KF (P≈35 kb)		RbI (P≈4.5 kb)		RbBr (P≈5 kb)		RbCl (P≈5 kb)		RbF (P≈12 kb)		CsF (P≈48 kb)	
	d	a	*d*	a	*d*	a	*d*	a	*d*	a	*d*	a	*d*	a	*d*	a	*d*	a
	cm^{-8}	*cm*$^{-8}$	*cm*$^{-8}$	*cm*$^{-8}$	*cm*$^{-8}$	*cm*$^{-8}$	*cm*$^{-8}$	*cm*$^{-8}$	*cm*$^{-8}$	*cm*$^{-8}$	*cm*$^{-8}$	*cm*$^{-8}$	*cm*$^{-8}$	*cm*$^{-8}$	*cm*$^{-8}$	*cm*$^{-8}$	*cm*$^{-8}$	*cm*$^{-8}$
100	3.920	3.920					3.076	3.076					3.876	3.876	3.300	3.300	3.370	3.370
(200 fcc)	3.316	fcc	3.206	fcc	3.081	fcc	2.667	fcc	3.621	fcc	3.410	fcc	3.263	fcc	2.826	fcc	2.995	fcc
110	2.783	3.936	2.647	3.743	2.533	3.582			3.090	4.370	2.881	4.074	2.757	3.898	2.315	3.274	2.394	3.386
(220 fcc)	2.382	fcc							2.590	fcc	2.408	fcc	2.318	fcc	1.989	fcc		
111	2.254	3.904					2.158	3.052									1.978	3.426
200	1.982	3.964	1.875	3.750					2.176	4.350	2.038	4.076	1.964	3.928	1.650	3.300	1.697	3.394
210	1.770	3.958															1.518	3.394
211	1.614	3.953	1.528	3.743	1.458	3.571			1.771	4.338	1.674	4.100	1.602	3.923			1.378	3.375
(420 fcc)											1.528	fcc						
220	1.396	3.948							1.527	4.320	1.452	4.107						
Average		3.94		3.74		3.58		3.06		4.34		4.09		3.91		3.29		3.39

TABLE 2. *Numerical data used for lattice energy calculations*

Halide	r at transition		C[a]		D[a]		P at transition[b]	β at transition[c]		β at 1 bar[d]	α at 1 bar[e]	$(\partial\beta/\partial T)_P$ at 1 bar[d]	$(\partial\beta/\partial P)_T$ at 1 bar[d]
	fcc	sc	fcc	sc	fcc	sc	10^9 dyne/cm^2	fcc	sc	fcc	fcc	fcc	fcc
	10^{-8} cm		10^{-60} erg cm^6		10^{-76} erg cm^8			10^{-12} cm^2/dyne		10^{-12} cm^2/dyne	10^{-6}/deg	10^{-15} cm^2/dyne deg	10^{-22} cm^4/dyne^2
KI	3.409	3.55	924	1472	1420	2516	17.85	6.6	5.2	8.54	125	5.12	3.3
KBr	3.203	3.23	605	930	800	1343	18.05	6.1	4.8	6.70	110	4.03	2.1
KCl	3.057	3.08	452	680	560	794	19.68	4.6	3.8	5.63	101	2.70	1.5
KF	2.601	2.76	167	246	150	249	(20.0)	2.2	(1.5)	3.31	100	0.40	0.66
RbI	3.628	3.76	1330	2039	2240	3675	3.97	8.5	7.1	9.58	119	6.52	4.1
RbBr	3.406	3.57	898	1346	1340	2085	4.51	7.2	5.1	7.94	104	(5.30)[f]	2.8
RbCl	3.257	3.39	691	1023	960	1267	4.90	6.1	4.9	6.70	98	5.30	(1.6)
RbF	2.783	2.84	278	409	290	442	(11.76)	(3.0)	(2.4)	(3.90)	(90)	(4.00)	(0.80)
CsF	2.943	3.04	495	1450	600	2390	(20.0)	2.5	(1.5)	4.30	95	4.40	1.2

[a] Values taken from ref. 20 or calculated from data of ref. 21.
[b] See ref. 6; values in parentheses estimated in these experiments.
[c] Calculated from data of ref. 4 and 8.
[d] See ref. 8 and 18.
[e] See ref. 18 and 19.
[f] This value is estimated. The value given in ref. 8 appears to be out of line with all the other values.

TABLE 3. *Volume change at the transition (fcc→sc)*

Halide	$-\Delta V/V_{fcc}\times 100$	
	Present work	P–V data (Bridgman [5])
KI	22.2	8.5
KBr	19.3	10.5
KCl	18.3	11.2
KF	10.8	----
RbI	13.9	10.7
RbBr	13.4	11.3
RbCl	13.4	14.6
RbF	17.3	----
CsF	10.0	----

pressure form could be identified at 20 kb but not at 15 kb.

Bridgman previously studied all the alkali fluorides except RbF and observed no transitions [17, 18]. His failure to obtain the transition in KF may be attributed to the fact that he did not carry the material to sufficiently high pressures. A similar explanation does not apply in the case of CsF because Bridgman studied this material to 42 kb at room temperature and to 56 kb at 137 °C. The probable explanation for the discrepancies in the findings is that Bridgman's specimen was not anhydrous. The transition reported here can be observed microscopically in the anhydrous salt but not in material exposed to the atmosphere for a very short time. In this connection it may be noted that if Bridgman's data on CsF and KF were obtained on partly hydrated materials the volume changes of table 2 may be in serious error. In addition all calculations involving the P–V data will be subject to similar errors.

The changes in volume at the transition points calculated from the lattice parameters are tabulated in table 3 with the corresponding values obtained by Bridgman [5] from volumetric measurements. It will be noted that the lattice parameters of the fcc phases involve correction of the 1 bar values by means of Bridgman's volume data. The agreement appears reasonably good for the rubidium halides, but not for the potassium halides. The discrepancy in the potassium halides may arise from the difficulties in estimating ΔV in the P–V studies on the potassium salts in which the transitions exhibit a 13 kg/cm^2 wide [5] region of indifference—an interval of apparent coexistence of t o phases in equilibrium. Under such circumstances it is believed that Bridgman's estimates of ΔV would tend to be low. The values for KF, RbF, and CsF obtained in the present studies appear to be somewhat erratic. This result is probably attributable in part to the absence of reliable P–V data on the flourides and in part to uncertainties in the transition pressures themselves.

4. Lattice Energies

4.1. Method of Calculation

Because Tosi and Fumi [3] have demonstrated that the repulsive parameters may not be considered independent of volume or structure in the alkali halides, they must be calculated by the method devised originally by Born and Mayer [1].

The first two derivatives of the internal energy are respectively,

$$(\partial U/\partial V)_T = T\alpha/\beta - P \quad (1)$$

and

$$(\partial^2 U/\partial V^2)_T = [1 + \{(\partial\beta/\partial T)_P + (\partial\beta/\partial P)_T \alpha/\beta\} T/\beta]/V\beta \quad (2)$$

where, in addition to the usual quantities, α represents the expansivity $[(\partial V/\partial T)_P/V_0]$ and β the compressibility $[-(\partial V/\partial P)_T/V_0]$.

The lattice energy, E, is taken to be

$$E = (-\delta e^2/r - C/r^6 - D/r^8 + Be^{-r/\rho})N \quad (3)$$

and the first two derivatives are given by

$$(\partial E/\partial V)_T = [\delta e^2/r + 6C/r^6 + 8D/r^8 - Bre^{-r/\rho}/\rho]N/3V \quad (4)$$

and

$$(\partial^2 E/\partial V^2)_T = -[4\delta e^2/r + 54C/r^6 + 88D/r^8 - Br(2 + r/\rho)e^{-r/\rho}/\rho]N/9V^2 \quad (5)$$

where δ is the Madelung constant, r, the nearest neighbor distance $\left(r_{fcc} = a_0/2; \quad r_{sc} = a_0\frac{\sqrt{3}}{2}\right)$, e, the electronic charge (4.80×10^{-10} esu), C and D, Van der Waals interaction coefficients, B and ρ, the repulsive parameters, and N, Avogadro's number.

Equations 1 and 4 and eqs 2 and 5 are set equal for each phase at the transition point and the systems of two equations may be solved for the parameters B and ρ applicable to each phase. In practice, the equations are solved for ρ and $Be^{-r/\rho}$ rather than for the parameters[2] B and ρ.

4.2. Data Used for Calculations

Experimental data used in the calculations were taken almost exclusively from the reports of Bridgman and differ somewhat from the data used by Tosi and Fumi [3]. Numerical values used are tabulated in table 2 with the sources being identified by the footnotes. Values enclosed in parentheses represent estimates for which experimental data were not available. Such estimates may be subject to errors exceeding the usual experimental uncertainties. The effect of errors on the calculated lattice energies will be discussed later.

[2] From the manner in which the equations are formulated it follows that the parameters and energies are determined for an ion pair. These units will be used throughout. Thus the energy in ergs will be understood to be ergs/ion pair.

4.3. Lattice Energies

Calculated values of ρ and $Be^{-r/\rho}$ for the two structures at the transition pressure are given in table 4. The lattice energies of both structures obtained from eq 3 using the data of table 2 and the values of $Be^{-r/\rho}$ from table 4 are given in cols 6 and 7 of table 4. Column 8 of table 4 gives the $P\Delta V$ term for the structure change calculated from the lattice parameters rather than from Bridgman's data [6].

TABLE 4. *Repulsive parameters and lattice energies of alkali halides at transition points*

Halide	ρ, 10^{-8} cm		$Be^{-r/\rho}$, 10^{-12} erg		Lattice energy, 10^{-12} erg		$P\Delta V$ at transition, 10^{-12} erg
	fcc	*sc*	*fcc*	*sc*	*fcc*	*sc*	
KI	0.417	0.409	2.34	2.51	−10.15	−10.41	0.31
KBr	.415	.401	2.48	2.47	−10.74	−10.88	.23
KCl	.369	.370	2.36	2.39	−11.45	−11.47	.21
KF	.308	.289	2.42	2.06	−13.69	−13.48	.06
RbI	.351	.354	1.49	1.49	−10.29	−10.10	.05
RbBr	.344	.305	1.62	1.41	−10.86	−10.81	.05
RbCl	.307	.293	1.56	1.44	−11.47	−11.30	.05
RbF	.250	.244	1.74	1.73	−13.43	−13.40	.09
CsF	.210	.189	1.52	1.74	−13.05	−13.80	.22

Although the numerical results of table 4 differ slightly from the corresponding values obtained by Tosi and Fumi [3] the agreement is encouraging because of the difference in the data used in the two calculations. It will be noted that the repulsive parameter, ρ, is generally smaller in the more compact CsCl type structure. This is in agreement with the findings of Tosi and Fumi [3], who observed that the experimental evidence for a smaller compressibility in the sc form required a smaller value for ρ. If the Born-Mayer treatment is adequate, then $E_{fcc} + P\Delta V - E_{sc} = 0$, provided the latent heat of the transition is negligible. The present data are less consistent with this requirement than the results of Tosi and Fumi [3]. Therefore, it is necessary to evaluate the latent heat and the effect of the experimental errors on the results.

4.4. Latent Heat of Transition

The anticipated agreement between lattice energies of the two structures when allowance is made for the work done at transition is predicated on the assumption that the entropy change at the transition is negligible. Although plausible arguments can be advanced to support this thesis [3], the experimental evidence has not been examined in detail. Jacobs [9] concluded that the latent heat could be neglected on the basis of Bridgman's data [2, 3] but, on close examination, Bridgman's results do not appear to be convincing. For example, Bridgman [4, 5] reported dT/dP positive for RbI, KI, and KCl but negative for RbBr, RbCl, and KBr and noted [4] that the accuracy of his data on the variation of transition pressure with temperature was questionable. Inspection of Bridgman's data shows that the inaccuracy arises principally from the fact that the transitions are sluggish; and the transition

pressures cannot be located with precision. In the rubidium halides there appears to be a region of indifference of about 1,000 kg/cm^2. Although his data and figures for the potassium halides do not indicate this region, Bridgman reported [5] that the region of indifference was about 13,000 kg/cm^2 for both KBr and KI.

Recently Clark [22] studied the effect of pressure on the melting points of some of the alkali halides and observed the triple points between the liquid phase and the two crystalline forms of CsCl, RbCl, and KCl. On the basis of his data $dT/dP>0$ for CsCl and he obtained a latent heat of 0.05×10^{-12} erg for the transition between the two crystalline forms. Combining his triple point data with Bridgman's data at lower temperatures indicates that $dT/dP>0$ for RbCl but $dT/dP<0$ for KCl. Assuming dT/dP independent of P and T, the latent heat for the transition in RbCl is estimated to be not more than 0.01×10^{-12} erg. For KCl the latent heat is negative but even smaller in magnitude. From the similarities in the properties of the alkali halides, it seems most probable that the latent heats for the other halides can be neglected on the scale of energies of interest here.

4.5. Effect of Errors on the Lattice Energies

As the entropy change at the transition appears to be negligible, the quantity $E_{fcc}+P\Delta V-E_{sc}$ should be zero for all the halides studied, provided the theory is adequate and the data used in the calculation are sufficiently precise. It is of interest to inquire whether, in view of the uncertainties in the data used for the calculation, the quantity $E_{fcc}+P\Delta V-E_{sc}$ is significantly different from zero.

To obtain the answer to this question the calculation of the lattice energies was analyzed by the law of propagation of errors and an estimate of the reliability of the lattice energies was obtained. The method of calculation and the results are given in the appendix. The standard deviations of the lattice energies given in table 5 of the appendix were used to evaluate the significance of the deviations of the energies from zero by investigating the ratio $|E_{fcc}+P\Delta V-E_{sc}|/\sqrt{\sigma^2_{fcc}+\sigma^2_{sc}+\sigma^2_{P\Delta V}}$. All values necessary for the evaluation are given in the tables except those for $\sigma^2_{P\Delta V}$ which are insignificant in comparison with σ^2_{fcc} and σ^2_{sc}.

If the rule is adopted to consider the deviations to be significantly different from zero only when such deviations exceed twice the respective standard deviations calculated, then only values for KI and CsF exceed these limits. From the fact that all other values are not significant in this sense it would appear that two possibilities exist, first the latent heats of transition in these two instances are not negligible, or second that the estimates of the experimental errors were too low. Of these two the latter seems much more probable. Some discrepancies in the data on KI were noted earlier and the assumed error was not sufficient to encompass such data in the calculations. It is by no means clear, as noted earlier, that Bridgman's data on CsF can be accepted as applying to the anhydrous salt. With these facts in mind it appears justified to conclude that, within

TABLE 5. *Individual variance terms in error calculations*

Halide	$\left(\frac{\partial E}{\partial T}\right)^2\sigma_T^2$	$\left(\frac{\partial E}{\partial c}\right)^2\sigma_c^2$	$\left(\frac{\partial E}{\partial D}\right)^2\sigma_D^2$	$\left(\frac{\partial E}{\partial \alpha}\right)^2\sigma_\alpha^2$	$\left(\frac{\partial E}{\partial \beta}\right)^2\sigma_\beta^2$	$\left(\frac{\partial E}{\partial P}\right)^2\sigma_P^2$	$\left(\frac{\partial E}{\partial r}\right)^2\sigma_r^2$	$\left(\frac{\partial E}{\partial \beta}\frac{\partial \beta}{\partial T}\right)^2\sigma_T^2$	$\left(\frac{\partial E}{\partial \beta}\frac{\partial \beta}{\partial P}\right)^2\sigma_P^2$	σ_E^2	$\sqrt{\sigma_E^2/N}$
	(±5° C)	(±10%)	(±10%)	*	(±10%)	**	***	(±25%)	(±25%)	†	
	10^{17} erg^2	10^{18} erg^2	10^{16} erg^2	10^{16} erg^2	10^{20} erg^2	10^{20} erg^2	10^{20} erg^2	10^{20} erg^2	10^{20} erg^2	10^{20} erg^2	10^{-12} erg
fcc											
KI	3	42	33	4	1	15	86	0	0	102	0.17
KBr	6	8	44	4	3	21	140	1	0	164	0.21
KCl	5	18	6	4	6	15	155	1	1	178	0.22
KF	20	2	39	5	33	6	253	0	1	293	0.28
RbI	11	14	6	5	6	0	107	1	1	116	0.18
RbBr	7	25	5	5	9	0	136	1	1	148	0.20
RbCl	16	7	6	5	13	0	139	1	0	154	0.21
RbF	5	15	0	5	52	0	210	3	3	268	0.27
CsF	4	116	124	1	1	3	126	0	0	132	0.19
sc											
KI	4	36	25	78	4	17	153	0	0	176	0.22
KBr	4	24	13	67	6	17	2	1	0	26	0.08
KCl	4	6	14	80	10	11	2	1	1	25	0.08
KF	26	12	81	114	7	5	2	1	27	42	0.11
RbI	8	19	13	90	8	0	28	1	1	38	0.10
RbBr	7	25	8	74	14	0	7	1	1	23	0.08
RbCl	13	21	36	60	16	0	31	1	0	49	0.12
RbF	12	46	64	66	77	0	226	2	3	309	0.29
CsF	11	324	4	48	29	5	32	4	2	74	0.14

*For the fcc structures the range of α was taken to be ±10%, for the sc structures ±25%.

**For the potassium halides the range of P was taken to be ±5 kb; for the rubidium halides, ±0.5 kb; for CsF, ±5 kb.

***For the fcc structures the range of r was taken to be 0.1A; for the sc structures the range was obtained from table 1.

†The data of the table have all been rounded off. The sum σ_E^2 was obtained from the unrounded data and subsequently rounded. Therefore, the values given for σ_E^2 may differ from the sums of the tabulated terms.

the experimental error of the available data, the Born-Mayer treatment with the modifications introduced by Tosi and Fumi produces a satisfactory representation of the energies of the high-pressure forms of the alkali halides.

5. Appendix

Given a quantity E which is an explicit function of variables $x_1, x_2 \ldots x_n$ each of which is a function of the quantities $y_1, y_2 \ldots y_n$, i.e.,

$$E=f(x_1x_2 \ldots x_n) \quad \text{with} \quad x_1=\varphi(y_1y_2 \ldots y_n),$$
$$x_2=\psi(y_1y_2 \ldots y_n) \quad \ldots \quad x_n=\xi(y_1y_2 \ldots y_n). \quad (1)$$

Then the variance of E, σ_E^2, can be expressed to a first approximation in terms of the variances of the quantities $y_1, y_2 \ldots y_n$, [$\sigma_{y_1}^2$, $\sigma_{y_2}^2 \ldots$ etc.], which are assumed to be statistically independent, as follows:

$$\sigma_E^2 \simeq \left(\frac{\partial E}{\partial y_1}\right)^2 \sigma_{y_1}^2+\left(\frac{\partial E}{\partial y_2}\right)^2 \sigma_{y_2}^2+ \ldots \left(\frac{\partial E}{\partial y_n}\right)^2 \sigma_{y_n}^2 \quad (2)$$

where

$$\frac{\partial E}{\partial y_1}=\frac{\partial E}{\partial x_1}\frac{\partial x_1}{\partial y_1}+\frac{\partial E}{\partial x_2}\frac{\partial x_2}{\partial y_1}+ \ldots \frac{\partial E}{\partial x_n}\frac{\partial x_n}{\partial y_1} \quad (3)$$

$$\frac{\partial E}{\partial y_2}=\frac{\partial E}{\partial x_1}\frac{\partial x_1}{\partial y_2}+\frac{\partial E}{\partial x_2}\frac{\partial x_2}{\partial y_2}+ \ldots \frac{\partial E}{\partial x_n}\frac{\partial x_n}{\partial y_2} \quad (4)$$

$$\frac{\partial E}{\partial y_n}=\frac{\partial E}{\partial x_1}\frac{\partial x_1}{\partial y_n}+\frac{\partial E}{\partial x_2}\frac{\partial x_2}{\partial y_n}+ \ldots \frac{\partial E}{\partial x_n}\frac{\partial x_n}{\partial y_n} \quad (5)$$

If the following definitions are made:

$$x=3y\left(\frac{T\alpha}{\beta}-P\right); \quad (6)$$

$$y=\left(\frac{\delta e^2}{r}+\frac{6C}{r^6}+\frac{8D}{r^8}\right)N; \quad (7)$$

$$z=-\left(\frac{4\delta e^2}{r}+\frac{54C}{r^6}+\frac{88D}{r^8}\right)N; \quad (8)$$

$$w=\left[1+\left\{\left(\frac{\partial \beta}{\partial T}\right)_P+\left(\frac{\partial \beta}{\partial P}\right)_T\frac{\alpha}{\beta}\right\}\frac{T}{\beta}\right]\frac{9V}{\beta}; \quad (9)$$

then it can be shown that

$$NBe^{-r/\rho}=(y-x)^2/[(w-z)-2(y-x)]. \quad (10)$$

If we define

$$R=-\left(\frac{\delta e^2}{r}+\frac{C}{r^6}+\frac{D}{r^8}\right)N \quad (11)$$

then the lattice energy can be written

$$E=R+(y-x)^2/[(w-z)-2(y-x)]. \quad (12)$$

The quantities x, y, z, w, and R are identified with the variables x of eqs 3–5 while each of the $y_1 \ldots y_n$ can be identified with one of the parameters r, T, α, $(\partial\beta/\partial T)_P$ etc. in the defining eqs 6–9 and 11. Therefore each of the appropriate partial derivatives in eqs 3–5 can be computed and evaluated. To evaluate eq 2 numerical values must be assigned to the variances of each parameter. The extreme range of each parameter was estimated. These estimates were based in part on previous experience in measuring such quantities and in part on available data. The range was arbitrarily defined to be equal to 5σ and the appropriate values of σ^2 calculated.

The results of the calculations are given in table 5 which gives values for the various terms of eq. 2 for both forms of each halide. Each column is headed by the term to which the data refer and the range assumed for the parameter involved. The range is shown in parenthesis where applicable to all data in the column or in the footnotes where variable ranges were used. Column 12 gives the square root of the sum of the individual terms divided by Avogadro's number. The values in this column represent the standard deviations of the lattice energies given in table 4.

The ranges were assigned as follows:

a. For a working temperature of 298° K, a variation of ±5° K appears to be the maximum expected under normal laboratory conditions.

b. No reasonable estimates for variations in the values of C and D were apparent. Consequently a range of ±10 percent was assumed. From the results it appears that the term in D will be negligible regardless of the range assumed.

c. Measured values of α are available for the fcc structures. Considering both experimental errors and the variation of α with P, a value of ±10 percent was assumed for the fcc phases. No data are available for the sc structures and to compensate for a change in α with structure the range was increased to ±25 percent for the sc materials. The term is unimportant and much larger variations could be tolerated without affecting the total error.

d. Measured values of β are available for most halides. The range of β was taken somewhat arbitrarily to be ±10 percent. With the present data this term may represent as much as 1/10 of σ_E^2. With better data for the other quantities better estimates for β will be necessary.

e. The uncertainties in the derivatives of β with P and T were set at ±25 percent. Both quantities are small and might not be expected to be sensitive to P and structure. They contribute only a very small amount to σ_E^2 so that even if the variations were outside the limits assumed they would not affect the results appreciably.

f. The limits on P correspond to the estimates of Bridgman [4, 5] of the region of indifference. For the potassium halides and CsF a range of ±5kb was assumed while for the rubidium halides ±0.5kb was taken. For a few of the sc structures this uncertainty in P is the direct cause of a large part of the

uncertainty (σ_E^2) in the lattice energy. For all of the fcc and most of the sc structures its effect is subordinate to that of the unit cell size.

g. The limits on r for the sc structures were obtained directly from the X-ray diffraction data given in table 1 and were taken to be the range of the values for a_0. The limits on r for the fcc structures are more difficult to estimate and it was finally decided to assume a range of ± 0.05Å. Despite the fact that this figure may be on the high side, it represents the maximum for the sc structures which were measured directly. Although Bridgman's compression data which were used to calculate r at the transition point for the fcc phases are presumably more precise than the estimated range, it is believed that the inherent difficulties involved in measurements where both phases coexist over a wide pressure range makes the variation in r assumed here not unreasonable.

The authors are indebted to J. Mandel for valuable advice concerning the propagation of error calculations.

6. References

[1] M. Born and J. E. Mayer, Z. Physik **75,** 1 (1932).
[2] For example, see D. Cubicciotti, J. Chem. Phys. **31,** 1646 (1959); **33,** 1579 (1960); **34,** 2189 (1961).
[3] M. P. Tosi and F. G. Fumi, J. Phys. Chem. Solids **23,** 359 (1962).
[4] P. W. Bridgman, Z. Krist. **67,** 363 (1928).
[5] P. W. Bridgman, Phys. Rev. **48,** 893 (1935).
[6] P. W. Bridgman, Proc. Am. Acad. Arts Sci. **76,** 1 (1945).
[7] G. J. Piermarini and C. E. Weir, J. Chem. Phys. **37,** 1887 (1962).
[8] J. C. Slater, Proc. Am. Acad. Arts Sci. **61,** 144 (1926).
[9] R. B. Jacobs, Phys. Rev. **54,** 468 (1938).
[10] J. C. Jamieson, J. Geol. **65,** 334 (1957).
[11] G. J. Piermarini and C. E. Weir, J. Research NBS **66A,** 325 (1962).
[12] L. F. Vereschagin and S. S. Kabalkina, Akad. Nauk. SSSR Dokl. **113,** 797 (1957).
[13] L. H. Adams and B. L. Davis, Proc. Nat. Acad. Sci. **48,** 982 (1962).
[14] Standard X-Ray Diffraction Powder Patterns, NBS Cir. 539, U.S. Dept. of Commerce (U.S. Government Printing Office, Washington, D.C., 20402) **1–7.**
[15] R. W. G. Wyckoff, Crystal Structures (Interscience Publ. Inc., New York, N.Y., 1951) **1.**
[16] A. Van Valkenburg, Rev. Sci. Inst. **33,** 1462 (1962).
[17] P. W. Bridgman, Proc. Am. Acad. Arts Sci. **66,** 255 (1931).
[18] P. W. Bridgman, Proc. Am. Acad. Arts Sci., **67,** 305 (1932).
[19] Wein-Harms, Handbuch d. Experimental Physik. **8,** p. 51.
[20] M. L. Huggins, J. Chem. Phys. **5,** 143 (1937); **15,** 212 (1947).
[21] J. E. Mayer, J. Chem. Phys. **1,** 270 (1933).
[22] S. P. Clark, J. Chem. Phys. **31,** 1526 (1959).
[23] See P. W. Bridgman, The Physics of High Pressure (G. Bell & Sons Ltd., London, 1952) Ch. VIII for discussion of behavior of α and β in transitions.

(Paper 68A1–258)

JOURNAL OF RESEARCH of the National Bureau of Standards—A. Physics and Chemistry
Vol. 68A, No. 1, January–February 1964

Calculation of the Higher Order Dipole-Dipole Effect in Paramagnetic Crystals

Paul H. E. Meijer

(August 13, 1963)

This report is an attempt to investigate the influence of dipole-dipole coupling in a paramagnetic spin system at low temperatures. It consists of two parts. The first part is a discussion of the use of $C_M=C_{H=0}$ for a system with mutual interaction. It is pointed out that only if the external field is large compared to the internal field is this equation correct.

The other part consists of a calculation of higher order correction of the dipole-dipole interaction on a system of paramagnetic spins which is subject to a crystalline field which we chose of the $Y_{2,0}$ type. The total Hamiltonian consists of a spin Hamiltonian in accordance with this symmetry, a term representing the external magnetic field and the dipole-dipole interaction between the spins. The partition function is calculated by means of the Schwinger trace formula considering a representation in which the first two terms of the Hamiltonian are diagonal. The trace of the density matrix can be expressed as the trace of a product, one factor is the density matrix of the noninteracting spins, the other factor consists of a sum of commutators. These commutators are worked out in detail and the result is given in the form of a finite series over the quantum number m. There seems to be no obvious way to perform these summations.

1. Introduction

In a system of paramagnetic dipoles in a crystalline field the magnetic specific heat at constant magnetization is equal to the specific heat in zero magnetic field. This is easily seen from

$$C_M=C_H+T\left(\frac{\delta M}{\delta T}\right)_H\left(\frac{\delta H}{\delta T}\right)_M \tag{1.1}$$

and the fact that the magnetization in a system without any spatial correlation (i.e., ideal gas-like) is always proportional to H for small fields, hence M as well as (dM/dT) will go to zero if there is no field and we have $C_M=C_{H=0}$.

As a consequence of the lack of correlation $M=0$ if $H=0$, hence the relation should be $C_{M=0}=C_{H=0}$. The general question when $C_M=C_{H=0}$ is discussed in appendix 1.

If there is no crystalline field both these quantities are zero and the magnetic specific heat at constant $H\neq 0$ is merely determined by the Curie law

$$C_H=\frac{CH^2}{T^2} \tag{1.2}$$

where C is the Curie constant.

For the case of dipole-dipole interaction between the spins the value of the specific heat at constant magnetic field was calculated by Van Vleck in 1937 [1].[1] The result can be expressed in the limit of high temperatures in the form of an internal magnetic field H_i, which has an average value zero, but a root mean square value H_i, that is non-zero; then

$$C_H=\frac{C(H^2+\frac{1}{2}H_i^2)}{T^2}. \tag{1.3}$$

[1] Figures in brackets indicate the literature references on page 118.

We want to calculate C_M again, the reason being that the ratio of C_M to C_H determines among other things the real part of the susceptibility at high frequencies. The result that $C_M=C_{H=0}$ was used in the calculation of this ratio [2], although this is correct only if a Curie law holds. Although the error is not very important, at least not at external fields large compared to the internal field, there is a certain inconsistency in the fact that $H_i\neq 0$ is in contradiction with the Curie law, which assumes the total absence of any mutual interaction.

In order to reconsider the equation of state, one can draw up a modification of the Curie equation by replacing the field H by either $H+H_i$ or by $\sqrt{H^2+H_i^2}$ and then recalculating the difference between C_H and C_M again; this is not equal to zero for $H=0$. As a matter of fact it is infinitely large with the second choice

$$M=C\frac{H+H_i}{T}\rightarrow C_H-C_M=-\frac{C(H+H_i)^2}{T^2} \tag{1.4}$$

$$M=C\frac{(H^2+H_i^2)^{1/2}}{T}\rightarrow C_H-C_M=-\frac{C}{T^2}\frac{(H^2+H_i^2)^{3/2}}{H}. \tag{1.5}$$

The failure of such attempts is due to the fact that the Curie law is a high-temperature expansion in the case where the internal field is small. That is, the internal field itself is temperature dependent in such a way that it will vanish for $T\rightarrow\infty$. The difference between C_M and C_H is now

$$C_H-C_M=-\frac{CH^2}{T^2}+\frac{2H}{T^2}H_i\left(1+\frac{C}{T}\right)$$

since for high temperature H_i is small and we find that this difference goes to zero for $H=0$ and that the correction is proportional to T^{-3}. This could have been obtained in a much simpler way if one assumed the Curie-Weiss law for the magnetization

$$M=C\frac{H}{T-\theta}, \tag{1.6}$$

which leads to

$$C_H-C_M=-CH^2\frac{T}{(T-\theta)^3}. \tag{1.7}$$

The introduction of interaction between the spins is not in contradiction with the assumption that ΔC goes to zero for $H\rightarrow 0$.

The considerations above were mainly intended to provide a reasonable excuse to introduce an internal field by means of those terms in $(kT)^{-1}$ which arise from the dipole-dipole interaction. These terms can be classified in two groups, classical and quantum mechanical. The quantum mechanical terms are the result of the noncommuting of the operators. For zero external field they occur only if there is a crystalline field splitting. It is the main purpose of this work to calculate these quantum mechanical effects in the internal field. The method followed is straightforward. The effects should be observable in the "intermediate" temperature region, that is, the high temperature expansion should hold far enough down, but not too close to the Curie temperature of the dipole-dipole interaction [3].

2. Operator Expansion

We will separate the Hamiltonian into two parts: the first part, $\mathcal{H}_1=a/kT$, contains the diagonal terms, the spin Hamiltonian in the crystalline and the external field; the second part, $\mathcal{H}_2=b/kT$ is the dipole-dipole interaction. It has no diagonal terms.

The expansion of the exponential needed for the evaluation of the partition function is

$$e^{-(a+b)}=e^{-a}+\sum_{n=1}^{\infty}(-1)^n e^{-a}S_n. \tag{2.1}$$

As is well-known [compare 4] S_n contains the b-operator n times. If one actually wants to have concrete values for S_n one has to perform another expansion, this time with respect to a. The practical question is how far do we calculate this double power series. The term $e^{-a} \cdot b$ contained in S_1 is a product of a purely diagonal term and a purely nondiagonal term. Hence the trace is zero [5], which means that the average value of the field created by the dipole-dipole interaction at a certain point is zero. The field has, however, a mean square value, and the first term in S_2 is the major contribution to its value. This is a purely "classical" term in the sense that it is also nonzero for commuting operators. All first terms in S_n are classical, but since we assume that the dipole-dipole interaction is small compared to the thermal energy of the system the description on the basis of the first term in S_2 will be sufficient for the classical part as long as there is no evidence of an approaching cooperative phenomenon. Another argument for dropping the next terms is to notice that the range of the dipole-dipole interaction squared is r^{-6}, and all higher classical terms with even n-value will give rise to weak interactions of extremely short range unless the temperature is so low that a strong correlation between the spins occurs.

The expressions for S_1 and S_2 are given by

$$S_1 = \int_0^1 ds_1 b(s_1);\ S_2 = \int_0^1 ds_1 \int_0^{s_1} ds_2 b(s_1) b(s_2) \tag{2.2}$$

and expanding $b(s)$:

$$b(s) = e^{as} b e^{-as} = b + s[a, b] + \ldots \tag{2.3}$$

The result of the integration is

$$e^{-(a+b)} = e^{-a}\{1 - S_1 + S_2\} = e^{-a}(1 - b + \tfrac{1}{2}[a, b] + \tfrac{1}{6}[a[a, b]] + \tfrac{1}{2}b^2 + \tfrac{1}{6}b[a, b] + \tfrac{1}{24}b[a[a, b]] + \tfrac{1}{3}[a, b]b + \tfrac{1}{8}[a, b]^2 + \tfrac{1}{8}[a[a, b]]b. \tag{2.4}$$

None of the terms of S_1 contribute to the trace since they are the product of a number of diagonal matrices and *one* nondiagonal matrix.

The terms of S_2 up to the second order in b are

$$\frac{1}{2} b^2 + \frac{1}{6} b[a, b] + \frac{1}{3} [a, b]b. \tag{2.5}$$

It is shown in the app. 2 that the only contribution to the weighted trace is

$$\text{tr}\ \{e^{-a}\ (\tfrac{1}{2}\ b^2 + \tfrac{1}{4}\ [b[a, b]])\}. \tag{2.6}$$

3. Calculation of the Double Commutator

In order to calculate the double commutator we introduce the following notation

$$\mathcal{H}_2 = g^2\beta^2 \sum_{k \neq l} \frac{S_k S_l - 3(S_k r_{kl})(S_l r_{kl})/r_{kl}^2}{r_{kl}^3} = \sum_{\alpha, \beta} \sum_{k \neq l} S_\alpha^k \Theta_{\alpha\beta}^{kl} S_\beta^l. \tag{3.1}$$

Where the position indices are written as superscripts and the matrix Θ is given by:

$$\begin{aligned} \Theta_{11} &= g^2\beta^2(y^2 + z^2 - 2x^2)/r^5; & \Theta_{12} &= \Theta_{21} = g^2\beta^2 xy \\ \Theta_{22} &= g^2\beta^2(x^2 + z^2 - 2y^2)/r^5; & \Theta_{23} &= \Theta_{32} = g^2\beta^2 yz \\ \Theta_{33} &= g^2\beta^2(x^2 + y^2 - 2z^2)/r^5; & \Theta_{13} &= \Theta_{31} = g^2\beta^2 xz \end{aligned} \tag{3.1a}$$

leaving out all superscripts.

Since the leading part of the Hamiltonian is of the form (a, b, and c are constants)

$$\mathcal{H}_1 = \sum_{\text{positions}} aS_z^2 + bS_z + c \tag{3.2}$$

we have to calculate the commutators C_n and double commutators D_n:

$$C_n=[S_\beta, (S_z)^n] \text{ and } D_n=[S_\alpha, [S_\beta, (S_z)^n]], \tag{3.3}$$

where all spins are at the same location. In order to avoid confusion with the superscripts, which have been omitted, the powers are placed outside parentheses. Table 1 shows that there are four nonzero values of D_1. However two have zero's in the diagonal, hence if multiplied by the (diagonal) weight factor only $\alpha=\beta=x$ or y will give a contribution. The same holds for D_2. The trace of the two elements of C is $\hbar^2 m$. The trace of the two elements of D is $-\hbar^3[3m^2-S(S+1)]$. This has to be inserted in the multiple sum over all positions containing two Θ's and multipled by the weight factor exp $(\mathcal{H}_1/kT)$.

Since both Hamiltonians are series over all positions and since all commutators with respect to two different positions are zero we have to figure out in which ways these two summations can "overlap". The first commutator gives $(k\neq l)$:

$$[\mathcal{H}_2, \mathcal{H}_1]=a\sum_{klm}\Big[\sum_{\alpha\beta} S_\alpha^k \Theta_{\alpha\beta}^{kl} S_\beta^l, (S_z^m)\Big]+b\sum_{klm}\Big[\sum_{\alpha\beta} S_\alpha^k \Theta_{\alpha\beta}^{kl} S_\beta^l, (S_z^m)^2\Big]. \tag{3.4}$$

The summation over m contains only two terms $m=k$ and $m=l$. These terms are equal since the matrix Θ is symmetric in both the upper and lower indices and since $k\neq l$ the operators commute.

$$[\mathcal{H}_2, \mathcal{H}_1]=2a\sum_{k\neq l}\sum_{\alpha,\beta}[S_\alpha^k, S_z^k]\Theta_{\alpha\beta}^{kl}S_\beta^l+2b\sum_{k\neq l}\sum_{\alpha\beta}[S_\alpha^k, (S_z^k)^2]\Theta_{\alpha\beta}^{kl}S_\beta^l. \tag{3.5}$$

The double commutator introduces a sum over four positions, say k, $l(k\neq l)$ and i, $j(i\neq j)$. There are six different terms (table 2). The first four give all the same contribution because of the symmetry of Θ mentioned above, and so do the last two. Writing for short

$$f(S_z^m)=a(S_z^m)^2+b(S_z)$$

we have

$$\begin{aligned}[[\mathcal{H}_2, [\mathcal{H}_2, \mathcal{H}_1]]=\sum_{\substack{\alpha\beta\\ \alpha'\beta'}}\Big(8\sum_{\substack{jkl\\ \text{all different}}}\{&[S_\alpha^k,[S_{\alpha'}^k, f(S_z^k)]]\Theta_{\alpha\beta}^{kj}\Theta_{\alpha'\beta'}^{kl}S_\beta^j S_{\beta'}^l\\ &+[S_\alpha^k, S_{\alpha'}^k]\Theta_{\alpha\beta}^{kj}\Theta_{\alpha'\beta'}^{kl}[S_{\beta'}^l, f(S_z^l)]S_\beta^j\}+4\sum_{k\neq l}\{S_{\alpha'}^k[S_\alpha^k, f(S^k)]\Theta_{\alpha\beta}^{kl}\Theta_{\alpha'\beta'}^{kl}[S_{\beta'}^l, S_\beta^l]\\ &+[S_{\alpha'}^k, [S_\alpha^k, f(S^k)]]\Theta_{\alpha\beta}^{kl}\Theta_{\alpha'\beta'}^{kl}S_{\beta'}^l S_\beta^l-[S_{\alpha'}^k, [S_\alpha^k, f(S^k)]]\Theta_{\alpha\beta}^{kl}\Theta_{\alpha'\beta'}^{kl}[S_{\beta'}^l, S_\beta^l]\}\Big),\end{aligned} \tag{3.6}$$

TABLE 1

$D_1/(i\hbar)^2$

	x	y	z
x	$-S_z$	0	0
y	0	$-S_z$	0
z	S_x	S_y	0

$D_2/(i\hbar)^2$

	$\beta=x$	y	z
$\alpha=x$	$2(S_x^2-S_y^2)$	$-(S_yS_x+S_xS_y)$	0
y	$(S_xS_y+S_yS_x)$	$2(S_x^2-S_y^2)$	0
z	$-(S_zS_x+S_xS_z)$	$(S_zS_y+S_yS_z)$	0

TABLE 2

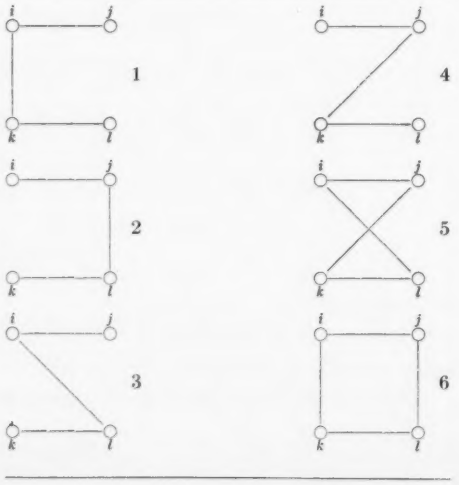

using for the second set of terms the following commutator identity:

$$[AB, CD]=AC[BD]+[AC]BD-[AC][BD]$$

if only

$$[AC]\neq 0 \text{ and } [BD]\neq 0$$

and all other commutators are zero. Only the diagonal part of this double commutator contributes to the partition sum, and as a result of this the summation over α, β, α' and β' has a number of restrictions:

First term: $\alpha=\alpha'=x$ or y; $\beta=\beta'=z$.

Second term is always zero since $[S_\beta, f(S_z)]$ has no diagonal elements for every β'.

Third term: α, $\alpha'=x$ or y, and β, $\beta'=x, y$ or y, x.

Fourth term: $\alpha=\alpha'=x$ or y and β', $\beta=z$. In case it is x, y it will be canceled by the diagonal contribution from y, x.

Fifth term: $\alpha=\alpha'=x$ or y and β', $\beta=x, y$ or y, x.

The diagonal parts of the spin operators to the second power are:

$$(S_x^2)_D=(S_y^2)_D=\tfrac{1}{2}[S(S+1)-S_z^2]$$

$$(S_xS_y)_D=-(S_yS_x)_D=\frac{\hbar S_z}{2i}$$

and using table 1 we find (combining the first and fourth term):

$$[\mathcal{H}_2, [\mathcal{H}_2, \mathcal{H}_1]]_{\text{Diag.}}=8\sum_{\substack{k\neq j\\ k\neq l}}(i\hbar)^2\left\{\frac{a}{2}[3(S_z^k)^2-(S^k)^2](\Theta_{xz}^{kj}\Theta_{xz}^{kl}-\Theta_{yz}^{kj}\Theta_{yz}^{kl})S_z^jS_z^l\right.$$

$$\left.+bS_z^k(\Theta_{xz}^{kj}\Theta_{xz}^{kl}+\Theta_{yz}^{kj}\Theta_{yz}^{kl})S_z^jS_z^l\right\}+\sum_{\substack{\alpha\beta\\ \alpha'\beta'}}4\sum_{k\neq l}\Big([S_\alpha^k, f(S^k)]S_{\alpha'}^k\Theta_{\alpha\beta}^{kl}\Theta_{\alpha'\beta'}^{kl}[S_{\beta'}^l, S_\beta^l]\Big). \quad (3.7)$$

The last term is calculated with the help of

$$[S^\pm, S_z^2]S^\mp=(\mp 2\hbar S_z+\hbar^2)S^\pm S^\mp+\hbar^2(S^2-3S_z^2)\pm\hbar^3S_z\mp 2\hbar S_z(S^2-S_z^2). \quad (3.8)$$

The summation over α, β, α', β' contains 8 terms. It turns out, however, that 4 cancel mutually: if α and β are equal (both x or both y) the subscripts $\alpha'\beta'$ are either x and y or y and x. Both have the same coefficient $\Theta_{xx}^{kl}\Theta_{xy}^{kl}$ but the commutators have the opposite sign. The fact that these cancel could have been seen on the following general grounds. A commutator is anti-Hermitian and a double commutator is Hermitian. Hence the last factor has imaginary diagonal elements and the total expression has real diagonal elements, and the first factor must have an imaginary diagonal part:

$$[S_y, f(S_z)^2]S_x=-[S_x, f(S_z)]S_y$$

$$=\frac{i}{4}([S^+, f(S_z)]S^--[S^-, f(S_z)]S^+$$

$$=-\frac{i}{2}[a\{2\hbar S_z(S^2-S_z^2)-\hbar^3S_z\}+b\hbar(S^2-S_z^2)]. \quad (3.9)$$

The final result for the last term is:

$$4\sum_{k\neq l}\hbar^2[(\Theta_{xz}^{kl}\Theta_{yy}^{kl})-(\Theta_{xy}^{kl})^2][2aS_z^2(S^2-S_z^2-\tfrac{1}{2}\hbar^2)+bS_z(S^2-S_z^2)]. \quad (3.10)$$

In order to obtain a value for the partition functions the trace has to be calculated numerically since the sums of the type

$$\sum\nolimits_p=\sum_{m=-S}^{S}m^pe^{am^2+bm} \qquad (p=0, 1, 2, 3) \quad (3.11)$$

cannot be evaluated in closed form.

4. Conclusion

The complication of the calculation lies mainly in the fact that the commutator of two spin operators is not a c-number but again an operator. This makes many tricks used to evaluate exponential operators useless. For instance, one could have written the original total Hamiltonian with step up and step down operators S^+ and S^-. The expansion of the exponential would have created a polynomial containing S^+, S^- and S_z to certain powers. A general conclusion is that only those terms which contain an equal number of S^+ and S^- at the same location will have a nonzero diagonal element. To calculate the actual value, however, one has to shift the S^+ and S^- operator such that they are all at the end or the beginning of the monomial and in conjunction to each other. This rearrangement of operations is accomplished with the help of Wick's theorem if we deal with creation and annihilation operations. It is still possible to formulate a Wick-like theorem for spin one-half. This was done by Kenan [6]. It introduces an additional numerical factor into each diagram. For spin not equal to one-half, his treatment fails. The crucial point is that only for spin one-half is $(S_z)^2$ a c-number. Otherwise S_z is an operator and hence can not be taken outside the trace and the contraction operator cannot be defined. These considerations indicate that it seems unavoidable to calculate the trace straightforwardly. Actually the straightforward calculation consists of doing the same steps as in the Wick-theorem.

Finally, the summation of the positions has to be performed. It is possible to restrict this to the immediate environment since the radial dependence decreases very rapidly.

5. References and Notes

[1] J. H. Van Vleck, J. Chem. Phys. **5,** 320 (1937).

[2] L. J. F. Broer, Considerations and measurements on paramagnetic relaxation (North-Holland Publishing Co., Amsterdam, 1945). Part of this work is reviewed in C. J. Gorter, Paramagnetic relaxation (Elsevier, Amsterdam, 1947).

[3] Another restriction is that the spin-Hamiltonian contains only S_z and the external field is in that direction. Or to formulate the same statement more generally: the spin-Hamiltonian and the field can be diagonalized simultaneously.

[4] See for instance references given in R. Bellman, Introduction to matrix analysis (McGraw Hill, New York, 1960), p. 178.

[5] That is if we take the partial trace of b or H_2. Each term in H_2 contains two traces, one over the $2S+1$ states connected with k, one over the $2S+1$ states connected with l. If one, say k, coincides with a certain point in a or H_1, which is a sum over positions, then the trace with respect to l gives zero.

[6] R. P. Kenan, A generalized molecular-field theory of antiferromagnetism. Thesis: The Ohio State University, 1962.

6. Appendix 1

We want to investigate under what conditions $C_M=C_{H=0}$ for arbitrary H. To calculate the specific heat at constant H we find from the Maxwell relation $\partial S/\partial H=\partial M/\partial T$

$$C_H=T\int_0^H \frac{\partial^2 M}{\partial T^2}\,dH+C_{H=0}$$

the second term at the right-hand side of (11) is

$$C_M=C_H+T\left(\frac{\partial M}{\partial T}\right)^2\Big/\frac{\partial M}{\partial H}$$

and the condition $C_M=C_{H=0}$ gives

$$T\int_0^H \frac{\partial^2 M}{\partial T^2}\,dH=T\left(\frac{\partial M}{\partial T}\right)^2\Big/\frac{\partial M}{\partial H}$$

which leads to the differential equation

$$\left(\frac{\partial M}{\partial H}\right)^2 \frac{\partial^2 M}{\partial T^2} - 2 \frac{\partial^2 M}{\partial T \partial H} \frac{\partial M}{\partial T} \frac{\partial M}{\partial H} + \left(\frac{\partial M}{\partial T}\right)^2 \frac{\partial^2 M}{\partial H^2} = 0$$

which is fulfilled by

$$M = f\left(\frac{H+c_1}{T+c_2}\right) - f\left(\frac{C_1}{C_2}\right)$$

where f is an arbitrary function and c_1 and c_2 two constants. The initial condition forces us to take $c_1=0$. For kT larger than the crystal field splitting this condition is fulfilled.

7. Appendix 2

From the sum and difference

$$b[a,b]+[a,b]b=ab^2-b^2a \qquad b[a,b]-[a,b]b=[b,[a,b]]$$

we find

$$b[a,b]=\tfrac{1}{2}[b,[a,b]]+\tfrac{1}{2}ab^2-\tfrac{1}{2}b^2a \qquad [a,b]b=\tfrac{1}{2}[b,[a,b]]-\tfrac{1}{2}ab^2+\tfrac{1}{2}b^2a.$$

Hence the relevant terms in (2.5) are

$$\tfrac{1}{6}b[a,b]+\tfrac{1}{3}[a,b]b=\tfrac{1}{12}[b,[a,b]]+\tfrac{1}{12}ab^2-\tfrac{1}{12}b^2a+\tfrac{1}{6}[b,[a,b]]-\tfrac{1}{6}ab^2+\tfrac{1}{6}b^2a=\tfrac{1}{4}[b,[a,b]]-\tfrac{1}{12}ab^2+\tfrac{1}{12}b^2a.$$

Since a is diagonal we have

$$\text{tr.}\{(f(a)ab^2)\}=\text{tr.}\{(f(a)b^2a)\},$$

hence the contribution to the trace is

$$\text{tr.}\{f(a)\tfrac{1}{4}[b[a,b]]\}.$$

(Paper 68A1–259)

JOURNAL OF RESEARCH of the National Bureau of Standards—A. Physics and Chemistry
Vol. 68A, No. 1, January-February 1964

Second and Third Virial Coefficients for Hydrogen

R. D. Goodwin, D. E. Diller, H. M. Roder, and L. A. Weber

Cryogenic Engineering Laboratory, National Bureau of Standards, Boulder, Colo.

(August 15, 1963)

Second and third virial coefficients for parahydrogen have been derived from closely spaced PVT data from 24 to 100 °K. They are in good agreement at 100 °K with published data for normal hydrogen. Analytical representations of the combined data from about 20 to 423 °K are presented which may be useful in computation of thermodynamic functions of the gas. These formulas are related to those resulting from the use of the Lennard-Jones potential.

1. Introduction

As part of an extensive program for determining the thermodynamic and transport properties of fluid parahydrogen, we have recently published new data on the P–V–T surface from 15 to 100 °K [1].[1] Earlier, we gave preliminary values of the second and third virial coefficients, $B(T)$ and $C(T)$, in a paper describing the apparatus [2].

In this paper we present final values of the virial coefficients derived from the smoothed compressibility data [1]. These differ but slightly from the preliminary values. Also we present and examine analytical representations of $B(T)$ and $C(T)$ which may be useful for computing thermodynamic functions of the gas.

In a forthcoming paper [3] we have used the following arbitrary representations [4] to fit our closely spaced data in order to facilitate computations of thermofunctions below 100 °K:

$$B=\sum_{i=0}^{3} b_i T^{-i}; \qquad C=\sum_{i=1}^{4} c_i T^{-i}.$$

On the other hand, in this paper use is made of other published virial coefficients as well as those from this laboratory to provide a more extensive tabulation from about 20 to 423 °K to which are fitted expressions having forms suggested by the use of the Lennard-Jones potential. All coefficients were determined by the method of least squares.

2. Derivation of the Virial Coefficients

The virial expansion [5] may be rearranged to a form which, when truncated, is linear in density on isotherms, convenient for graphical or analytical determination of the second and third coefficients,

$$\Phi\equiv(Pv-RT)v=RTB+RTC/v+ \ldots . \qquad (1)$$

Parameters RTB and RTC of eq (1) as truncated have been determined on isotherms by least-squares using the reported compressibility data [1] and the orthobaric densities [6]. The number of datum pairs, n, on each isotherm is given in column (a) of table 1. It was found by trial that data for densities above 0.007 g mol/cm^3 diverge from the linear behavior of eq (1). These data were omitted, with the result that a maximum of eight points per isotherm were applicable above 29 °K. (The above maximum density for validity of eq (1) with only two terms is less than half the critical density of 0.0156 g mol/cm^3 [6].) Derived values of B and C are given in tables 2 and 3, respectively, at integral temperatures from 24 through 100 °K.

Equation (1) also was used for smoothing and interpolation of compressibility data to the highest densities by admitting as many terms as required by the experimental precision [1]. At temperatures below critical (32.98 °K), a single isotherm of eq (1) was used to represent both vapor and compressed liquid. The number of datum pairs, n', and number of terms, N, in polynomial (1) are given in column (b) of table 1 which includes also the maximum density multiplied by 10^3 for each isotherm. With increasing number of terms, the mean deviation decreases more at an odd number than at an even number of terms. Since coefficients of the higher-order terms of these divergent, alternating polynomials show no regular temperature-dependence, the expansions cannot be interpreted as virial equations [7]. Nevertheless, values of B and C obtained in this way are presented in appendix, table 1, to meet the commonplace question of the effect upon them of an increased number of terms in eq (1). It may be seen that values of B are essentially the same as in table 2. Values of C, while of similar magnitude to those in table 3, scatter badly.

[1] Figures in brackets indicate the literature references at the end of this paper.

JOURNAL OF RESEARCH of the National Bureau of Standards—A. Physics and Chemistry
Vol. 68A, No. 1, January-February 1964

Second and Third Virial Coefficients for Hydrogen

R. D. Goodwin, D. E. Diller, H. M. Roder, and L. A. Weber

Cryogenic Engineering Laboratory, National Bureau of Standards, Boulder, Colo.

(August 15, 1963)

Second and third virial coefficients for parahydrogen have been derived from closely spaced PVT data from 24 to 100 °K. They are in good agreement at 100 °K with published data for normal hydrogen. Analytical representations of the combined data from about 20 to 423 °K are presented which may be useful in computation of thermodynamic functions of the gas. These formulas are related to those resulting from the use of the Lennard-Jones potential.

1. Introduction

As part of an extensive program for determining the thermodynamic and transport properties of fluid parahydrogen, we have recently published new data on the P–V–T surface from 15 to 100 °K [1].[1] Earlier, we gave preliminary values of the second and third virial coefficients, $B(T)$ and $C(T)$, in a paper describing the apparatus [2].

In this paper we present final values of the virial coefficients derived from the smoothed compressibility data [1]. These differ but slightly from the preliminary values. Also we present and examine analytical representations of $B(T)$ and $C(T)$ which may be useful for computing thermodynamic functions of the gas.

In a forthcoming paper [3] we have used the following arbitrary representations [4] to fit our closely spaced data in order to facilitate computations of thermofunctions below 100 °K:

$$B=\sum_{i=0}^{3} b_i T^{-i}; \qquad C=\sum_{i=1}^{4} c_i T^{-i}.$$

On the other hand, in this paper use is made of other published virial coefficients as well as those from this laboratory to provide a more extensive tabulation from about 20 to 423 °K to which are fitted expressions having forms suggested by the use of the Lennard-Jones potential. All coefficients were determined by the method of least squares.

2. Derivation of the Virial Coefficients

The virial expansion [5] may be rearranged to a form which, when truncated, is linear in density on isotherms, convenient for graphical or analytical determination of the second and third coefficients,

$$\Phi\equiv(Pv-RT)v=RTB+RTC/v+ \ldots . \qquad (1)$$

Parameters RTB and RTC of eq (1) as truncated have been determined on isotherms by least-squares using the reported compressibility data [1] and the orthobaric densities [6]. The number of datum pairs, n, on each isotherm is given in column (a) of table 1. It was found by trial that data for densities above 0.007 g mol/cm^3 diverge from the linear behavior of eq (1). These data were omitted, with the result that a maximum of eight points per isotherm were applicable above 29 °K. (The above maximum density for validity of eq (1) with only two terms is less than half the critical density of 0.0156 g mol/cm^3 [6].) Derived values of B and C are given in tables 2 and 3, respectively, at integral temperatures from 24 through 100 °K.

Equation (1) also was used for smoothing and interpolation of compressibility data to the highest densities by admitting as many terms as required by the experimental precision [1]. At temperatures below critical (32.98 °K), a single isotherm of eq (1) was used to represent both vapor and compressed liquid. The number of datum pairs, n', and number of terms, N, in polynomial (1) are given in column (b) of table 1 which includes also the maximum density multiplied by 10^3 for each isotherm. With increasing number of terms, the mean deviation decreases more at an odd number than at an even number of terms. Since coefficients of the higher-order terms of these divergent, alternating polynomials show no regular temperature-dependence, the expansions cannot be interpreted as virial equations [7]. Nevertheless, values of B and C obtained in this way are presented in appendix, table 1, to meet the commonplace question of the effect upon them of an increased number of terms in eq (1). It may be seen that values of B are essentially the same as in table 2. Values of C, while of similar magnitude to those in table 3, scatter badly.

[1] Figures in brackets indicate the literature references at the end of this paper.

TABLE 1. *Number of datum pairs,* n, *and of terms* N, *for eq (1)*

T, °K	[a]	[b]			T, °K	[a]	[b]		
	n	n'	N	$10^3/v_{min}$		n	n'	N	$10^3/v_{min}$
24	3	24	9	44.1	40	8	45	11	40.4
					42	8	42	11	40.3
25	3	25	9	44.1	44	8	41	9	39.7
26	4	25	9	43.8	46	8	40	9	39.1
27	5	27	9	43.8	48	8	39	9	38.4
28	6	29	9	43.4					
29	7	31	9	43.4	50	8	38	9	37.6
					55	8	37	9	36.6
30	8	33	11	42.9	60	8	36	9	35.9
31	8	35	13	42.9	65	8	34	9	34.6
32	8	38	13	42.5	70	8	33	7	34.0
33	8	47	15	42.4					
34	8	48	13	42.0	75	8	30	7	31.8
					80	8	29	7	30.8
35	8	48	11	42.0	85	8	28	7	29.8
36	8	47	11	41.5	90	8	27	7	28.9
37	8	47	11	41.5	95	8	26	5	28.1
38	8	46	11	40.9					
39	8	46	11	40.9	100	8	24	5	26.6

[a] For $N=2$ and $0.001 \leq 1/v \leq 0.007$ g mol/cm³.
[b] To the highest experimental densities, $10^3/v_{min}$.

TABLE 2. *Derived and calculated values of* B, *cm³/g mol*

T, °K	Derived	Calculated		T, °K	Derived	Calculated	
		(2a)	(2b)			(2a)	(2b)
15		−219.4	−222.3	50	−33.39	−33.25	−33.47
16	−204.2	−200.8	−202.8	55	−27.48	−27.29	−27.53
17		−184.7	−186.1	60	−22.70	−22.43	−22.67
18	−172.9	−170.6	−171.5	65	−18.64	−18.40	−18.63
19		−158.2	−158.7	70	−15.22	−15.01	−15.23
20	−148.8	−147.1	−147.4	75	−12.42	−12.13	−12.32
21		−137.2	−137.4	80	−9.88	−9.65	−9.82
22	−129.7	−128.4	−128.4	85	−7.63	−7.50	−7.63
23		−120.3	−120.3	90	−5.66	−5.61	−5.72
24	−112.8	−113.1	−113.0	95	−3.99	−3.95	−4.02
25	−106.2	−106.5	−106.3	98.15	−3.06	−2.99	−3.05
26	−100.3	−100.4	−100.3	100	−2.52	−2.47	−2.51
27	−94.80	−94.88	−94.74	103.15	−1.69	−1.62	−1.65
28	−89.66	−89.78	−89.65	113.15	+0.67	+0.73	+0.75
29	−85.03	−85.08	−84.96	123.15	2.63	2.65	2.73
30	−80.73	−80.72	−80.62	138.15	5.01	4.96	5.09
31	−76.75	−76.68	−76.60	153.15	6.89	6.76	6.94
32	−72.99	−72.93	−72.86	173.15	8.84	8.62	8.85
33	−69.53	−69.43	−69.39	198.15	10.65	10.37	10.62
34	−66.22	−66.16	−66.14	223.15	11.98	11.68	11.93
35	−63.17	−63.09	−63.10	248.15	12.97	12.70	12.94
36	−60.26	−60.22	−60.25	273.15	13.76	13.51	13.72
37	−57.54	−57.53	−57.58	298.15	14.38	14.17	14.34
38	−54.99	−54.99	−55.06	323.15	14.87	14.71	14.85
39	−52.60	−52.60	−52.69	348.15	15.27	15.17	15.25
40	−50.32	−50.34	−50.45	373.15	15.60	15.56	15.59
42	−46.19	−46.19	−46.33	398.15	15.86	15.90	15.87
44	−42.50	−42.46	−42.62	423.15	16.08	16.19	16.10
46	−39.18	−39.09	−39.28				
48	−36.17	−36.03	−36.24				

Uncertainty in B, estimated from eq (1) for low densities, is

$$\delta B = [2Z - 1 + C/v^2]\,\delta v - vZ\delta T/T \qquad (1a)$$

where $Z \equiv Pv/RT$, or approximately

$$\delta B \approx v[\delta v/v - \delta T/T]. \qquad (1b)$$

Experimental uncertainty in v was estimated to be 0.2 percent at low densities [2]. Examination of the sensitivity of the shape of isotherms of $(Pv-RT)v$ to errors in density, however, indicates a precision near 0.02 percent. This is illustrated by figure 1

TABLE 3. *Derived and calculated third virial coefficients*

T, °K	C, (cm³/g mol)²		T, °K	C, (cm³/g mol)²	
	Derived	Calc'd.		Derived	Calc'd.
20	----------	−405	50	964	968
21	----------	+218	55	889	893
22	----------	680	60	838	835
23	----------	1018	65	785	789
24	1207	1259	70	743	750
25	1402	1425	75	726	718
26	1580	1533	80	694	690
27	1627	1596	85	659	665
28	1612	1625	90	636	643
29	1615	1629	95	624	624
30	1600	1614	98.15	530	613
31	1585	1586	100	609	606
32	1550	1549	103.15	560	596
33	1516	1507	113.15	540	567
34	1466	1463	123.15	560	542
35	1426	1418	138.15	540	510
36	1377	1373	153.15	522	483
37	1331	1330	173.15	500	454
38	1290	1290	198.15	458	424
39	1252	1251	223.15	437	399
40	1209	1215	248.15	415	378
42	1144	1151	273.15	404	360
44	1091	1095	298.15	370	345
46	1046	1047	323.15	340	331
48	1005	1005	348.15	313	319
			373.15	303	308
			398.15	310	298
			423.15	302	289

in which the upper curve is an experimental linear isotherm, and the lower curve shows the effect of an artificially introduced error of 0.263 percent in density [2]. As a further illustration figure 2 gives deviations of the data from the least-squared, truncated virial expression at 44 °K and compares these with the boundary for a deviation of ±0.02 percent in density. From such considerations, the precision of these lowest experimental densities appears to be within 0.03 percent. Since this applies to all isotherms, the corresponding error in B should be roughly independent of temperature. For the lowest density, $v=1000$ cm³/g mol; uncertainty in B thus is estimated to be about 0.3 cm³/g mol. Systematic deviations in the temperature-dependence of B, on the other hand, may be sought in absolute deviations of the NBS temperature scale for platinum resistance. For $\delta T=0.02$ °K, $v=1000$ cm³/g mol, and $25° \leq T \leq 100$ °K, the range of uncertainty is $0.8 \leq \delta B \leq 0.2$ cm³/g mol.

Since B is derived as the intercept of linear plots of $(Pv/RT-1)v$ versus $1/v$, it may be seen that all of the above arguments for precision apply equally to absolute errors in v or in T. Absolute uncertainty in B therefore is estimated to be in the range 1.1 cm³/g mol at 25 °K to 0.5 cm³/g mol at 100 °K.

To the above virial coefficients for parahydrogen from 24 to 100° in tables 2 and 3 have been added values for normal hydrogen at higher and lower temperatures in order to provide a more extensive set. Of the published values of virial coefficients for normal hydrogen [4, 8, 9, 10, 11, 12], values from Woolley, Scott, and Brickwedde [9] below 24 °K are included in table 2, while values from Michels, de Graaff, and Ten Seldam [10] at nonintegral temperatures above 98 °K are given in tables 2 and

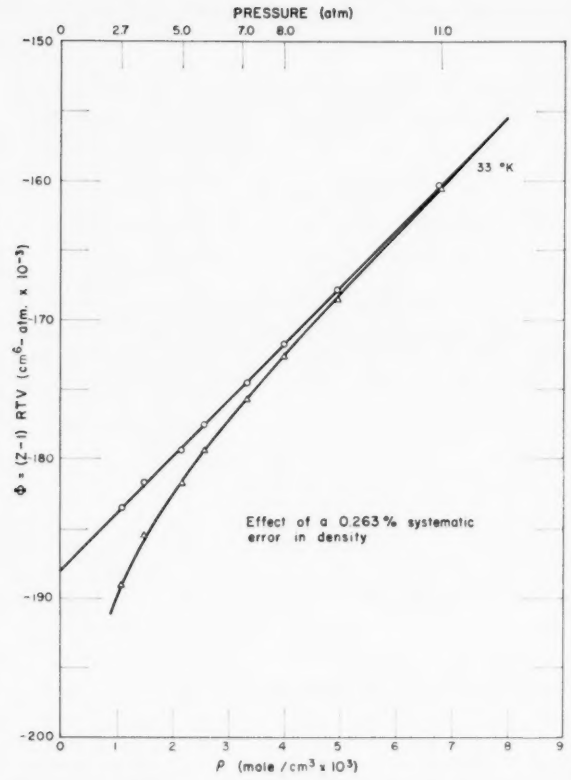

FIGURE 1. *Effect of systematic error in density [2] upon the linear behavior of eq. (1), for the 33 °K isotherm.*

The notation is $Z \equiv Pv/RT$. Circles: experimental linear isotherm. Triangles: same data with artifically introduced error of 0.263 percent.

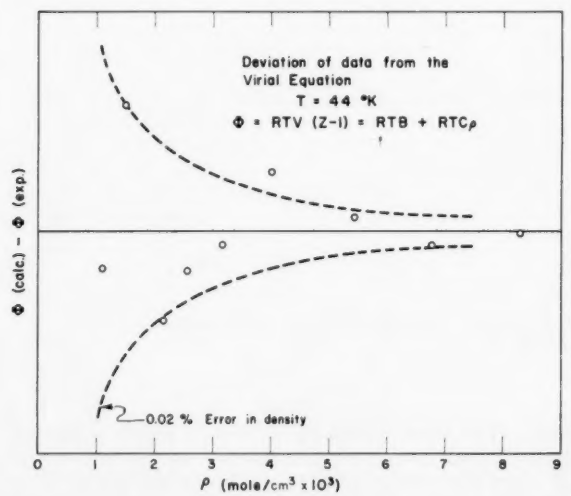

FIGURE 2. *Deviations of data,* $\Phi \equiv (Z-1)RTv$, *where* $Z \equiv Pv/RT$, *from eq. (1) at 44 °K.*

Dashed lines correspond to ±0.02 percent systematic error in density.

3. Uncertainty of the data of Michels et al., was estimated by them to be 0.15 cm³/g mol in B, and about 15 percent in C. Excellent agreement of the independent data at 100 °K suggests that the virial coefficients of these hydrogen modifications may be indistinguishable at this and higher temperatures. Small differences have been detected at lower temperatures [13].

3. Representation of Second Virial Coefficient

Figure 3 presents the derived data of table 2 as a function of $T^{-5/4}$. The data for normal hydrogen at low temperatures are seen to deviate from the straight line extrapolated from the parahydrogen data, in agreement with the experimental comparison of the two modifications made by Beenakker et al. [13].

Systematic deviations persist with all analytical representations which have been investigated for the temperature-dependence of B. It therefore does not appear possible to select a form which is best for all purposes from among the following two, which utilize two and four constants, respectively, with notation $x \equiv T_0/T$:

$$B = B_0[1 - x^{5/4}], \qquad T_0 = 109.83\ °\text{K},$$

$$B_0 = 19.866\ \text{cm}^3/\text{g mol}, \qquad \Delta = 0.125\ \text{cm}^3/\text{g mol}. \quad (2a)$$

$$B = \sum_{i=1}^{4} B_i x^{(2i-1)/4}, \qquad T_0 = 109.781\ °\text{K},$$

$$B_1 = +42.464, \qquad B_2 = -37.1172,$$

$$B_3 = -2.2982, \qquad B_4 = -3.0484,$$

$$\Delta = 0.066\ \text{cm}^3/\text{g mol}. \quad (2b)$$

Mean deviations, given for each equation above, are defined as

$$\Delta \equiv (n-N)^{-1} \sum^{n} |B - B_{\text{calc}}|,$$

wherein $n=49$ is the number of datum pairs, and N is the number of constants in the equation. Calculated results from these equations are given in table 2, and the individual deviations are plotted in figure 4.

The form of (2a) is that used by Keesom for helium [14], the constant high-temperature limit corresponding to the rigid-sphere model for molecular interaction [5]. The value of B_0 in (2a) is comparable with the volume 22.65 cm³/g mol of solid normal hydrogen at 4.2 °K [9]. The rather good fit provided by this simple equation is indicated by figure 3. Equation (2b) consists of the leading terms of an expansion derived from the Lennard-Jones potential [5]. Appendix, table II, gives coefficients for that expansion with increasing number of terms. (The form of the expansion given in

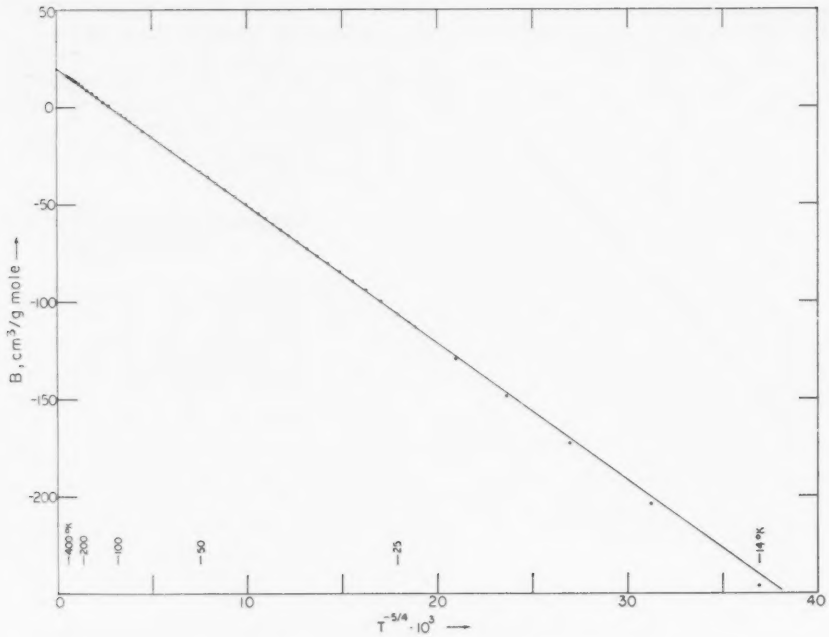

FIGURE 3. *Second virial coefficient,* B, *versus* $T^{-5/4}$.

Open circles are for parahydrogen. Filled circles for normal hydrogen below 24 °K are from [9] and above 100 °K from [10].

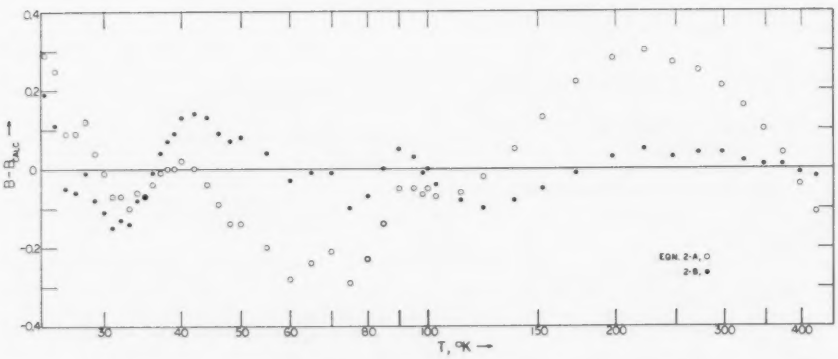

FIGURE 4. *Deviations of second virial coefficient,* B, *in cm³/g mol, from eq (2a), open circles and from (2b), filled circles.*

the appendix does not include the root, T_0.) It is seen that four terms give an acceptable representation. Whereas use of additional terms improves the fit, the similarity in form of the two sets of deviations in figure 4 suggests the presence of systematic experimental errors. If such errors are present, it is doubtful that use of higher terms would be justified. The form of the deviations in figure 4 having been found also with analytical representations of B other than polynomials, it is improbable that they arise from the selected polynomial forms of (2a) and (2b). It appears equally improbable that they arise entirely from deviations of the NBS temperature scale used.

4. Representation of Third Virial Coefficient

The Lennard-Jones potential yields an expansion in powers of $T^{-1/2}$ [5]. From this key, eq (3) was evolved, using notation $x \equiv T_0/T$,

$$C = C_0 x^{1/2}[1 + cx^3]\,[1 - \exp\,(1 - x^{-3})],$$
$$T_0 = 20.615\ °\text{K}, \qquad C_0 = 1310.5\ (\text{cm}^3/\text{g mol})^2,$$
$$c = 2.1486, \qquad \Delta = 17.4\ (\text{cm}^3/\text{g mol})^2. \quad (3)$$

It represents the third virial coefficient within the apparent precision of the data. The last factor on the right of (3) differs significantly from unity only at temperatures below 40 °K. Calculated values of C are given in table 3.

The series

$$C = \sum_{i=1}^{n} C_i T^{-i/2} \quad (3a)$$

requires at least six terms to give a better representation than eq (3). The alternating series obtained by least-squares, however, are highly divergent; for example, the fifth term for $N=6$ exceeds the value of C by factor 240 at 24 °K.

5. Note on Two-Term Representations

The behavior of plots of $y \equiv B$ or C as functions of $x \equiv T_0/T$ suggests an empirical relation of the form

$$y/y_0 = x^{\mu} - x^{\nu} \quad (4)$$

with constants $\mu < \nu$. The limitations of (4) having been examined in obtaining (2) and (3) above, it is reasonable next to examine the relation

$$y/y_0 = \exp\,(kx^{\mu}) - \exp\,(kx^{\nu}). \quad (4a)$$

Since the five parameters in (4a) must be found tediously by trial, the exploration has been discontinued with preliminary results in the following table. It is concluded that (4a) may be sufficiently flexible to offer promise of accurate representations of both B and C.

y	μ	ν	k	T_0	y_0	n	Δ
B	¼	½	0.6	110.9	92.18	49	0.20
C	½	1	4	20	135	32	55

$$\Delta \equiv (n-3)^{-1}\sum^{n}|y - y_{\text{calc}}|.$$

Robert J. Corruccini and Paul F. Wacker of this laboratory made numerous suggestions for improving the manuscript, for which the authors are most appreciative. This work was supported by the National Aeronautics and Space Administration.

6. Appendix

TABLE I. *Virial coefficients from extended isotherms of eq (1)*

T, °K	B, cm³/g mol	C, cm³/g mol²	T, °K	B, cm³/g mol	C, cm³/g mol²
24	−115.3	5601	40	−50.18	1027
			42	−46.02	919
25	−106.5	1952	44	−42.54	1134
26	−101.1	2736	46	−39.25	1108
27	−95.01	2032	48	−36.28	1103
28	−90.36	2624			
29	−85.72	2561	50	−33.49	1050
			55	−27.67	1068
30	−80.96	1725	60	−22.93	1057
31	−77.24	2180	65	−18.77	906
32	−73.69	2042	70	−15.30	809
33	−69.14	554			
34	−66.27	1549	75	−12.57	854
			80	−9.96	767
35	−63.29	1537	85	−7.58	615
36	−60.30	1402	90	−5.57	559
37	−57.51	1280	95	−4.00	637
38	−55.04	1335			
39	−52.66	1321	100	−2.52	620

TABLE II. *Polynomial coefficients in Lennard-Jones expansion for second virial coefficient*

$$B = \sum_{i=1}^{N} b_i T^{-(2i-1)/4}, \text{ (cm}^3\text{/g mol)}. \quad (2b)$$

N / b_i	3	4	5	6
b_1	+1.18579. 10^2	+1.37452. 10^2	+1.45098. 10^2	+1.20054. 10^2
b_2	−7.32017. 10^2	−1.25884. 10^3	−1.55190. 10^3	−3.70405. 10^3
b_3	−5.21897. 10^3	−8.16662. 10^3	+3.04443. 10^3	−1.78006. 10^4
b_4		−1.13500. 10^4	−3.24136. 10^4	+1.41284. 10^4
b_5			+4.07085. 10^4	−6.48921. 10^4
b_6				+1.05121. 10^5
Δ	0.2991	0.0664	0.0615	0.0408

7. References

[1] R. D. Goodwin, D. E. Diller, H. M. Roder, and L. A. Weber, Pressure-density-temperature relations of fluid parahydrogen from 15 to 100 °K at pressures to 350 atm, J. Res. NBS **67A** (Phys. and Chem.) No. 2, 173 (1963).

[2] R. D. Goodwin, Apparatus for determination of pressure-density-temperature relations and specific heats of hydrogen to 350 atm. at temperatures above 14 °K, J. Res. NBS **65C** (Eng. and Instr.) No. 4, 231 (1961).

[3] H. M. Roder, L. A. Weber, and R. D. Goodwin, Thermodynamic and related properties of parahydrogen from the triple point to 100 °K at pressures to 340 atm (to be published).

[4] L. Holborn and J. Otto, On the isotherms of some gases between +400 and −183°, Z. Physik **33,** 1(1925); **38,** 359 (1926).

[5] J. O. Hirschfelder, C. F. Curtiss, and R. B. Bird, Molecular theory of gases and liquids (John Wiley and Sons Inc., New York, N.Y., 1954).

[6] H. M. Roder, D. E. Diller, L. A. Weber, and R. D. Goodwin, The orthobaric densities of parahydrogen, derived heats of vaporization and critical constants, Cryogenics **3,** 16 (1963).

[7] A. Michels, J. C. Abels, C. A. Ten Seldam, and W. de Graaff, Polynomial representation of experimental data; application to virial coefficients of gases, Physica **26,** 381 (1960).

[8] H. L. Johnston, I. I. Bezman, and C. B. Hood, Joule-Thomson effects in hydrogen at liquid air and room temperatures, J. Am. Chem. Soc. **68,** 2367 (1946)

[9] H. W. Woolley, R. B. Scott, and F. G. Brickwedde, Compilation of thermal properties of hydrogen in its various isotopic and ortho-para modifications, J. Res. NBS **41,** 379 (1948) RP1932.
[10] A. Michels, W. de Graaff, and C. A. Ten Seldam, Virial coefficients of hydrogen and deuterium at temperatures between −175°C and +150°C. Conclusions from the second virial coefficient with regard to the intermolecular potential, Physica **26,** 393 (1960).
[11] Roseann Piser, The virial coefficients of hydrogen, Thesis, Dept. of Chem., Brooklyn College (Jan. 1960).
[12] H. F. P. Knaap, M. Knoester, C. M. Knobler, and J. J. M. Beenakker, The second virial coefficients of the hydrogen isotopes between 20 and 70 °K, Physica **28,** 21 (1962).
[13] J. J. M. Beenakker, F. H. Varekamp, and H. F. P. Knaap, The second virial coefficient of ortho and para hydrogen at liquid hydrogen temperatures, Physica **26,** 43 (1960).
[14] W. H. Keesom, Helium (Elsevier Publ. Co., (1942).

(Paper 68A1–260)

JOURNAL OF RESEARCH of the National Bureau of Standards—A. Physics and Chemistry
Vol. 68A, No. 1, January–February 1964

Heats of Solution, Transition, and Formation of Three Crystalline Forms of Metaboric Acid

Marthada V. Kilday and Edward J. Prosen

(October 3, 1963)

The three crystalline forms of metaboric acid HBO_2 were prepared, purified, and analyzed. Heats of solution in water or of reaction with sodium hydroxide solution were compared with those of orthoboric acid H_3BO_3(c). The best values for the heats of transition at 25 °C are: (c,I) to (c,II), 2.33 ± 0.23 kcal/mole; (c,II) to (c,III), 1.30 ± 0.05 kcal/mole; (c,I) to (c,III), 3.63 ± 0.24 kcal/mole. The following heats of formation at 25 °C were derived: -192.77 ± 0.35 kcal/mole for the cubic HBO_2(c,I), -190.43 ± 0.34 kcal/mole for the monoclinic HBO_2(c,II), and -189.13 ± 0.34 kcal/mole for the orthorhombic HBO_2(c,III).

1. Introduction

Three crystalline forms of metaboric acid HBO_2 were identified and described by Kracek, Morey, and Merwin [1] [1] in 1938. The three forms are the cubic form HBO_2(c,I), the monoclinic form HBO_2(c,II), and the orthorhombic form HBO_2(c,III). Although heat-of-solution data [2–6] and other thermodynamic data are available on the monoclinic and orthorhombic forms, no heat of solution or formation data and little other thermodynamic information other than that of Kracek, Morey, and Merwin are available on the most stable form, the cubic. (See, however, the preliminary report of part of the present work [7].) An investigation [18] of the equilibrium decomposition pressures of orthoboric acid into water vapor and each of the three metaboric acids yielded both heat-of-formation [(c,I), −192.6; (c,II), −190.6; (c,III), −189.0 kcal/mole] and entropy values for each of the forms. However, since the uncertainty in the heat of formation derived from those measurements was large, it was desirable to determine the heats of formation (or differences in heat of formation) by a more direct means.

The three crystalline forms of metaboric acid were prepared, purified, and analyzed. Heats of hydrolysis in water and heats of neutralization in sodium hydroxide solution were measured and compared with similar heats using orthoboric acid. From these heats of solution or neutralization, heats of transition and formation of the three forms of metaboric acid may be derived, since, as indicated by the work of Hibben [8], H_3BO_3 and HBO_2 form the same final products in solution.

2. Preparation and Analyses of Samples

The experiences of Kracek [1] and Tazaki [9] as well as other thermodynamic and mechanism studies [18] of the decomposition pressures of orthoboric acid were considered in the development of the methods of preparation of the metaboric acid samples described in this paper.

[1] Figures in brackets indicate the literature references at the end of this paper.

In general the samples were identified by X-ray diffraction,[2] refractive index,[3] and density measurements which were in agreement with the work of Kracek [1] and Tazaki [9]. The boron content of the various materials was determined from titrations (in the presence of an excess of D-mannitol) of aqueous solutions of weighed samples using $0.1N$ sodium hydroxide and a Beckman pH meter with a glass electrode and a calomel reference electrode.

Quick identification and separation of the various crystals were made by flotation in the liquids listed in table 1 which also lists the densities of the metaboric acids and orthoboric acid.

TABLE 1. *Densities of boric and metaboric acid crystals, and liquids used for flotation*

Substance	Density
	g/cm³
H_3BO_3(c)	1.44
Carbon tetrachloride	1.60
HBO_2(c,III)	1.78
Ethyl Iodide	1.92
HBO_2(c,II)	2.04
Ethylene bromide	2.17
HBO_2(c,I)	2.49

For the sake of brevity in this paper HBO_2(c,I), HBO_2(c,II), and HBO_2(c,III) will sometimes be referred to as (c,I), (c,II), and (c,III), respectively.

2.1. H_3BO_3(c)

Orthoboric acid, analytical grade reagent, was recrystallized three times from aqueous solution and air-dried at room temperature. It was stored in a desiccator containing a saturated solution of calcium bromide which maintains a relative humidity of about 20 percent at room temperature. A spectroscopic analysis [4] of a sample prepared in this manner indicated a total impurity of not more than 0.001 mole percent. Titration analyses of the

[2] A. Perloff of the Constitution and Microstructure Section of the Minera Products Division.
[3] C. P. Saylor of the Pure Substances Section of the Analytical and Inorganic Chemistry Division.
[4] Spectrochemistry Section of the Analytical and Inorganic Chemistry Division.

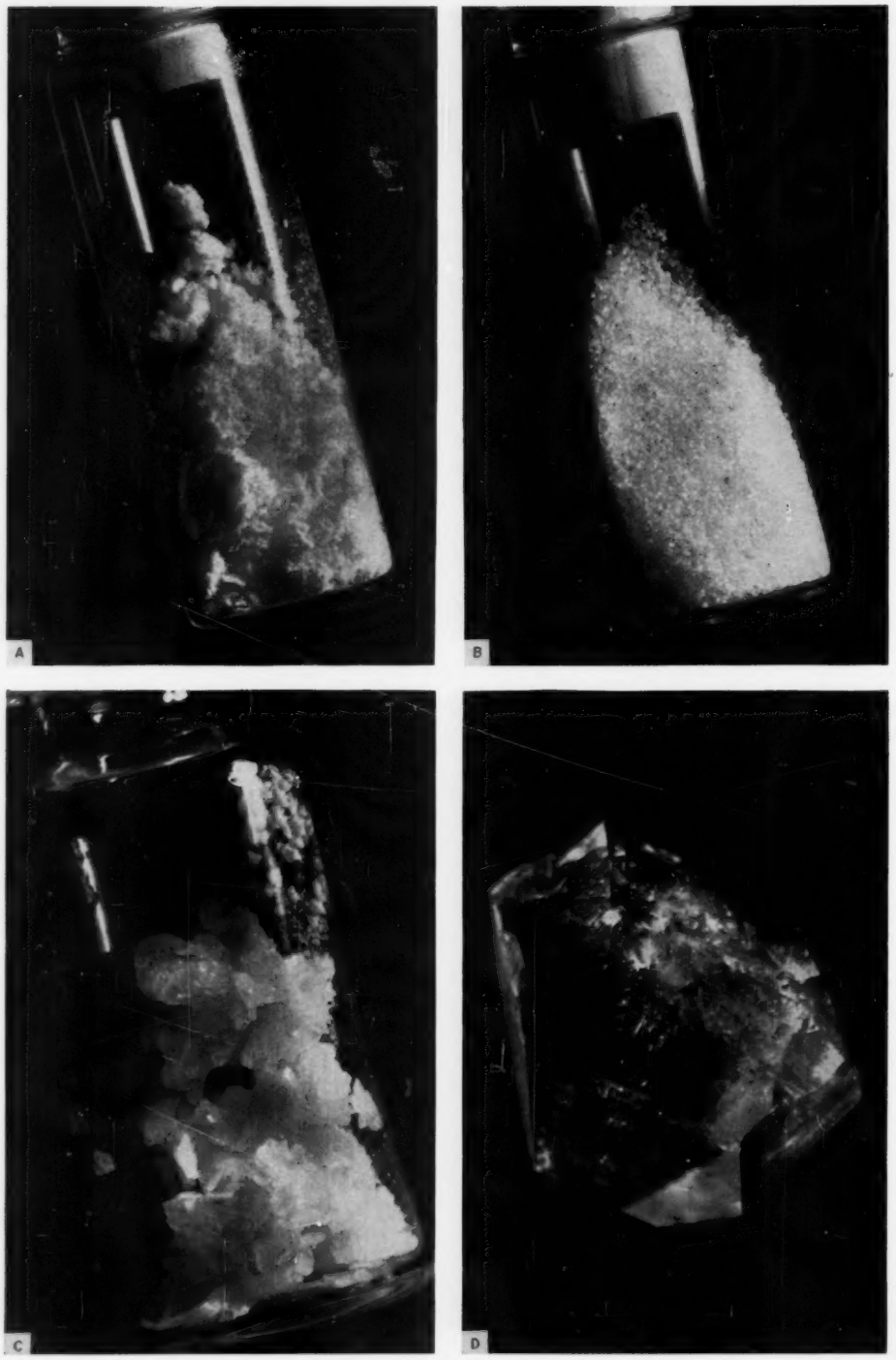

FIGURE 1. *The various crystal forms of metaboric acid:*
A. orthorhombic, B. cubic, C. monoclinic, and D. a large single cyrstal of the cubic HBO_2(c,I), *actual size, approximately 3.5 mm; A, B, and C are approximately actual size.*

final calorimetric solutions of boric acids in water indicated a weight of boric acid averaging 99.72± 0.09 (sdm) percent of the sample weight; the accuracy of the titration analyses was estimated to be a few tenths of a percent the total boric acid.

2.2. HBO_2(c,III)

It should be possible in preparing the metaboric acids from orthoboric acid to choose conditions of temperature, pressure, and humidity which would result in pure products if the conditions were accurately controlled. However, the preparations described here contained mixtures of the metaboric acids and orthoboric acid which were separated by flotation methods and/or analyzed to determine the composition of the sample.

The orthorhombic form of metaboric acid was obtained by dehydration of orthoboric acid in open Petri dishes at 65 °C and the samples were weighed every 2 or 3 days during the dehydration. The relative humidity of the atmosphere generally ranged from 15 to 30 percent but occasionally for brief periods it was as high as 55 percent. The theoretical weight for metaboric acid was reached in 1 to 3 weeks, however, this was not an exact indication of the completeness of dehydration since orthoboric acid volatilizes to an appreciable extent at 65 °C. At this temperature and humidity the only impurity expected and found in the product was orthoboric acid, the amount of which varied somewhat with the atmospheric conditions during preparation. The products generally contained 80 to 90 percent (c, III). The samples were stored in glass-stoppered bottles over anhydrous magnesium perchlorate drying agent, and subsequent manipulations were performed in a dry box. The appearance of the product may be seen in figure 1a.

2.3. HBO_2(c,II)

The monoclinic form of metaboric acid was prepared at 120 °C by dehydration of wet orthoboric acid in bottles with loose-fitting glass stoppers to impede the escape of water vapor. The dehydration generally required 3 to 4 weeks. Extended heating was not desirable because greater contamination with (c,I) developed. Formation of (c,II) was apparent from the presence of globules or treelike structures. The best yield of the (c,II) was obtained when the starting material was orthoboric acid which had not been thoroughly dried but was still moist with the liquid from recrystallization.

These preparations contained the three crystal forms of metaboric acid as well as some orthoboric acid. The purification and all subsequent manipulations of the (c,II) were performed in a dry box to prevent the sample from reacting with atmospheric moisture. The product was first washed thoroughly with spectroscopic-grade (H_2O-free) carbon tetrachloride to remove H_3BO_3(c) and (c,III) by flotation and solution. Figure 1c shows the material at this stage of the purification. The remaining clusters of crystals were crushed (but not ground) in a mortar. When they were added to ethyl iodide (analytical reagent), the (c,II) and (c,I) sank to the bottom. The floating crystals and the ethyl iodide were removed before adding ethylene bromide in which (c,II) floats but (c,I) does not. The floating crystals, mostly needlelike in form were removed, washed with H_2O-free CCl_4, and dried at 120 °C for about 30 min before storing in a glass-stoppered bottle over anhydrous magnesium perchlorate.

Flotation did not completely separate (c,I) from (c,II) due to air-bubble effects and to inclusion of (c,I) by (c,II). However, (c,II) dissolves moderately rapidly in water at 25 °C while (c,I) is only very slightly soluble at that temperature, thus it was possible to determine the amount of (c,II) by titration of an aqueous solution of the sample. About 1 percent of (c,I) was found in the best samples; details will be given in the analyses of the calorimetric solutions.

2.4. HBO_2(c,I)

The most stable form of metaboric acid, the cubic HBO_2(c,I), has been prepared by several methods. One method was similar to the preparation of (c,II) except that the orthoboric acid was not wet initially and a period of 4 to 5 weeks was required to complete the dehydration. This product consisted of crystals of (c,I) approximately 1 mm in size mixed with some (c,II). Figure 1b shows this product after purification.

Another method of preparing the (c,I) resulted in a product which contained essentially no impurities. Thin glass spherical bulbs, 1.5 cm diam, were blown at the end of 4 mm (o.d.) glass tubing; the overall length was approximately 12 cm. The bulbs were filled with orthoboric acid and weighed. After heating at 110 °C for approximately 4 weeks the samples had reached constant weight at approximately that of metaboric acid.

A third method produced crystals which were generally smaller than those formed in the other two methods, but occasionally larger crystals were formed; the largest single crystal obtained was approximately 3.5 mm in size and is shown in figure 1d. In this method 5 g of orthoboric acid, 15 g of (c,III), and a few seed crystals of (c,I) were sealed, after brief evacuation, in a 100-ml Pyrex-glass ampoule and heated at 180 °C. Sometimes in a day or two, the melt developed "cloudiness" indicating crystal formation, but at other times it was as much as a week before crystallization was visible; 2 to 5 weeks was allowed for crystal aggregation but this was no guarantee of large crystal formation. As the ampoule cooled, the mixture formed a solid mass which adhered tightly to the surface of the glass but apparently did not attack the glass, because it was possible after soaking with water to scrape off the crystals leaving a smooth glass surface.

Samples of (c,I) of high purity were obtained by washing the products of the above preparations with water since the cubic form is only very slightly soluble. The cubic crystal surfaces were attacked

711-046—64——9

after several hours exposure to water at room temperature, but extended washing with methanol effectively dissolved the other forms of HBO_2 and did not mar the crystal surfaces. We feel that a sample of high purity was obtained in this way although it was not possible to obtain a quantitative analysis with respect to the crystal form. When weighed samples were dissolved in boiling water and titrated in the presence of excess D-mannitol, 99.89 ± 0.03 percent of the theoretical amount of boric acid was found in the analyses of four samples.

3. Apparatus and Procedures

3.1. Calorimetric Apparatus and Procedures

The calorimeter employed in these experiments is shown in figure 2 and described in [10]. The temperature of the water bath was maintained at approximately 25 °C or 40 °C and normally varied by ±0.003 °C during an experiment. The bath, temperature controls, and method and instruments for measuring time, temperature, and electrical energy have been described previously [10, 11, 12].

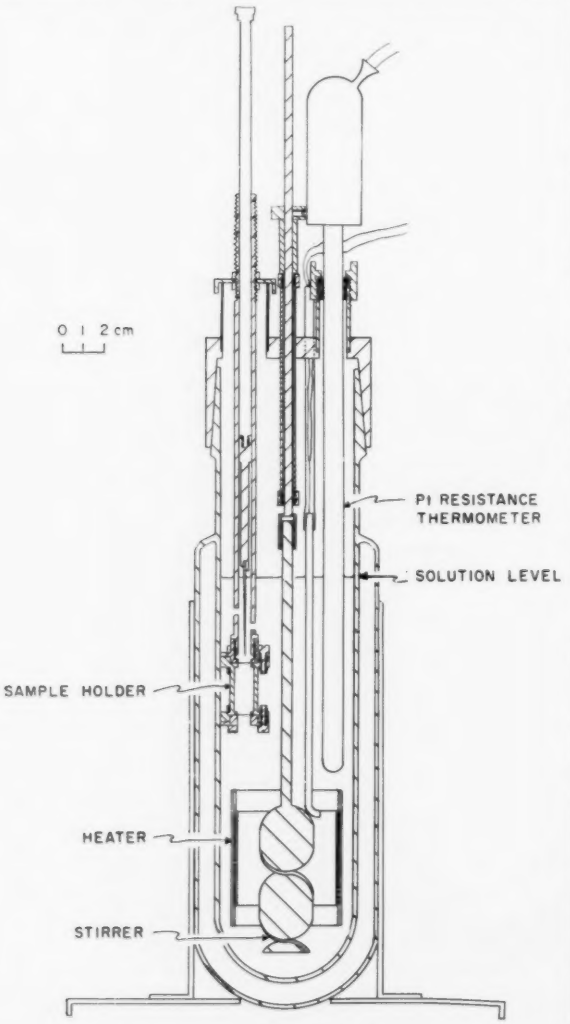

FIGURE 2. *The solution calorimeter.*

Each calorimetric experiment included a preliminary equilibration period of 20 to 30 min, a 20-min initial rating period, an electrical calibration period, a 20-min middle rating period, a chemical reaction period, and a 20-min final rating period. The temperature was recorded at 2-min intervals during the rating periods, and at 1-min intervals during the calibration and chemical reaction periods. The electrical calibration period lasted either 20 min with 7 or 9 min of heating or 10 min with 5 min of heating; temperature rises were 0.01 ohm per minute of heating. The chemical reaction periods generally made 40 min long for the solution in water and 20 or 30 min long for the solution in sodium hydroxide to insure complete solution.

In early experiments glass bulbs were used to contain the samples with a holder similar to that described in [12]. In later experiments the Monel capsule shown in figure 2 was used and platinum disks, 1 mil thick, closed the ends of the sample holder. The stirring rate in early experiments was 500 rpm but was later increased to 1000 rpm in order to prevent the (c,I) from settling to the bottom, and to dissolve the samples within a reasonable length of time for calorimetric measurements.

Three series of calorimetric experiments to be reported differ somewhat in procedure and in the composition of the calorimetric systems.

Series I—In the earlier experiments, the samples were contained in glass bulbs and the stirring rate of 500 rpm was used. The heats of solution in water were measured using 500 g (27.8 moles) of water in the calorimeter. For measuring the heat of reaction in $2N$ sodium hydroxide solution, the calorimetric solution was prepared in the calorimeter by adding 135 g of a stock solution of $10N$ sodium hydroxide to 402 g (22.3 moles) of water. In this series, heats of solution in water and in $2N$ sodium hydroxide were measured at 25 °C for orthoboric acid and metaboric acid (c,II), and heats of solution in $2N$ sodium hydroxide were measured at 40 °C for orthoboric acid and metaboric acids (c, II) and (c,I).

The process of filling the thin glass bulbs with the samples of the metaboric acids was a tedious and time-consuming one, and the evacuation and sealing of the bulbs after filling introduced the possibility of decomposition of the samples. These difficulties were eliminated in later experiments where the Monel capsule replaced the glass bulb as the sample container. The containers for the metaboric acids were always filled in a dry box but those for orthoboric acid were filled in the room atmosphere.

Series II—These experiments were similar to those of Series III except that the samples were enclosed in glass bulbs rather than in the Monel capsule.

Series III—In these experiments, using the Monel capsule and the 1000-rpm stirring rate, the heat capacity of the system was reduced. For the heats of solution in water the calorimeter contained 452 g (25 moles) of water. For the heats of reaction in 2*N* sodium hydroxide the calorimeter contained 362 g (20 moles) of water plus 122 g of the stock solution of 10*N* sodium hydroxide. In this series heats of solution in water were measured at 25 °C for orthoboric acid, metaboric acids (c,III) and (c,II); and heats of reaction in 2*N* sodium hydroxide at 25 °C were measured for orthoboric acid, metaboric acids (c,III), (c,II), and (c,I).

The cubic HBO_2(c,I) is the most stable form of metaboric acid and the solution in which the (c,I) dissolved completely within a reasonable length of time and under conditions suitable for calorimetric measurements was also used for measurements of the heats of solution of the two less stable forms of metaboric acid and of orthoboric acid. Solution of (c,I) was accomplished in a 2*N* sodium hydroxide solution at 40 °C in approximately 30 min at a stirring rate of 500 rpm when the sample was crushed to pass a No. 200 standard sieve. The crushing and sieving of the sample was a tedious operation which was performed in the room atmosphere; the gain in weight resulting from reaction with and/or adsorption of moisture from the atmosphere amounted to less than 1 percent of the sample weight. No difference was detected by X-ray analysis between the sieved and the uncrushed samples.

In preparing the calorimetric samples of (c,I), the freshly sieved material was heated at 120 °C for 1 hr and cooled in a desiccator. Thin glass bulbs were filled with the sample in a dry box; the bulbs were then removed from the dry box, attached to a vacuum manifold, and sealed off under reduced pressure. These samples were used for solution in sodium hydroxide at 40 °C. It was later learned that the sample could also be dissolved at 25 °C in approximately 50 min by doubling the stirring rate. In the two experiments under these conditions the Monel capsule was used as the sample container rather than the glass bulbs; the capsule was filled in a dry box.

3.2. Determination of Energy for Initiating Reactions

The energy for breaking the glass bulbs was too small to be measured in this system; the limit of detection was about 0.4 j. Other investigators [14] have measured the energy and found that 0.2 j or less was required to break thin glass bulbs. When the Monel capsule was used to contain the sample, the energy required to break the two platinum disks was affected by several factors other than the properties of the disks, namely, the reaction rate, the particle size, and the extent to which the capsule was filled. Thus there was a large percentage of uncertainty in the determination of this energy.

The disk-breaking energy was determined as follows. In two experiments where the capsule contained only water the energy for breaking the the disks was found to be approximately 1.5 j/expt.; this was near the limit of detection in this calorimeter, and not typical of the energies involved in the metaboric acid experiments because there was no friction resulting from the presence of crystalline samples. It was believed that disk-breaking energies more comparable to those of the experiments reported later in this paper were obtained in three series of experiments in which the heats of solution in water at 25°C were measured for NaCl and KCl. The disk-breaking energy was obtained from the difference between the measured energy and the theoretical energy calculated from the weight of sample, using the following heats of solution: 1.001 kcal/mole for NaCl (dilution=1000 H_2O) [15] and 4.187 kcal/mole for KCl (dilution=1500 H_2O) [15]. The average disk-breaking energies obtained were, respectively, 3.86 ± 0.24 (sdm) j/expt. and 9.84 ± 1.01 (sdm) j/expt. The mean of these values, 7 ± 4 j/expt., was used to correct the experiments of series III.

3.3. Thermal Equilibrium

A disadvantage in the use of a glass, vacuum-jacketed calorimeter is that thermal equilibrium is reached slowly between the constant-temperature bath, the glass walls of the calorimeter, and the calorimeter solution after a change in the temperature of the calorimeter solution. In order to determine the magnitude of errors resulting from failure to acheive thermal equilibrium in both exothermic and endothermic reactions, an experiment was performed which involved no chemical energy. An increase in temperature was produced by electrical heating; a decrease, by inserting a copper rod precooled in liquid nitrogen into a copper tube which extended into the calorimeter solution and withdrawing the rod when the desired temperature drop was acheived. A 2-hr equilibration period was followed by a 50-min initial rating period, a 10-min heating period, which included 5 min of electrical heating, a 60-min middle rating period, a 10-min cooling period during which the copper rod was inserted for 1½ min, and a 60-min final rating period. The results indicated that equilibrium was not reached until at least 45 min after the cessation of electrical heating or withdrawal of the cold rod. It was estimated that an error of 0.5 percent for a temperature rise of 0.05 ohm resulted from using reaction periods of only 10 or 20 min (as in the calibrations), and an error of 1.0 percent for a temperature drop of 0.02 ohm. For the experiments reported in this paper, the largest errors (1 to 2 percent of the total energy absorbed by the system) occurred in the aqueous solutions which were endothermic. The errors in the exothermic reactions (solutions in sodium hydroxide) were about 0.5 percent or less. Although these errors were considered in the overall uncertainties, they tend to cancel in the calculation of the heats of formation and transition.

3.4. Chemical Analyses and Procedure

The actual composition in terms of species of the final calorimetric solutions was not determined.

However, Hibben [8] found from infrared and Raman measurements on aqueous solutions of boric acid and borates that only H_3BO_3 and BO_2^- are present in dilute solutions. Thus, when ortho- or metaboric acid is dissolved in water, H_3BO_3(aq) is the product; and, when dissolved in aqueous bases, the metaborate ion is formed. By assuming that the products of solution are the same for orthoboric acid and for the three metaboric acids, the heat of formation for any of the metaboric acids can be calculated knowing only the heat of solution of orthoboric acid and of the metaboric acid, and the heats of formation of water and of orthoboric acid.

The final calorimetric solutions in water were analyzed by titration for orthoboric acid, but it was not possible to obtain an accurate analysis of the solutions in the sodium hydroxide. Therefore, these heats of reaction are based on the number of moles calculated from the sample weight and the average composition of the samples obtained from analyses of the aqueous solutions. The final calorimetric solution from the water experiments was diluted to 500 ml or 1000 ml and appropriate aliquots were taken for titration in the presence of excess D-mannitol with a standard 0.1*N* sodium hydroxide solution. A Beckman *p*H meter was used to indicate the end points which occurred at about *p*H 7.8. These titrations are probably accurate to a few tenths of a percent. The ratio of the amount of boric acid found in the titrations to the amount of boric acid based on the sample weight is an indication of the purity of the sample with respect to chemical composition but not to crystal form. From the boric acid ratio it was possible to calculate the amount of orthoboric acid present in the samples of HBO_2(c,III), and the average composition of these samples was applied in corrections calculated for the solutions of the same sample in sodium hydroxide where it was not possible to obtain an accurate analysis of the final calorimetric solutions.

The final calorimetric solutions of the samples of metaboric acid (c,II) in water contained the undissolved (c,I). Therefore, the final solution was filtered through a coarse filter paper and the filtrate was titrated as described above; the number of moles of boric acid found in this titration was assumed to be equal to the number of moles of (c,II) in the sample. the difference between this and the number of moles of metaboric acid in the sample as calculated from its weight, was taken as the amount of (c,I) in the sample. An approximate check on this value was obtained from titration of an aqueous solution of the undissolved residue. This value was not as accurate as that obtained from the weight of sample because the amount of (c,I) was only about 1 to 5 percent of the sample, and losses during the manipulations of such small crystals were likely to occur.

The approximate amount of (c,I) which dissolved in water at 25 °C was determined by adding a weighed sample of (c,I) to 452 ml of distilled water in the calorimeter and stirring at about 1000 rpm for 2 hr. The solution was then filtered through a fine filter paper and the filtrate was titrated for boric acid. As would be expected, more rapid solution occurred when the samples were of small particle size. Approximately 9 mg dissolved from a 0.3-g sample which was 40–70 mesh, 15 mg dissolved from a similar sample which was less than 100 mesh, and 2 mg dissolved from a 0.030 g sample (<100 mesh). The time during which the samples were exposed to the water in these experiments was about twice that in the calorimetric experiments; therefore, the solution of not more than 0.2 mg of (c,I) (or 0.02% of *S*) would be expected in the experiments given in table 3. The acutal amount of (c,I) which dissolved in water was so small and uncertain because of particle size that no correction was made for it.

Solutions prepared in the same manner as the calorimetric solutions of sodium hydroxide were analyzed by titration against weighed samples of potassium acid phthalate (NBS standard sample No. 84) using phenolphthalein indicator. These analyses were only approximations since no special precautions were used to exclude carbon dioxide from the calorimetric solutions. An analysis of a solution prepared from stock soln No. 1 [used in reactions of (c,I) at 40 °C] indicated a normality of 1.94; a solution prepared from stock soln No. 3 [used in reactions of H_3BO_3(c) at 25 °C] was found to be 2.27*N*; and one prepared from stock soln No. 4 [used in reactions of H_3BO_3 at 40 °C, and (c,II) at 40 °C and 25 °C] was 1.88*N*. Two stock solutions, A and B, were used alternately in the preparation of calorimetric solutions for the experiments in Series III. Initial analysis of a solution prepared from stock soln A indicated a normality of 1.79, and from stock soln B, 1.96; no change was observed in the final analyses of similar solutions.

4. Units and Physical Constants

The unit of energy for the calorimetric experiments reported in this paper is the absolute joule. For conversion to the thermochemical calorie, 1 thermochemical calorie=4.1840 j.

Values for atomic weights were taken from the 1961 Table of Atomic Weights [16].

The masses of all samples given in the following tables have been corrected to the weights in vacuo using buoyancy factors calculated from densities given by Kracek, Morey, and Merwin [1].

5. Experimental Results

The heats of formation of the three metaboric acids were calculated from the heats of reaction of the metaboric acids and of orthoboric acid in water and in solutions of sodium hydroxide. The results of the experiments where these heats of reaction were determined are given in tables 2 through 6. Tables 2 through 5 give details of experiments on which our "best values" are based, and in table 6 the average values of 4 to 6 experiments for all other reactions are given.

In all experiments *S* is the weight (in vacuo) of sample in grams; E_a is the energy equivalent of the initial system as determined from the electrical cali-

TABLE 2. $HBO_2(c, III)$ *in water at 25 °C—Series III*

Expt. No.	S	H_3BO_3 total titr.	H_3BO_3 ratio	H_3BO_3 calc.	HBO_2 (c,III) calc.	E_a	ΔRc	Q	$q_{H_3BO_3}$	$\Delta H(25\ °C)$ [1]
	g	*Mole*		*Mole*	*Mole*	*j/ohm*	*Ohm*	*j*	*j*	*kj/mole* HBO_2(c,III)
1	0.83071	0.01824	0.9623	0.001747	0.01649	21,313.7	−0.002740	−58.40	−38.0	1.662
2	.64787	.01425	.9640	.001303	.01295	21,304.2	−.002212	−47.12	−28.3	1.994
3	.73979	.01621	.9604	.001637	.01457	21,315.3	−.002643	−56.34	−35.6	1.904
4	.66889	.01464	.9582	.001520	.01312	21,300.4	−.002361	−50.29	−33.1	1.844
5	.81347	.01788	.9633	.001666	.01621	21,319.8	−.002845	−60.65	−36.2	1.940
Mean										1.869
Standard deviation of the mean										±0.057
Overall uncertainty, 10%										±0.19

[1] Another correction, $q_d = -7.0$ j/expt., was added to Q.

TABLE 3. $HBO_2(c,II)$ *in water at 25 °C—Series III*

Expt. No.	S	Undissolved Residue HBO_2(c,I) titr.	HBO_2 (c,II) titr.	H_3BO_3 ratio	E_a	ΔRc	Q	$\Delta H(25\ °C)$ [1]
	g	*Mole*	*Mole*		*j/ohm*	*Ohm*	*j*	*kj/mole* HBO_2 (c,II) titr.
1	1.11827	0.00016	0.02523	0.9951	21,314.1	−0.008501	−181.19	7.459
2	1.15561	.00018	.02615	.9986	21,303.6	−.008403	−179.01	7.113
3	1.19328	.00008	.02713	.9994	21,318.3	−.009094	−193.87	7.404
4	1.24525	.00019	.02816	.9978	21,322.9	−.009263	−197.51	7.262
5	1.20517	.00026	.02719	.9983	21,286.4	−.009069	−193.05	7.357
6	1.24061	.00020	.02802	.9970	21,302.6	−.009407	−200.39	7.401
Mean								7.333
Standard deviation of the mean								±0.051
Overall uncertainty, 3%								±0.220

[1] A correction, $q_d = -7.0$ j/expt., was added to Q.

TABLE 4. $HBO_2(c,II)$ *in* 2N *sodium hydroxide solution at 25 °C—Series III*

Expt. No.	S	HBO_2(c,I) calc.	HBO_2(c,II) calc.	E_a	ΔRc	Q	$q_{(c,I)}$	$\Delta H(25\ °C)$ [1]
	g	*Mole*	*Mole*	*j/ohm*	*Ohm*	*j*	*j*	*kj/mole* HBO_2(c,II)
1	1.09860	0.000174	0.024670	21,175.9	0.043611	923.50	4.8	−36.956
2	1.23190	.000197	.027918	21,090.1	.049811	1050.52	5.4	−37.185
3	1.32026	.000211	.029920	21,133.0	.053130	1122.80	5.8	−37.099
4	1.39278	.000222	.031563	21,086.4	.056267	1186.47	6.1	−37.175
Mean								−37.104
Standard deviation of the mean								±0.053
Overall uncertainty, 2%								±0.74

[1] Another correction, $q_d = -7.0$ j/expt. was added to Q.

TABLE 5. $HBO_2(c,I)$ *in* 2N *sodium hydroxide solution at 25 °C—Series III*

Expt. No.	S	E_a	ΔRc	Q	$\Delta H(25\ °C)$ [1]
	g	*j/ohm*	*Ohm*	*j*	*kj/mole* HBO_2(c,I)
1	0.54449	21,067.7	0.016479	347.17	−27.375
2	.26108	21,073.9	.008065	169.96	−27.350
Mean					−27.362
Overall uncertainty, 2%					±0.55

[1] A correction, $q_d = -7.0$ j/expt., was added to Q.

bration which preceded each chemical reaction experiment; ΔRc is the corrected temperature rise of the system [13]; Q, the product of E_a and ΔRc, is the total energy absorbed by the system; and ΔH, the enthalpy of reaction, is the heat absorbed ($-Q$, less any applicable corrections, $-q$) per mole of orthoboric acid or metaboric acid calculated from the weight of sample or determined from the number of moles of orthoboric acid found in the titrations of the final calorimetric solutions, H_3BO_3 titr. The overall uncertainty includes twice the experimental standard deviation of the mean and other uncertainties discussed in section 5.1. The H_3BO_3 ratio is the ratio of the number of moles of orthoboric acid found in

TABLE 6. *Average results of other solution experiments*

Group	Compound	Series	S[1]	Undissolved residue HBO_2(c,I) titr.	Calc. HBO_2(c,II) or HBO_2(c,III)	H_3BO_3 titr.	E_a	ΔRc	Q	$q_{(c,I)}$ or $q_{H_3BO_3}$	Dilution H_2O/ H_3BO_3	Experimental sdm	$\Delta H(40\ °C)\pm$ uncertainty
			g	*g*	*Mole*	*Mole*	*j/ohm*	*Ohm*	*j*	*j*		*kj/mole*	*kj/mole* *kcal/mole*
Solutions in 2*N* sodium hydroxide at 40 °C													
1	H_3BO_3(c)	I	1.64442 (1.47–1.76)				23,238.7	0.024556	570.65			±0.007	−21.46±0.21 −5.13±0.05
2	HBO_2(c,II)	I	1.45515 (1.11–1.91)	0.0359			23,222.7	.049235	1,143.37	32.2		±.077	−35.61±1.78 −8.51±0.43
3	HBO_2(c,I)	I	0.37354 (0.33–0.42)				23,143.7	.010105	233.85			±.021	−27.43±0.27 −6.56±0.07
Solutions in 2*N* sodium hydroxide at 25 °C													
													$\Delta H(25\ °C)\pm$ uncertainty
4	H_3BO_3(c)	I	0.59862 (0.57–0.62)				22,859.7	.009924	226.86			±0.071	−23.43±0.23 −5.60±0.06
5	H_3BO_3(c)	III	0.97140 (0.95–1.00)				21,129.8	.017354	366.68	[2]		±.044	−22.90±0.34 −5.47±0.08
6	HBO_2(c,II)	I	1.34726 (1.19–1.52)	0.0472			22,884.8	.047484	1,086.60	21.2		±.132	−36.87±1.84 −8.81±0.44
7	HBO_2(c,III)	III	0.69948 (0.66–0.74)		0.013861		21,129.4	.029520	623.75	[3] 33.8		±.62	−42.07±2.10 −10.05±0.50
Solutions in water at 25 °C													
8	H_3BO_3(c)	II	1.57140 (1.38–1.70)			0.02530	21,000.1	−0.026502	−556.55		1000	±0.088	[3] 22.00 ±0.22 5.26 ±0.05
9	H_3BO_3(c)	III	1.10529 (1.06–1.14)			0.01784	21,276.1	−.017780	−378.28	[2]	1400	±.024	[3] 21.60 ±0.22 5.16 ±0.05
10	HBO_2(c,II)	I	1.12472 (1.10–1.17)	0.0647	0.024192		23,122.8	−.007262	−167.91		1000	±.057	6.94 ±0.35 1.659±0.083

[1] The range of sample weights is given in parentheses below the average sample weight.
[2] A correction, $q_d = -7.0$ j/expt., was also added in the experiments of Series III.
[3] Based on moles H_3BO_3 titr.

titrations of the final calorimetric solutions to the number of moles of orthoboric acid calculated from the sample weight; q_d is the correction for the energy required to break the platinum disks used in Series III.

The heats of solution of orthoboric acid in water at 25 °C and in sodium hydroxide solution at 25 °C and 40 °C are used in the calculations of the heats of formation of the three metaboric acids. The heat of solution in water at 25 °C has been determined by several investigators [2–5, 10, 19–25] and their values at a dilution of 1000 H_2O range from 5.17 kcal/mole to 5.56 kcal/mole; the more recent values are grouped between 5.24 and 5.28 kcal/mole.

We have measured the heat of solution of orthoboric acid in water in two groups of experiments and the results are given in table 6, groups 8 and 9 for Series II and Series III which are described in section 3.1. The samples in Series II were enclosed in glass bulbs which had been sealed after pumping for several hours at 10^{-5}mm Hg pressure at room temperature; the samples in Series III were enclosed in the Monel capsule. The reaction periods for the experiments in group 8 were of 20-min duration while those in group 9 were of 40-min duration, thus the latter should be nearer thermal equilibrium at the end of the reaction period.

According to Smisko and Mason [19] the heat of solution of orthoboric acid in water does not change significantly between the dilutions of 500 H_2O and 5000 H_2O. Therefore no corrections for dilutions of H_3BO_3 are made in this paper since all values fall within the range of 900 to 2700 H_2O.

The data for the measurements of the heats of solution of orthoboric acid in sodium hydroxide solution at 40 °C and at 25 °C are given in table 6, groups 1, 4, and 5. The largest uncertainty considered for these reactions was the possible variation in the concentration and/or composition of the calorimetric solutions of sodium hydroxide.

Our best value for the heat of transition from (c,III) to (c,II) is derived from the heats of solution in water at 25 °C (Series III) given in tables 2 and 3, and group 9 of table 6. The equation representing the mean heat of solution given in table 2 is

$$HBO_2(c,III) + 1501\ H_2O(liq) \rightarrow H_3BO_3(1500\ H_2O)$$

$$\Delta H(25\ °C) = 1.869 \pm 0.187\ kj/mole$$

$$= 0.447 \pm 0.045\ kcal/mole \qquad (1)$$

and that for table 3 is

$$HBO_2(c,II) + 901\ H_2O(liq) \rightarrow H_3BO_3(900\ H_2O)$$

$$\Delta H(25\ °C) = 7.33 \pm 0.22\ kj/mole$$

$$= 1.752 \pm 0.053\ kcal/mole \qquad (2)$$

The experimental uncertainty, 2(sdm), is large for eq (1) because the amount of heat absorbed during

the reaction was small. The uncertainty with respect to sample composition also made a relatively large contribution to the overall uncertainty for eq (2).

The heat of reaction in table 2 is based on the number of moles of (c,III) calculated from the stoichiometric relationship between the weight of sample and the amount of boric acid found in titrations of the final calorimetric solutions. The corrections for the energy absorbed during the solution of the orthoboric acid were calculated from the results of group 9, table 6. The composition of the samples in group 7, table 6 was assumed to be the same as the average of those in table 2.

In table 3, the H_3BO_3 ratio is the ratio of the sum of the number of moles of (c,II) and of (c,I) titrated, to the number of moles of HBO_2 calculated from the sample weight. From this it can be seen that only a few tenths of 1 percent of the sample weight was not accounted for in the titration analyses and this is within the limits of accuracy expected of the analytical methods employed. The extra care taken in the purification of this sample is evidenced by the fact that the amount of (c,I) impurity is much smaller and the composition of the samples is more uniform than those of the experiments in Series I given in group 10 of table 6, on which the average composition, 6 percent of (c,I), of the samples in groups 2 and 6 was based. The amount of (c,I) dissolved during the latter experiments was determined from the difference between the amount assumed to be present initially and the amount found in the undissolved residue at the end of the experiment. A correction for the heat of reaction of the (c,I) which dissolved, $q_{(c,I)}$, was made using the results obtained in group 3 of table 6 and in table 5. A large uncertainty with respect to composition of sample was considered in the results of groups 2, 6, and 10; groups 2 and 6 had an additional uncertainty in the concentration of sodium hydroxide solutions.

The results given in tables 4 and 5 were used with the results of group 5, table 6, to calculate our best value for the heat of transition from (c,II) to (c,I). The mean heat of reaction for the experiments in table 4 is given by the equation,

$$HBO_2(c,II)+NaOH(aq)\rightarrow[NaBO_2+H_2O](soln)$$
$$\Delta H(25\ ^\circ C)=-37.10\pm0.74\ \text{kj/mole}$$
$$=-8.87\pm0.18\ \text{kcal/mole} \qquad (3)$$

and for those in table 5,

$$HBO_2(c,I)+NaOH(aq)\rightarrow[NaBO_2+H_2O](soln)$$
$$\Delta H(25\ ^\circ C)=-27.36\pm0.55\ \text{kj/mole}$$
$$=-6.54\pm0.13\ \text{kcal/mole}. \qquad (4)$$

The uncertainties in the compositions of the sodium hydroxide solutions and of the samples of (c,II) contributed largely to the overall uncertainties assigned to these equations. In table 4, the corrections for the heat evolved during the solution of (c,I) was made according to eq (4) assuming 0.7 wt percent of (c,I) was present in the samples. This was the average composition found in the samples of table 3. A value comparable to eq (4) at 40 °C is given in group 3, table 6.

The equations representing the reactions of orthoboric acid which were used with eqs (1), (2), and (4) in calculating our best values for the heats of formation of the metaboric acids given in table 8 are

$$H_3BO_3(c)+1400\ H_2O(liq)\rightarrow H_3BO_3(1400\ H_2O)$$
$$\Delta H(25\ ^\circ C)=21.60\pm0.22\ \text{kj/mole}$$
$$=5.16\pm0.05\ \text{kcal/mole} \qquad (5)$$

and

$$H_3BO_3(c)+NaOH(aq)\rightarrow[NaBO_2+2H_2O](soln)$$
$$\Delta H(25\ ^\circ C)=-22.90\pm0.34\ \text{kj/mole}$$
$$=-5.47\pm0.08\ \text{kcal/mole}. \qquad (6)$$

The average values of the experimental data for these reactions are given in groups 9 and 5 of table 6.

5.1. Uncertainties

The estimated error in the analyses of the products by titration was about 0.3 percent. An uncertainty in composition and weight of samples was considered because the samples could not be quantitatively analyzed as to crystal form. This uncertainty was highest in the samples of (c,II) or solution in sodium hydroxide where it was difficult to determine accurately the amount of (c,I) impurity present initially or that which dissolved during the experiment. A greater uncertainty was present in the experiments where the products were not analyzed by titration and the composition of the sample was assumed to be the same as that of another series of experiments. An uncertainty was also considered for the solution of orthoboric acid samples in water in series I where the samples were enclosed in glass bulbs, because some decomposition may have occurred while the samples were under vacuum or during the sealing of the bulbs.

In section 3.3 the failure to reach thermal equilibrium in the calorimeter was discussed and possible errors of 2.0 percent were considered in extreme cases.

It was assumed that the uncertainty in the energy for breaking the platinum disks used in series III did not exceed 4 j/expt. This assumption is based on the work described in section 3.2 where the energies for breaking the disks were determined when the capsule contained water, NaCl, and KCl.

For the experiments in Series I it had been assumed that the variations in the calorimetric sodium hydroxide solutions could be neglected. However, the experiments of Series III were arranged so as to expose any significant effects caused by the variations in the sodium hydroxide solutions on the heats of reaction and to nullify that effect on the heats of

TABLE 7. *Table showing the possible effects of time and different concentrations of sodium hydroxide solutions on the measured heats of reaction for experiments in Series III*

Sample No.		$-\Delta H$(25 °C)		
		NaOH stock soln [1]		Mean
		A	B	
		kj/mole	*kj/mole*	*kj/mole*
H_3BO_3(c)	1		23.032	
	2	22.935		22.985
	3		22.987	
HBO_2(c,III)	1	43.08		
	2		44.22	43.33
	3	42.71		
HBO_2(c,II)	1	36.956		
	2		37.185	37.104
	3	37.099		
	4		37.175	
HBO_2(c,I)	1		27.375	
	2	27.350		27.362
HBO_2(c,III)	4		40.46	
	5	40.51		40.80
	6		41.42	
H_3BO_3(c)	4	22.832		
	5		22.836	22.806
	6	22.751		

[1] Initial analysis of a calorimetric solution prepared from NaOH stock soln A indicated a normality of 1.79, and from stock soln B, 1.96; no change was indicated in similar analyses made 4 weeks later at the end of these experiments.

formation. These variations were caused by (1) slightly different compositions in the 10N stock solutions, (2) changes in the composition of a given stock solution over a period of time, and (3) errors in the amounts weighed during the preparation of the calorimetric solutions. The method of preparing the calorimetric solutions and the analyses of the stock solutions are given in sections 3.1 and 3.4. All of the heats of reaction in sodium hydroxide at 25° C of series III are given in table 7. Two stock solutions, A and B, were used alternately in the preparation of the calorimetric solutions for these experiments, and the experiments are arranged in the table in the chronological order in which they were run. The difference between the results obtained with the two stock solutions is small and within the limits of experimental error. However, a change in composition of the stock solutions with time is indicated by the fact that the results of the earlier experiments with H_3BO_3 and (c,III) have a higher mean heat of reaction than those of the comparable later experiments; we have no reason to suspect a change in the composition of the sample. Based on these results we have assigned an uncertainty of 3 percent for the reaction of (c,III) and 1 percent for all other reactions in sodium hydroxide solutions.

Although the overall uncertainties are large for the measured heats of reaction, most of them tend to cancel out in the calculatons of the heats of formation and transition.

6. Discussion and Summary

The heats of formation calculated from the various measured heats of reaction are summarized in table 8. ΔH_r was derived from the measured heats of reaction and is represented by the general equation

$$HBO_2(c, X)+H_2O(liq)\rightarrow H_3BO_3(c).$$

From this, the heats of formation of the metaboric acids were obtained using the following heats of formation at 25 °C: −262.16 kcal/mole for H_3BO_3(c) [11, 28], and −68.317 kcal/mole for H_2O(liq) [17]. The uncertainties given in table 8 were calculated as the square root of the sum of the squares of the individual uncertainties; the largest uncertainty was ±0.32 kcal/mole in the heat of formation of orthoboric acid. We have selected the following as the best values for the heats of formation of the metaboric acids at 25 °C: (c,I), −192.77±0.35 kcal/mole; (c,II), −190.43±0.34 kcal/mole; and (c,III), −189.13±0.34 kcal/mole. These values agreed with the respective values of −192.6, −190.6, and −189.0 kcal/mole obtained by Prosen [18] from measurements of the equilibrium decomposition pressures of orthoboric acid into water vapor and the three metaboric acids.

The best values for the heats of transition were obtained from eq (1) and eq (2),

$$HBO_2(c,III)\rightarrow HBO_2(c,II),$$
$$\Delta H(25\ °C)=-1.30\pm0.05\ \text{kcal/mole},$$

and from eq (3) and eq (4)

$$HBO_2(c,II)\rightarrow HBO_2(c,I),$$
$$\Delta H(25\ °C)=-2.33\pm0.23\ \text{kcal/mole}.$$

TABLE 8. *Heats of formation of the metaboric acids as calculated from various reactions*
(kcal/mole)

Compound	Calorimetric solution	ΔH(40 °C) for HBO_2	ΔH(40 °C) for H_3BO_3	H_r(40 °C)	ΔH(25 °C) for HBO_2	ΔH(25 °C) for H_3BO_3	ΔH_r(25 °C)	$\Delta Hf°$(25 °C)
HBO_2(c,I)	NaOH				−6.54	−5.47	−1.07	−192.77±0.35
	NaOH	−6.56	−5.13	−1.43			[1] −1.28	−192.56±0.33
HBO_2(c,II)	NaOH				−8.87	−5.47	−3.40	−190.44±0.38
	NaOH				−8.81	−5.60	−3.21	[2] −190.63±0.55
	NaOH	−8.51	−5.13	−3.38			[1] −3.23	[2] −190.61±0.55
	H_2O				1.66	5.26	−3.60	[2] −190.24±0.35
	H_2O				1.75	5.16	−3.41	−190.43±0.34
HBO_2(c,III)	H_2O				0.45	5.16	−4.71	−189.13±0.34
	NaOH				−10.05	−5.47	−4.58	[2] −189.26±0.61

[1] Estimated thermal coefficient, $\Delta Cp\sim-10$ cal/deg mole.
[2] These values are subject to large uncertainties in the composition of the samples.

Combination of these two values gives the following heat of transition:

$$HBO_2(c,III) \rightarrow HBO_2(c,I),$$
$$\Delta H(25\ °C) = -3.63 \pm 0.24 \text{ kcal/mole.}$$

Roth, Börger, and Bertram [3] measured the heat of solution of a mixture of metaboric acid and orthoboric acid in 0.1*N* sodium hydroxide solution at 19 °C. The crystalline form of the metaboric acid used was not identified; however, they state that the hydration and solution of the metaboric acid may not have been complete in the experiments. This would suggest that their sample contained the monoclinic form which reacts more slowly than the orthorhombic form and usually contains (c,I). They calculate a heat of solution for the metaboric acid, $\Delta H(19\ °C) = -8.0$ kcal/mole, which is comparable to our value for the monoclinic form given in eq (3).

In the work of von Stackelberg, Quatram, and Dressel [5], the heat of solution in water was measured at a dilution of 500 H_2O/H_3BO_3 at 20 °C for a mixture of orthoboric acid and metaboric acid. Although their metaboric acid was crystallographically identified as the monoclinic form, they obtained a heat of solution (after correcting for the orthoboric acid) of 0.56 kcal/mole which is near the value we obtained in eq (1) for the orthorhombic form.

The more recent work of Sokolova and coworkers [6] yielded the following values for the heats of solution at 20 °C at a final dilution of 500 H_2O/H_3BO_3: $\Delta H = 0.47$ kcal/mole for the orthorhombic, HBO_2(c,III); and $\Delta H = 1.76$ kcal/mole for the monoclinic, HBO_2(c,II). These values are in good agreement with our eq (1) and eq (2). Their heat of transition from the orthorhombic to the monoclinic metaboric acid is -1.29 kcal/mole which agrees with our value of -1.30 kcal/mole.

(Paper 68A1–261)

7. References

[1] F. C. Kracek, G. W. Morey, and H. E. Merwin, Am. J. [5] Sci. **35A,** 143 (1938).
[2] W. A. Roth and E. Börger, Ber. **70B,** 48 (1937).
[3] W. A. Roth, E. Börger, and A. Bertram, Ber. **70B,** 971 (1937).
[4] W. A. Roth, Z. Naturforsch. **1,** 574 (1946).
[5] M. von Stackelberg, F. Quatram, and J. Dressel, Z. Elektrochem. **43,** 14 (1937).
[6] N. D. Sokolova, S. M. Skuratov, A. M. Shemonaeva, and V. M. Yuldasheva, Zhur. Neorg. Khim. **6,** 774 (1961).
[7] M. V. Kilday and E. J. Prosen, J. Am. Chem. Soc. **82,** 5508 (1960).
[8] J. H. Hibben, Am. J. Sci. [5] **35A,** 113 (1938).
[9] H. Tazaki, J. Science Hiroshima Univ. Ser. A **10,** 37 (1940); ibid., 109.
[10] M. V. Kilday, W. H. Johnson, and E. J. Prosen, J. Res. NBS **65A,** (Phys. and chem.) 435 (1961).
[11] E. J. Prosen, W. H. Johnson, and F. Y. Pergiel, J. Res. NBS **62,** 43 (1959) RP2927.
[12] W. H. Johnson, A. A. Gilliland, and E. J. Prosen, J. Res. NBS **63A,** 161 (1959).
[13] E. J. Prosen, Experimental Thermochemistry, F. D. Rossini, ed., ch. 6, Vol. **I** (Interscience Publishers, Inc., New York, N.Y., 1936).
[14] S. R. Gunn and L. G. Green, J. Phys. Chem **64,** 1066 (1960).
[15] V. S. Barfield, NBS, private communication (1961).
[16] A. E. Cameron and E. Wichers, J. Am. Chem. Soc. **84,** 4175 (1962).
[17] F. D. Rossini, D. D. Wagman, W. H. Evans, S. Levine, and I. Jaffe, Selected values of chemical thermodynamic properties, NBS Circ. 500 (U.S. Government Printing Office, Washington, D.C., 20402, 1952).
[18] E. J. Prosen, NBS, unpublished data (1960).
[19] H. L. Johnston, H. N. Hersh, and E. C. Kerr, J. Am. Chem. Soc. **73,** 1112 (1951).
[20] N. S. Osborne, H. F. Stimson, and D. C. Ginnings, J. Res. NBS **23,** 197 (1939) RP1228.
[21] J. Smisko and L. S. Mason, J. Am. Chem. Soc. **72,** 3679 (1950).
[22] E. R. Van Artsdalen and K. P. Anderson, J. Am. Chem. Soc. **73,** 579 (1951).
[23] K. Linderstrøm-Lang, Compt. rend. trav. lab. Carlsberg, Ser. chim. **15,** No. 4, 65pp (1924).
[24] M. Berthelot, Ann. chim. phys. [5] **17,** 132 (1879).
[25] J. Thomsen, Thermochemische Untersuchungen, Vols. **I–IV** (Verlag J. A. Barth, Leipzig. 1882-1886).
[26] C. Katz, MS Thesis, Cornell University (1949); quoted in [22].
[27] W. C. Blasdale and C. M. Slansky, J. Am. Chem. Soc. **61,** 917 (1939).
[28] W. H. Evans, E. J. Prosen, and D. D. Wagman, Thermochemistry and Thermodynamic Functions of Some Boron Compounds in Thermodynamic and transport properties of gases, liquids, and solids, p. 231, Y. S. Touloukian, ed. (McGraw-Hill Book Co., Inc., New York, N.Y., 1959).

JOURNAL OF RESEARCH of the National Bureau of Standards—A. Physics and Chemistry
Vol. 68A, No. 1, January–February 1964

Publications of the National Bureau of Standards*

Selected Abstracts

Solutions of the equation $\Psi_{xx}+\frac{1}{x}\Psi_x+Kx^ne\Psi=0$, E. A. Kearsley, *J. Res. NBS* **67B** (*Math. and Math. Phys.*), *No. 4,* (*Oct.–Dec. 1963*).

The general solution of the equation $\Psi_{xx}+\frac{1}{x}\Psi_x+Kx^ne\Psi=0$ is displayed in terms of simple tabulated functions. The existence and uniqueness of solutions of a simple boundary value problem are determined as a function of the parameter K.

On the graphs of finite idempotent Boolean relation matrices, D. Rosenblatt, *J. Res. NBS* **67B** (*Math. and Math. Phys.*), *No. 4,* (*Oct.–Dec. 1963*).

This paper presents a graph-theoretic characterization of idempotent Boolean relation matrices of finite order. A relation-theoretic point of view is adopted in the paper. Idempotent matrices appear in the sequence of powers of any Boolean relation matrix, and are of purely theoretical as well as applied interest in connection with issues of convergence. The results provide a detailed description of the connectivity and cyclic structure of the directed graphs of idempotent matrices. The study is basically motivated by certain connectivity and flow problems which arise in the analysis of large-scale information systems. The formal results are exemplified in an investigation of the asymptotic forms of a recursive model of an information system which affords a conjoint representation of processes of communication and derivation of information. A second principal application is given in a process formulation for the generation of consistent rank orderings. The relation between system design and idempotent forms is exhibited in the two applications.

Long waves associated with disturbances produced in plasmas, H. Bremmer, *J. Res. NBS* **68D** (*Radio Sci.*), *No. 1,* (*Jan. 1964*).

The disturbances produced in a homogeneous plasma by passing charges is analyzed.

Reflection of electromagnetic waves from a lossy magneto-plasma, J. R. Wait and L. C. Walters, *J. Res. NBS* **68D** (*Radio Sci.*), *No. 1,* (*Jan. 1964*).

A method is outlined for calculating the reflection coefficient from a horizontally stratified ionized medium. The profiles of electron density and the collision frequencies are both taken to be exponential functions. The d-c magnetic field is taken to be horizontal and transverse to the direction of propagation. The specific results described are applicable to the oblique reflection of VLF radio waves in the D layer of the ionosphere for propagation along the magnetic equator. It is confirmed that the reflection coefficient is nonreciprocal in both amplitude and phase. For a wide range of the parameters, the magnitude of the reflection coefficient is greater for west-to-east propagation than for east-to-west propagation.

Electron optical studies of low-pressure gases, L. Marton, D. C. Schubert, and S. R. Mielczarek, *NBS Mono. 66* (*Aug. 16, 1963*), *35 cents.*

This document is the final report of research carried on in the Electron Physics Section of the National Bureau of Standards during the period from February 1, 1955 to March of 1962 in developing an electron optical method for the visualization of low-pressure gas flow. The goal of this work was to develop and demonstrate the suitability of electron optical techniques for recording the spatial distribution of gas molecules at fixed times with sufficient accuracy that the velocity distribution could be derived. The work concentrated on the properties of chopped molecular beams of cadmium at extremely low pressures where the densities of the particles in the molecular beam pulse correspond to a pressure of less than 10^{-7} Torr. The project was successful. During the course of this program, equipment was built, methods of operation were developed, the theory of the electron optical schlieren was developed in some detail, and ways of efficiently converting the data obtained into velocity distributions of the gas molecule were investigated.

Experimental statistics, M. G. Natrella, *NBS Handb. 91* (*Aug. 1, 1963*), *$4.25.*

This Handbook is a collection of statistical procedures which are useful in research and development programs. It is intended for the user with a scientific or engineering background who has an occasional need for statistical techniques, but does not have the time or inclination to become an expert on statistical theory or methodology. It is organized in five sections. Section 1 provides an elementary introduction to basic statistical concepts and furnishes full details on standard statistical techniques for the analysis and interpretation of measurement data. Section 2 provides detailed procedures for the analysis and interpretation of enumerative and classificatory data. Section 3 has to do with the planning and analysis of comparative experiments. Section 4 is devoted to consideration and exemplification of a number of important but as yet non-standard statistical techniques, and to discussion of other special topics. Section 5 contains all the mathematical tables needed for application of the procedures given in Sections 1 through 4.

Proceedings of the 1962 Standards Laboratory Conference, *NBS Misc. Publ. 248 (Aug. 16, 1963), $1.75.*

This publication comprises technical papers together with discussions thereof, presented at the 1962 Standards Laboratory Conference, August 8–10, 1962.

Choking two-phase flow literature summary and idealized design solutions for hydrogen, nitrogen, oxygen, and refrigerants 12 and 11, R. V. Smith, *NBS Tech. Note 179* (*Aug. 3, 1963*), *75 cents.*

The literature summary presents a brief description and discussion of papers on choking, two-phase flow. These papers are arranged with respect to analysis methods and experimental systems. The idealized solutions utilize models intended to provide upper and lower limits for the actual flow cases. Charts are presented to provide for rapid determination of choking flow for the choking point condition and for Fanno and isentropic flow for the fluids H_2, N_2, O_2, CCl_2F_2, and CCl_3F. A discussion of choking flow and relaxation phenomena is included.

Report of the investigation of slow-flow meters for fuel oil distribution systems, D. R. Mackay, *NBS Tech. Note 196* (*Sept. 5, 1963*), *20 cents.*

A recent development in the retail distribution of fuel oil to individual residences and to mobile homes involves the use of small, slow-flow meters. A technical investigation was conducted by the Office of Weights and Measures to develop testing equipment and test procedures that could be used to evaluate the accuracy characteristics of these meters. This report describes the testing systems and test procedures that were developed, as well as the data that were obtained during the course of the investigation.

Research on crystal growth and characterization at the National Bureau of Standards during the period January to June 1963, Ed. by H. S. Peiser, *NBS Tech. Note 197* (*Sept. 23, 1963*), *30 cents.*

The National Bureau of Standards with partial support from

the Advanced Research Projects Agency is continuing diverse research projects on the growth and characterization of crystals. This note summarizes the individual NBS activities in this and closely related fields during January to July 1963. Lists of NBS publications appertaining to that period and of participating NBS scientists are appended.

Monte Carlo calculations of the penetration and diffusion of fast charged particles, M. J. Berger, *Book, Methods in Computational Physics, Ed. B. Alder, S. Fernbach, and M. Rotenberg,* **I,** *135–215 (Academic Press, Inc., New York, N.Y., 1963).*
This is an expository article describing a Monte Carlo method for treating the multiple Coulomb scattering of fast charged particles. The method involves the setting up of a schematized random walk each step of which takes into account the effect of many successive collisions, and this random walk is simulated by random sampling. The transition probabilities for the random walk are obtained from the appropriate multiple scattering theories, including those of Moliere, Goudsmit and Saunderson, Landau, etc. After a detailed description of the required computational procedures, a review is given of the results that have been obtained by this method. The problems discussed include the backscattering and transmission of electrons and positrons by foils, the spatial distribution of energy dissipation by electrons, the slowing-down spectrum and pathlength distribution of electrons, and the penetration of protons. Numerous comparisons are made with experiments and other calculations.

Infrared dispersion of some oxide glasses, I. H. Malitson, G. W. Cleek, O. N. Stavroudis, and L. E. Sutton, *Appl. Opt.* **2,** *741 (July 1963).*
The refractive indices of four types of oxide glasses were measured for the wavelength range from 0.4μ to 5.3μ. The experimental data were fitted to a Sellmeier dispersion equation of the form $n_2=1+\Sigma A_j\lambda^2/(\lambda^2-\lambda_j^2)$. Dispersive curves were plotted which indicate the expected dispersive power, contribution to chromatic aberration, and spectral limit of resolution of the glasses as a function of wavelength. An attempt was made to correlate the parameters of the dispersion equation with the chemical composition of the glasses.

The structure of hexagonal silver iodide, G. Burley, *J. Chem. Phys.* **38,** *No. 12, 2807–2812 (June 1963).*
A detailed three dimensional refinement of the structure of hexagonal silver iodide from room temperature photographic data showed very little deviation from the ideal wurtzite-type structure. Using anisotropic temperature factors a final R value of 7.4% was obtained. The space group is $P6_3mc$. $a=4.592$, $c=7.510$, $c/a=1.635$, $\mu=0.374_4$. A general linear relation of the position parameter μ to the c/a axial ratio was found to apply to compounds having this structure type.

Radiolysis of propane-d_8 in the presence of organic compounds other than hydrocarbons, I. B. Sandoval and P. J. Ausloos, *J. Chem. Phys.* **38,** *No. 10, 2454–2460 (May 15, 1963).*
The gas phase radiolysis of propane-d_8 has been investigated in the presence of dimethylmercury, azomethane, acetone, methyliodide, methanol, nitromethane and methylamine. The cross section of the hydride transfer reaction

$$C_2D_5^+ + RH \rightarrow C_2D_5H + R^+$$

is, in all cases, at least ten times smaller than that of the reaction

$$C_2D_5^+ + C_3D_8 \rightarrow C_2D_6 + C_3D_7^+$$

Evidence for the occurrence of the proton transfer reaction

$$C_2D_5^+ + RH \rightarrow C_2D_4 + RHD^+$$

has been obtained. For the mixtures containing methanol, the cross section of this proton transfer reaction is about fifty times that of the hydride transfer process. Approximate values of $G(CH_3^+)$ have been determined for most of the additives.

Stark energy levels of symmetric-top molecules, J. H. Shirley, *J. Chem. Phys.* **38,** *2896–2913 (June 15, 1963).*
Calculations have been performed to determine the Stark energy levels of rigid symmetric top molecules. The continued fraction expression for the eigenvalues of the energy matrix is presented and techniques of evaluation described. Tables of reduced energy levels as a function of electric field are given for all rotational states through $J=4$. Graphs of these values and the effective dipole moments are included.

The microwave spectrum of normal propyl chloride, T. N. Sarachman, *J. Chem. Phys.* **39,** *No. 2, 469–473 (July 15, 1963).*
The microwave spectrum of gaseous normal propyl chloride reveals the presence of two rotational isomers, the *trans* and *gauche* conformations. The ground vibrational state rotational constants found for the more abundant Cl^{35} species are, for the *gauche* form, $A=11829.22$, $B=3322.58$, $C=2853.06$ Mc/sec; for the *trans* form, $B=2379.7$, $C=2271.7$ Mc/sec. Analysis of quadrupole hyperfine splittings in the spectrum of the *gauche* form gives the quadrupole coupling constants $\chi_{aa}=-19.41$ Mc/sec, $\eta=2.10_5$, in the principal axis system of the Cl^{35} species. Satellite spectra rising from excited vibrational states were also observed: in the *gauche* form, the first and second excited states of the skeletal torsion were assigned, and another satellite is believed to be from the excited methyl torsion; in the *trans* form, only the first excited state of the skeletal torsion was assigned. From relative intensity measurements, it is concluded that the energy difference between the *trans* and *gauche* isomers is $0 \pm .5$ kcal/mole.

Vacuum ultraviolet photochemistry. VI. Photolysis of cyclopropane with the Xenon resonance lines, C. L. Currie, H. Okabe, and J. R. McNesby, *J. Phys. Chem.* **67,** *No. 7, 1494–1497 (July 1963).*
The photolysis of cyclopropane has been carried out at 1470 Å at room temperature.
The relative yields of products as well as isotopic analyses of hydrogen, methane, and ethylene resulting from the photolysis of equimolar mixtures of cyclopropane and cyclopropane-d_6 indicate the following primary processes in order of decreasing importance.

$$\text{c-}C_3H_6 \rightarrow CH_2 + C_2H_4$$
$$\text{c-}C_3H_6 \rightarrow H_2 + C_3H_4$$
$$\text{c-}C_3H_6 \rightarrow H + C_3H_5$$

Atomic hydrogen probably forms molecular hydrogen by wall recombination. It is suggested that methane and ethane are formed from the methyl radical produced in the reaction:

$$CH_2 + \text{c-}C_3H_6 \rightarrow \text{c-}C_3H_5CH_3^* \rightarrow CH_3 + C_3H_5$$

The mechanism of formation of other products is discussed briefly.

Atomic frequency standards at the National Bureau of Standards, J. M. Richardson, R. E. Beehler, R. C. Mockler, and R. L. Fey, *Comite Consultatif, Definition de la Seconde aupres du Comite Intern. des Poids et Measures, pp. 57–67 (Sept. 1962).*
Many laboratories in various countries have now shown that certain atomic resonance frequencies have such desirable properties that they may be considered suitable for a definition of the unit of time. Details in the performance of actual atomic resonance devices are given. Also, estimates are made of how closely a given device approaches the idealized resonance frequency. Recently, two cesium beam frequency standards of independent design and construction have been completed, evaluated, and compared at Boulder. The main characteristics and performance details of these standards are analyzed and listed.
An analysis is given of comparisons of the U.S. Frequency Standard, by standard frequency broadcasts, with other frequency standards in the world.

Whistlers, R. M. Gallet, *Grenoble, Univ. Ecole Phys, Theorique, Les Houches, Geophysique Exterieur, pp. 551–590* (*Gordon and Breach, New York, N.Y., 1963*).
The whistlers and the very low frequency emissions (VLF Emissions) are two different classes of natural radio phenomena observed at very low frequency (few kilocycles per second). Both classes are characterized by very distinctive variations of frequency with time, which give them quasi-musical qualities in listening. They can be heard after the voltage, which the electromagnetic signals induce in an antenna, is amplified by a wide band audio-amplifier without frequency conversion. Their principal physical interest is that their characteristics are directly due to the structure of the Earth's exosphere. They can be considered as natural and highly sensitive electromagnetic probes for studying the physics of the exosphere. In both classes a radio-propagation phenomenon is experienced, which has the unique property of *guiding* the energy of radio waves along curved paths defined by the magnetic lines of force of the Earth's magnetic field. These paths reach far out into space, as far as 3 or 4 earth's radii in the plane of the magnetic equator, and bring the energy back to earth at the point in the opposite hemisphere which is the magnetic conjugate of the position of the radio emission in the case of the whistlers. The length of such one way path can easily be as long as 30,000 to 50,000 km. Furthermore, the energy can be almost perfectly reflected at the end of the path, and propagating again along the same path can be received in the area near the original point of emission. Along such long paths the speed of propagation of the energy is very slow (as low as c/10 to c/100), and its local value depends strongly on frequency.

Theory of the deep penetration of electrons and charged particles, L. V. Spencer and J. Coyne, *Phys. Rev.* **128,** *No. 5, 2230–2237 (Dec. 1, 1963).*
Charged particle penetration is amenable to elementary analysis if the continuous-slowing-down, small-angle, and diffusion-in-angle approximations are made. Such calculations are carried out in this paper, partly for their own interest and partly to demonstrate procedures of use in more realistic calculations. The present calculations can be considered an extension of Yang's work to problems including energy loss. One section of the paper goes beyond the approximation of diffusion-in-angle to derive results for a scattering function with a large-angle tail.

Correlation effects in two- and three-electron systems, J. W. Cooper and J. B. Martin, *Phys. Rev.* **131,** *No. 3, 1183–1186 (Aug. 1, 1963).*
Correlation effects in the lithium isoelectronic series $(1s)^2\ 2s\ ^2S$ have been studied by computing the expectation values of a number of one- and two-electron operators. Calculations were performed using both Hartree-Fock and configuration interaction wave functions.
For comparison purposes the same expectation values were computed from configuration interaction wave functions of comparable accuracy for the two electron systems $(1s)^2\ ^1S$. The main conclusions are (a) correlation has little effect on the one-electron expectation values, (b) the expectation values of $\sum_{i>j}(r_i \cdot r_j)$ and $\sum_{i>j}(p_i \cdot p_j)$ are proportionately larger for three- than for two-electron systems, and (c) the configuration interaction approach probably gives poor estimates of the expectation values of $\sum_{i>j}\delta^3(r_{ij})$ even though this value appears to converge as the number of terms in the wave function is increased.

Mechanical and electrical relaxation in theorium oxide containing calcium oxide, J. B. Wachtman, Jr., *Phys. Rev.* **131,** *517 (July–Sept. 1963).*
The dynamic behavior of oxygen vacancies associated with the solid solution of CaO in ThO_2 is treated using an 8-position nearest neighbor model. This treatment predicts an internal friction peak characterized by a single relaxation time and a dielectric loss peak with a single relaxation time equal to twice the mechanical relaxation time. Both peaks have been observed and are in accord with these predictions within experimental error. The activation energy for the motion of an oxygen vacancy neighboring a substitutional Ca ion in $98.5\ ThO_2 + 1.5\ CaO$ is $0.93 \pm .02$ e.v.

A study of embrittlement of high strength steels by hydrogen isotopes. I. Testing of steel rings as specimens, a comparison of hydrogen and deuterium embrittlement, and permeation studies, G. B. Wood, *J. Electrochem. Soc.* **110,** *No. 8, 867–877 (Aug. 1963).*
The embrittling nature of deuterium in steel is demonstrated. A comparison of the retention of embrittlement with retained gas content in uncoated steel is discussed. The separation factor for the electrodeposition of hydrogen and denterium on SAE 4130 steel was found to be 5.9. Permeation of the mixture of these isotopes through steel resulted in further enrichment with respect to hydrogen. The diffusion coefficients and permeation rates for hydrogen and deuterium in steel were compared.

A study of embrittlement of high strength steels by hydrogen isotopes. II. A comparison of gas contents and hydrogen or deuterium embrittlement resulting from electroplating processes, G. B. Wood, *J. Electrochem. Soc.* **110,** *No. 8, 877–885 (Aug. 1963).*
Plating processes introduce more deuterium into steel from heavy water solutions than hydrogen from ordinary water solutions, yet hydrogen embrittles steel more than deuterium. There is no simple relation between the total gas content and embrittlement. Embrittlement appears to be dependent on factors other than the total gas content. The present work does not preferentially support any one of the mechanisms which have been proposed for hydrogen embrittlement. The difference in the chemical affinity of steel for hydrogen and deuterium is demonstrated.

Optical observation of pressure induced transitions in polymers, A. Van Valkenburg and J. Powers, *J. Appl. Phys.* **34,** *No. 8, 2433–2434 (Aug. 1963).*
Pressure induced transitions in polytetrafluoroethylene, nylon 6, natural rubber, and polyethylene were observed optically between diamond anvils. In all polymers examined, the decrease in thickness and in birefringence is irreversible, at least on the time scale of a few months.

Visual observations of high pressure transitions, A. Van Valkenburg, *Rev. Sci. Instr. Letter* **33,** *No. 12, 1462 (Dec. 1962).*
Phase changes at routine pressures of 70 kilobars have been visibly observed in transparent solids and liquids using a diamond squeezer cell and polarizing microscope.

Some intra-atomic correlation correction studies, M. Krauss and B. J. Ransil, *J. Chem. Phys.* **33,** *840 (1960).*
The applicability of the "intra-atomic correlation correction" (ICC) formulation of Hurley is discussed. It is shown that accurate bond energies can not be obtained with the usual restricted basis set without employing another empirical procedure although it may be possible to obtain accurate excitation energies.

Band spectrum analysis of mercury hydride, T. L. Porter, *J. Opt. Soc. Am.* **52,** *1201 (1962).*
The emission spectrum of mercury hydride has been photographed in the second and third orders of a 21-foot concave grating in the region 2930–4550 A. The light source was an electrodeless discharge tube containing a drop of mercury in an atmosphere of hydrogen and argon. Twenty-six bands of the A–X system and four bands of the B–X system have been analyzed, most of them to their predissociation limits. A table of these bands and a vibrational energy-level diagram are given. The behavior of the lambda-type doubling in the $^2\Pi$ state for which the electronic coupling is Hund's case a is compared with the theoretical prediction.

Remarks on coincidence experiments with visible light, Z. Bay and P. S. Farago, *Proc. Royal Soc. Edinburgh, Sec. A. Math. and Phys. Sci.* **LXVI,** *pt. 11, No. 10, 111–115 (Royal Society of Edinburgh, Edinburgh, Scotland, 1963).*
After the detection of correlations in two coherent light beams by Hanbury, Brown, and Twiss, objections were raised by Brannan and Ferguson on the basis of the experiments of Adam, Janossy, and Varga and their own experiments in which no correlations were detected. It is pointed out here

that the opposing groups were looking for two entirely different effects, one being quadratic, the other one linear in the number or photons involved. The quadratic effect is in agreement with photon theory while the linear effect is not and therefore the experimental proof of the existance or nonexistence of the linear effect is of fundamental importance. It was shown by Purcell and by Hanbury, Brown, and Twiss that the choice of parameters in the experiments of Janossy and Brannen and Ferguson was inadequate to show the quadratic effect. It is shown in this paper that their experiments were also inadequate to decide between the existence or nonexistence of the linear effect.

Other NBS Publications

J. Res. NBS 67B (Math. and Math. Phys.), No. 4 (Oct.–Dec. 1963) 75 cents.

Zonal harmonic perturbations of an accurate reference orbit of an artificial satellite. J. P. Vinti.

Optimal periodic inspection programs for randomly failing equipment. G. H. Weiss.

An analysis of pedestrian queueing. G. H. Weiss.

Solutions of the equation $\Psi_{zz}+\frac{1}{x}\Psi_z+Kx^n e^{\Psi}=0$, E. A. Kearsley. (See above abstract.)

On the graphs of finite idempotent Boolean relation matrices. D. Rosenblatt. (See above abstract.)

J. Res. NBS 68D (Radio Sci.), No. 1 (Jan. 1964) $1.00.

Comparison of observed VLF attenuation rates and excitation factors with theory. A. D. Watt and R. D. Croghan.

Field Intensity measurements at 10.2 kc/s over reciprocal paths. J. C. Hanselman, C. J. Casselman, M. L. Tibbals, and J. E. Bickel.

The propagation of VLF waves over distances between 1000 and 3000 km. B. Burgess.

Some experimental results concerning nonreciprocal east-west VLF wave propagation. B. Burgess.

An experimental study of the phase stability of VLF signals. D. E. Hampton.

Some particular observations on diurnal phase variations of VLF transmission received in Paris. B. Decaux and A. Gabry.

Periodic fading of VLF signals received over long paths during sunrise and sunset. D. D. Crombie.

Effects of wall perturbations in multimode waveguides. S. W. Maley and E. Bahar.

VLF Utilization at NASA satellite tracking stations. C. H. Looney, Jr.

Long wave associated with disturbances produced in plasmas. H. Bremmer. (See above abstract.)

Some remarks on the Watson transformation and mode theory. L. A. Berry.

Concerning limitations and further corrections to geometric-optical theory for LF/VLF propagation between the ionosphere and the ground. J. R. Johler. (See above abstract.)

Some remarks on mode and ray theories of VLF radio propagation. J. R. Wait.

Two-dimensional treatment of mode theory of the propagation of VLF radio waves. J. R. Wait.

Reflection of electromagnetic waves from a lossy magnetoplasma. J. R. Wait and L. C. Walters.

Propagation of ELF waves below an inhomogeneous anisotropic ionosphere. J. Galejs and R. V. Row.

VLF propagation under the ionosphere in the lowest mode of horizontal polarization. H. A. Wheeler.

Propagation of VLF waves under disturbed conditions. B. Burgess.

VLF disturbances caused by trapped beta-rays from the decay of neutrons produced in high-altitude nuclear explosions. A. J. Zmuda, B. W. Shaw, and C. R. Haave.

VLF anomalies observed at State College, Pa., during the U.S. 1962 high-altitude nuclear tests. C. F. Sechrist.

J. Res. 68D (Radio Sci.), No. 2 (Feb. 1964). $1.00.

Generation of an electromagnetic pulse by an expanding plasma in a conducting half-space. A. P. Stogryn and R. N. Ghose.

Impedance of a monopole antenna with a radial-wire ground system on an imperfectly conducting half-space, part II. S. W. Maley and R. J. King

Capacitor type biconical antennas. J. Galejs.

Simulated angular response patterns for transhorizon propagation. J. W. Strohbehn and A. T. Waterman, Jr.

Radio-star scintillations from ionospheric waves. J. W. Warwick.

Ionosonde studies of some chemical releases in the ionosphere. J. W. Wright.

Diurnal changes and transmission time in the arctic propagation of VLF waves. W. T. Blackband.

Geometrical optics convergence coefficient for the whistler case. J. H. Crary.

Comments on a paper 'Collisional Detachment and the Formation of an Ionospheric' by E. T. Pierce. H. R. Arnold.

The quasi-longitudinal approximation in the generalized theory of radio wave absorption. R. F. Benson.

Diurnal phase variation of VLF waves at medium distances. H. Volland.

Application of diffractions by convex surfaces to irregular terrain situations. H. T. Dougherty and L. J. Maloney.

Effect of lossy earth on antenna gain. R. J. Coe and W. L. Curtis.

Propagation of radio waves with frequency 99.9 Mhz as a function of the vertical structure of the atmosphere derived from daily radiosonde observations. G. P. A. Braam.

Bibliography of temperature measurement, July 1960 to December 1962, C. Halpern, NBS Mono. 27, Suppl. 1 (Sept. 13, 1963), 20 cents.

1963 Supplement Screw-thread standards for federal services, (Parts I, II, and III) Handb. H28 (1957) (Oct. 15, 1963), 70 cents.

Clinical Dosimetry, Recommendations of the International Commission on Radiological Units and Measurements, NBS Handb. 87 (Aug. 9, 1963), 40 cents. (This publication supersedes parts of H78. Handbooks 84 through 89 will completely replace H78.)

Methods of evaluating radiological equipment and materials, Recommendations of the International Commission on Radiological Units and Measurements, NBS Handb. 89 (Aug. 23, 1963), 35 cents. (This publication supersedes parts of H78. Handbooks 84 through 89 will completely replace H78.)

Hydraulic research in the United States, 1963, NBS Misc. Publ. 249 (Aug. 9, 1963), $1.00.

Mean electron density variations of the quiet ionosphere, No. 11—January 1960, J. W. Wright, L. R. Wescott, and D. J. Brown, NBS Tech. Note 40–11 (Aug. 30, 1963), 40 cents.

Mutual interference between surface and satellite communication systems, W. J. Hartman and M. T. Decker, NBS Tech. Note 126 (Aug. 1, 1963), 35 cents.

Antenna beam elevation angle for control of tropospheric interference between space system earth terminals and terrestrial stations, S. G. Lutz and W. J. Hartman, NBS Tech. Note 180 (Aug. 25, 1963), 15 cents.

Computer program for ionospheric mapping by numerical methods, M. E. Hinds and W. B. Jones, NBS Tech. Note 181 (Aug. 20, 1963), 50 cents.

A note on antipodal focussing, J. R. Wait, NBS Tech. Note 182 (Aug. 20, 1963), 15 cents.

Report on technical investigation of odometers, D. R. Mackay, NBS Tech. Note 195 (Aug 6, 1963), 25 cents.

Synthesis of perfluorostyrene and (2,2-difluorovinyl)perfluorobenzene (α-hydroheptafluorostyrene). A general method for synthesis of highly fluorinated styrenes, J. M. Antonucci and L. A. Wall, SPE Trans. **3,** No. 3, 225–230 (July 1963).

Radiation transfer problems in the rocket ultra-violet lines, C. Pecker and R. N. Thomas, J. Quant. Spectry. Radiative Transfer **3,** No. 2, 163–165 (June 1963).

Stress-corrosion cracking of type 304 stainless steel at 455 to 615 F, H. L. Logan, M. J. McBee, and M. Romanoff, Mater. Res. Std. **3,** No. 8, 635–639 (Aug. 1963).

Lines of constant correlated color temperature based on MacAdam's (u,v) uniform chromaticity transformation of the CIE diagram, K. L. Kelly, J. Opt. Soc. Am. **53,** No. 8, 999–1002 (Aug. 1963).

Intrinsic attenuation, R. W. Beatty, IEEE Trans. Microwave Theory Tech. **MTT–11,** No. 3, pp. 179–182 (May 1963).

A note on modular groups, M. Newman, Proc. Am. Math. Soc. **14,** No. 1, 124–125 (Feb. 1963).

Leaf temperature and energy exchange, D. M. Gates, Archiv Meteorol. Geophys. Bioklimatol. Ser. B, **12,** 321–336 (1963).

Equatorial ionospheric variations during geomagnetic storms, S. Matsushita, J. Geophys. Res. **68,** 2595–2601 (May 1, 1963).

The calibration of inductive voltage dividers, T. L. Zapf, ISA Proc. 1962, **17,** pt. I, pp. 10.2.62–1 to 10.2.62–8 (1962).

Effects of the nuclear explosion over Johnston Island observed in Peru on July 9, 1962, M. Casaverde, A. Giesecke, and R. Cohen, J. Geophys. Res. **68,** No. 9, 2603–2611 (May 1, 1963).

Derivation of electron density profiles in the lower ionosphere using radio absorption measurements at multiple frequencies, R. Parthasarathy, G. M. Lerfald, and C. G. Little, J. Geophys. Res. **68,** 3581–3588 (June 15, 1963).

Radiolysis of methane, P. J. Ausloos and S. G. Lias, J. Chem. Phys. **38,** No. 9, 2207–2214 (May 1, 1963).

The stress-corrosion cracking of type 304 stainless steel at 455 to 615 F, H. L. Logan, M. J. McBee, and M. Romanoff, Mater. Res. Std. **3,** No. 8, 625–639 (Aug. 1963).

The redefinition of the second and the velocity of light, G. E. Hudson and W. Atkinson, Physics Today **16,** No. 5, 30–36 (May 1963).

Thermal conductivity, R. L. Powell, American Institute of Physics Handb. 2d Ed. pp. 4–76–4–101 (McGraw-Hill Book Co., Inc., New York, N.Y., 1963).

Digital pattern recognition by moments, F. L. Alt, Book, Optical Character Recognition, Ed. G. L. Fischer, D. K. Pollack, B. Raddick, and M. E. Stevens pt. II, pp. 153–179 (Spartan Books, Washington, D.C., 1962).

D-gluco-L-glycero-3-octulose, a crystalline ketose from D-erythrose, R. Schaffer and A. Cohen, J. Organ. Chem. **28,** 1929–1930 (1963).

A phenomenological theory of overvoltage for metallic particles, J. R. Wait. Book, Overvoltage Research and Geophysical Applications, Ed. J. R. Wait, ch. **3,** p. 22 (Pergamon Press, Inc., New York, N.Y., 1959).

Statistics in chemical analysis, W. J. Youden, Handbook of Analytical Chemistry, Sec. 14, pp. 14–1—14–9 (McGraw-Hill Book Co., Inc., New York, N.Y., 1963).

Radiation, L. S. Taylor, Americana Annual 620–622 (Americana Corporation, Chicago, Ill., 1961).

Ten year weathering data on aluminum alloys, W. H. Ailor, Jr., and F. M. Reinhart, Materials Protect. **2,** No. 6, 30–36 (June 1963).

Modulary groups of $t \times t$ matrices, M. Newman and J. R. Smart, Duke Math. J. **30,** 253–257 (1963).

An experimental method of estimating *F*-region collision frequencies (research note), J. K. Hargreaves, J. Atmospheric and Terrest. Phys. **25,** 300–304 (May 1963).

Optical Character Recognition, Ed., G. L. Fischer, D. K. Pollack, B. Raddick, and M. E. Stevens (Spartan Books, Washington, D.C. 1962).

Achievement of measurement of agreement among electrical standards laboratories, F. D. Weaver, Instr. Control Systems **36,** 128–131 (July 1963).

A He^3 cryostat for performing experiments with oriented nuclei, E. Ambler, R. Dove, and R. Kaeser (Proc. 1962 Cryogenic Engineering Conf.), Book, Advances in Cryogenic Engineering **8,** Sec. H–2, 443–554 (Plenum Press Inc., New York, N.Y., 1963).

Spectroscopic absorption of NO in crystalline and liquid krypton, G. L. Pollack and H. P. Broida, J. Chem. Phys. **38,** No. 8, 2012–2015 (Apr. 15, 1963).

The possibility of guided electromagnetic waves in the earth's crust, J. R. Wait, IEEE Trans. Ant. Prop. **AP–11,** 330–335 (May 1963).

The nature of the compound obtained from aqueous cesium chloride solution and hydrogen chloride, A. G. Maki and and R. West, Inorganic Chem. **2,** 657 (1963).

Laboratory investigation of overvoltage, L. S. Collett, A. A. Brant, W. E. Bell, K. A. Ruddock, H. O. Siegel, and J. R. Wait, Book, Overvoltage Research and Geophysical Applications, Ed. J. R. Wait, ch. 5, p. 50 (Pergamon Press, Inc., New York, N.Y., 1959).

1,2,2-trifluorovinyl phenyl ether and 2,3,4,5,6-pentafluorophenyl 1,2,2-trifluorovinyl ether and their polymers, W. J. Pummer and L. A. Wall, SPE Trans. **3,** No. 3, 220–224 (July 1963).

Radiometry, M. M. Reynolds, R. J. Corruccini, M. M. Fulk, and R. M. Burley, American Institute of Physics Handb. 2d ed., pp. 6–153—6–172 (McGraw-Hill Book Co., Inc., New York, N.Y., 1963).

Classification of resonances in the electron scattering cross section of Ne and He, J. A. Simpson and U. Fano, Phys. Rev. Letters **11,** 158 (1963).

Bolometric microwave power calibration techniques at NBS, R. F. Desch and R. E. Larson, Proc. ISA 17th Annual Instrument-Automation Conf. & Exhibit (Oct. 1962).

Criteria from the transient decay curves, J. R. Wait and L. S. Collett, Book, Overvoltage Research and Geophysical Applications, Ed. J. R. Wait, ch. 6a, p. 71 (Pergamon Press, Inc., New York, N.Y., 1959).

On the interpretation of prominence spectra. VI. Temperature determination and a model for quiescent prominences, J. T. Jefferies and F. Q. Orrall, Astrophys. J. **137,** 1232–1241 (May 15, 1963).

The lifetime and movement of artificially produced electron clouds observed with spaced ionosondes, J. W. Wright, J. Geophys. Res. **68,** No. 10, 3011–3020 (May 15, 1963).

Isopiestic vapor pressure measurements of the tenary system: Sorbitol-sodium chloride-water at 25°, V. E. Bower and R. A. Robinson, J. Phys. Chem. **67,** 1540–1541 (1963).

The intermediate state of some hard superconductors, V. Arp, R. H. Kropschot, and T. S. Craig, Book, Superconductors, pp. 135–141 (Interscience Publ., New York, N.Y., 1962).

Ferromagnetic resonance and shape dependent effects, L. A. Steinert, J. Appl. Phys. Letter **34,** 2106–2107 (July 1963).

Characteristics of spread *F* at high geomagnetic latitude, W. K. Klemperer, J. Geophys. Res. **68,** No. 10, 3191–3196 (May 15, 1963).

The thermodynamics of the ternary system: Urea-sodium chloride-water at 25°, V. E. Bower and R. A. Robinson, J. Phys. Chem. **67,** 1524–1527 (1963).

Verification of the tenfold assignment of the Baryon resonances, S. Meshkov, C. A. Levinson, and H. J. Lipkin, Phys. Rev. Letters **10,** No. 8, 361–364 (Apr. 15, 1963).

Vapor snakes in solid argon, G. L. Pollack and H. P. Broida, J. Chem. Phys. **38,** No. 4, 968–969 (Feb. 15, 1963).

The day-to-night ratio of cosmic noise absorption during polar cap absorption events, C. S. Gilmor, J. Atmospheric Terrest. Phys. **25,** 263–266 (May 1963).

Photographic dosimetry, megaroentgen range, W. L. McLaughlin, Encyclopaedia of X-rays and Gamma Rays, Ed. G. L. Clark, pp. 307–309 (Reinhold Publ. Corp., New York, N.Y., 1963.)

Proposed experiment to measure effects of ground roughness on the dose rate from fallout radiation, C. Eisenhauer, Health Phys. **9,** 503–506 (1963).

Standards for dental radiographic film, G. C. Paffenbarger, Mag. Std. **34,** 148 (May 1963).

The variable-frequency method, J. R. Wait, Book, Overvoltage Research and Geophysical Applications, Ed. J. R. Wait, ch. 4, p. 29 (Pergamon Press, Inc., New York, N.Y., 1959).

Heat transfer between a cryo-surface and a controlled atmosphere, Suppl. Bull. Intern. Inst. Refrigeration Annexe 1962–1, p. 89 (Aug. 1962).

Polymers and telomers of 4-chloroperfluoroheptadiene-1,6, J. E. Fearn and L. A. Wall, SPE Trans. **3,** No. 3, 231–234 (July 1963).

Excitation of pi-electrons in polystyrene and similar polymers by 20 Kev electrons, N. Swanson and C. J. Powell, J. Chem. Phys. **39,** 630–634 (Aug. 1, 1963).

Cane sugar refining. II. Decolorization with adsorbents, V. R. Deitz and F. G. Carpenter, Cane Sugar Handb. Ed,

G. P. Meade, 9th edition, pp. 342–385 (John Wiley & Sons Inc., New York, N.Y., Aug. 1963).

Klystron protection circuit, W. E. Case and N. T. Larsen, Rev. Sci. Instr. **34,** No. 7, 809–810 (July 1963).

Stable 6300 Å auroral arcs in mid-latitudes, F. E. Roach and J. R. Roach, Planetary Space Sci. **11,** 523–545 (1963).

Parable of the Fisherman, W. J. Youden, Phys. Teacher Editorial **1,** No. 3, 120–121 (Sept. 1963).

The wear of magnetic recording tape and solubility of the binder, F. Nesh, IEEE Trans. Audio **AU–11,** No. 3, 97 (May–June 1963).

Special techniques for use in sugar analysis, V. R. Deitz and F. G. Carpenter, Cane Sugar Handb. Ed. G. P. Meade, 9th edition, pp. 605–619 (John Wiley & Sons, Inc., New York, N.Y., Aug. 1963).

Humidity (measurement of moisture in gas), A. Wexler, ISA Transducer Compendium, pp. 502–508 (Sept. 1963).

Convection phenomena from plants in still air, D. M. Gates and C. M. Benedict, Am. J. Botony **50,** 563–573 (July 1963).

Triboluminescence in a mercury bubbler, L. Schoen, Can. J. Phys. **38,** 967–970 (1960).

Deuterium isotope effect on glass transformation temperatures of aqueous inorganic solutions, L. C. Shepley and A. B. Bestul, J. Chem. Phys. **39,** No. 3, 680–687 (Aug. 1, 1963).

Mechanical reading of characters and recognition, M. E Stevens (Proc. Intern. Patent Office Workshop on Information Retrieval), 125th Anniversary of the U.S. Patent Act of 1836, pt. II, p. 205 (1962).

One year trial for new voltmeter standard, C. Stansbury, Mag. Std. **34,** No. 3, 240–241 (Aug. 1963).

Pressure-density-temperature relations of freezing liquid parahydrogen to 350 atmospheres, Cryogenics **3,** No. 1, 12–15 (Mar. 1, 1963).

Status of sugar color and turbidity measurements, F. G. Carpenter and V. R. Deitz, Am. Soc. Sugar Beet Technologists **12,** No. 4, 326–347 (Jan. 1963).

Portable 2 flow counter for the detection of α and β particles in smear samples, L. Costrell, A. Schwebel, and G. W. Zimmer, Health Phys. **9,** No. 6, 643 (June 1963).

The occurrence of short-duration cosmic noise absorption events inside the southern auroral zone, C. S. Gillmor, Jr., and J. K. Hargreaves, J. Atmospheric and Terrest. Phys. **25,** 311–317 (June 1963).

An unmodulated twin channel microwave attenuation measurement system, D. H. Russell, ISA 18th Annual Conf., pp. 1–17 (Sept. 1963).

Application of distillation techniques to radiochemical separations, J. R. DeVoe, Natl. Acad. Sci.-Natl. Res. Council Nuclear Science Series, Radiochemical Techniques NAS–NS3108 (Aug. 1962).

Physical measurements and experiment design, W. J. Youden (Colloq. Intern. Centre Natl. Recherche Sci., Aug.–Sept. 1961), Book, Le Plan d'Experiences, No. 110, p. 115 (Centre National de la Recherche Scientifique, Paris, France, 1963).

Airglow research, F. E. Roach, Trans. Am. Geophys. Union **44,** No. 2, 431–432 (June 1963).

The National Bureau of Standards reactor facility, C. O. Muehlhause, Capital Chemist **12,** No. 1, 7–10 (Jan. 1962).

Determination of rhodium in rhodium-uranium alloys by precipitation with hydrogen sulfide, E. J. Maienthal, Anal. Chem. **35,** 1094–1095 (July 1963).

Determination if bitumen content in expansion joint fillers, E. Horowitz and J. Mandel, Mater. Res. Std. **3,** No. 9, 723–725 (Sept. 1963).

Time and frequency broadcasting, A. H. Morgan, ISA J. **10,** No. 6, 49–54 (June 1963).

Distillation, A. T. Leslie and E. C. Kuehner, Analytical Chemistry Handb. **XIII,** Methods of Separation, Ed. L. Meites, Sect. 10, pp. 10–23—10–42 (1963).

Precision and accuracy in electromagnetic measurements, R. D. Huntoon (Intern. Conf. Precision Electromagnetic Measurements, Boulder, Colo., Aug. 14–17, 1962), IRE Trans. Instr. **I–11,** Nos. 3 and 4, 84 (Dec. 1962).

Quadrupole coupling constants from the microwave spectrum of hydrazoic acid, R. A. Forman and D. R. Lide, Jr., J. Chem. Phys. **39,** No. 4, 1133–1134 (Aug. 15, 1963).

The following papers were published in Ionospheric Sporadic *E*, Ed. E. K. Smith and S. Matsushita (Pergamon Press, Inc., New York, N.Y., 1962).

A note on the heights of the different IGY types of E_s, S. C. Gladden, pp. 178–181.

A study of radio wave scattering from sporadic *E* near the magnetic equator, K. L. Bowles and R. Cohen, pp. 51–77.

A theoretical study of sporadic-*E* structure in the light of radio measurements, K. Tao, pp. 235–257.

Lunar tidal variations of sporadic *E*, S. Matsushita, pp. 194–214.

On the width of the equatorial E_s belt, R. W. Knecht and R. E. McDuffie, pp. 215–218.

Recent sporadic-*E* experimental work in the United States, J. F. DeGregorio, J. W. Finney, K. Kildahl, and E. K. Smith, pp. 141–142.

Sporadic-*E* propagation with 3μ sec pulses, G. R. Ochs, R. J. Carpenter, and E. K. Smith, pp. 143–148.

The night-*E* layer, G. A. M. King, pp. 219–231.

The occurrence of sporadic *E*, E. K. Smith, pp. 3–12.

The occurrence of sporadic *E* during the IGY, H. I. Leighton, A. H. Shapley, and E. K. Smith, pp. 166–177.

Variations in frequency of occurrence of sporadic *E*, 1949–1959, W. B. Chadwick, pp. 182–193.

**Publications for which a price is indicated are available by purchase from the Superintendent of Documents, Government Printing Office, Washington, D.C., 20402 (foreign postage, one-fourth additional). Reprints from outside journals and the NBS Journal of Research may often be obtained directly from the authors.*

U.S. GOVERNMENT PRINTING OFFICE:1964

(Continued from inside front cover)

Troposphere and Space Telecommunications. Data Reduction Instrumentation. Radio Noise. Tropospheric Measurements. Tropospheric Analysis. Spectrum Utilization Research. Radio-Meteorology. Lower Atmosphere Physics.

Radio Systems. Applied Electromagnetic Theory. High Frequency and Very High Frequency Research. Frequency Utilization. Modulation Research. Antenna Research. Radiodetermination.

Upper Atmosphere and Space Physics. Upper Atmosphere and Plasma Physics. High Latitude Ionosphere Physics. Ionosphere and Exosphere Scatter. Airglow and Aurora. Ionospheric Radio Astronomy.

Radio Standards Laboratory

Radio Standards Physics. Frequency and Time Disseminations. Radio and Microwave Materials. Atomic Frequency and Time-Interval Standards. Radio Plasma. Microwave Physics.

Radio Standards Engineering. High Frequency Electrical Standards. High Frequency Calibration Services. High Frequency Impedance Standards. Microwave Calibration Services. Microwave Circuit Standards. Low Frequency Calibration Services.

NBS Laboratory Astrophysics Group

(Joint Institute for Laboratory Astrophysics at Univ. of Colo.)

U.S. DEPARTMENT OF COMMERCE
Luther H. Hodges, Secretary

NATIONAL BUREAU OF STANDARDS
A. V. Astin, Director

Order all publications from the Superintendent of Documents
U.S. Government Printing Office, Washington, D.C., 20402

Use of funds for printing this publication approved by the Director of the Bureau of the Budget (June 19, 1961).

UNIVERSITY MICROFILMS
313 NORTH FIRST STREET
ANN ARBOR, MICHIGAN
SJR-A-OCT

UNITED S...
GOVERNMENT PRINTING OFFICE
DIVISION OF PUBLIC DOCUMENTS
WASHINGTON, D.C. 20402
OFFICIAL BUSINESS

PENALTY FOR PRIVATE USE TO AVOID PAYMENT OF POSTAGE, $300 (GPO)

JOURNAL OF RESEARCH of the National Bureau of Standards Vol. 68A, No. 1 January–February 1964
A. Physics and Chemistry

Contents

	Page
Fast neutron dose measurements for a D–D source in water. W. B. Beverly and V. Spiegel, Jr.	1
X-ray spectrometric analysis of noble metal dental alloys. B. W. Mulligan, H. J. Caul, S. D. Rasberry, and B. F. Scribner.	5
The first spectrum of manganese, Mn I. Miguel A. Catalán, William F. Meggers, and Olga García-Riquelme.	9
Transition probabilities of forbidden lines. R. H. Garstang.	61
Franck-Condon factors to high vibrational quantum numbers III: CN. R. W. Nicholls.	75
Infrared absorption spectrum of nitrous oxide (N_2O) from 1830 cm^{-1} to 2270 cm^{-1}. Earle K. Plyler, Eugene D. Tidwell, and Arthur G. Maki.	79
An absolute light scattering photometer: II. Direct determination of scattered light from solutions. Donald McIntyre.	87
High pressure microscopy of the silver and cuprous halides. A. Van Valkenburg.	97
Lattice parameters and lattice energies of high-pressure polymorphs of some alkali halides. C. E. Weir and G. J. Piermarini.	105
Calculation of the higher order dipole-dipole effect in paramagnetic crystals. Paul H. E. Meijer.	113
Second and third virial coefficients for hydrogen. R. D. Goodwin, D. E. Diller, H. M. Roder, and L. A. Weber.	121
Heats of solution, transition, and formation of three crystalline forms of metaboric acid. Marthada V. Kilday and Edward J. Prosen.	127
Publications of the National Bureau of Standards.	139

Library of Congress Catalog Card Number: 62–37059

For sale by the Superintendent of Documents, U.S Government Printing Office, Washington, D.C., 20402. Price 70 cents (single copy)
Subscription price: $4 a year; 75 cents additional for foreign mailing.
UNITED STATES GOVERNMENT PRINTING OFFICE, WASHINGTON : 1964